

# Romanian Journal of MINERAL DEPOSITS

continuation of

DARI DE SEAMA ALE SEDINTELOR INSTITUTULUI DE GEOLOGIE SI GEOFIZICA  
COMPTES RENDUS DES SÉANCES DE L'INSTITUT DE GÉOLOGIE ET GÉOPHYSIQUE  
(2. Zacaminte)

Founded 1910 by the Geological Institute of Romania

ISSN 1220-5648

**VOL. 91**  
**No. 1-2**

## CONTENT

*page*

- Adolf Heinrich HORN, Paulo Roberto Antunes ARANHA, Henrique Chaves JONCEW**  
Combined mineralochemical, statistical and geophysical (GPR) data as support for the  
exploration of pegmatite-hosted gemstones: example from the Santa Rosa mine, MG, Brazil ..... 1
- Paulo Roberto Antunes ARANHA, Adolf Heinrich HORN, Henrique Chaves JONCEW**  
Use of GPR in pegmatite mining: example of a sheetlike body from northern Minas Gerais, Brazil ..... 7
- Ioan PINTEA, Maria-Lidia NUȚU-DRAGOMIR, Sorin Silviu UDUBAȘA, Daniel BÎRGĂOANU,  
Luisa Elena IATAN, Ion BERBELEAC, Oana-Claudia CIOBOTEA-BARBU**  
Hydrosilicate aqueous -, and vapor - “melt” inclusions in some specific rocks and minerals  
from Romania ..... 13
- George DINCĂ, Gheorghe C. POPESCU, Oana-Claudia CIOBOTEA-BARBU,  
Daniel BÎRGĂOANU**  
Silver sulfotellurides and other Te-sulfosalts in alabandite-bearing veins from Săcărâmb  
Au-Ag-Te ore deposit, Metaliferi Mountains, Romania ..... 19
- Elena-Luisa IATAN, Ion BERBELEAC**  
Neogene mineralizations of Bucium Rodu-Frasin Au-Ag deposits, South Apuseni Mountains,  
Romania ..... 25
- Călin G. TĂMAȘ, Paul IVĂȘCANU, Gabriela BENA, Laurențiu IGNA, Nicolae HAR**  
Neogene distal skarn mineral assemblage from Ruda Brad, Apuseni Mountains, Romania ..... 31

*- continued on the outside back cover -*



**Geological Institute of Romania**  
**Society of Economic Geology of Romania**  
**București – 2018**



## **DIRECTORS OF THE JOURNAL**

**Dr. Ștefan Marincea**, General Director of the Geological Institute of Romania

**Prof. Dr. Gheorghe Damian**, President of the Society of Economic Geology of Romania

**Editor in Chief:** Sorin Silviu Udubașa (University of Bucharest).

**Editorial Secretary:** Monica Macovei (University of Bucharest)

### **Editorial board**

**Gheorghe Udubașa**, Romanian Academy; University of Bucharest

**Peter Andráš**, Matej Bel University, Banská Bystrica, Slovakia

**Anne-Sylvie Andre-Mayer**, Université de Lorraine, Nancy, France

**Andrei Ionut Apopei**, "Alexandru Ioan Cuza" University, Iași

**Essaid Bilal**, Ecole des Mines, Saint Etienne, France

**Grigore Buia**, University of Petrosani

**Andrei Buzatu**, "Alexandru Ioan Cuza" University, Iași

**Nicolae Buzgar**, "Alexandru Ioan Cuza" University, Iași

**Georgios Christofides**, Aristotle University of Thessaloniki, Greece

**Floarea Damian**, Technical Univ. Cluj-Napoca – North Center Baia Mare

**Gheorghe Damian**, Technical Univ. Cluj-Napoca – North Center Baia Mare,

**János Földessy**, Miskolc University, Hungary

**Ovidiu Gabriel Iancu**, "Alexandru Ioan Cuza" University, Iași

**Gheorghe Ilinca**, University of Bucharest

**Marian Lupulescu**, New York State Museum, USA

**Mihai Marinescu**, University of Bucharest

**Marcel Mărunțiu**, Geological Institute of Romania

**Vasilios Melfos**, Aristotle University of Thessaloniki, Greece

**Ferenc Molnar**, Geological Survey of Finland

**Marian Munteanu**, Geological Institute of Romania

**Antonela Neacsu**, University of Bucharest

**Bogdan Niculescu**, University of Bucharest

**M.S. Pandian**, Pondicherry University, India

**Lucian Petrescu**, University of Bucharest

**Ioan Pinte**, Geological Institute of Romania

**Gheorghe Popescu**, University of Bucharest

**Relu Roban**, University of Bucharest

**Ioan Seghedi**, Institute of Geodynamics of the Romanian Academy, Bucharest

**Dan Stumbea**, "Alexandru Ioan Cuza" University, Iași

**Călin Tămaș**, Babeș-Bolyai University, Cluj-Napoca

**George Tudor**, Geological Institute of Romania

**Mircea Țicleanu**, Geological Institute of Romania

**Sorin Silviu Udubașa**, University of Bucharest

**Rom. J. Mineral Deposits** is also the Bulletin of the Society of Economic Geology of Romania

**The authors are responsible for the ideas presented in the papers.**

**ISSN 1220-5648**



Geological Institute of Romania  
Society of Economic Geology of Romania



## Romanian Journal of MINERAL DEPOSITS

ISSN 1220-5648

VOL. 91  
No. 1-2

2018

### CONTENT

<b>Adolf Heinrich HORN, Paulo Roberto Antunes ARANHA, Henrique Chaves JONCEW</b> Combined mineralochemical, statistical and geophysical (GPR) data as support for the exploration of pegmatite-hosted gemstones: example from the Santa Rosa mine, MG, Brazil .....	1
<b>Paulo Roberto Antunes ARANHA, Adolf Heinrich HORN, Henrique Chaves JONCEW</b> Use of GPR in pegmatite mining: example of a sheetlike body from northern Minas Gerais, Brazil .....	7
<b>Ioan PINTEA, Maria-Lidia NUȚU-DRAGOMIR, Sorin Silviu UDUBAȘA, Daniel BÎRGĂOANU, Luisa Elena IATAN, Ion BERBELEAC, Oana-Claudia CIOBOTEA-BARBU</b> Hydrosilicate aqueous -, and vapor - “melt” inclusions in some specific rocks and minerals from Romania .....	13
<b>George DINCĂ, Gheorghe C. POPESCU, Oana-Claudia CIOBOTEA-BARBU, Daniel BÎRGĂOANU</b> Silver sulfotellurides and other Te-sulfosalts in alabandite-bearing veins from Săcărâmb Au-Ag-Te ore deposit, Metaliferi Mountains, Romania .....	19
<b>Elena-Luisa IATAN, Ion BERBELEAC</b> Neogene mineralizations of Bucium Rodu-Frasin Au-Ag deposits, South Apuseni Mountains, Romania .....	25
<b>Călin G. TĂMAȘ, Paul IVĂȘCANU, Gabriela BENA, Laurențiu IGNA, Nicolae HAR</b> Neogene distal skarn mineral assemblage from Ruda Brad, Apuseni Mountains, Romania .....	31
<b>Daniel BÎRGĂOANU, Gheorghe DAMIAN, Andrei BUZATU</b> The Fe content in the sphalerites from the Breiner-Băiuț deposit .....	37
<b>Réka KOVÁCS, Călin G. TĂMAȘ</b> New geochemical data and mineralogical interpretation for Cisma ore deposit, Gutâi Mountains .....	43
<b>Mădălina Paula ANDRII, Călin Gabriel TĂMAȘ</b> Ore mineralogy and geochemistry relationships in Băița Bihor ore deposit, Apuseni Mountains, Romania - Blidar Contact case study .....	49

**Ioan E. BARBU, Gheorghe BRĂNOIU**

Depositional systems for the sedimentary deposits from the Lighidia perimeter, Bozovici,  
Caraş-Severin county ..... 55

**Heloiza M. HORN, Adolf H. HORN, Reginaldo A. SAMPAIO, Essaid BILAL**

Decontamination of middle to low-grade contaminated areas, using a lowcost method ..... 61

**João P. S. KESSLER, Thiago P. ARAUJO, Fernando M. MELLO, Essaid BILAL**

Characterization of clay minerals from the reject of the sand extraction in  
Capela de Santana-RS, Brazil ..... 67

**Andreea-Elena MAFTEI, Andrei BUZATU, Nicolae BUZGAR, Andrei-Ionut APOPEI**

Preliminary assessment of anthropogenic contribution and influencing factors on major  
elements and total organic carbon in Tazlău River sediments, Romania ..... 73

**Marius C. SANDU, Gabriel O. IANCU, Ciprian CHELARIU Mihai NICULITA**

Preliminary study on the geochemistry of stream sediments from Grintiesul Mare brook,  
Eastern Carpathians, Romania ..... 79

**Lucica NICULAE**

The dynamics, geomorphology and the relationship of the mass movement with the geology  
in the Subcarpathian Area, between the Buzău and the Călnău Rivers ..... 85

**Fernando M. MELLO, Essaid BILAL, Gustavo N. C. MESQUITA,**

**Maria Eduarda L. R. TEODORO, Thiago P. ARAUJO, Frédéric GALLICE**

Background and reference values for the cadmium contents of brazilian soils compared ..... 91

**Adrian Theodor TONCO, Antonela NEACȘU, Delia Georgeta DUMITRAȘ**

Evaluation of the present demand and supply of gems, minerals and rocks of aesthetic value in the  
exhibitions organized by the Geological Institute of Romania - National Museum of Geology ..... 97



# COMBINED MINERALOCHEMICAL, STATISTICAL AND GEOPHYSICAL (GPR) DATA AS SUPPORT FOR THE EXPLORATION OF PEGMATITE-HOSTED GEMSTONES: EXAMPLE FROM THE SANTA ROSA MINE, MG, BRAZIL

Adolf Heinrich HORN\*, Paulo Roberto Antunes ARANHA, Henrique Chaves JONCEW

Federal University of Minas Gerais; Belo Horizonte, Brazil

\* *hahorn@ufmg.br*; Tel.: +55 31 34417505; Fax: +55 31 3409 5410

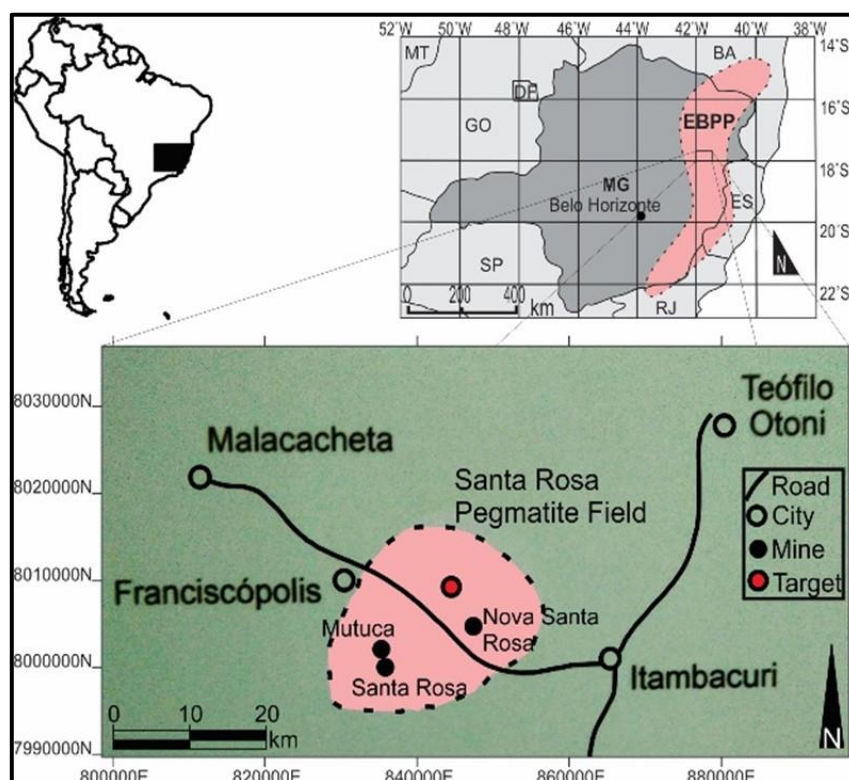
**Abstract:** The Santa Rosa Pegmatite Field, near Teófilo Otoni, Brazil, is known for its gem-quality tourmalines. The investigated pegmatite formed from late-stage fluids during crystallization of the Santa Rosa Granite in the late phase of the Neoproterozoic Araçuaí Orogen, is weakly zoned, with border, wall and intermediate zones and a discontinuous quartz core. However, even though gemstones are fundamental for the local economy, exploitation remains a rudimentary practice. ICP-MS, electron microprobe and Principal Components Analyses were conducted on selected mineral samples. There are distinct chemical characteristics and statistical distributions that provide enough information to differ between mineralized and non-mineralized zones. These data combined with GPR readings to evaluate if geophysical anomalies might be considered to detect potential gem sources. This methodology is based on the application of simple techniques to easily separable minerals, making it an accessible way to guide and optimize the exploration and exploitation of gemstones.

**Keywords:** GPR, pegmatites, prospection, colored stones, geochemistry

## 1. Introduction

Gemstone mining is a traditional economic practice in Northeastern Minas Gerais State, Brazil. This region is located in the Eastern Brazilian Pegmatite Province (EBPP) (Paiva, 1946), and hosts several pegmatite districts, including the Santa Rosa Pegmatite Field (SRPF) (Netto et al., 1997), 40km SW of Teófilo Otoni (Fig. 1).

Despite the importance of gemstones for the local economy, exploitation is still rudimentary and efforts to optimize prospecting are scarce. In an attempt to partially fill that lacuna, pegmatite-hosted minerals were sampled in an underground pegmatite dig and subjected to basic chemical analyses to compare mineralized and non-mineralized points, and ground-penetrating radar profiles were performed to locate anomalies within the pegmatite, which may guide excavations.



**Fig. 1.** Location of the Santa Rosa Pegmatite Field, its most important mines and the target dig in the Eastern Brazilian Pegmatite Province (modified from Cornejo et al., 2014).

## 2. Regional setting

The SRPF is located between the cities of Franciscópolis and Itambacuri, in the crystalline core of the Neoproterozoic Araçuaí Orogen. Its formation relates to the emplacement of the Santa Rosa Granite, a late-collisional suite (Bayer et al., 1985; Pedrosa-Soares et al., 2001). The granite intruded paraderived biotite schists and gneisses of the São Tomé and Tumiritinga Formations, marine units deposited in arc-related basins. This was the second plutonic event in the area, following the also late-tectonic intrusion of the São Vitor Tonalite (Oliveira, 2016; Vieira, 2007). B assimilation occurred during emplacement, causing schist tourmalinization (Oliveira, 2016; Fig. 2c).

## 3. Geology of the studied area

The studied pegmatite is an 8m thick dike, intruding biotite schists of the São Tomé Formation concordantly to its foliation. Its structure is zoned (Fig. 2a), marked by crystal growth towards the center and a small, discontinuous quartz core. Tourmaline crystals or agglomerates growing from the margin of a zone to its center are a frequent feature. Subordinate pegmatite intrusions and apophyses are found in the main dike's vicinities.

Gem-tourmalines in the dig are blue or green and may occur in pockets, cavities formed by late-stage substitution processes controlled by the exsolution of fluxing components from the melt (London, 1986, 1987). These geodes may also contain black, non-gemological tourmaline or no tourmaline whatsoever, on which case filling is composed of clay, mud and water. Pocket frames in the studied dig are usually marked by the presence of star-shaped muscovite crystals (Fig. 2b).



**Fig. 2.** Typical aspects from the Santa Rosa Pegmatite area. a. Zoned structure; b. Star-shaped muscovite framing pocket; c. Tourmalinization of schist xenolith (Oliveira, 2016).

## 4. Material and methods

### 4.1. Sampling and preparation

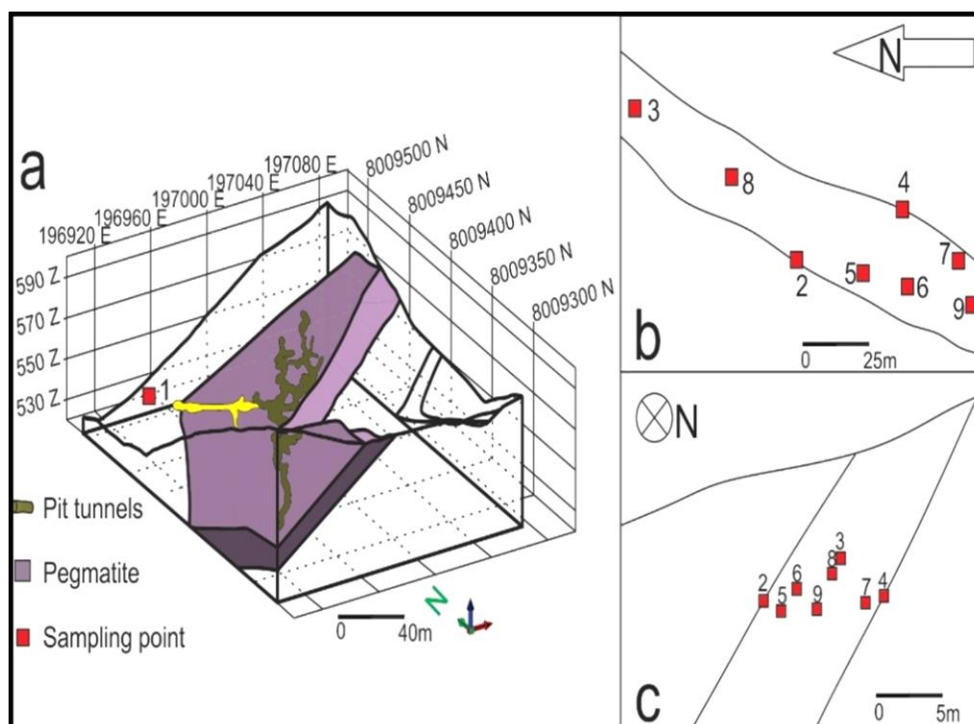
Pegmatite sampling took place in the underground galleries (Fig. 3), in different zonal contexts of the dig, including points surrounding representative pockets with both gemological and non-gemological tourmalines, and a clay-filled pocket. Tourmaline, feldspar and garnet were then manually separated from the rock samples and prepared for chemical analyses. Finally, polished thin sections were prepared: 14 made of tourmaline, 9 made of garnet.

### 4.2. Analytical methods

Electron microprobe analyses (EMPA) were conducted in the Center of Microscopy at the Universidade Federal de Minas Gerais, Belo Horizonte, MG, by cross-sections in several mineral grains to provide data about internal zoning and chemical variations. The equipment used was a JXA-8900RL probe. Readings

were conducted under 15kV voltage and 20nA current, with a counting time of 15s (Si, Na, Ti, P, F, K, Mg, Ca and Fe) and 30s (Al, Cr, Mn).

ICP-MS chemical analyses of total minerals were done in the laboratories of SGS Geosol Ltda., Vespasiano, MG, using pulverized samples (16 of tourmaline; 9 of garnet; 16 of feldspar) in Lithium metaborate flux.



**Fig. 3.** Santa Rosa Pegmatite (a), with sampling points relative positions in plant view (b) and cross-section (c).

#### 4.3. Ground-penetrating radar (GPR)

Ground-penetrating radar was proved a successful tool for gemstone prospecting in pegmatites by Patterson and Cook (1999). Being so, nine GPR profiles were executed on different sections of the dig, aiming to detect the contacts between the pegmatite and the hosting schist, as well as the planar and punctual anomalies within the rock structure. The data were acquired using antennas of 100 and 200MHz central frequencies.

#### 4.4. Principal Component Analysis (PCA)

The PCA method was applied to major element compositional data obtained by ICP-MS analyses. The raw data were converted using the *centered logratio* transform (Aitchison, 1982) and scores were calculated with the assistance of correlation matrices. It was not the scope of this work to determine possible correspondences between the components and physical factors acting during the mineral crystallization, although studies regarding that matter might be performed in the future. PCA was rather used as a basic tool, to identify whether certain groups of minerals (particularly those sampled near mineralized pockets) would stand out from the general distribution.

### 5. Results

#### 5.1. Mineral characterization

Feldspars are mostly white or tan, and occasionally pink. Closer to the surface, due to alteration, yellowish shades and kaolinization processes are observed. Graphic texture is often present in the intermediate zones of the pegmatite, where crystals reach up to decametric size. Samples belong to the series defined by the microcline and albite vertices of the K-Na-Ca classification diagram.

Tourmalines are dark-colored, with shades of gray, brown, blue and black. A discrete magnetism is also observed. Intergrowth with feldspar and/or quartz is often present. Millimetric sulfide and mica crystals are scarcely observed as inclusions. The analyzed specimens belong to the alkali and X-vacant groups and were classified as Li-poor-rock schorl. Elements distribution in tourmalines may vary throughout the mine, but no pattern was observed.



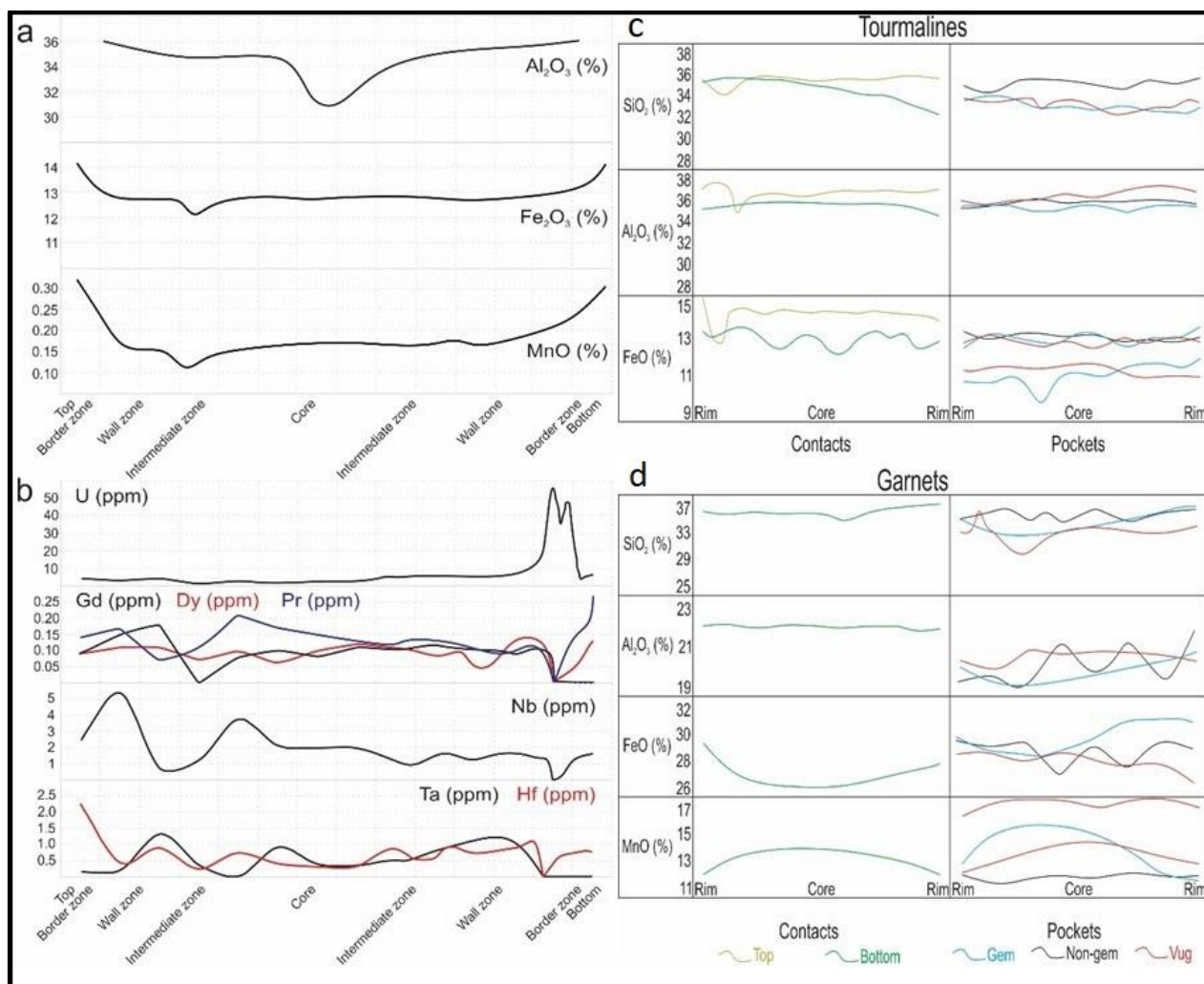
Garnets are red or brown in color and, like tourmalines, are slightly magnetic. Small quartz or zircon crystals are frequent as inclusions. Samples are Mn-rich. Chemical compositions form an intermediate range between almandine and spessartine ( $\text{Alm}_{58-76\%}$ ,  $\text{Spss}_{21-40\%}$ ).

## 5.2. Element distribution

Throughout the dig, peculiarities can be observed in the compositions of tourmaline and feldspar samples. In tourmalines, Al contents decrease from the border zones of the pegmatite to the core, maintaining an approximately constant level in the intermediate zones. Fe and Mn percentages are also highest in the borders and roughly constant in the rest of the dike. However, near the gem-bearing pocket, these elements reach their lowest values (Fig. 4a).

Nearly all elements are evenly distributed in feldspars. Yet, samples from the barren pocket stand out from this trend, as Dy, Gd, Pr, Hf, Nb and Ta contents fall below detection limits, while U percentages are much higher than the average (Fig. 4b). Furthermore, high-K specimens occur solely near the mineralized pocket.

As for the internal compositions, fluctuations in element percentages inside mineral grains are common but discrete. This is valid even for samples from the vicinities of the pockets – which are affected by late-stage substitution processes. Nevertheless, some distinguishing features are observed between minerals from various sampling points.

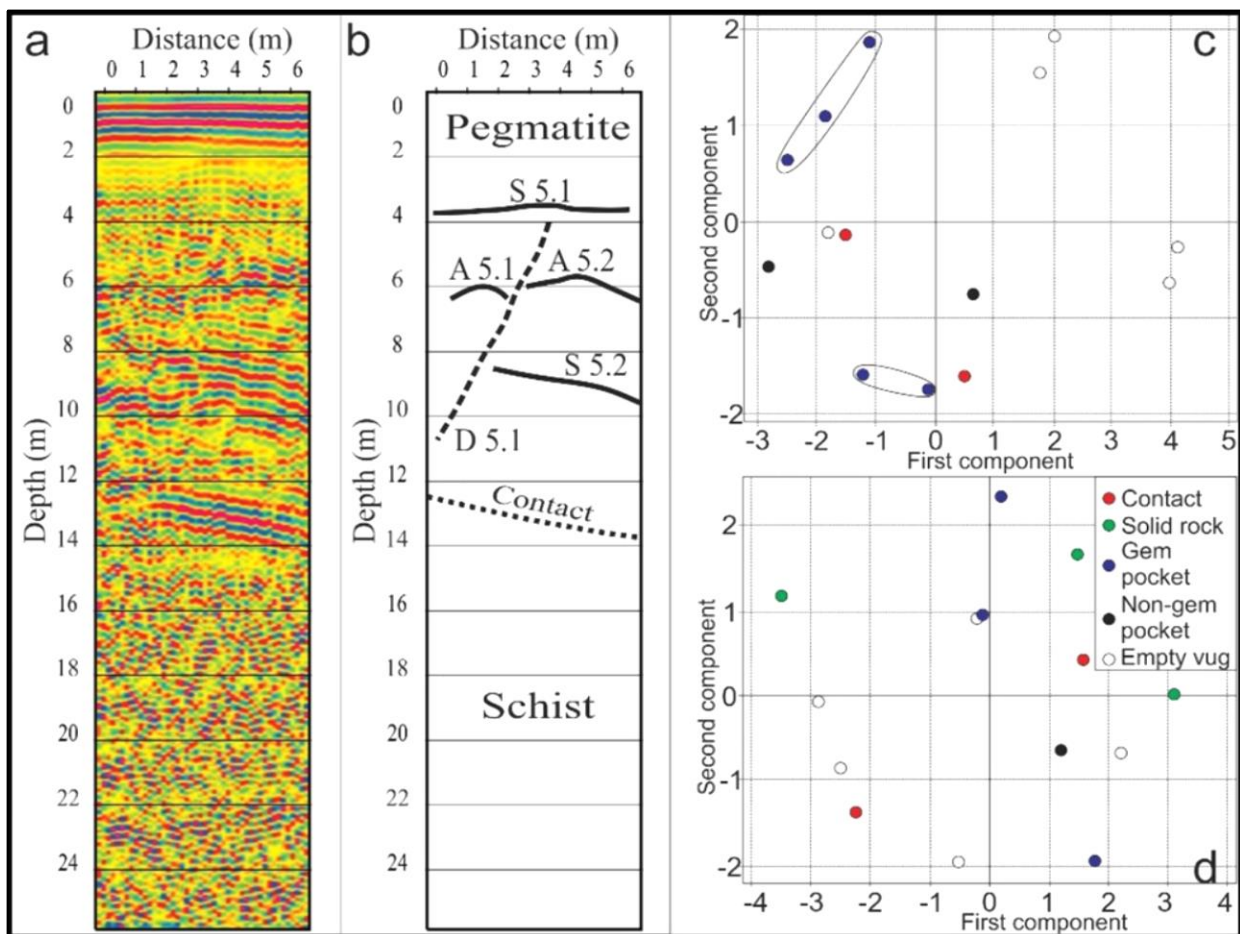


**Fig. 4.** Representative scheme synthesizing element distribution patterns from the Santa Rosa Pegmatite. a. Selected main elements distribution in tourmalines in an idealized cross-section of the pegmatite by whole mineral composition; b. Selected trace elements distribution in feldspars in an idealized cross-section of the pegmatite by whole mineral composition; c. Tourmaline grain profiles by microprobe; d. Garnet grains profiles by microprobe.

Figures 4c and 4d present the most important internal variations in mineral compositions. In tourmaline grains from the upper and base contacts, Fe content has a constant distribution in the former, but a more erratic behavior in the latter. Some garnets – including all samples from the gem-bearing pockets – are zoned, with an increase in Si and Al from the core to the rims, accompanied by Mn decrease. Minerals from the pocket zones also have traits that may be used for comparison. Tourmaline grains from the gem pocket and the barren, clay-filled cavity are characterized by  $Al > Si$ . Also, some of these samples have lower Fe content than those from the other pockets. Tourmalines from the non-gemological pocket show similar Al and Si quantities and high Fe percentages.

### 5.3. Principal Components Analysis

The PCA method showed no particular distribution that distinguished tourmaline (Fig. 5d) and garnet samples from mineralized and non-mineralized zones. For feldspars, however, an important feature is observed. When the analysis is applied to major element composition, samples from gem-producing pockets fall into two isolated groups from the rest (Fig. 5c). Both groups have negative score values for the first component and high module values for the second (positive for K-feldspars and negative for Na-feldspars).



**Fig. 5.** Radargram (a) and interpretation (b) from the 5<sup>th</sup> GPR reading. Anomalies indicated by “A” are punctual, while planar anomalies are designated by “S” and linear discontinuities are represented by “D”. Score plot generated with the use of the PCA method for major element compositional data of feldspar (c) and tourmaline (d) samples.

### 5.4. Ground-penetrating radar

The GPR profiles were successful at finding various structures in the pegmatitic body, as exemplified by Figures 5a and 5b. Radargram interpretation made it possible to create a digital model of the pegmatite body (Fig. 3a) and a total of eight hyperboles were detected, which means that GPR was able to locate punctual anomalies inside the rock.

## 6. Discussion

Distinguishing features are present near the pocket zones. Feldspars from these vicinities stand out from the others in the statistical distribution, and high-K minerals are restricted to mineralized zones. Moreover,  $Al > Si$  and low Fe and Mn contents in tourmalines and Fe and Mn zonation in garnets also indicate gem-bearing pockets. Combining this information with GPR readings may importantly assist the search for gems in the dig. It not only directs excavations towards punctual anomalies, but also allows the evaluation of the effort's potential for success beforehand.

This methodology may be expanded to studies regarding not only gemstone prospecting, but also the geologic evolution of the Santa Rosa Pegmatite Field and its relation with the surrounding granitic intrusions. GPR proved itself a useful tool for underground geologic mapping, Patterson and Cook (1999) showing that higher central frequencies on GPR are capable of making the difference between mineralized and non-mineralized pockets. Even though this work employed a basic approach, the Principal Components Analysis, if performed to a larger extent, it is a powerful statistical method that may assist the identification of various factors that controlled crystallization, which may provide important insights regarding how the SRPF was formed.

## 7. Conclusions

The analyses performed in this work provided data that may objectively guide and optimize the search for gems in the tourmaline dig. ICP-MS and PCA analyses of tourmalines and feldspars produced criteria to establish whether a mineral was formed near a mineralized pocket. This information, combined with GPR readings, has the potential to significantly increase the mine productivity, which currently still has to resort to trial and error.

## 8. Acknowledgements

We thank CNPQ, FAPEMIG for the financial, UFMG, and Mine Invest LTDA for the logistical support.

## 9. References

- Aitchison J. (1982) The statistical analysis of compositional data. *Journal of the Royal Statistical Society. Series B (Methodological)* 44, p. 139–177.
- Bayer P., Horn A.H., Schmidt-Thomé R., Lammerer B., Wiedemann C.M., Weber-Diefenbach K. (1985) The Brazilian Mobile Belt in southern Espírito Santo (Brazil) and its igneous intrusions. *Zentralblatt für Geologie und Paläontologie* 9, p. 1429–1439.
- Cornejo C., Bartorelli A., Menezes-Filho L.A.D. (2014) A subclasse dos ciclossilicatos. In: Cornejo, C., Bartorelli, A. (Eds.), *Minerais E Pedras Preciosas Do Brasil*. Solaris, São Paulo, p. 444–593.
- London D. (1987) Internal differentiation of rare-element pegmatites: Effects of boron, phosphorus, and fluorine. *Geochimica et Cosmochimica Acta* 51, p. 403–420.
- London D. (1986) Formation of tourmaline-rich gem pockets in miarolitic pegmatite. *American Mineralogist* 71, p. 396–405.
- Netto C., Araújo M.C., Pinto C.P., Drumond J.B. V. (1997) Cadastramento de recursos minerais: Pegmatitos. In: *Projeto Leste. SEME/COMIG/CPRM*, Belo Horizonte.
- Oliveira B.N. (2016) Mapeamento geológico da área entre Itambacuri-Franciscópolis, microregião de Teófilo Otoni - MG. UFMG, Belo Horizonte.
- Paiva G. (1946) Províncias pegmatíticas do Brasil, *Bulletin* 78. DNPM/DFPM, Rio de Janeiro.
- Patterson J.E., Cook F.A. (1999) Successful application of Ground Penetrating Radar in exploration for gem tourmaline. *Canadian Mineralogist* 37, p. 862–863.
- Pedrosa-Soares A.C., Noce C.M., Wiedemann C.M., Pinto C.P. (2001) The Araçuaí-West-Congo Orogen in Brazil: An overview of a confined orogen formed during Gondwanaland assembly. *Precambrian Research* 110, p. 307–323.
- Vieira V.S. (2007) Significado do Grupo Rio Doce no Contexto do Orógeno Araçuaí. UFMG, Belo Horizonte.

## USE OF GPR IN PEGMATITE MINING: EXAMPLE OF A SHEETLIKE BODY FROM NORTHERN MINAS GERAIS, BRAZIL

Paulo Roberto Antunes ARANHA\*, Adolf Heinrich HORN, Henrique Chaves JONCEW

Federal University of Minas Gerais; Belo Horizonte, Brasil

\* *aranha1941@gmail.com*; Tel.: +55 31 3409 5442; Fax: +55 31 3409 5410

**Abstract:** Located in the region of Teófilo Otoni, Brazil, the Santa Rosa Pegmatite Field is known for its gem-quality tourmalines. It formed from late-stage fluids during crystallization of the Santa Rosa Granite in the late-tectonic phase of the Neoproterozoic Araçuai Orogen. The pegmatite structure is zoned, with wall, mural and intermediate zones and a small, discontinuous quartz core and gem mineral pockets distributed along determined zones (lines) between the intermediate zone and the core. The investigations with GPR in surface and subsurface profiles, at the galleries, allows the identification of the limits of the pegmatite and the zones, and also the orientation of pocket bearing areas (lines), the distribution of these mineralized corps (substitution pockets) and the estimation of the orientation of pocket evolution (lines). This is possible due to changes and differences in the density of the different compartments of the pegmatite, the wall rock and the pockets, permitting to register their contacts. The GPR profiles interpretation allows the detection at least two anomalies (hyperbolae shape) with gems in its interior.

**Key words:** Pegmatite, ground penetrating radar, prospecting

### 1. Introduction

Gemstone mining is a traditional economic practice in Northeastern Minas Gerais State, Brazil. This region is located in the Eastern Brazilian Pegmatite Province (EBPP) (Paiva, 1946; Putzer, 1976), and hosts several pegmatite districts, including the Santa Rosa Pegmatite Field (SRPF) (Netto et al., 1997), localized at 40km SW of Teófilo Otoni city.

Despite the importance of gemstones for the local economy, exploitation takes place in rudimentary digs and efforts to optimize their prospecting are scarce. In an attempt to partially fill those voids, pegmatite-hosted minerals were sampled in an underground work and subjected to basic chemical analyses to compare mineralized and non-mineralized points and to help understanding the pegmatite crystallization process and its possible implications for gem tourmaline formation, as well as interpreting the tourmaline setting by the use of GPR radargrams to positioning the pockets relative to the pegmatite/schist contact.

The Ground Penetrating Radar, GPR, is an electromagnetic geophysical research method, applied to subsurface surveys, based on the interaction of radio waves, between 10 MHz and 1.3 GHz frequency, with underground structures. The method has been applied in various fields, especially in forensic, geoscientific and archaeological investigations (Busby et al., 2004; Daniels, 2004; Everett, 2013).

In Earth Sciences, several areas make use of GPR in their research, with satisfactory results, as in stratigraphy (Hager and Carnevale, 2006), geotechnics (Aranha et al., 2006; Benson, 1995; Hara and Sakayama, 1984; Santos, 2014), pedology (Chaplot et al., 2004; Huggenberger et al., 1994), geomorphology (Aranha, 2002; Augustin and Aranha, 2006), environmental geology (Parizzi et al., 2011) and mining (Francke, 2012; Rafezi et al., 2015).

The GPR operates in a similar way to seismic reflection method. However, it employs electromagnetic waves instead of acoustic ones, and has a depth of investigation centimeters to decameters. A source emits the electromagnetic wave, which penetrates the underground and interacts with its structures, suffering changes in reflection patterns due to contrasts of electric permittivity, which is caused by structural anomalies or geological contacts. A receiver captures the reflected wave. A processing unit amplifies and adjusts the acquired signal and relays it to a computer, which displays and stores the information (Busby et al., 2004; Davis and Annan, 1989; Everett, 2013; Milson, 2003; Santos, 2014).

Academic papers about the application of GPR in pegmatites are still rare. In general, the surveys conducted are private property and the access to their results, restricted. In fact, only two authors have produced publications regarding in the State of California (USA): Frederick A. Cook, PhD, and Jeffrey E. Patterson, PhD, originally producing independent works and later in joint research. Patterson (1996) conducted the first survey focused on detection of pockets in pegmatites using GPR at the Little 3 Mine. Later, Cook (1997, 2002) included the GPR in a report of geophysical methods applied to gem exploration. Together, Patterson and Cook (1999, 2000, 2002, 2004) disseminate the results of their investigations in a Himalaya mine, these being the most important publications up to date. Their research was driven by observation of patterns like form, color and organization of the minerals. The

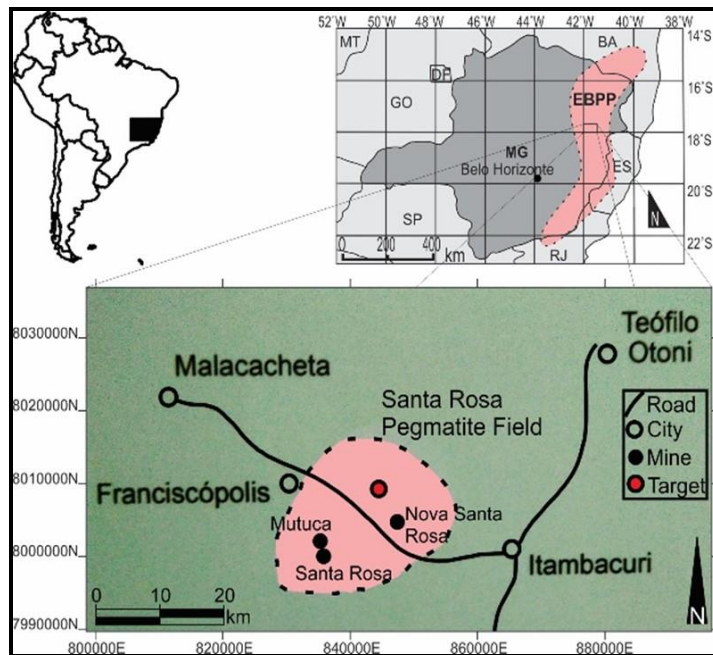


gems were found usually in oblong, flattened, and filled with clay or zeolite cavities with their edges parallel to the contact between the pegmatite and the host rock.

## 2. Regional setting

The SRPF is located between the cities of Franciscópolis and Itambacuri, in the crystalline core of the Neoproterozoic Araçuaí Orogen (Fig. 1). Its formation is associated to the emplacement of Santa Rosa Granite, a late-collisional suite (Bayer et al., 1985, 1987; Oliveira, 2016; Paes, 1997).

The granite intruded biotite schists and gneisses of the São Tomé and Tumiritinga Formations, metasedimentary marine units deposited in arc-related basins. This was not the first plutonic event in the area, as it followed the also late-tectonic intrusion of the São Vitor Tonalite (Oliveira, 2016; Vieira, 2007) B-assimilation occurred during emplacement, causing schist tourmalinization (Oliveira, 2016).



**Fig. 1:** Map of the Santa Rosa Pegmatite Field localization.

## 3. Geology of the studied area

### Santa Rosa Pegmatite

The studied pegmatite is an 8m thick dyke, which intruded biotite schists of the São Tomé Formation concordantly to its foliation, zone with thick (blocky) feldspar crystals; and d) small, discontinuous quartz core. Tourmaline crystals or agglomerates that grow from the margin of a zone to its center are a frequent feature. Subordinate pegmatite intrusions and apophyses are found in the main dyke's vicinities.

Gem-tourmalines in the pegmatite are blue or green, and may occur in pockets (miaroles), cavities formed by late-stage substitution processes controlled by fluxing components exsolution from the melt (London, 1986 a, b, 1987; Simmons et al., 2012). These geodes may also bear black, non-gemological tourmaline or contain no tourmaline whatsoever, on which case filling is composed by clay, mud and water. Pocket frames in the studied dig usually show star-shaped muscovite crystals.

## 4. Material and methods

In nine profiles from the walls of the tunnels in the pegmatite, were taken GPR data with structures that could match the possible cavities (popularly known as potholes or pockets).

The antennas, with central frequency of 100 and 200 MHz, were arranged parallel (common offset), connected via the processing unit to a computer, which retransmitted the signal (Fig. 2). The registration was done using the program Malå Groundvision. The capture, horizontal step, was executed every 5cm travelled and the Computer processing of the collected data consisted of: Declipping, Dewow, Set time zero, Window time range, Removal background, Gaussian Filter, Elevation static (wall static), Time to depth conversion.





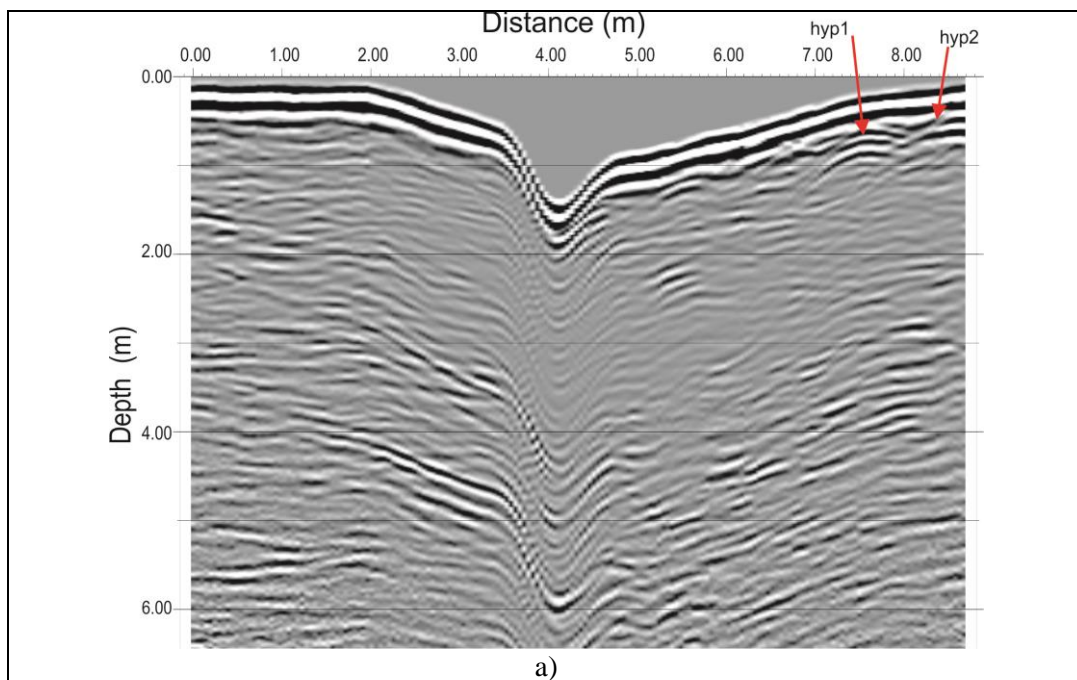
**Fig. 2:** Photo of the acquisition of GPR profile on the wall of the pegmatite rock.

## 5. Results

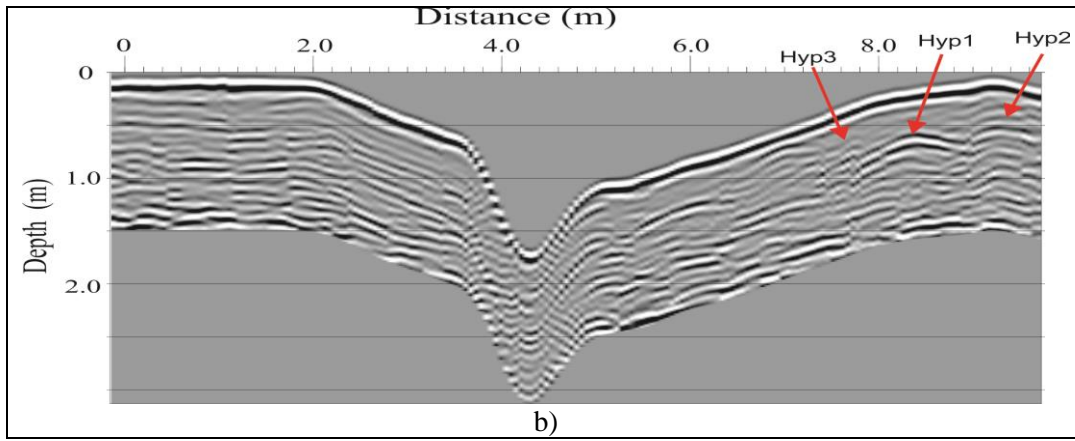
In the radargrams obtained by GPR profiles, it was possible to observe variation patterns in the reflection of electromagnetic waves patterns, corresponding to puncture-like and planar structural anomalies within the pegmatite, or to the contact between the pegmatite and the host rock (Micaschists s.l.).

Using the detected hyperbolae, the velocity of electromagnetic waves propagation in the pegmatite was set to 110 m/ $\mu$ s. Associating the performed profiles to topographic survey of the walls, it was possible to spatially locate the anomalies.

The radargrams obtained on the wall of the tunnel 1 show two distinct hyperbolae at well-defined distances of 7.5 and 8.4m. These two hyperbolae are clearly visible in both radargrams, one obtained with antennas of 100 MHz (Fig. 3a), and another obtained with antennas of 200 MHz (Fig. 3b). Also, is to note in the second radargram a little hyperbolae (hyp3), less pronounced, on the left side of the hyperbolae - hyp1. These anomalies were investigated and underground works were made, resulting in the finding of pockets filled with gems.

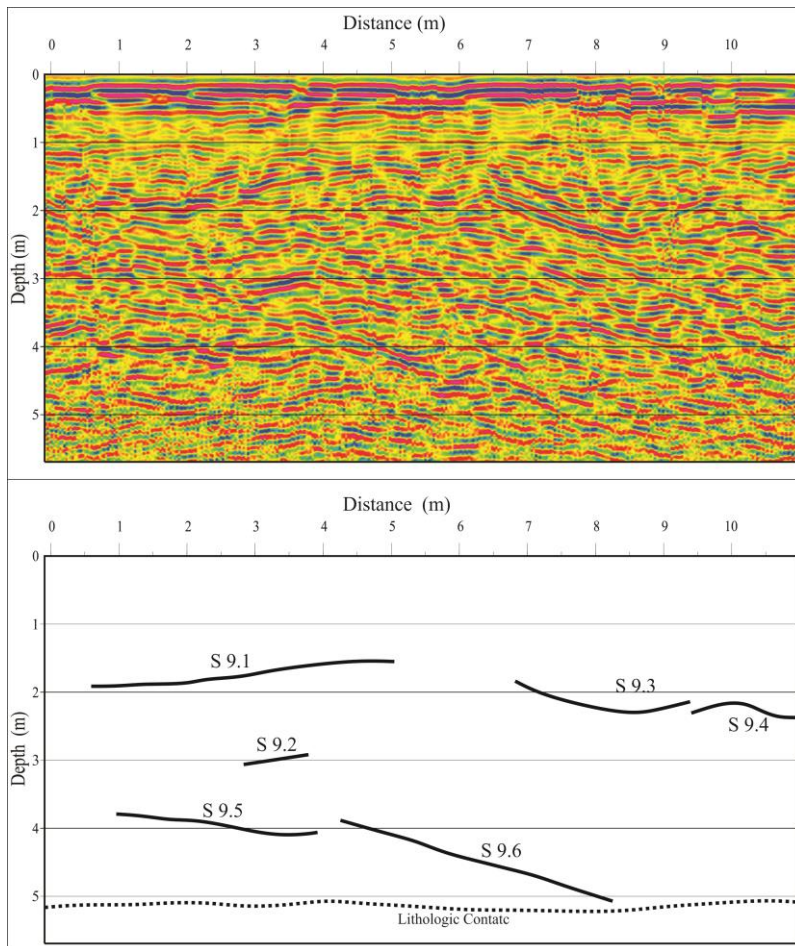


**Fig. 3.** (see explanation on the next page)



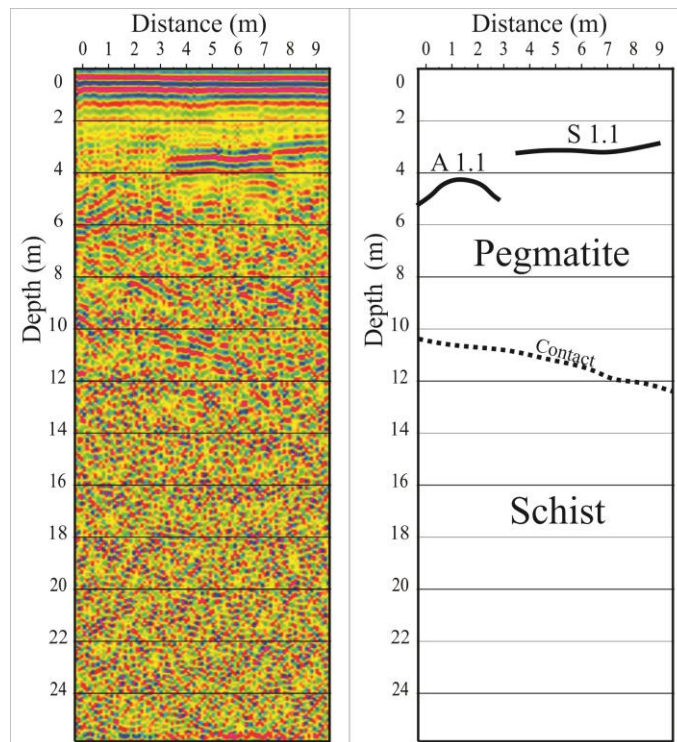
**Fig. 3:** a) Radargrams obtained with the 100 MHz antennas, showing two hyperbolae - pockets indicated by the red arrows; b) radargrams obtained with the 200 MHz antennas on the same wall showing three hyperbolae.

Other profiles were performed on different walls and it was possible to observe in the radargrams obtained with antennas of 100 MHz (Fig. 4) the presence of reflections, probably associated with structures in pegmatite. In general, these structures may be related to fractures filled with clay.



**Fig. 4:** The radargram at the top obtained in wall 9, is showing such related reflections correlated with the internal structure of the pegmatite. The lower part of the figure shows the interpretation of the upper radargram.

Another result well marked by GPR investigation was the identification of the contact between the pegmatite and the host rock formed by micaschists. In Fig. 5 one may observe various types of reflections, hyperbolae; indicating pockets; and linear reflections indicating the contact and clay-filled fractures.



**Fig. 5:** Typical radargram obtained in the research and its interpretation.

## 6. Conclusions

In the same way as in various fields of Geosciences, the GPR method proved to be an effective tool in the investigation of the pegmatites, corroborating the proposals of Cook (1997, 2002) and Patterson and Cook (1999, 2000, 2002, 2004). The investigation profiles carried out have not only detected the pegmatite-host rock limits, but also structural anomalies inside the pegmatite, especially represented by  $\sigma$  hyperbolic patterns, indicating pockets filled with gems.

The planar anomalies found in the pegmatite are predominantly parallel to the direction of intrusive body. Their meaning is debatable. These surfaces can be related to compositional or structural variations within the pegmatite, marking, for example, the boundary between the wall and the border zone. Another possibility is that these anomalies correspond to a set of fractures parallel to the foliation of the schist of São Thomé Formation. These diachyses, besides the schistosity of the host rock, can be considered in this way as a facilitator for the emplacement of the pegmatite veins and dykes.

## 7. Acknowledgements

We thank CNPQ for the financial support (481382/2012-7), UFMG, and Mine Invest LTDA for the logistical support.

## 8. References

- Aranha P.R.A. (2002) Estudo das coberturas superficiais e sua dinâmica na região de Gouveia, Serra do Espinhaço, MG: Utilizando o Radar de Penetração no Solo (GPR). PhD thesis, UFOP, Ouro Preto. 312p.
- Augustin C.H.R.R., Aranha P.R.A. (2006) Piping em área de voçorocamento, noroeste de Minas Gerais. *Revista Brasileira de Geomorfologia* 7, p. 9–18.
- Bayer P., Schmidt-Thomé R., Weber-Diefenbach K., Horn, A.H. (1987) Complex concentric granitoid intrusions in the Coastal Mobile Belt, Espírito Santo, Brazil: The Santa Angélica Pluton. *Geologische Rundschau* 76, p. 357–361.
- Benson A.K. (1995) Applications of GPR in assessing some geological hazards: Examples of ground water contamination, faults, cavities. *Journal of Applied Geophysics* 33, p. 177–193.
- Busby J.P., Cuss R.J., Raines M.G., Beamish D. (2004) Application of Ground Penetrating Radar to geological investigations. British Geological Survey, Keyworth. 125p.
- Chaplot V., Walter C., Curmi P., Hollier-Larousse A., Robain H. (2004) Combining geophysical methods to estimate the spatial distribution of soils affected by water saturation. *Comptes Rendus Geoscience* 336, p. 553–560.
- Cook F.A. (1997) Application of geophysics in gemstone exploration. *Gems & Gemology* 33, p. 4–23.

- Cook F.A. (2002) Geophysical methods used in exploration for gemstones. Available at <http://csegrecorder.com/articles/view/geophysical-methods-used-in-exploration-for-gemstones>. Accessed on 11.10.2014.
- Daniels D.J. (2004) Ground Penetrating Radar. 2<sup>nd</sup> ed. IEE Radar Series. The Institution of Electrical Engineers, London. 25p.
- Davis J.L., Annan, A.P. (1989) Ground Penetrating Radar for high resolution mapping of soil and rock stratigraphy. *Geophysical Prospecting* 37, p. 531–551.
- Everett M.E. (2013) Near-surface applied geophysics. 1<sup>st</sup> ed. Cambridge University Press, New York.
- Francke J. (2012) A review of selected ground penetrating radar applications to mineral resource evaluations. *Journal of Applied Geophysics* 81, p. 29–37.
- Hager J., Carnevale M. (2006) The application of low frequency GPR to stratigraphic investigations. Available at [http://www.hagergeoscience.com/pdf\\_files/MLF\\_paper.pdf](http://www.hagergeoscience.com/pdf_files/MLF_paper.pdf). Accessed on 19.8.2014.
- Hara T., Sakayama T. (1984) The applicability of ground probing radar to site investigations. Technical note, OYO Corp., Tóquio.
- Huggenberger P., Meier E., Pugin A. (1994) Ground-Probing Radar as a tool for heterogeneity estimation in gravel deposits: Advances in data-processing and facies analysis. *Journal of Applied Geophysics* 31, p. 171–184.
- London D. (1987) Internal differentiation of rare-element pegmatites: Effects of boron, phosphorus, and fluorine. *Geochimica et Cosmochimica Acta* 51, p. 403–420.
- London D. (1986a) Magmatic-hydrothermal transition in the Tanco rare-element pegmatite: Evidence from fluid inclusions and phase-equilibrium experiments. *American Mineralogist* 71, p. 376–395.
- London D. (1986b) Formation of tourmaline-rich gem pockets in miarolitic pegmatite. *American Mineralogist* 71, p. 396–405.
- Milson J. (2003) Field Geophysics. 3<sup>rd</sup> ed. The geological field guide series. John Wiley & Sons Ltd., Chichester.
- Netto C., Araújo M.C., Pinto C.P., Drumond J.B.V. (1997) Cadastramento de recursos minerais: Pegmatitos. In: Projeto Leste. SEME/COMIG/CPRM, Belo Horizonte.
- Oliveira B.N. (2016) Mapeamento geológico da área entre Itambacuri-Franciscópolis, microrregião de Teófilo Otoni - MG. Thesis of undergraduate degree, UFMG, Belo Horizonte.
- Paes V.J.C. (1997) Geological map - sheet Teófilo Otoni - SE.24-V-C-IV, scale 1:100.000. In: Projeto Leste. SEME/COMIG/CPRM, Belo Horizonte.
- Paiva G. (1946) Províncias pegmatíticas do Brasil. *Boletim* 78. DNPM/DFPM, Rio de Janeiro.
- Parizzi M.G., Aranha P.R.A., Costa R.D., Silva-Filho J.A., Tupinambás M.M., Cajazeiro J.M.D. (2011) Geofísica e sedimentologia aplicadas à avaliação do grau de assoreamento de trecho do Rio das Velhas em Rio Acima, Minas Gerais. *Geonomos* 19, p. 152–162.
- Patterson J.E. (1996) Modeling of layered aplitic pegmatite dikes using Ground Penetrating Radar, Little Three Mine, Ramona District, San Diego County, California. Research report, University of Arizona, Tucson.
- Patterson J.E. (2003) Application of Ground Penetrating Radar (GPR) at the Cryo-Genie gem 87. San Diego County, California. University of Calgary, Calgary. 25p.
- Patterson J.E., Cook F.A. (1999) Successful application of Ground Penetrating Radar in exploration for gem tourmaline. *Canadian Mineralogist* 37, p. 862–863.
- Patterson J.E., Cook F.A. (2000) Application of complex trace analysis for improved target identification in gem-tourmaline-bearing pegmatites in the Himalaya mine, San Diego County, California. In: Noon D.A., Stickley G.F., Longstaff D. (Eds.) *Eight International Conference on Ground Penetrating Radar*. Gold Coast, p. 653–657.
- Patterson J.E., Cook F.A. (2002) Successful application of ground-penetrating radar in the exploration of gem tourmaline pegmatites of Southern California. *Geophysical Prospecting* 50, p. 107–117.
- Patterson J.E., Cook F.A. (2004) Ground penetrating radar (GPR) as an exploration tool in near surface pegmatite mining. In: SEG Technical Program Expanded Abstracts 2004. Denver, p. 1472–1475.
- Putzer H. (1976) *Metallogenetische Provinzen in Südamerika*. 1<sup>st</sup> ed. E. Schweizerbart'sche Verlagbuchhandlung, Stuttgart.
- Rafezi H., Novo A., Hassani F. (2015) An investigation into application of Ground Penetrating Radar (GPR) in surface mining. In: *Symposium on the Application of Geophysics to Engineering and Environmental Problems*, Austin, Texas. p. 1–7.
- Santos V.R.N. (2014) Detecção e classificação automática de interferências do subsolo com GPR utilizando redes neurais artificiais: Estudo no SCGR do IAG/USP. PhD Thesis, USP, São Paulo.
- Simmons W.B., Pezzotta F., Shigley J.E., Beurlen H. (2012) Granitic pegmatites as sources of colored gemstones. *Elements* 8, p. 281–287.
- Vieira V.S. (2007) Significado do Grupo Rio Doce no Contexto do Orógeno Araçuai. PhD Thesis, UFMG, Belo Horizonte.

## HYDROSILICATE AQUEOUS -, AND VAPOR - “MELT” INCLUSIONS IN SOME SPECIFIC ROCKS AND MINERALS FROM ROMANIA

Ioan PINTEA<sup>1,\*</sup>, Maria-Lidia NUȚU-DRAGOMIR<sup>2</sup>, Sorin Silviu UDUBAȘA<sup>3</sup>, Daniel BÎRGAOANU<sup>1</sup>, Luisa Elena IATAN<sup>2</sup>, Ion BERBELEAC<sup>2</sup>, Oana-Claudia CIOBOTEA-BARBU<sup>1</sup>

<sup>1</sup> Geological Institute of Romania, 1, Caransebeș St., 012271 Bucharest, Romania

<sup>2</sup> Institute of Geodynamics of Romanian Academy, 19-21, Jean-Louis Calderon St., 020032 Bucharest, Romania

<sup>3</sup> University of Bucharest, 1, Nicolae Bălcescu Blvd., 010041 Bucharest, Romania

\* *ipinteaflincs@yahoo.com*

**Motto:** “Terminology that is readily applicable to a one-component system, such as “gas”, “liquid”, “boiling” and critical point, can be very misleading when applied to complex multicomponent system” (Roedder and Coombs, 1967).

**Abstract.** The paper deals with uncommon aqueous-, and vapor-rich “melt” inclusions from various rocks and minerals from Romania. It is envisaged that complex hydrosilicate  $\pm$  chloride  $\pm$  carbonate  $\pm$  sulphate  $\pm$  phosphate  $\pm$  CO<sub>2</sub>  $\pm$  CH<sub>4</sub> fluid/melt was released from deep, intermediate and shallow environments during subduction processes in the Carpathian zone. Heterogeneous fluid inclusions of silicothermal fluids containing liquid/melt $\pm$ vapor $\pm$ solid(s) were formed in quartz and ore minerals from epithermal systems, pegmatites and sedimentary rocks. In porphyry copper systems (Upper Cretaceous and Miocene terrains from Romania) the counterparts of silicate melt -, and brine inclusions as vapor-rich “melt” inclusions are representative for the released fluid/melt phases during magma crystallization and endogenous metasomatic processes.

**Keywords:** hydrosilicate vapor “melt” inclusions, epithermal ores, pegmatites, porphyry copper, sedimentary rocks, Carpathians

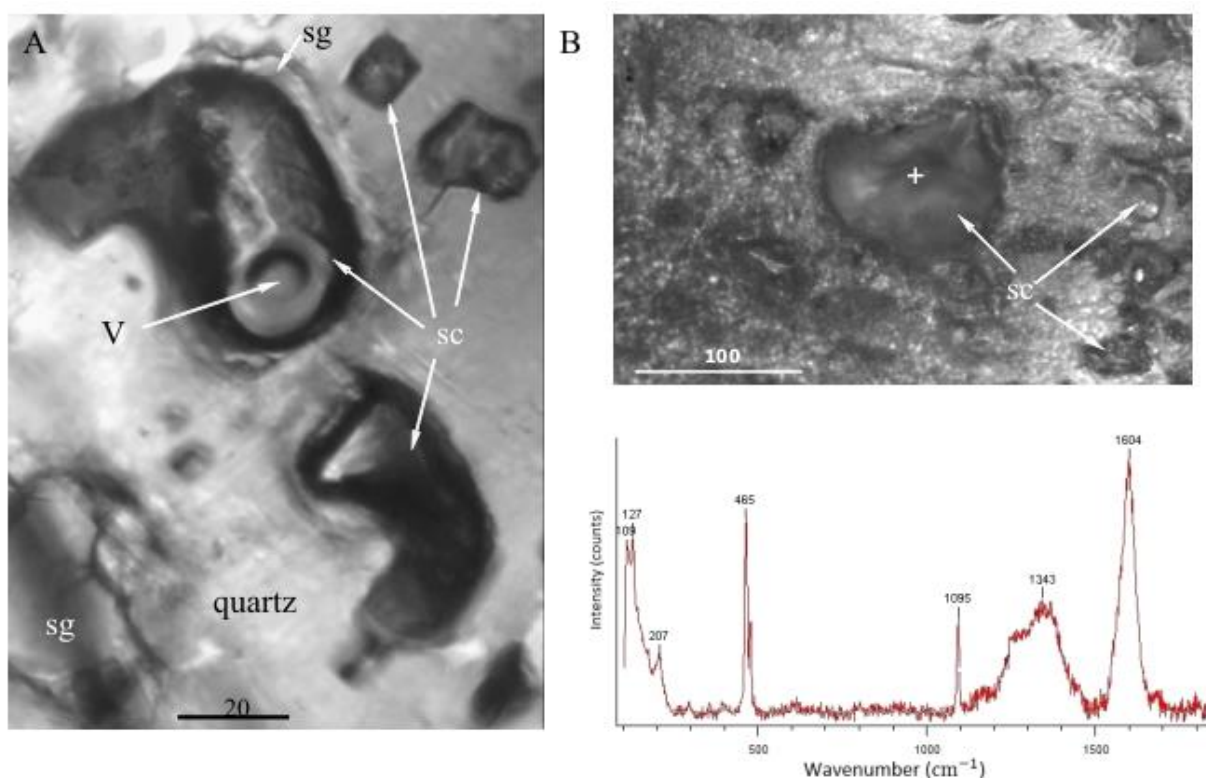
### Introduction

In specific geological conditions (e.g. epithermal veins and breccias, granitic pegmatites, porphyry copper systems, sedimentary salty rocks, etc) the ubiquitous vapor-rich inclusion, aqueous multiphase, and vapor bubbles in brine or melt inclusions are represented at room temperature conditions by a mixture of low temperature alkali-hydrosilicate  $\pm$  chloride  $\pm$  sulfate  $\pm$  carbonate “melt”- like with consistency of glycerin (10<sup>2</sup> Pa·s) which at room temperature conditions seems to be a certain fragile solid phase (e.g. Thomas and Davidson, 2012, and references therein; Wilkinson et al., 1996, 2015). Generally, an opaque bubble could be seen under the transmitted light microscope. These bubbles are isolated or randomly distributed as primary inclusions but frequently are present along other melt or fluid inclusion types (i.e. aqueous - liquid biphasic, brine or melt inclusions) in crystal growth zones or cicatrized microfissures (trails) being the counterpart assemblages of the boiling or immiscibility processes, formed mainly by heterogeneous trapping.

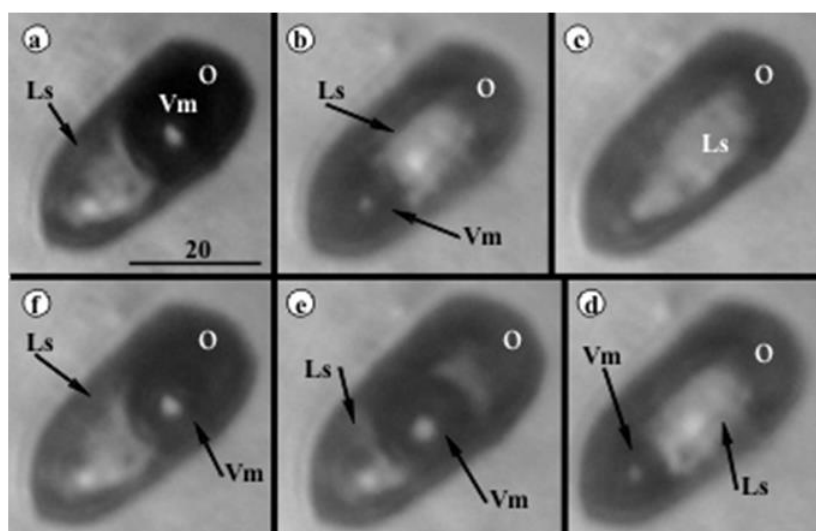
### Hydrosilicate melt in vapor - rich “melt” inclusions

An open cavity on the surface of a polished slide from a conspicuous quartz pseudomorphose after halite from a brecciated salty rock (Marginal folds nappe, Vrancea zone in Romania) showed that the opaque bubble visible in transmitted light is formed by a solid carapace of an empty inner space which probably contained a vapor or liquid immiscible phase rich in CO<sub>2</sub> and CH<sub>4</sub> (Nuțu and Vaselli, 2015; Fig. 1). Generally, it is presumed that in many cases the vapor bubble inside the brine and silicate melt inclusions could be assigned to a second immiscible phase instead of a pure gaseous volatile phase (e.g. Pinteau, 2014, 2016; Pinteau et al., 2017). A hydrous rind around the vapor bubble in silicate melt inclusion as a reaction product between gas and silicate melt during cooling was noted by Lowenstern (1993) in quartz from rhyolites erupted at the Valley of Ten Thousand Smokes, Alaska. Amazing graphite rim covering the gas bubble containing traces of CO<sub>2</sub>, N<sub>2</sub> and CH<sub>4</sub> in two-phase (L+V) aqueous fluid inclusion (H<sub>2</sub>O-NaCl) in coarse quartz veins from BIF-hosted iron ores from Krivoy Rog, Ukraine was detected by Raman spectroscopy (Sośnicka et al., 2015). Biphasic aqueous bubbles in silicate melt inclusions formed by shrinkage or heterogeneous trapping were described as aqueous fluid inclusions formed at various pressure conditions in volcanic environments worldwide (Davidson et al., 2005; Kovalenker et al., 2006; and reference therein). In Romania such complex aqueous bubble in silicate melt inclusions were described in quartz phenocrysts from “Laleaua Alba” dacite by Naumov et al. (2014) and elsewhere by Pinteau (2010, 2016). Generally, they have relatively low homogenization temperatures (< 100° up to around 300-350°C) and show specifically “bubble collapse” phenomena during quenching





**Fig. 1. A.** Low-temperature alkali-hydrosilicate melt inclusions in quartz pseudomorphose after halite in a sedimentary brecciate salty rocks (Marginal fold nappe, Vrancea zone, Romania). During polishing a small hole (V) was opened at the inclusion surface showing the real content of the presumed vapor-rich inclusion. But, in short time, around 2-3 days, the content disintegrated in air suggesting metastability, perhaps a kind of foam assemblage (or hydrate microtexture) formed by a melt (now glass) and gas bubbles ( $\text{CO}_2$ ,  $\text{CH}_4$  etc). **B.** Based upon preliminary Raman spectroscopy (e.g. Raman spectra enclosed) it is presumed that inclusions are silicate-carbonate melt (sc) occurring together with another glassy counterpart inclusions (sg), suggesting immiscibility. During heating microthermometry several small bubbles formed around 200°C and then homogenized on further heating near 400°C (i.e. inclusion formation temperature). Scale bar in  $\mu\text{m}$ .



**Fig. 2.** Microthermometric sequence (from a to f) for a hydrosilicate – chloride – carbonate - sulphate -  $\text{CO}_2$  biphasic inclusion from pegmatitic quartz from Vlădeasa granite (Upper Cretaceous). During heating-quenching cycles (multiple and reproducible) the presumed solidified low temperature hydrosilicate glass (Ls) was liquefied between 221-237°C marked by the releasing of the internal vapor-rich bubble (the second immiscible phase). On further heating Vm was consumed completely in the liquid hydrosilicate phase at 299°C. During quenching Vm renucleated at 277°C and the hydrosilicate liquid phase (Ls) solidified between 237° and 197°C. At 197°C bubble (Vm) suddenly collapsed suggesting a contraction phenomenon reminding the bubble collapse during normal freezing experiment in the microthermometry of the aqueous biphasic inclusions. Notations: Ls-hydrosilicate glass/gel phase, Vm- immiscible vapor-“melt” bubble, o- Fe-rich amorphous opaque phase. Scale bar in  $\mu\text{m}$ .

under the microscope reminding the freezing moment during criometry of the aqueous biphasic fluid inclusions (Fig. 2). Besides the bubble and liquid, these inclusions often contain a lot of solid phases which remain unmelted during heating, similar to the colloidal-silica inclusions in chalcedony (Prokofiev et al., 2016). Uncommon fluid inclusions were mentioned in porphyry copper systems by Roedder (1971) and also by Rosasco and Roedder (1979) in Brazilian pegmatite quartz where the authors measured homogenization temperatures between 92-113°C for vapor bubble + aqueous phase, and 95-152°C for presumed liquid “H<sub>2</sub>S” droplets from various individual inclusions and finally suggested that they could be immiscible liquid hydrocarbons, possibly with some H<sub>2</sub>S in solution. The presence of hydrosilicate-chloride-carbonate-sulfate-CO<sub>2</sub>-vapor-rich “melt”, “hydrosilicate gel” (Vasyukova, 2011) or “silicothermal fluid” (Wilkinson et al., 1996) is suggested by the presence of multiple solid microphases which remain unmelted during microthermometry in quartz from epithermal ore deposits in Eastern Carpathians and Metaliferi Mountains or in Carpathian metamorphic environments mentioned long time ago by Pomârleanu (1971), Murariu and Dumitrescu (1976), Pinteă (1991) in Udubaşa et al., 1991, IGR report - from Udubaşa et al., 2003), suggesting heterogeneous trapping.

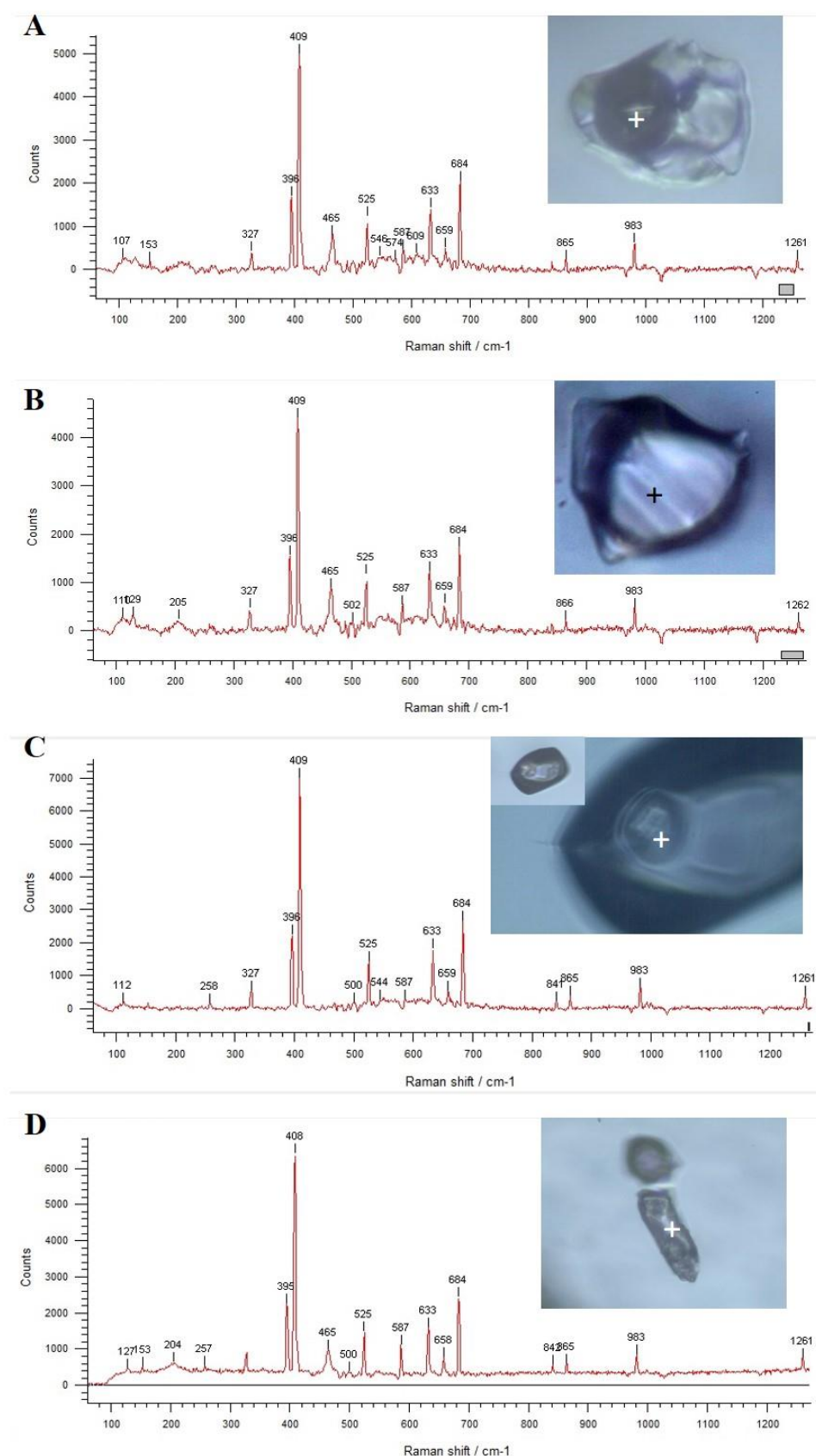
## Results and discussions

Recent non-destructive Raman spectroscopy analyses (Fig. 3) indicate specific vibrational stretching lines and bands which could be assigned for SO<sub>4</sub><sup>2-</sup>, HCO<sub>3</sub><sup>-</sup>, CO<sub>3</sub><sup>2-</sup>, P<sub>2</sub>O<sub>5</sub> or PO<sub>4</sub><sup>3-</sup> molecules detected in the vapor-rich type inclusions from pegmatite quartz from Vlădeasa granite (upper Cretaceous), Miocene porphyry copper systems from Metaliferi Mountains, quartz from xenoliths brought out by alkaline basaltic andesite rocks in the Igriş Mountains, quartz and sphalerite from Căvnic mining prospect from Maramureş district (Romania). Sulphates, carbonates, phosphates, quartz, dawsonite and other solid phases were envisaged by optical microscopy during microthermometry of such heterogeneous aqueous inclusions (Pomârleanu, 1975, 2007; Pinteă, 1995, Grancea et al., 2002, a.m.o.). Questioned many years ago by Roedder and Stalder (1981) in several volcanic environments from USA, the vapor-rich inclusion characterizing a “pneumatolysis” process (*i.e.* vapor-phase crystallization) are nowadays described as hydrosilicate vapor-“melt” or hydrothermal gel solution in pegmatites from Transbaikalia, Russia, Volhin in Ukraine, Tin Mountain from South Dakota (USA), Ehrenfriedersdorf (Germany), Rønne granite and pegmatite in Norway (*e.g.* Touret et al., 2007; Sîrbescu and Nabelek, 2003, Thomas and Davidson, 2012) or in porphyry copper deposits from South America (*e.g.* Davidson and Kamenetsky, 2001; Kamenetsky et al., 2004; Wilkinson et al., 2015).

Experimental works on Na<sub>2</sub>O-K<sub>2</sub>O-Al<sub>2</sub>O<sub>3</sub>-SiO<sub>2</sub>-H<sub>2</sub>O system at various PTX-conditions suggest that three immiscible highly concentrated alkali silicate aqueous fluid can be generated at temperature as low as 450°C up to 900°C and pressure of 0.1-0.2 GPa in equilibrium with quartz and K-feldspar or synthetic granite compositions (Veksler et al., 2002, 2006). A hydrosilicate liquid (HSL) was released from water and alkali rich silicate melt (Na<sub>2</sub>O-SiO<sub>2</sub>-H<sub>2</sub>O+NaF+NaCl+Ta) around 600°C, and special mass transfer and metal transport properties were assigned to this unconventional fluid phase by Smirnov et al. (2012). Kotelnikova and Kotelnikov (2010) studied immiscibility in sulfate-bearing fluid system at high P and T and suggested that fluid phases exsolved at magmatic stage undergo unmixing by decreasing temperature between 180-200°C. The occurrence of such a complex immiscibility in silicate melt containing alkalis and carbonates with volatile phases including F, Cl, S, P and CO<sub>2</sub> it seems to be conditioned by the high activity of the alkalis in the alkali-aluminosilicate melts (Panina and Usoltseva, 2004).

## Conclusions

Published data worldwide and our recent microthermometry and Raman spectroscopy in various samples from geological formations in Romania allowed us to (preliminary) conclude that vapor-rich inclusions and heterogeneous aqueous inclusions are representative for a complex hydrosilicate ± chloride ± carbonate ± sulfate ± phosphate (and Fe-rich) supercritical fluid phase originating from deep upper mantle and mid crustal environment released from various melt types (batches) during magmatic flare-up or metamorphism (metasomatic) associated with the subduction processes of different ages in the Carpathians. Alternatively, they could be representative for successive phase separation process related to specific stage of melt evolution in magma chambers and volcanic conduits such as magma mixing, mingling or assimilation. The separation of vapor, liquid and multiple microsolid phases in these inclusions (*i.e.* vapor-rich or aqueous-rich) took place after trapping during decreasing temperature and pressure and their homogenization temperature recorded by microthermometry is not their original



**Fig. 3.** Raman spectra in some selected samples from Carpathian zone (Romania). **A.** Vlădeasa pegmatite quartz; **B.** Quartz from Roșia Poieni porphyry copper deposit; **C.** Săpânța quartz xenolith (Pintea, 2014 - Fig. 1h); **D.** Quartz from Cavnic-Bolduț mining prospect. Measurements were performed at Romanian Geological Institute in Bucharest by a Raman Renishaw spectrometer equipped with a Leica DM 2700M and 50x objective lense. Excitation was provided by two laser types: 532 nm with resolution of 1200l/mm to 1800l/mm and 785 nm with resolution of 1200l/mm, respectively. Laser time exposure ranged between 5 to 15 sec and counting time from 1 to 55. Fluid inclusion length around 60  $\mu\text{m}$ .



formation temperature. Moreover, it was demonstrated by experimental microthermometry in the H<sub>2</sub>O-NaCl (Bodnar et al., 1985) or H<sub>2</sub>O-CO<sub>2</sub> (Sterner, 1992) systems that the final homogenization temperature in the vapor phase could be underestimated suggesting exsolution from magmas (or metamorphism) at much higher temperatures comparatively to their homogenization values recorded under the microscope.

Anyhow, it is worth noting that the interpretation of the microthermometric data in the H<sub>2</sub>O-NaCl, H<sub>2</sub>O-CO<sub>2</sub> and other well studied model systems is the most important tool in fluid phase applications and interpretations in various geological setting mentioned above, and still remaining the best proxy in fluid geochemistry and geothermobarometry, also taking into account the inherent post-entrapment modifications.

**Acknowledgements.** This work has been partially supported by the Research Projects no. PN18470201/2018 financed by Romanian Ministry of Research and Innovation and no. 29 PCCDI/2018 “GEORES” financed by UEFISCDI, Romania.

## References

- Bodnar R.J., Burnham C.W., Sterner S.M. (1985) Synthetic fluid inclusions in natural quartz. III. Determination of phase equilibrium properties in the system H<sub>2</sub>O-NaCl to 1000°C and 1500 bars. *Geochim. Cosmochim. Acta*, 49, p. 1861-1873.
- Davidson P., Kamenetsky V.S. (2001) Immiscibility and continuous felsic melt-fluid evolution within the Rio Blanco porphyry system, Chile: evidence from inclusions in magmatic quartz. *Econ Geol.*, 96, 1921-1929.
- Davidson P., Kamenetsky V.S., Cooke D.R., Frikker P. (2005) Magmatic precursor of hydrothermal fluids at the Rio Blanco Cu-Mo deposit, Chile: links to silicate magmas and metal transport. *Econ. Geol.*, 100, p. 963-978.
- Grancea L., Bailly L., Leroy J., Banks D., Marcoux E., Milési J.P., Cuney M., André S.A., Istvan D., Fabre C. (2002) Fluid evolution in the Baia Mare epithermal gold/polymetallic district, inner Carpathians, Romania. *Min. Deposita*, 37, 630-647.
- Kamenetsky V.S., Naumov V.B., Davidson P., Achterberg van E., Ryan C.G. (2004) Immiscibility between silicate magmas and aqueous fluids: a melt inclusion pursuit into magmatic-hydrothermal transition in the Omsukchan granite (NE Russia). *Chem. Geol.*, 210, p. 73-90.
- Kotelnikova Z.A., Kotelnikov A.R., (2010) Immiscibility in sulfate-bearing fluid systems at high temperatures and pressures. *Geochem. Internat.*, 48, 4, p. 381-389.
- Kovalenker V.A., Naumov V.B., Prokofiev V.Yu., Jelen S., Gaber M. (2006) Compositions of magmatic melts and evolution of mineral-forming fluids in the Banska Stiavnica epithermal Au-Ag-Pb-Zn deposit, Slovakia: a study of inclusions in minerals. *Geochem. Internat.*, 44, 2, p. 118-136.
- Lowenstern J.B. (1993) Evidence for a copper-bearing fluid in magma erupted at the Valley of Ten Thousand Smokes, Alaska. *Contrib. Mineral. Petrol.*, 114, p. 409-421.
- Murariu T., Dumitrescu M. (1976) Contributions to geochemistry and geothermometry of Copalnic pegmatites (massif Preluca-Lăpuș) (in Romanian). *D.S. Inst. Geol. Geof.*, LXII/1 (1974-1975), p. 379-398, Bucharest.
- Naumov V.B., Kovalenker V.A., Damian G., Abramov S.S., Tolstykh M.L., Prokofiev V.Yu., Damian F., Seghedi I. (2014) Origin of the Lăleuș Alba dacite (Baia Sprie volcanic area and Au-Pb-Zn ore district, Romania): evidence from study of melt inclusions. *Central Eur. Geology*, 57/1, p. 83-112.
- Nuțu M.-L., Vaselli O. (2015). Fault related fluid flow within the subcarpathian nappe domain (East Carpathians) during the post-collision stage. *Conference Proceedings, 15<sup>th</sup> Internat. Multidisciplinary GeoConf.*, Book 1, vol. 1, p. 141-150.
- Panina L.I., Usoltseva I.M. (2004) Liquid carbonate-carbonate-salt immiscibility and origin of calciocarbonatites. In: "Deep seated magmatism, its sources and their relation to plume processes". *UDK 552.11.548.4*, p. 212-238.
- Pomârleanu V. (1971). Geothermometry and their application to some minerals from Romania. *Edit. Acad. Române*, 158 p. (in Romanian), Bucharest.
- Pomârleanu V. (1975). Decrepitometry and their applications in mineral prospection. *Edit. Tehn*, 180 p. (in Romanian), Bucharest.
- Pomârleanu V. (2007). Microinclusions in minerals from extraterrestrial and terrestrial environments. *Ed. AGIR*, 173 p. (in Romanian), Bucharest.

- Pintea I., (1995). Fluid inclusions microthermometry. Some typical examples. *Rom. J. Mineralogy*, 76, 2, p. 25-36.
- Pintea I. (2010) Fluid and melt inclusions evidences for autometasomatism and remelting in the alpine porphyry copper genesis from Romania. *Rom. J. of Mineral Deposits*, Vol. 84, Spec. Iss. - The 7<sup>th</sup> Nat. Symp. on Econ Geol. "Mineral Resources of Carpathian area", 10-12 Sept. 2010, Baia Mare, Romania, p. 15-18.
- Pintea I. (2014) The magmatic immiscibility between silicate-, brine-, and Fe-S-O melts from the porphyry (Cu-Au-Mo) deposits in the Carpathians (Romania): a review. *Rom. Jour. of Earth Sci.*, Vol 87, issue 1, p. 1-32.
- Pintea I. (2016) A self-perspective research topic revealed during the elaboration of the Atlas "Fluid and Melt Inclusions from Romania". *Rom. J. of Mineral Deposits*, Vol. 89, no. 1-2, p. 1-6.
- Pintea I., Berbeleac I., Udubaşa S.S., Nutu-Dragomir L.M., Iatan L.E. (2017) Fluid and melt inclusions study related to the magmatic-hydrothermal apatite-anhydrite association from Voia porphyry Cu-Au (Mo) prospect (Metaliferi Mountains, Romania). *ECROFI 2017*, 23-29 June 2017, Nancy (France), p. 206.
- Prokofiev V.Yu., Kamenetsky V.S., Selektor S.L., Rodeman T., Kovalenker V.A., Vatsadze Z.S., (2016) First evidence for natural occurrence of colloidal silica in chalcedony-hosted vacuoles and implications for ore-forming processes. *Geology*, 45, 1, p. 71-74.
- Roedder E., Coombs D.S. (1967) Immiscibility in granite melts, indicated by fluid inclusions in ejected granitic blocks from Ascension Island. *Jour. of Petrology*, 8, 3, p. 417- 451.
- Roedder E. (1971) Fluid inclusion studies on the porphyry - type ore deposits at Bingham, Utah, Butte, Montana, and Climax, Colorado. *Econ. Geol.*, 66, p. 98-120.
- Rosasco G.J., Roedder E. (1979) Application of a new Raman microprobe spectrometer to nondestructive analysis of sulfate and other ions in individual phases in fluid inclusions in minerals. *Geochim. Cosmochim. Acta*, 43, p. 1907-1915.
- Roedder E., Stalder H.A. (1981) Pneumatolysis and fluid-inclusion evidence for crystal growth from a vapor phase. *Mem. Geol. Soc. of India.*, 11, p. 1-12.
- Sîrbescu M.-L.C., Nabelek P.I. (2003) Crustal melt below 400°C. *Geology*, 31, 8, p. 685-688.
- Smirnov S.Z., Thomas V.G., Kamenetsky V.S., Kozmenko O.A., Large R.R. (2012) Hydrosilicate liquids in the system Na<sub>2</sub>O-SiO<sub>2</sub>-H<sub>2</sub>O with NaF, NaCl and Ta: evaluation of their role in ore and mineral formation at high T and P. *Petrology*, 20, 3, p. 271-285.
- Sośnicka M., Bakker R.J., Broman C., Pitcairn I., Paranko I., Burlinson K. (2015) Fluid types and their genetic meaning for the BIF-hosted iron ores, Krivoy Rog, Ukraine. *Ore Geol. Rev.*, 68, p. 171-194.
- Sterner M.S. (1992) Homogenization of fluid inclusions in the vapor phase: the apparent homogenization phenomenon. *Econ. Geol.*, 87, p. 1616-1623.
- Thomas R., Davidson P. (2012) Evidence of a water-rich silica gel state during the formation of a simple pegmatite. *Mineral. Mag.*, 76(7), p. 2785-2801.
- Touret J.L.R., Smirnov S.Z., Peretyzhko I.S., Zagorsky V.Y., Thomas V.G. (2007) Magmatic-hydrothermal transition in tourmaline-bearing miarolitic pegmatites: hydrosaline fluids or silica gels? In: *Granitic Pegmatites: The State of the Art* (T.Tartins and R.Vieira, editors). *Memorias*, 8, p. 92-93, Departamento de Geologia, Universidade do Porto, Portugal.
- Udubaşa S.S., Lespinnasse M., Udubaşa G., Popescu C.G., Leroy J., Bilal E. (2003) Fluid inclusions data on quartz samples from Costesti gold mineralization, southern Carpathians, Romania. *ECROFI XVII*, Budapest, 2003, *Acta Min.-Petrogr. Abstract Series 2*, Szeged, p. 220-221.
- Veksler I.V., Thomas R., Schmidt C. (2002) Experimental evidence of three coexisting immiscible fluids in synthetitic granitic pegmatite. *Amer. Min.*, 87, p. 775-779.
- Veksler I.V., Schmidt C., Thomas R. (2006) Low temperature alkali silicate melt and fluid in the system Na<sub>2</sub>O-K<sub>2</sub>O-Al<sub>2</sub>O<sub>3</sub>-SiO<sub>2</sub>-H<sub>2</sub>O. *Geochim. Cosmochim. Acta*, 70 (18), p. 671.
- Vasyukova O.V. (2011) Types and origin of quartz and quartz-hosted fluid inclusions in mineralised porphyries. Ph D thesis, University of Tasmania.
- Wilkinson J.J., Nolan J., Rankin A.H. (1996) Silicothermal fluid: a novel medium for mass transport in the lithosphere. *Geology*, 24, p. 1059-1062.
- Wilkinson J.J., Vasyukova O., Laird J.S., Ryan C., Kamenetsky V.S. (2015) Hydrosilicate liquids: unconventional agents of metal transport in porphyry ore systems. *ECROFI –XXIII*, Leeds, UK, 27-29 June 2015, *Extended Abstr. Volume*, p. 116.

## SILVER SULFOTELLURIDES AND OTHER Te-SULFOSALTS IN ALABANDITE-BEARING VEINS FROM SĂCĂRÂMB Au-Ag-Te ORE DEPOSIT, METALIFERI MOUNTAINS, ROMANIA

George DINCĂ<sup>1</sup>, Gheorghe C. POPESCU<sup>1</sup>, Oana-Claudia CIOBOTEA-BARBU<sup>2,3</sup>, Daniel BÎRGĂOANU<sup>2,4</sup>

<sup>1</sup> Department of Mineralogy, Faculty of Geology and Geophysics, University of Bucharest, 1, Nicolae Bălcescu Blvd., Bucharest, Romania;

<sup>2</sup> Geological Institute of Romania, 1 Caransebeș St., Bucharest, Romania;

<sup>3</sup> University Politehnica of Bucharest, Faculty of Applied Chemistry and Materials Science, Depart. of Inorganic Chemistry, Physical Chemistry and Electrochemistry, Bucharest;

<sup>4</sup> Department of Geology, Faculty of Geography and Geology, "Alexandru Ioan Cuza" University, 20A, Carol I Blvd., Iași, Romania.

**Abstract.** This paper addresses Ag-sulfotellurides and Te-sulfosalts occurring in Săcărâmb epithermal Au-Ag-Te ore deposit, Metaliferi Mountains, Romania. Cerveleite-like minerals were identified in close association with galena, sylvanite, bournonite and native tellurium. It is optically isotropic, it has a blue-grey colour and a chemical composition of  $\text{Ag}_{2.1}\text{Te}_1\text{S}_{2.8}$  (stoichiometric  $\text{Ag}_2\text{TeS}_3$  from EDS analyses of three grains). Benleonardite associated with tennantite, bournonite, galena and jordanite was found in two samples, with the composition  $\text{Ag}_{16.1}(\text{Sb}_{0.9}\text{As}_{1.5})_{2.4}\text{S}_{7.3}\text{Te}_{3.3}$ . The chemical composition of one grain shows a high concentration of Cu with a calculated empirical formula of  $(\text{Ag}_{12}\text{Au}_{0.3}\text{Cu}_{3.8})_{15.9}(\text{As}_{0.3}\text{Sb}_{1.4})_{1.7}\text{Te}_{9.2}\text{S}_{2.2}$ , which indicates a substitution between Ag and Cu. Two goldfieldite grains were found in association with bournonite, galena and tellurides. One grain has the chemical composition  $\text{Cu}_{10.2}\text{Ag}_{1.5}\text{Sb}_{1.3}\text{As}_{0.6}\text{Te}_{1.8}\text{S}_{11.5}$  and the second goldfieldite is Bi-bearing with the chemical composition  $\text{Cu}_{11.5}\text{Ag}_{0.2}\text{Bi}_{0.8}\text{Te}_{2.55}\text{S}_{12}$ . Sulfotellurides are an indicator for low  $f\text{Te}_2$ , this indicates that at Săcărâmb the Te/S ratio varied in the alabandite rich veins. The Ag-Te-S system is still poorly studied despite its significant scientific and economic importance.

**Keywords:** sulfotellurides, sulfosalts, alabandite, cervelleite, benleonardite, goldfieldite, Săcărâmb

### Introduction

Natural compounds of silver containing both sulfur and tellurium are known as two main groups: cervelleite-like compounds and sulfosalts like benleonardite  $\text{Ag}_8(\text{Sb,As})\text{Te}_2\text{S}_3$ . Cerveleite was found in Romania by Cook and Ciobanu (2003) at Băița Bihor and Ocna de Fier skarn deposits. Te bearing sulfosalts are more widespread in the Gold Quadrilater. The most important Te-sulfosalt is nagyagite discovered at Săcărâmb Au-Ag-Te ore deposit. Other Te-sulfosalts found at Săcărâmb are: museumite (Bindi and Cipriani, 2004), aleksite (Shimizu, 2003), tetradyomite (Posepny, 1868) and goldfieldite (Udubasa et al., 2002). Recently, at Roșia Montană Au-Ag deposit were discovered two Te-sulfosalts: alburnite-*locus typicus* (Tămaș et al., 2014) and Ge-bearing benleonardite (Sabău et al., 2016). In this study, it is reported a new occurrence of benleonardite, Cu-Au bearing benleonardite, cervelleite, Bi-bearing goldfieldite and an unknown cervelleite-like minerals.

### Geological Setting

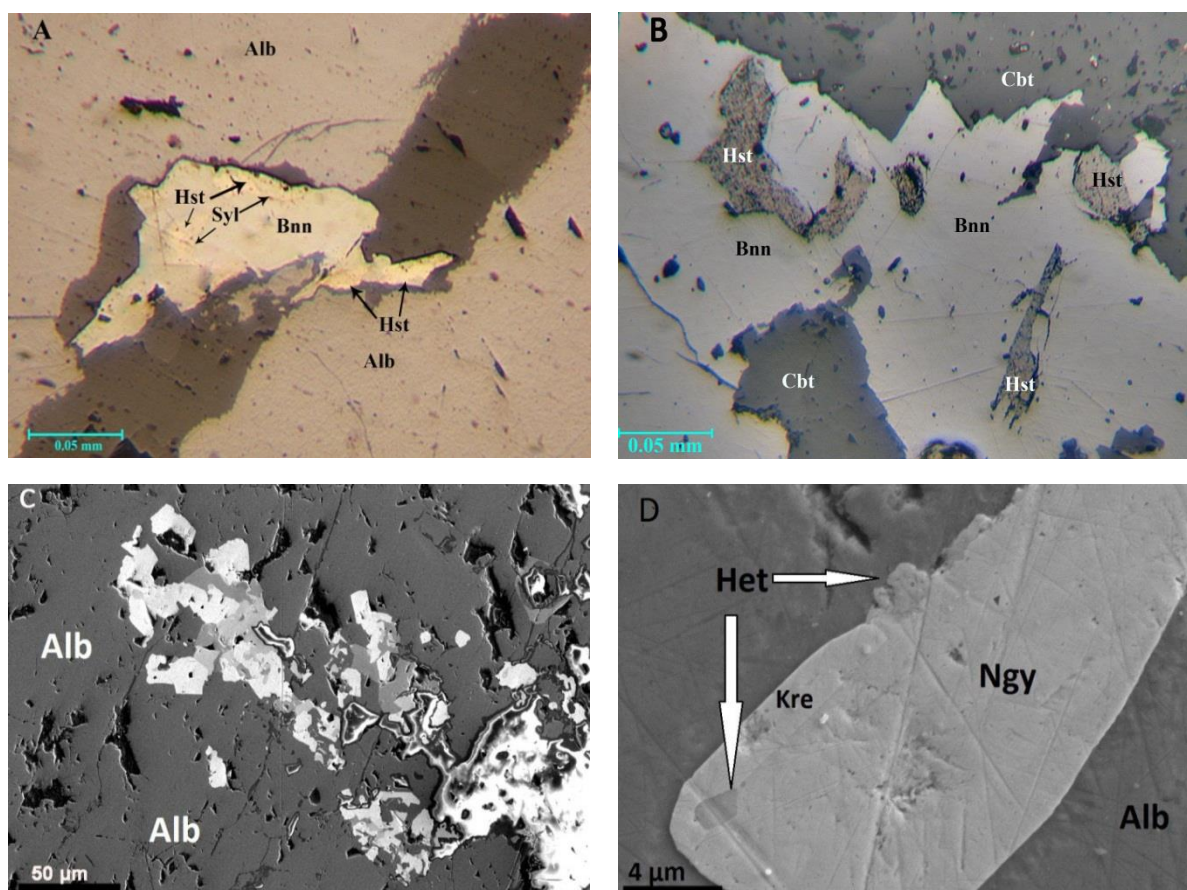
The Săcărâmb Au-Ag-Te ore deposit is located in the Metaliferi Mountains in Romania; it is the largest telluride mineral accumulation in Europe with a total of 14 minerals containing Te, Au and Ag. The ore mineralization has a Miocene-Pliocene age (14.7-7.4 Ma) and is related to the Neocene volcanic activity in the region, being part of the Alpine-Carpathian-Dinaride area (Udubașa et al. 1992). The ore mineralization is of hydrothermal origin, Săcărâmb is classified as a low-sulphidation Au-Ag-Te epithermal deposit (Ciobanu et al. 2005). The host of the mineralization is an andesitic neck with about 230 veins in a 1000 m<sup>2</sup> area with a 600 m vertical extent. The vein fields include four vein groups perpendicularly oriented, disposed as: Magdalena-Carolina and Nepomuc groups, having a NE-SW direction while Longhin-Antelongo and Ertzbau groups have a NW-SE orientation (Ianovici et al. 1976). The majority of the veins are rich in Au-Ag tellurides. What constitutes its uniqueness from other Au-Ag-Te deposits is the widespread presence of alabandite.

## Materials and methods

Over 50 polished sections were studied from ore samples found in two waste dumps (Sector 2 and Sector 3). Microscopic observations were carried out on a Leitz Wetzlar reflected light microscope and the images were taken using a PANPHOT Leitz Wetzlar reflected light microscope equipped with a Nikon Eclipse E-400 camera. Chemical analyses and SEM images were realized with a Zeiss Merlin GEMINI II SEM-EDS spectrometer, with a working regime: accelerating voltage ranging between 15-20 kV, beam current ranging between 1-2 nA, background time 20 s and a beam diameter that varies depending of the scale.

## Telluride assemblages

The first association observed was in the form of: krennerite, hessite ( $\text{Ag}_2\text{Te}$ ) and nagyagite inclusions in alabandite however in some cases sulfosalts were present as well (Fig. 1). The second type of association identified was the presence of native tellurium, sylvanite hessite and krennerite in the secondary rhodochrosite veins that crosscut the massive alabandite (Fig. 1). In this occurrence tellurides are usually associated with these sulfosalts: tetrahedrite, jordanite ( $\text{Pb}_{14}(\text{As,Sb})_6\text{S}_{23}$ ), dufrenoyite ( $\text{Pb}_2\text{As}_2\text{S}_5$ ) and bournonite. A third assemblage was discovered with native tellurium, sylvanite, hessite, nagyagite, goldfieldite, benleonardite and an unknown silver sulfotelluride (Fig 1). All of the tellurides from this assemblage are included in a sulfosalt-sulfide association comprised of bournonite, tetrahedrite-tennantite, galena, sphalerite and alabandite.



**Fig. 1.** Examples of tellurides and sulfosalt associations from Săcărâmb: A) association of hessite and sylvanite in bournonite with alabandite (parallel polarized light) B) hessite crystals included in bournonite (parallel polarized light) C) SEM image of a complex association of galena-sulfosalts-sulfotellurides and tellurides included in alabandite D) SEM image of nagyagite crystal with krennerite inclusion and on the margin heteromorphite  $\text{Pb}_7\text{Sb}_8\text{S}_{19}$ , all included in alabandite. Hst- hessite, Syl- sylvanite, Ngy- nagyagite, Alb- alabandite, Bnn- bournonite, Kre-krennerite, Het-heteromorphite and Cbt- carbonate.

## Sulfotellurides

Cervelleite-like minerals were found in 3 polished sections. The grain size of this mineral phases varies between 1 to 10  $\mu\text{m}$ . Under the microscope, these phases are isotropic and bluish grey. The Ag sulfotellurides coexist with hessite and sylvanite, presenting a replacement texture (Fig. 2). The tellurides and sulfotellurides appear as inclusions in tetrahedrite and bournonite associations, or in carbonate veins. The chemical compositions of cervelleite is presented in Table 1. After the calculation based on 6 total number of atoms, the empirical formula of Săcărâmb cervelleite is  $(\text{Ag}_{3.8}\text{Te}_{0.6}\text{S}_{1.6})$ . The unknown Ag-sulfotellurides have an empirical formula of  $(\text{Ag}_{2.1}\text{Te}_1\text{S}_{2.8})$  calculated based on 6 total number of atoms, it is possible that this phase has a simplified formula of  $\text{Ag}_2\text{TeS}_3$ .

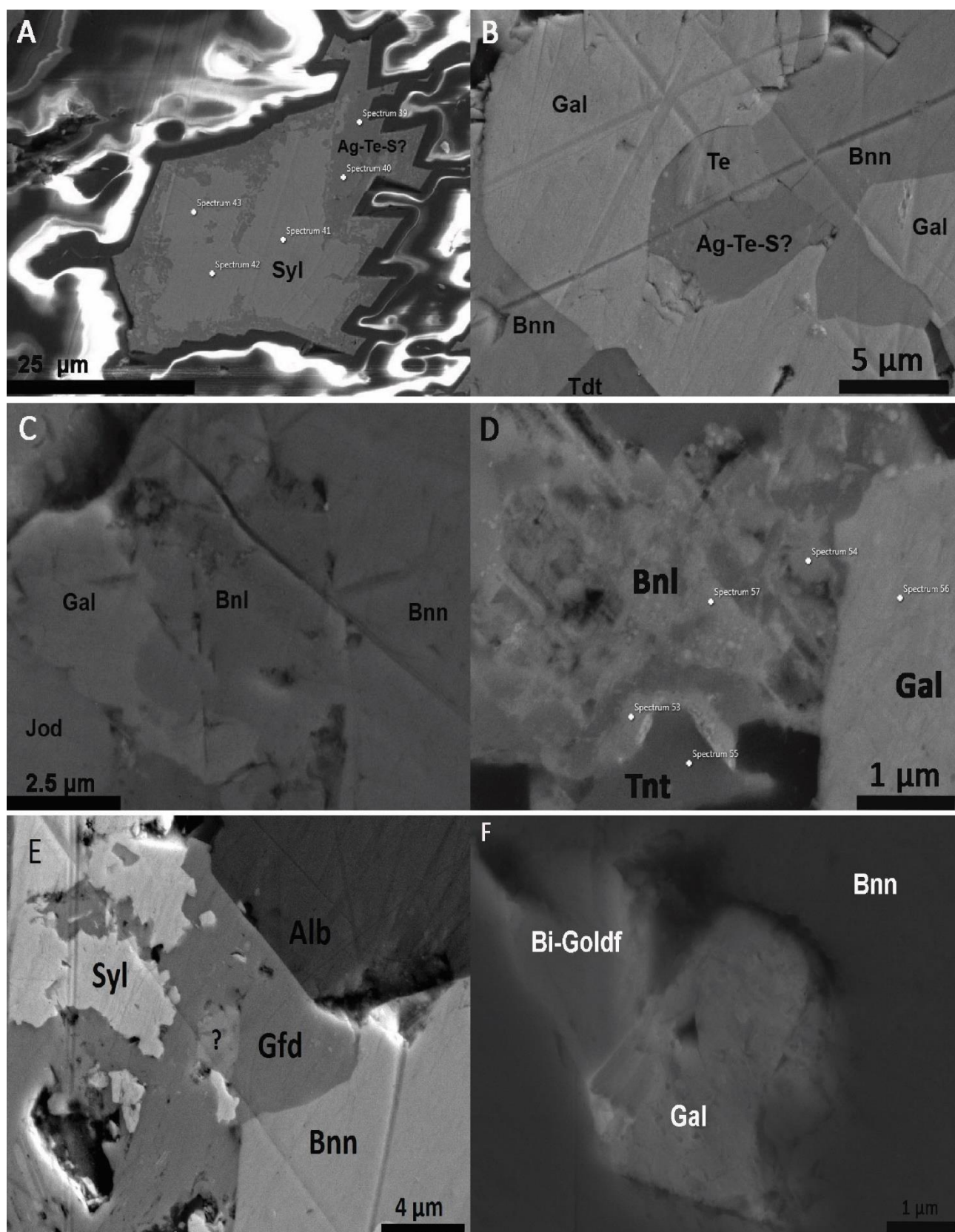
**Table 1.** Representative EDS chemical analyses of cervelleite and cervelleite-like minerals from Săcărâmb. The analyses were corrected to 100Wt% by the AZtecEnergy EDS analysis software.

Element Wt%	S3K2 cervelleite	S3K4 Unknown mineral	S3K4 Unknown mineral	S3K2 Unknown mineral
Ag	76.53	51.52	50.89	57.54
S	9.66	20.31	20.61	17.90
Te	13.81	28.17	28.5	24.57
Total	100	100	100	100
At%	Chemical formula based on sum of 6 atoms			
Ag	3.80	2.15	2.12	2.49
S	1.61	2.85	2.88	2.60
Te	0.58	0.99	1.00	0.90

Benleonardite,  $\text{Ag}_8(\text{Sb,As})\text{Te}_2\text{S}_3$ , was identified in two polished sections in association with bournonite, jordanite, tetrahedrite and galena (Fig. 2). It has a bluish grey colour and a moderate anisotropy. The empirical formula was calculated using 29 atoms per formula unit:  $\text{Ag}_{16.1}(\text{Sb}_{0.9}\text{As}_{1.5})_2\text{S}_{7.3}\text{Te}_{3.3}$ . To calculate the empirical formula, it was used the chemical data of benleonardite from Bindi et al. (2015), in which benleonardite is considered a member of the pearceite-polybasite group. In the material from Săcărâmb, it was discovered a Cu-bearing benleonardite which indicates a clear substitution of Ag by Cu, indicating the possibility of a Cu homologue of benleonardite. This hypothesis is sustained by the new data regarding the crystal-chemical formula of benleonardite  $(\text{Ag}_{15}\text{Cu}(\text{Sb,As})_2\text{S}_7\text{Te}_4)$  and the membership in the pearceite-polybasite group Bindi et al. (2015). Cu enrichment of benleonardite relates to the association with tennantite.

Goldfieldite appears in two polished sections in association with bournonite, galena, jordanite and tellurides (Fig. 2). The chemical composition of Săcărâmb goldfieldite is varied (Table 2), in one probe goldfieldite is rich in Ag, with an empirical formula of  $\text{Cu}_{11}\text{Ag}_{1.7}\text{Sb}_{1.4}\text{As}_{0.6}\text{Te}_2\text{S}_{12.3}$ . The calculation was based on 29 atoms, for minerals with 2 or less Te a.p.f.u. after the chemical study of goldfieldite by Trudu and Knittel (1998). The second goldfieldite is Bi-bearing with concentrations above 10 Wt%. The calculated empirical formula for Bi-bearing goldfieldite is  $\text{Cu}_{11.5}\text{Ag}_{0.2}\text{Bi}_{0.8}\text{Te}_{2.55}\text{S}_{12}$  (based on 27 atoms). It is the first known presence of Bi-bearing goldfieldite at Săcărâmb ore deposit. Bismuth is known to be found in tennantite and tetrahedrite commonly known as „annivite” and it has the same position as As and Sb in the crystal-chemical formula Gołębiewska et al. (2012).





**Fig. 2.** SEM images of sulfotellurides and Te-bearing sulfosalts found at Săcărâmb: A- unknown silver sulfotelluride replacing a sylvanite crystal, B –silver sulfotelluride with native tellurium, galena, tetrahedrite and bournonite, C- benleonardite crystal between galena and bournonite in association with jordanite, D- benleonardite replacing tennantite, E- sylvanite with an unidentified sulfotelluride in goldfieldite, associated with bournonite and alabandite F – inclusions of galena bismuth-bearing goldfieldite in bournonite. Alb-alabandite, Syl-sylvanite, Gfd-goldfieldite, Bi-Goldf- bismuth bearing goldfieldite, Bnl-benleonardite, Bnn-bournonite, Jod-jordanite, Tnt-tennantite, Te-native tellurium Ag-Te-S?- unknown sulfotelluride

**Table 2.** Representative EDS chemical analyses of benleonardite and goldfieldite from Săcărâmb. The analyses were corrected to 100Wt% by the AZtecEnergy EDS analysis software.

Element Wt%	S3K2	S3K2	S3K4	S3K4	S3C1	S3C1	S3K4	S3K4
<b>benleonardite</b>			<b>Cu- benleonardite</b>		<b>Bi-goldfieldite</b>		<b>Ag-goldfieldite</b>	
<b>Au</b>	0	0	3.61	1.68	-	-	-	-
<b>Ag</b>	66.87	66.67	55.94	53.33	1.44	1.42	10.02	10.02
<b>Cu</b>	0	0	7.41	13.1	45.05	45.17	40.22	40.74
<b>Sb</b>	4.15	3.83	8.55	6.04	-	-	10.66	9.14
<b>As</b>	4.31	3.99	0	2.28	-	-	2.87	2.59
<b>S</b>	9.05	8.9	11.6	11.72	23.41	23.69	22.93	22.60
<b>Te</b>	15.62	16.62	12.89	11.83	19.71	19.61	13.29	14.91
<b>Bi</b>	-	-	-	-	10.38	10.1	-	-
<b>Total</b>	100	100	100	100	100	100	100	100
<b>At%</b>	sum of 29 atoms				sum of 27 atoms		sum of 29 atoms	
<b>Au</b>			0.4	0.2	-	-	-	-
<b>Ag</b>	16.1	16.1	12.7	11.5	0.22	0.2	1.61	1.62
<b>Cu</b>	0	0	2.8	4.8	11.5	11.5	10.98	11.16
<b>Sb</b>	0.9	0.8	1.7	1.2	-	-	1.52	1.3
<b>As</b>	1.5	1.4	0.0	0.7	-	-	0.66	0.6
<b>S</b>	7.3	7.3	8.8	8.5	11.9	12	12.4	12.3
<b>Te</b>	3.2	3.4	2.5	2.2	2.5	2.5	1.8	2
<b>Bi</b>	-	-	-	-	0.8	0.8	-	-

## Conclusions

An interesting fact about these associations is that Au-tellurides in alabandite are much rarer than Ag-tellurides and native tellurium, furthermore an abundance of Au-tellurides are found in the secondary carbonate veins with sulfosalts. This indicates that the first telluride phase was rich in Ag and Pb and the second one that came with sulfosalts was rich in As, Sb and Au. The discovery of Bi-goldfieldite, indicates the existence of another member of the tetrahedrite group and a possible series between goldfieldite and a Bi homologue. Formation of the sulfotellurides indicates relative low  $f\text{Te}_2$  in some areas of the hydrothermal system. Numerous finds of unusual and poorly characterized telluride compositions in low-sulfidation epithermal veins reveal the still incomplete knowledge of the Ag-Te-S system and consequently deficient exploration and economic significance.

## Acknowledgments

We thank Eldorado Gold Corporation, for the support provided in the field research and the Microcosmos Laboratory, Geological Institute of Romania, for the SEM-EDS chemical analyses.

## References

- Bindi, L., Cipriani, C. (2004) Museumite,  $\text{Pb}_5\text{AuSbTe}_2\text{S}_{12}$ , a new mineral from the gold-telluride deposit of Săcărâmb, Metaliferi Mountains, western Romania. *European Journal of Mineralogy*, 16(5), 835-838
- Bindi, L., Stanley, C. J., Spry, P. G., (2015) New structural data reveal benleonardite to be a member of the pearceite-polybasite group. *Mineralogical Magazine*, 79(5), p. 1213-1221
- Ciobanu C. L., Cook N. J., Capraru N., Damian G., Cristea P. (2005) Mineral assemblages from the vein salband at Săcărâmb, Golden Quadrilateral, Romania: Sulphides and sulphosalts. *Geochemistry mineralogy and petrology* 43 Sofia.

- Cook, N. J., & Ciobanu, C. L. (2003) Cerveleite,  $\text{Ag}_4\text{TeS}$ , from three localities in Romania, substitution of Cu, and the occurrence of the associated phase,  $\text{Ag}_2\text{Cu}_2\text{TeS}$ . *Neues Jahrbuch für Mineralogie-Monatshefte*, 2003(7), 321-336.
- Cook N. J., Ciobanu C. L., Damian G., Damian F. (2004) Tellurides and sulphosalts from deposits in the Golden Quadrilateral, IAGOD Guidebook Series 12, 25-88, 31st August–7th September 2004, Alba Iulia Romania, p. 111-114.
- Gołębiowska, B., Pieczka, A., Parafiniuk, J. (2012) Substitution of Bi for Sb and As in minerals of the tetrahedrite series from Rędziny, Lower Silesia, Southwestern Poland. *The Canadian Mineralogist*: 50: p. 267-279.
- Ianovici, V., Borcos, M., Bleahu, M., Patrulius, D., Lupu, M., Dimitrescu, R., and Sava, H. (1976); *Geologia Muntilor Apuseni:Romania*. Editura Academiei Republicii Socialiste Romania, 631 p.
- Posepny, F. (1868) *Zur Geologie der Siebenburgischen Erzebirges*. Jahrbuch.Reichsanstalt, 18.
- Sabau G., Cioaca M. E., Munteanu M., Birgaouanu D., Ciobotea-Barbu O. C.; A new occurrence of arsenian alburnite, its associated phases and erratum to a previous report, *Rom. J. Mineral Deposits*, vol. 89, nr. 1-2, p. 93-98.
- Shimizu, M., Stanley, C.J., (2003) Re-study of nagyagite from Săcărâmb, Romania. *Mineral Exploration and Sustainable Development*. Millpress, Rotterdam, p. 527-528.
- Tămaş, C. G., Grobety, B., Bailly, L., Bernhardt, H. J., & Minuţ, A. (2014) Alburnite,  $\text{Ag}_8\text{GeTe}_2\text{S}_4$ , a new mineral species from the Roşia Montana Au-Ag epithermal deposit, Apuseni Mountains, Romania. *American Mineralogist*, 99(1), p. 57-64.
- Trudu, A.G., Knittel, U. (1998) Crystallography, mineral chemistry and chemical nomenclature of goldfieldite, the tellurian member of the tetrahedrite solid-solution series. *The Canadian Mineralogist*: 36: 1115-1137.
- Udubaşa G., Ďud'a R., Szakáll S., Kvasnytsya V., Koszowska E., Novák M., (2002); *Minerals of the Carpathians*. Granit Prague, 479 p.
- Udubasa, G., Strusievicz, R.O., Dafin, E., and Verdes, G., (1992); Mineral occurrences in the Metaliferi Mts., Romania: *Romanian Journal of Mineralogy* v. 75 (suppl. no. 2), 35 p.



## NEOGENE MINERALIZATIONS OF BUCIUM RODU-FRASIN Au-Ag DEPOSITS, SOUTH APUSENI MOUNTAINS, ROMANIA

Elena-Luisa IATAN\*, Ion BERBELEAC

Institute of Geodynamics of Romanian Academy, 19-21 Jean Louis Calderon St., 020032, Bucharest, Romania  
\*luisaiatan@yahoo.com

**Abstract:** The Miocene Bucium Rodu-Frasin deposit is a maar-diatreme complex structure hosting gold-silver epithermal LS mineralizations, in association with quartz-andesite intrusions. There is an intimate spatial and temporal association between the mineralization stages and the Miocene intrusions of the Frasin quartz-andesite. In Rodu area, the mineralizations follow the western diatreme contact with the Cretaceous flysch. In contrast, the Frasin structure mineralizations are focused in or near the NW and NE dome contacts with polymictic breccias. The ore deposition from hydrothermal fluids had a pulsating character, developed in three stages, gold being placed at shallow levels and during the last two epithermal LS stages, from alkaline liquid rich fluids.

The main mineral assemblages are: 1) magnetite (hematite) - pyrite (marcasite) - quartz and pyrite - quartz  $\pm$  base metal sulfides in the first stage; 2) carbonates (calcite, aragonite, dolomite, ankerite,  $\pm$  rhodochrosite  $\pm$  kutnohorite) - quartz - adularia, in the epithermal low sulfidation second stage; 3) quartz - pyrite - marcasite - carbonates (dominant rhodochrosite) - Au and alabandite - rhodochrosite - quartz in the third, epithermal low sulfidation stage. The mineralizing hydrothermal fluids had near neutral pH and gold was probably transported as a bisulfide complex; first boiling seems to be the main trigger of gold precipitation. Alterations as adularia, phyllic and carbonatizations show close relationships with the gold mineralization.

**Keywords:** Neogene Au-Ag mineralization, veins, stockworks, breccias, South Apuseni Mountains.

### Introduction

The Bucium Rodu-Frasin Neogene volcanic structure and related Au-Ag deposits (Fig. 1) are located in the north-eastern part of South Apuseni Mountains, within the so called "Golden Quadrilateral". They are situated about 10 km east of the Abrud city and 5 km south of the Rosia Montana deposit, being part of the Rosia-Bucium-Baia de Aries metallogenic district.

The Au-Ag ore deposits have been exploited from old times, traces of those works being provided by large surface excavations. The total resources for the Rodu and Frasin deposits currently stand 43.3M t with 1.3 g/t Au and 3 g/t Ag, equals 1.8 M oz of gold, and 4.7M oz of silver (Verbeek, 2005, in Hewson et al., 2005).

In this brief review, we highlight the basic features of the mineralizations, and the relationships between volcanic structures, hydrothermal alterations and mineralization styles from Bucium Rodu-Frasin area.

### Geological setting

The Apuseni Mountains have been considered as an isolated massif situated inside of the Carpathian arc, in the western part of Romania (Sandulescu, 1984; Balintoni, 1994), or as an interior segment (Seghedi et al., 2004) in the Alpine-Carpathian-Balkan orogenic system. They are composed of two major units: North Apuseni Mountains and South Apuseni Mountains. The South Apuseni Mountains consist of Palaeozoic and older metamorphic rocks, Mesozoic and Neogene igneous and sedimentary rocks.

The Neogene magmatic products (15-7 Ma, Rosu et al., 1997) have a calc-alkaline character (Ianovici et al., 1976; Cioflica et al., 2002), with some adakite-like features (Seghedi and Downes, 2011), being prevalently andesitic in composition.

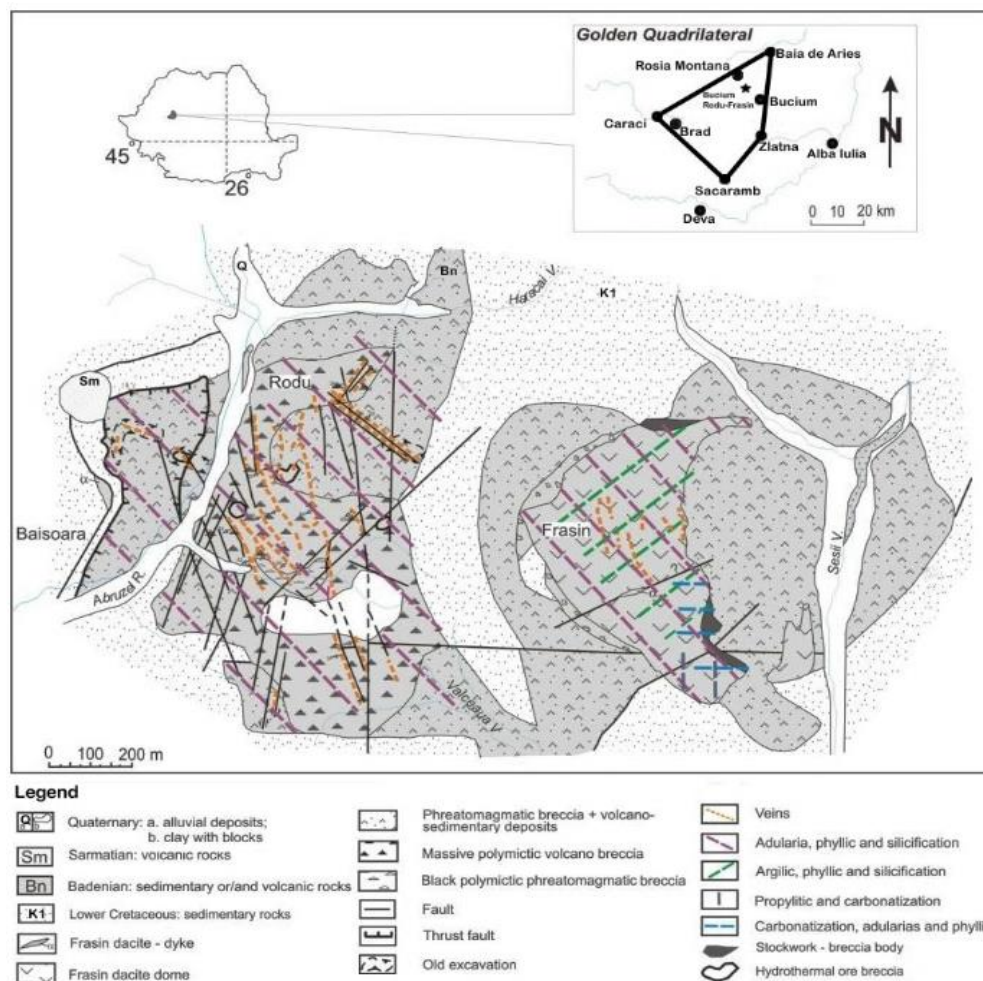
In Mesozoic-Tertiary times, the Bucium Rodu-Frasin area underwent a multi-stage evolution characterized by a strong mobility regime explained, at least partially, by the presence of the north-western segment of an important fault, designated here as Vintu-Aries dextral strike-slip fault.

Structural interpretation of detailed mappings, mining and exploration drilling works, magnetotelluric sounding data and laboratory studies (Ianovici et al., 1976; Borcoş and Vlad, 1997; Leary et al., 2004; Nadasan and Hewson, 2005) suggest that Bucium Rodu-Frasin area represents a small Upper Cretaceous-Lower Miocene collapse basin and a complex maar-diatreme structure, resulted from normal reactivation of older, steeply dipping fault structures related to the Vintu-Aries Fault (Berbeleac et al., 2016).

The geology of Bucium Rodu-Frasin area consists mainly of the following lithological units: 1) Lower Cretaceous marine sediments; 2) Badenian Frasin quartz-andesite, volcano - sedimentary deposits, epiclastic deposits and volcanoclastic products (mono- and polymictic breccias); 3) Badenian Frasin hornblende-biotite-quartz andesite intrusions; 4) Barza type Sarmatian(?) andesite lavas, 5) Detunata

basalt - andesite; 6) intra - maar - diatreme and subsequent sedimentary deposits and 7) Quaternary alluvial deposits.

Bucium Rodu-Frasin maar-diatreme complex volcanic structure consists of two separate eruptive craters, each excavated 400-500 m into Cretaceous sediments, filled with pyroclastic and epiclastic sequences. One is the Rodu maar-diatreme, crosscut by the Abruzel River, and the other one, the Frasin maar - diatreme structure, crosscut by Seasa Valley (Fig. 1). Both structures cover about 5 km<sup>2</sup> and are situated in a high mobility zone with intense deformation related to the Vintu-Aries Fault (Hewson et al., 2005). The Rodu maar-diatreme has an elliptical shape ~ 1500/1000 m with its long axis striking N-S and the southern and eastern sides exhibiting an irregular contour. In contrast, the Frasin maar-diatreme is nearly circular in shape with the diameter of about 1100 m.



**Fig. 1.** Geological map of Bucium Rodu-Frasin area (after R.M.G.C. data with additions, modified after Berbelean et al., 2016).

### Hydrothermal alteration

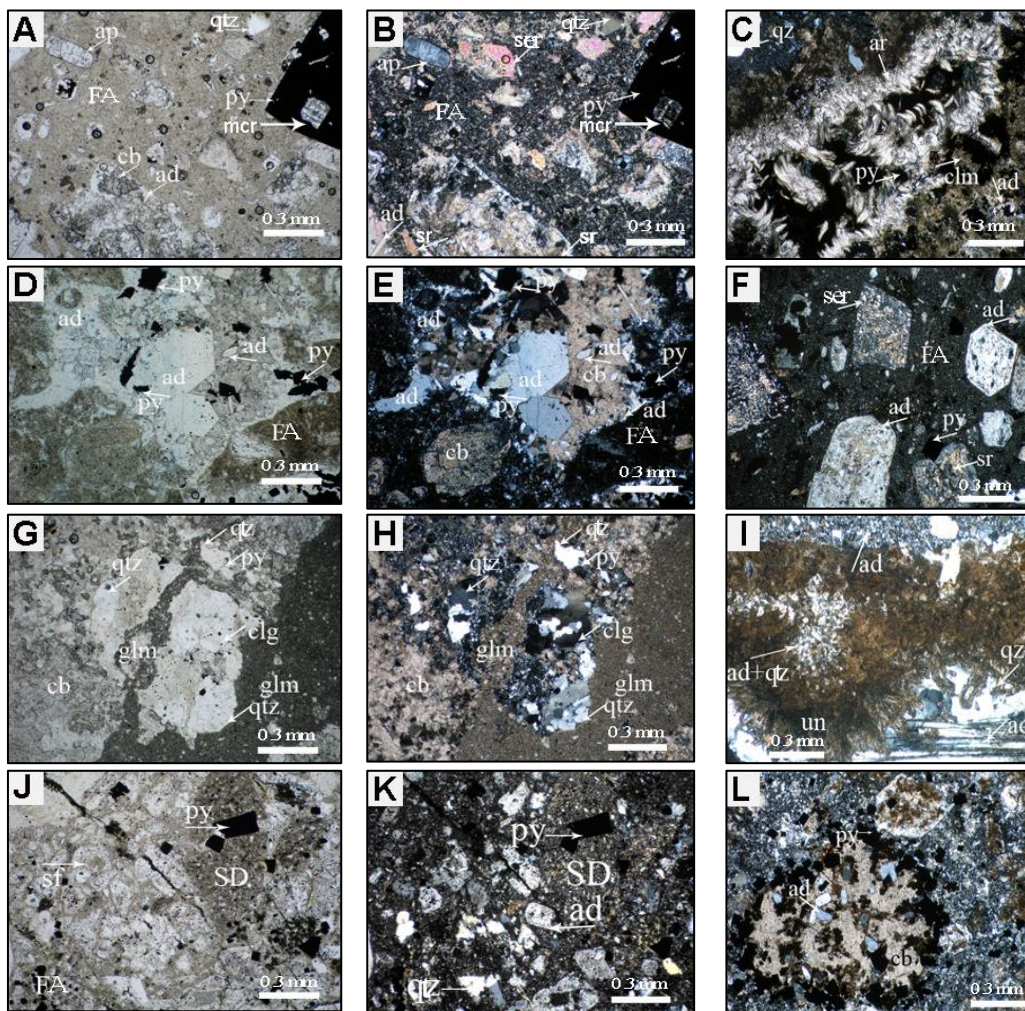
Hydrothermal alteration in Bucium Rodu-Frasin area is pervasive and widespread throughout the volcanic structure and surrounding Cretaceous formations. Altered rocks contain multiple overprinted hydrothermal mineral assemblages, as well as minerals formed by weathering. Five main types of hydrothermal alteration were distinguished (Fig. 2, 3): propylitic, potassic, phyllic, carbonatization and silicic. Argillic alteration is present just locally.

**Propylitic alteration:** At the surface, this alteration type was recognized in the andesite dike on the right side of Abruzel River and in the south-eastern half of the Frasin quartz-andesite flow dome. Its color is greenish and carbonate, chlorite and minor amounts of albite, sericite, epidote, pyrite and rutile are the most common new mineral assemblages. The Ca-plagioclase is replaced by albite ± chlorite, calcite, and epidote. Pyrite, chlorite, calcite, epidote and rutile replaced hornblende and biotite.

**Potassic (Adularia) alteration:** This alteration type is quite widespread. Its main characteristic is a total or partial replacement of plagioclase and mafic minerals by adularia, sericite and carbonates ± quartz and

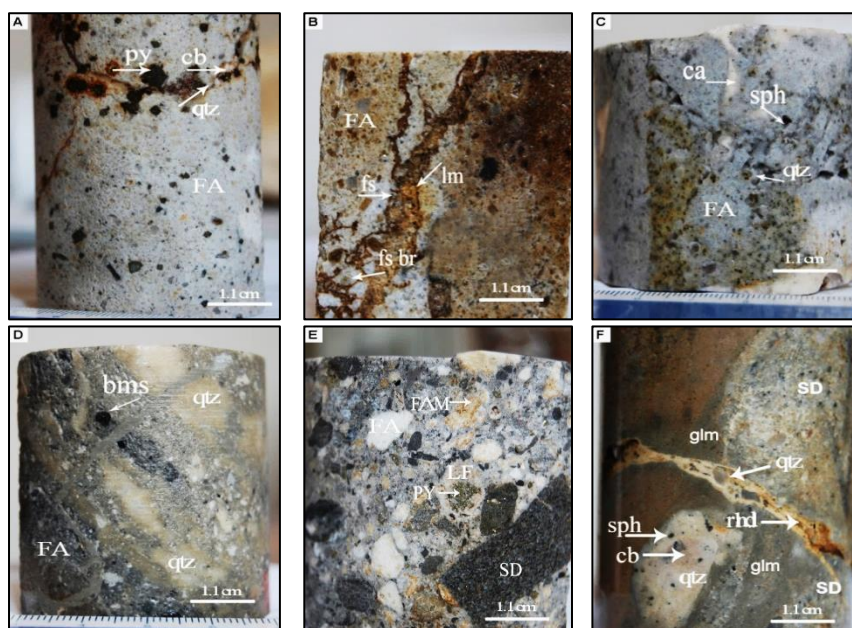


pyrite - rutile; the initial rock textures are preserved. The adularia processes seem to have evolved in stages II and III of ore deposition, characterized by following major mineral assemblages (Fig. 2, 3): arsenopyrite (Au?) - base metal sulfides - quartz - sericite - chlorite - adularia and pyrite (Au) - quartz - adularia in stage II and Au - base metal sulfides - carbonates - quartz - adularia with alabandite - rhodochrosite - quartz - pyrite characteristic for stage III. In stage II the feldspar and mafic phenocrysts were substituted by adularia (ad I  $\pm$  sericite), calcite and pyrite (Fig. 2A-B, F, K), while the III<sup>rd</sup> stage gave birth to quartz - adularia (- ad II), sericite, carbonates, pyrite  $\pm$  base metal sulfides, gold and rutile mineral assemblage (Fig. 2D- E, K, F, I).



**Fig. 2.** The ore textures and mineralogy of some samples from Bucium Rodu and Frasin gold deposits. A. (N II) and B. (N +). Frasin quartz andesite (FA) with porphyritic and cryptocrystalline groundmass textures. Phenocrysts replaced by adularia (ad), sericite (ser), clay minerals (clm), carbonates (cb) and pyrite (py) (Stage II); C. (N +). Frasin andesite with glassy groundmass and fissure partially filled with aragonite (ar), clay minerals (clm) and pyrite (py) (Stage III); D. (N II) and E. (N +) Vug of jigsaw-fit andesite filled up by quartz (qtz), carbonate (cb), pyrite (py) and adularia II (Stage II); F. (N +). Glassy Frasin andesite (FA) with phenocrysts replaced by adularia (ad), sericite (ser) and pyrite (py) (Stage II); G. (N II) and H. (N+): Polymictic lithoclast breccias with ash clasts. Conglomeratic clast (cgl) consisting of quartzite (qtz), glassy ash clasts and elongate cylindrical glassy vesicles (gvs) filled with quartz, cross-cut by a “glam” (local mining term) fissure (glm). Carbonates (cb), quartz (qtz) and pyrite (py) replace clasts and breccia matrix. I. (N +) Polymictic reworked breccia (Stage II) with a fissure filled with kutnahorite, quartz (qtz) and adularia II (Stage II); J. (NII) Polymictic breccia with interclast relict classical vesicles – spherulites (sf). K. (N+) adularized (ad) vesicles-spherulites and phenocrysts of glassy ash, marginal volcanic sandstone clast (SD) (Stage II); L. (N +). Lithophysae filled with carbonates (cb), adularia (ad) and pyrite (py) in porphyritic quartz andesite clast matrix (Stage II). N II = plane-polarized light; N + = cross-polarized light; all scale bars are 0.3 mm.

*Phyllic alteration* seems to be younger than adularia alteration. Adularia is overprinted, in various amounts, by sericite. The maximum intensity of this alteration type occurs within mineralized zones situated at the eastern contact of Frasin andesite dome with polymictic breccias, as well as in Rodu area. In these areas, there are fine to medium foliated sericite (illite) aggregates, in various percentages, plagioclase and/or adularia remnants (Fig. 2A, B, F).



**Fig. 3.** Photographs of some representative core slabs showing the alteration - mineralization stages: A. F1, D 019, m 453.72-473.80. Fissure filled with oxidized pyrite (py), quartz (qtz) and carbonates (cb) in porphyritic Frasin quartz andesite (FA) (stage II); B. D 030, m 94.40-94.45. Fissure (fs) with breccia (br) texture cemented by limonite (lm) in FA (Stage I); C. D 039, m. 107.32-107.37. Stockwork mineralization: sphalerite (sph), quartz (qtz) and carbonates (cb) in vugs of jigsaw-fit texture in fine, moderately porphyritic FA (Stage II); D. D 023, m. 105.85-105.90. A fracture with reworking breccia and bedded texture mineralized with (bms) and quartz (qtz), cut by a (glm) fissure (Stage II + I). E. D 053 A. m. 226-226.05. Massive reworking hydrothermal polymictic breccia with subangular and rounded (FA) clasts altered and mineralized (FAM). Pyrite (py) in lithophysae and angular sandstone (SD) in lithic supported matrix (Stage I?). F. D 005, m. 186.90-186.95. An older "glam" vein and younger vein filled with (qtz), (cb) and (sph) (Stage II), both cut by rhodochrosite (rhd) and (qtz) fissure (Stage III).

Carbonatization is subsequent to the adularia and phyllic alterations and in the mineralized zones it is the most widespread. Carbonatization displays a two stages evolution. Partial sometimes up to 60-70% replacement took place in the stage II, feldspar and feric minerals of the quartz-andesite, breccia clasts and Frasin quartz andesite body (Fig. 2A-B) being replaced with fine- to medium-grained carbonates as calcite, ankerite and pyrite. The stage III of alteration is recognized by the presence of lithophysae, veins and veinlets with fine- to large-grained carbonates (calcite, dolomite, aragonite, rhodochrosite) and  $\pm$  quartz, precious metals, base metals sulfides, alabandite, rutile, iron and manganese hydroxides (Fig. 2C-E, G, H; 3C, F).

Silicic alteration displays close relationships to the direct pathways of the ore fluids. Its products consist of amorphous silica as dark-grey small fissures and "Chinga" veins and white-brown fine grained quartz crystals  $\pm$  adularia, sericite, pyrite and argillic minerals (Fig. 3D, F).

Argillic alteration: The origin of the argillic alteration products is epigenetic, diagenetic and supergene, the clay minerals outlying, in the mineralized zones, the adularia-sericite and phyllic alteration zones.

White, (2003, in Leary et al., 2004), relying on mineralized zones petrology data, identified two types/phases of alteration: 1. adularia-clay illite-smectite - carbonate Mg-calcite  $\pm$  kutnahorite  $\pm$  rhodochrosite  $\pm$  silica alteration; and 2. later carbonate dolomite  $\pm$  siderite - kaolinite alteration, due to a low salinity bicarbonate fluid.

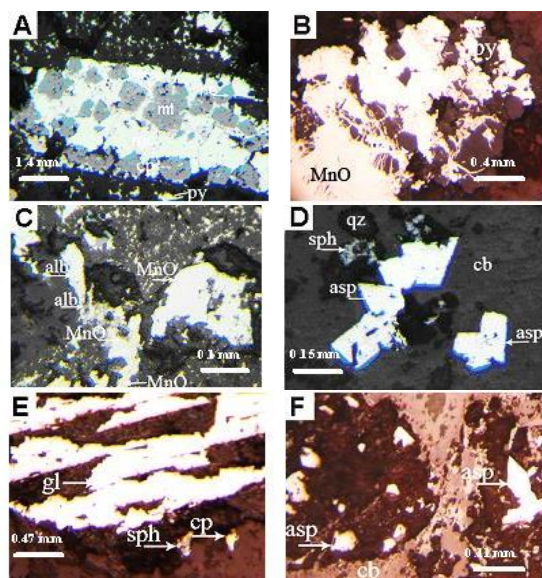
### Mineralization

In Bucium Rodu-Frasin area the Au-Ag-base metals mineralization occurs in close genetic relationships with the hydrothermal breccias and phreatomagmatic fracturing. The high-grade mineralization was present mainly in gently dipping veins. Major veins, as in the case of Rodu area, are partly paralleled by preexisting faults. The veins include carbonates, quartz, along with minor pyrite, sphalerite, galena, chalcopryrite, tetrahedrite and gold. Magnetite with minor hematite and sulfides mineralization, probably formed in the mesothermal conditions (?) has been recognized only as metasomatic substitutions of a probable Cretaceous limestone clasts fragmented from the depth.

According to the mineral parageneses, homogenization temperatures and free gold abundance, the mineralization has been considered by White (2003, in Leary et al., 2004) and Szentesy et al., (2004) as LS epithermal style; we think that it probably passes, at larger depths, into the mesothermal domain, or even

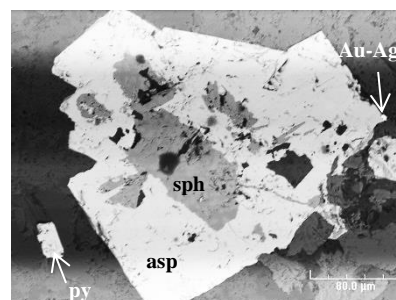


into skarn in Cretaceous limestone. The ore has been apparently emplaced in subsurface and subaerial conditions. It is situated in the more permeable polymictic breccias at the shallow levels of the Rodu-Frasin maar-diatreme complex structure. In addition, it is present within and immediately adjoining the Frasin quartz-andesite dome, as well as in Cretaceous sediments. The mineralization can be classified, according to the deposition forms, in the following styles: 1) vein which cut the Frasin quartz-andesite dome and volcanoclastic breccias in the Rodu maar-diatreme and Cretaceous sediments; 2) disseminations and hydrothermal breccia in maar-diatreme breccias, quartz-andesite bodies and Cretaceous sediments and 3) stockworks in the Frasin quartz-andesite dome and the contact breccias.



**Fig. 4.** Reflected light photomicrographs of some ore minerals from Rodu and Frasin deposits. A. (N+) Frasin quartz andesite (FA) replaced by euhedral and subhedral coarse-grained magnetite (mt), less substituted by hematite and cemented by marcasite aggregates (mc) and py (stage I); B. (N+) A vug in FA filled with manganese and iron oxides, pyrite and hydrothermal quartz (qtz) (Stage III); C. (N+). Alabandite (alb) near total replaced by manganese oxides (MnO) (Stage III); D. (N +) Fissure filled with arsenopyrite (asp), carbonates (cb), quartz (qtz) and sphalerite (Stage II); E. (N+) Galena (gl), chalcopyrite (cp) and sphalerite (sph) grains, disseminated in polymictic breccia (Stage II). F. (N+) Arsenopyrite (asp) euhedral crystals within lithophysae clast (Stage II).

Mineral	Zn (Wt%)	As (Wt%)	Fe (Wt%)	S (Wt%)	Au (Wt%)	Ag (Wt%)	Sum (Wt%)
Sphalerite	34.20	0.00	2.30	62.12	0.80	2.30	99.42
Pyrite	2.97	0.23	31.06	62.55	2.85	0.00	99.66
Pyrite	2.74	0.27	29.45	63.42	3.94	0.00	99.82
Arsenopyrite	3.55	15.84	36.19	42.59	1.10	0.00	99.26
Arsenopyrite	2.05	16.20	36.91	42.86	1.65	0.00	99.67
Electrum	0.11	0.00	0.22	0.00	72.62	26.62	99.57



**Fig. 5.** SEM image (right) and SEM-EDS analysis (table, left) of “electrum” (Au-Ag)-arsenopyrite (asp)-sphalerite (sph)-pyrite (py) assemblage.

The ore deposition had a pulsating character (Fig., 3A-D, F) with the evolution occurring, probably, in three stages to which the following mineral assemblages were associated (Fig. 4): a) magnetite (hematite) - pyrite (marcasite) -quartz and pyrite - quartz  $\pm$  base metal sulfides in the first stage (mesothermal?) (Fig. 10A); b) arsenopyrite - Au -base metal sulfides - quartz - adularia (Fig. 4 D), “Chinga” pyrite - Au - quartz - adularia and base metal sulfides - carbonates (calcite, aragonite, dolomite, ankerite,  $\pm$  rhodochrosite  $\pm$  kutnohorite) - quartz - adularia, in the epithermal low sulfidation - second stage (Fig. 4 E) and c) quartz - pyrite - marcasite - carbonates (dominant rhodochrosite) - Au and alabandite - rhodochrosite - quartz in the third, epithermal low sulfidation stage.

**Veins:** The pyrite-base metal sulfides-gold-carbonates (calcite, dolomite, rhodochrosite, aragonite)-quartz- adularia vein style is especially present in the Rodu maar-diatreme, where it occurs as single veins or/and vein sets, sometimes accompanied by Au - Ag disseminations and hydrothermal breccias. The veins usually have NW-SE strikes and N-S trends, show an “en échelon” tension veins distribution, being related to late normal movement on steeply east-dipping faults (Hewson et al., 2005). The most important veins are: Sperlea, Scaunul Camarii and Scaunele Bradului, Crucile Bradului and Buhaiului” (Ghitulescu and Socolescu, 1941).

**Disseminations and breccias:** These mineralization styles occur especially on restricted areas of the Rodu shallow-dipping maar-diatreme polymictic breccias and surrounding Cretaceous sediments, and also in shallow-dipping polymictic quartz-andesite breccias situated along the eastern contact of the Frasin andesite dome (Fig. 1). Some parts of the breccias show evidence of multiple events of brecciation, cementation and reworking (Fig. 3E).

**Au-Ag stockwork mineralizations:** The gold is present in various proportions, either as small grains or as sub-microscopic occurrences, within all Rodu-Frasin Au-Ag -base metal sulfide mineralization styles. The individual gold grains in native state have been observed as thin sheets on pyrite, sphalerite and quartz grains or as short wires, and sheets in geodes. It is accompanied by pyrite, sphalerite, calcite, rhodochrosite and quartz. Local gold concentrations are also common at the intersection zones of the so called “chairs” (“scaune”) veins with “crosses” (“cruci”) veins. According to White (2003, in Larry et al., 2004) and confirmed by our study (Fig. 5) the gold has been geochemically identified as “electrum”.

## Conclusions

The Neogene geologic evolution of the Bucium Rodu-Frasin magmatic-hydrothermal system took place in close relationships with the tectonic, magmatic and metallogenetic activity in the Bucium-Rosia Montana-Baia de Aries district. The ore occurs in a structurally complex environment, typically with some generations of faults or fractures oriented in two or more directions. Ore minerals consist roughly of sulfides, gold, carbonates, adularia and quartz. They have been prevalently emplaced as veins, breccia bodies and disseminations in open fractures and breccias in the Rodu diatreme, and as stockworks, veins and disseminations in relationship to the Frasin dome structure.

**Acknowledgments:** The authors show their gratitude to S.C. Roșia Montană Gold Corporation S.A. especially to Mr. Adrian Minuț, for the logistic support in the field, and for the access to the primary data. Also, we thank Prof. Dr. Essaid Bilal and Ecole Nationale Supérieure des Mines of Saint-Etienne (France) for the help with SEM-EDS analysis. This study was partially supported by the 29 PCCDI/2018 “GEORES” research project financed by UEFISCDI, Romania.

## References:

- Balintoni I. (1994) Structure of the Apuseni Mountains. Rom. J. of Tectonics and Regional Geology, 72, p. 51-58, Bucuresti.
- Berbeleac I., Nutu-Dragomir M.-L., Udubasa S.S. (2016) Miocene maar and flow dome complex structures from Bucium Rodu and Frasin, Metaliferi Mountains, Romania. Rom. J. of Mineral Deposits, 89/1-2, p. 59-64.
- Borcoș M., Vlad S.N. (1997) Late Tertiary epithermal systems in the Romanian Carpathians. IGCP Project no. 356 – Stip, Macedonia.
- Cioflica G., Jude R., Berbeleac I., Jude R., Udubasa S.S. (2002) Types of gold mineralization in Romania. Geologica Carpathica, 53, Special Issue (on-line), Bratislava.
- Ghitulescu T. P., Socolescu M. (1941) Étude géologique et minière des Monts Metallifères. An. Inst. Geol. XXI, p. 181-464, Bucuresti.
- Hewson N., Leary S., Feier N. (2005) Tarina and Rodu: Gold mineralization hosted in maar-diatreme contact environments in the Apuseni. Mountains, Romania. Au-Ag-Te-Se deposits - IGCP Project 486, Field Workshop, Kiten, Bulgaria, 14-19 Sept 2005. Bulgarian Academy of Sciences Geochemistry, Mineralogy and Petrology, 43, 2, p. 94-101, Sofia.
- Ianovici V., Borcos M., Bleahu M., Patrușiu D., Lupu M., Dimitrescu R., Savu H. (1976) Geologia Munților Apuseni. Ed. Acad. Republicii Socialiste. Romania, 631 p., Bucuresti
- Leary S.F., O'Connor G.V., Howie K., Nădăsan L. (2004) The Rodu-Frasin Deposit. In: Cook N.J., Ciobanu C.L. (Eds.) Gold-Silver-Telluride Deposits of the Golden Quadrilateral, South Apuseni Mts., Romania. IAGOD Guidebook, Series 12, p. 99-104.
- Nadasan L., Hewson J.N. (2005) Relogging of the Rodu vent breccia. RMGC Internal Technical Memorandum.
- Rosu E., Pécskay Z., Stefan A., Popescu G., Panaiotu C., Panaiotu, C.E. (1997) The evolution of the Neogene volcanism in the Apuseni Mountains Romania: Constraints from new K-Ar data. Geologica Carpathica 48, 6, p. 353-359.
- Sandulescu M. (1984) Geotectonica Romaniei. Ed. Tehnica, 366 p., Bucuresti.
- Seghedi I., Downes H. (2011) Geochemistry and tectonic development of Cenozoic magmatism in the Carpathian-Pannonian region. Gondwana Research 202011 p. 655-672.
- Szentesy C., Minut A., O'Connor G. (2004) Exploration progress on Bucium Rodu Frasin gold deposit. Fourth National Symposium on Economic Geology “Gold in Metaliferi Mountains” 3<sup>rd</sup>-5<sup>th</sup> September 2004, Alba Iulia. Rom. J. of Mineral Deposits, 81, p. 186-187.

## NEOGENE DISTAL SKARN MINERAL ASSEMBLAGE FROM RUDA BRAD, APUSENI MOUNTAINS, ROMANIA

Călin G. TĂMAȘ<sup>1\*</sup>, Paul IVĂȘCANU<sup>2\*\*</sup>, Gabriela BENA<sup>2</sup>, Laurențiu IGNA<sup>2</sup>, Nicolae HAR<sup>1</sup>

<sup>1</sup> Babeș-Bolyai University, Department of Geology, 1, M. Kogălniceanu str., 400084, Cluj Napoca, Romania

<sup>2</sup> Deva Gold, 89, Principală str., 337190, Certeju de Sus, Romania

\* *calin.tamas@ubbcluj.ro*; \*\* *paul.ivascanu@eu.eldoradogold.com*

**Abstract:** Skarn-type mineral assemblage linked to Neogene volcanism and consisting of garnet, vesuvianite, actinolite, chlorite, brucite, hematite, magnetite and calcite was identified by optical microscopy and X-ray diffraction in drill core samples from Ruda Brad, Apuseni Mountains. On the basis of spatial relationships to the igneous source the identified mineral assemblage is interpreted as a distal skarn occurrence.

**Keywords:** garnet, vesuvianite, brucite, hematite, distal skarn, Neogene, Ruda Brad, Apuseni Mountains, Romania

### Introduction

The Neogene skarns represent an unusual mineral assemblage occurrence in Romania as compared to Laramian skarns. An overview of the Neogene skarns in Romania was made by Mârza (1992), who noticed that there are two types of skarn-related mineralizations, *i*) skarn occurrences related to carbonate replacement/manto deposits, *e.g.* Valea Vinului and Cobășel from Rodna Veche, and Baia de Arieș; *ii*) skarn occurrences not related to carbonate replacement/manto deposits, *e.g.* Țibleș and Băiuț. The present work reports the first Neogene related distal skarn mineral assemblage from Brad-Săcărâmb metallogenetic district, which was discovered in Ruda Brad area.

### Regional geological setting

Ruda Brad area belongs to Brad-Săcărâmb metallogenetic district from the South Apuseni Mountains, Romania. Due to its elevated economic and scientific importance, this Neogene metallogenetic district was intensely studied and various aspects of its geology were presented by many authors, *e.g.* Ghițulescu and Socolescu (1941), Ianovici et al. (1969 and 1976), Roșu et al. (1997, 2004), Udubașa et al. (2001), etc. According to the above mentioned and many other authors, the basement is represented by Middle Jurassic-Lower Cretaceous ophiolites, which are covered by Maastrichtian-Palaeocene (Borcoș et al., 1989)/Palaeocene (Borcoș et al., 1998) and Miocene sedimentary rocks. The associated Neogene volcanic activity started around 14.7 Ma and ended at about 10.5 Ma being followed by a late pulse at 1.6 Ma (Roșu et al., 2004). Significant Au-Ag and Cu ore deposits (epithermal and porphyry) formed in connection to the Neogene volcanism.

### Local geology

The samples used in this research have been collected from the northern extension of the Ruda vein system at depth of over 350 m below the Ruda valley floor, where the fault-controlled vein system and associated andesitic dikes intercept a significant body of Maastrichtian-Palaeocene sedimentary rocks (coarse to medium grained clastic unit) overlying the Jurassic ophiolite sequence. Skarns are formed both on the massive limestone clasts (reworked Jurassic limestones) and/or on the carbonate rich matrix of the sedimentary units (conglomerates to greywackes). While early stage skarns are relatively restricted, important carbonate replacement-style mineralization (related to lower temperature epithermal stage hydrothermal activity) is observed as low grade disseminate and stock-style mineralization, resembling similar setting observed at Certej.

### Materials and methods

Several drill core fragments were selected from drill cores based on preliminary macroscopic and hand-lens observations. The material was used for optical microscopy in transmitted and reflected light. X-ray diffraction was used for the identification of a mineral species from the garnet group using a Bruker D8 Advance diffractometer with Cu  $K\alpha$  radiation ( $\lambda = 1.541874 \text{ \AA}$ ) and a LynxEye detector from the Department of Geology, Babeș-Bolyai University, Cluj-Napoca, Romania.

## Results

The studied samples were selected from a matrix-supported coarse siliciclastic sequence with carbonate pebbles up to 3 cm across (Fig. 1). Some of these pebbles were replaced by a mineral assemblage that contains black needle-like crystals accompanied by light brown isometric crystals and pyrite associated to relict calcite (Fig. 2).



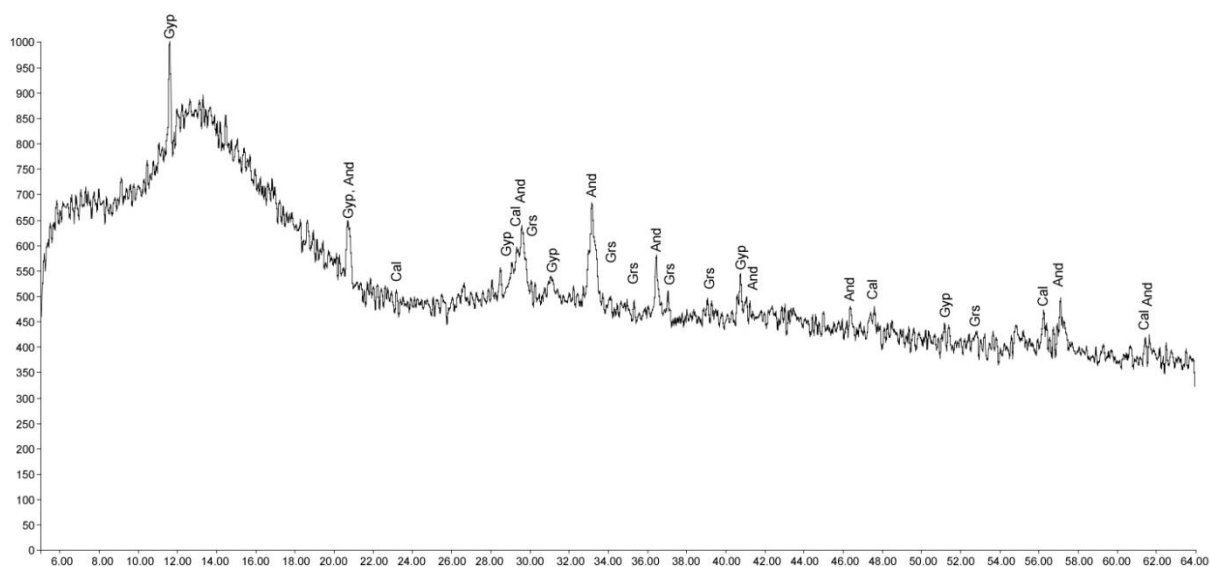
**Fig. 1.** Matrix-supported conglomerate with carbonate pebbles; dimensions of the sample: 6.5 x 5.5 cm.



**Fig. 2.** A nest composed of remnant calcite, black needle-like crystals, light brown isometric crystals and pyrite; approx. dimensions of the field view: 4 x 3 cm.

## XRD data

Several light brown crystals were separated for an XRD analysis that facilitated the identification of andradite ( $\text{Ca}_3\text{Fe}_2(\text{SiO}_4)_3$ ), grossular ( $\text{Ca}_3\text{Al}_2(\text{SiO}_4)_3$ ), gypsum and calcite (Fig. 3).



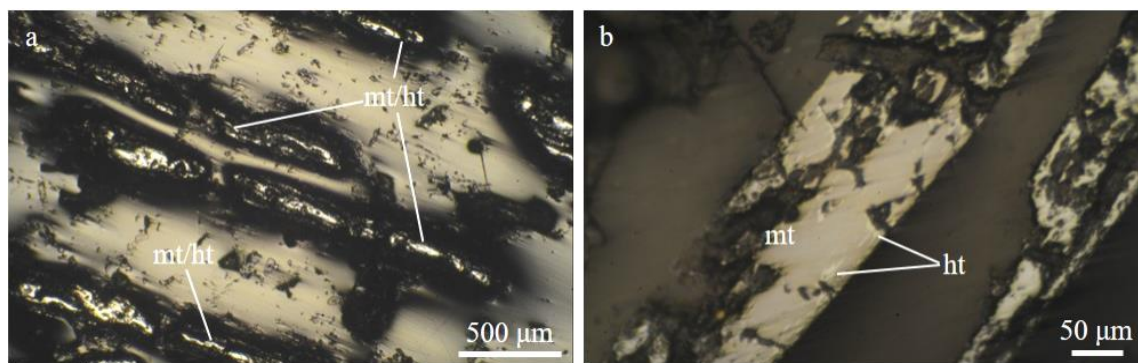
**Fig. 3.** The X-ray diffraction obtained for the sample selected from the light brown isometric crystals visible in Fig. 2 confirms the occurrence of andradite (And) and grossular (Grs) accompanied by calcite (Cal) and gypsum (Gyp).

## Ore microscopy

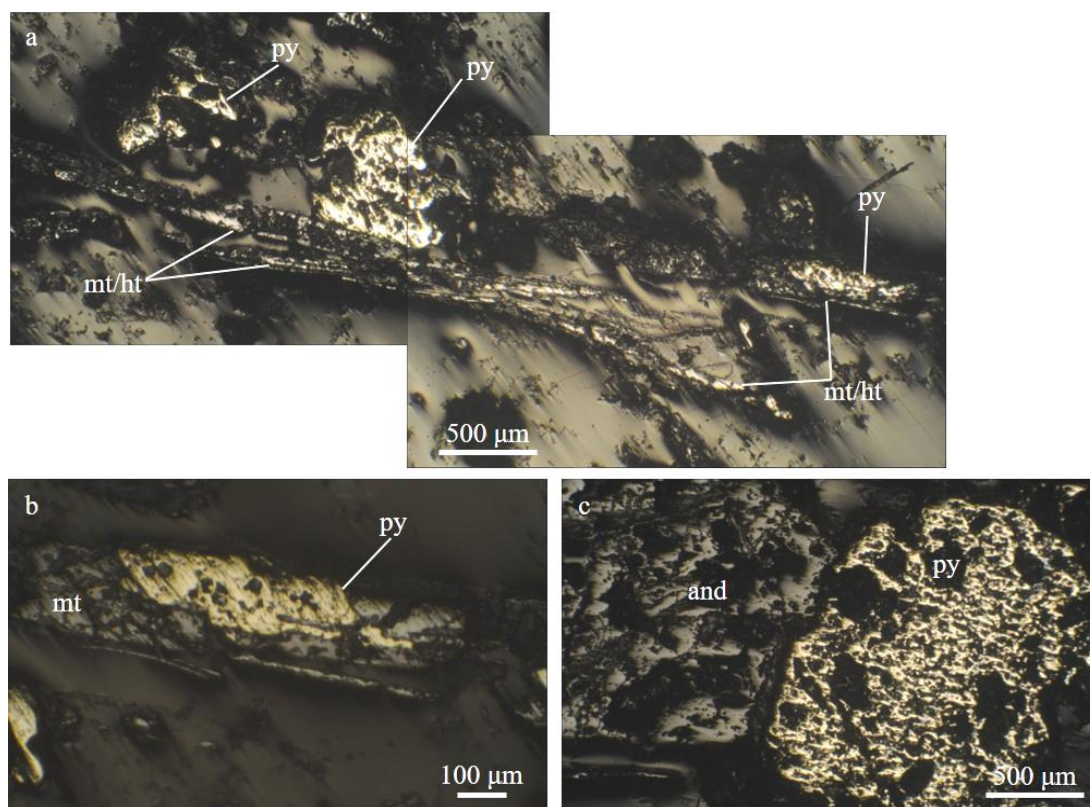
The ore microscopy study revealed the mineralogy of the black needle-like crystals (Fig. 4a-b). The shape of these crystals is characteristic for hematite, but their optical properties are those of magnetite. At higher magnification minute hematite relics are visible in magnetite being preserved within the needle-like crystals (Fig. 4a,b). These observations indicate the replacement of hematite by magnetite or the so-called muschetovitization.

Pyrite crystals or crystal groups are sometimes deposited on magnetite lamellae (Fig. 5a) or they may be intergrown with magnetite (Fig. 5b). Euhedral large-sized pyrite crystals are also related to euhedral garnet/andradite crystals (Fig. 5c).





**Fig. 4.** Photomicrographs in plane polarized reflected light that reveal the relationships between magnetite and hematite. a) General view of the needle-like crystals hosted by the calcite gangue; b) detail of a lamella that contains hematite relics hosted by magnetite. Abbreviations: ht-hematite; mt-magnetite.



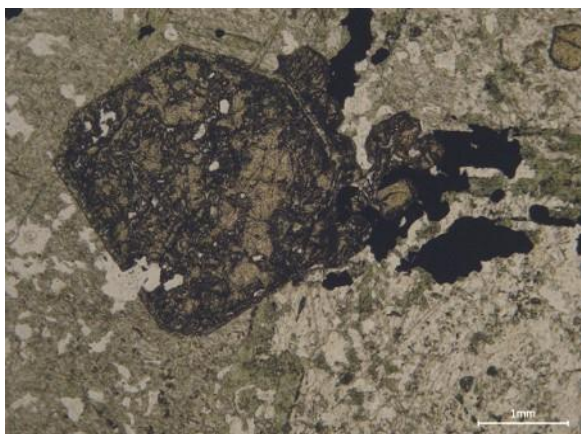
**Fig. 5.** Photomicrographs in plane polarized reflected light of magnetite/hematite – pyrite mineral assemblage. a) General view of needle-like hematite crystals almost entirely transformed in magnetite (muscovitization) intergrown with pyrite; b) detail of (a) that shows pyrite intergrown with magnetite, previously hematite; c) pyrite-andradite assemblage. Abbreviations: and-andradite; ht-hematite; mt-magnetite; py-pyrite.

### ***Transmitted light microscopy***

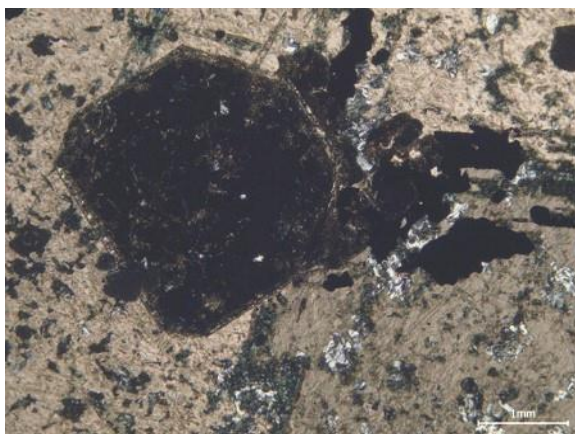
The transmitted light microscopy allowed the identification of the transparent minerals associated to hematite-magnetite and pyrite. The garnets occur as characteristic octagonal euhedral crystals with high relief, brown color and isotropic character (Fig. 6 and 7). They are hosted by calcite and are associated to chlorite (Fig. 6 and 7), vesuvianite (Fig. 8 and 9), and brucite (Fig. 10 and 11).

The garnet growth was sequential with at least two main growth stages (Fig. 8 and 10). The first garnet generation - garnet I consists of euhedral octagonal crystals several millimeters across (Fig. 6 and 8), which show homogeneous optical properties. However, they show sometimes parallel growing zones towards their border (Fig. 10). This garnet generation was followed by vesuvianite, which occurs as a complete rim around the already formed garnets (Fig. 8 to 11). The vesuvianite rim was partly covered by a new garnet generation deposited outward towards the calcite host (Fig. 8 to 11). This later garnet generation - garnet II consists of smaller sized, less than 1 mm in size, anhedral to subhedral crystals or crystal aggregates. The first garnet generation may possess an outward zoning that reflect the growth zones (Fig. 10), while the second one shows no zoning (Fig. 8 and 10).

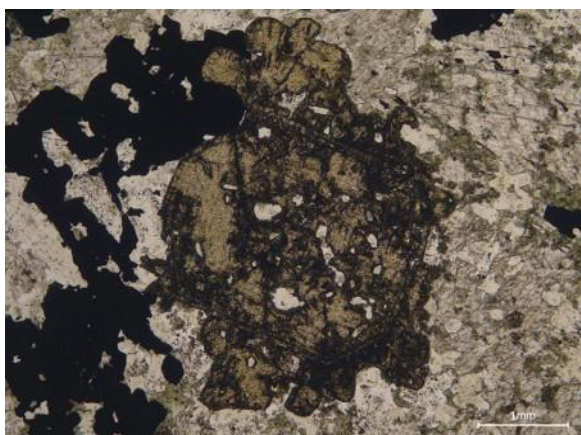




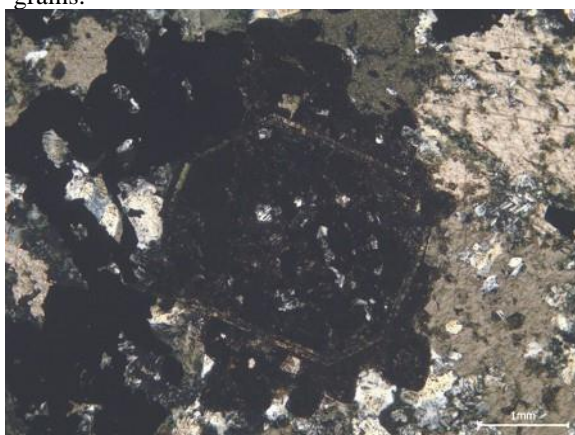
**Fig. 6.** Euhedral brown octagonal garnet/andradite crystal hosted by calcite and associated to chlorite.



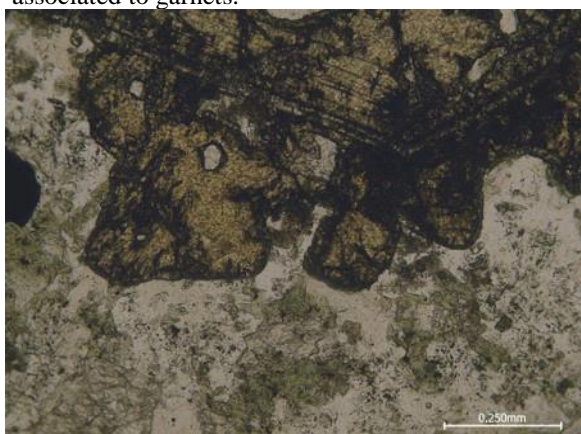
**Fig. 7.** Same image as Fig. 6 in crossed polarizers light (XPL), which presents the isotropic character of the garnet and shows the large size of calcite grains.



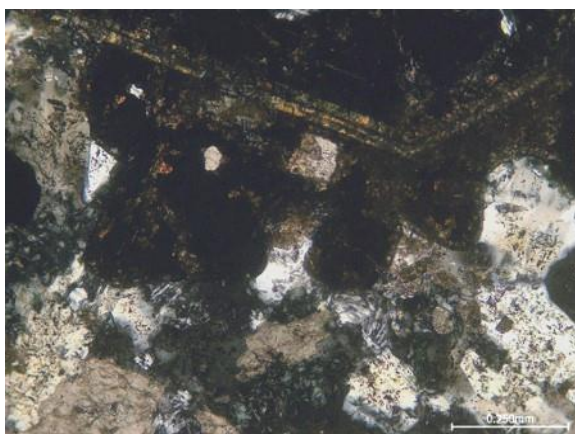
**Fig. 8.** Garnet nest composed of a euhedral octagonal central part-garnet I, surrounded by a vesuvianite rim, and outer subhedral garnet grains-garnet II. Calcite, chlorite and metallic minerals are associated to garnets.



**Fig. 9.** Same image as Fig. 8 (XPL), which presents the anisotropic vesuvianite rim that separates the two garnet generations.



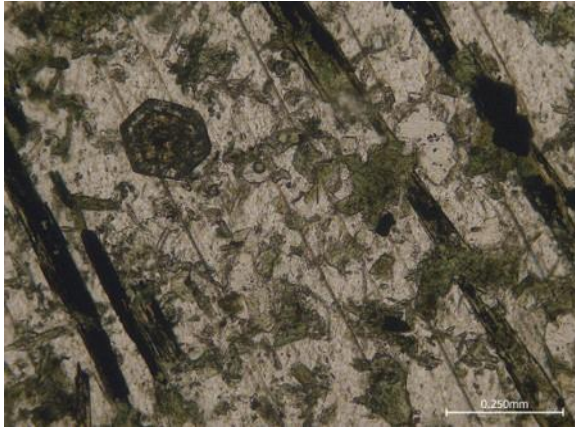
**Fig. 10.** Detail of Fig. 8 that shows the zoning of the garnet I, the anhedra/subhedral garnet II grains, and the continuous vesuvianite rim that separates the two garnet generations.



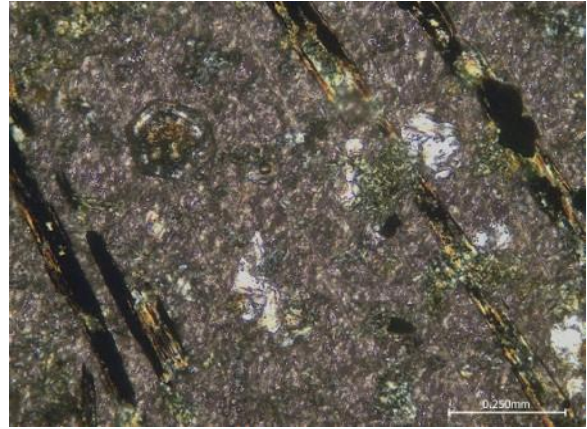
**Fig. 11.** Same image as Fig. 10 (XPL), detail of Fig. 9 that confirms the paragenetic sequence garnet I, vesuvianite, garnet II, and the associated gangue minerals, *i.e.* calcite, chlorite, and brucite.

Vesuvianite is also denominated hydro-garnet due to its optical properties and chemical composition resemblances with those of garnets. In the examined thin section, vesuvianite occurs as outer rim of the garnet I generation and as characteristic euhedral hexagonal zoned crystals (Fig. 12 and 13). Vesuvianite is hosted by large sized calcite grains, which also contain chlorite and brucite. Sometimes, vesuvianite

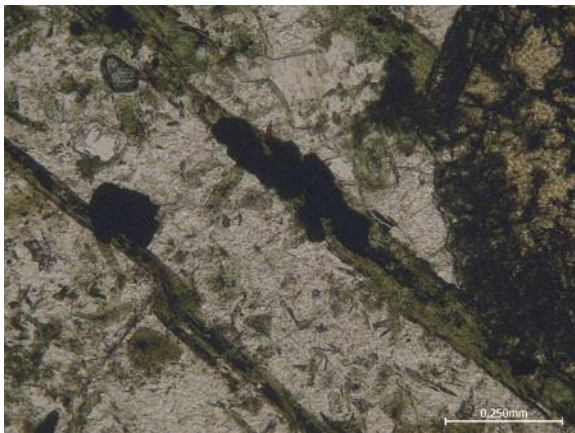




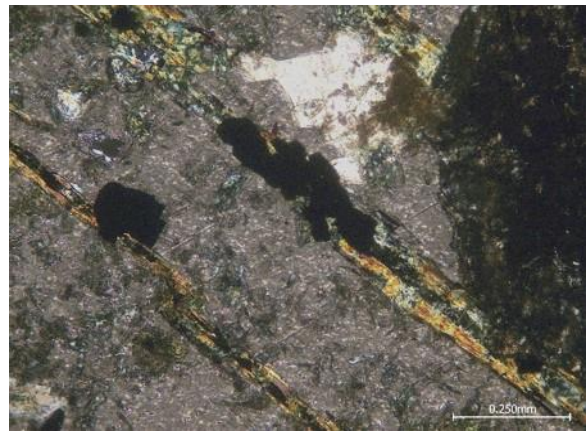
**Fig. 12.** Euhedral vesuvianite crystal with specific zoning; note the presence of Fe-oxides (black needle-like crystals), chlorite and brucite hosted by calcite.



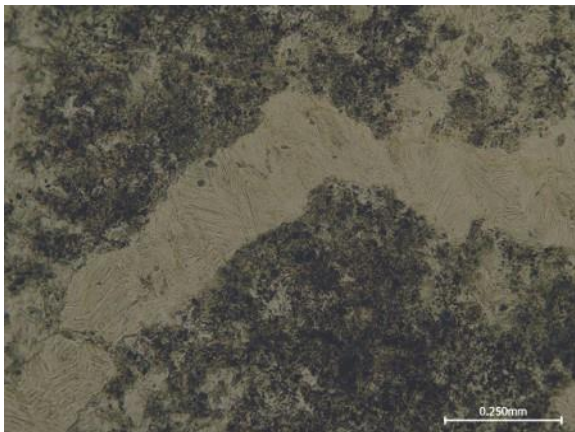
**Fig. 13.** Same image as Fig. 12 (XPL) that confirms the anisotropy of vesuvianite euhedral crystal and the presence of brucite hosted by calcite.



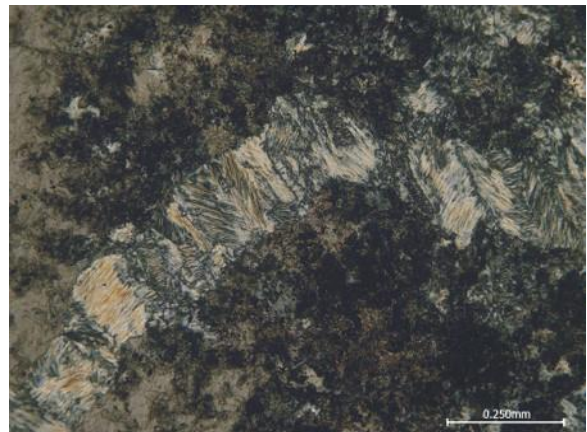
**Fig. 14.** Actinolite needle-like green crystals hosted by calcite and abutting to a garnet.



**Fig. 15.** Same image as Fig. 14 (XPL) that shows actinolite needle-like crystals associated to garnet, chlorite, and brucite and hosted by calcite. Note that the inner part of actinolite elongated crystals is replaced by chlorite and metallic minerals.



**Fig. 16.** Brucite vein that cuts calcite-chlorite mineral assemblage.



**Fig. 17.** Same image as Fig. 16 (XPL), with characteristic interference colours for calcite, chlorite and feathery morphology of brucite vein.

could be misinterpreted at microscope in plane-polarised light as garnet due to its hexagonal habit and high relief, but in cross-polarised light it is clearly anisotropic (Fig. 13). The needle-like hematite transformed in magnetite crystals is frequently associated to a green mineral that shows a higher relief than chlorite. According to its optical properties, this mineral (Fig. 14 and 15) is actinolite. It occurs as elongated crystals, sometimes with an inner spine-like zone replaced by chlorite. Actinolite is hosted by re-crystallized calcite and is frequently in contact to garnets.

Brucite occurs as small-sized grains hosted in re-crystallized calcite closely associated to other skarn-minerals, *e.g.* garnets, vesuvianite, hematite transformed in magnetite. It was also observed as monomineral veinlets that cut the skarn-mineral assemblage (Fig. 16 and 17). The maximum observed width of brucite veins is 3 mm.

## Conclusions

Hematite-magnetite±pyrite associated to garnet/andradite-grossular, vesuvianite, brucite, actinolite, chlorite, and calcite developed on carbonate pebbles from a matrix-supported conglomerate from Ruda Brad area under the influence of hydrothermal fluids related to Neogene volcanic activity. This mineral assemblage is a characteristic skarn association. Due to their position with respect to the igneous source, these skarn nests could be interpreted as small-scale distal skarn occurrences.

The exploration activity in Brad-Săcărâmb metallogenetic district allowed to discover other skarn and replacement-type mineral assemblages, usually of small-scale, *e.g.* Bolcana, Voia, and Certej. All these unexpected mineral assemblages within Brad-Săcărâmb area developed on Jurassic carbonate rocks or carbonate pebbles from Palaeocene-Miocene conglomerates affected by hydrothermal fluids derived from the Neogene magmatism. The skarn and the replacement mineral assemblages are controlled by the distance from the igneous bodies. However, skarn-related and replacement mineralization styles were until now completely ignored in the area even if the presence of carbonate rocks within the basement and the Neogene subvolcanic bodies represent favourable control factors for the genesis of such ore body types, which are completely covered today by Neogene volcanic and sedimentary units.

The recognition of favourable reactive units that could host carbonate replacement or even skarn style mineralization adjacent to the mined epithermal veins could become an interesting exploration target in Ruda-Barza area. Similar setting was found at Certej, where high grade replacement-style mineralization of basal limestone-bearing conglomerates (Palaeocene - Early Miocene) contributed to the increase of the ore reserves.

## References

- Borcoş, M., Roşu, E., Ştefan, A., Popescu, G. (1989) Le volcanism banatitic des Monts Apuseni (Romania). XIVth KBGA, Extended Abstracts, p. 194-197.
- Borcoş, M., Vlad, Ş., Udubaşa, G., Găbudeanu, B. (eds.) (1998) Qualitative and quantitative metallogenetic analysis of the ore genetic units in Romania. Rom. J. Mineral Deposits, 78, special issue, p. 1-158.
- Ghiţulescu, T.P., Socolescu, M. (1941) Etude géologique et minière des Monts Métallifères (Quadrilatère aurifère et régions environnantes). An. Inst. Geol. Rom., vol. XXI, p. 181-465, Bucureşti.
- Ianovici, V., Giuşcă, D., Ghiţulescu, T.P., Borcoş, M., Lupu, M., Bleahu, M., Savu, H. (1969) Evoluţia geologică a Munţilor Metaliferi. Ed. Acad., 741 p., Bucureşti.
- Ianovici, V., Borcoş, M., Bleahu, M., Patrulius, D., Lupu, M., Dimitrescu, R., Savu, H. (1976) Geologia Munţilor Apuseni. Ed. Acad., 631 p., Bucureşti.
- Mârza, I. (1992) Geneza zăcămintelor de origine magmatică. Vol. III, Petrometalogenia skarnului (pirometasomatoza), greisenului (pneumatoliza). Ed. Dacia Cluj-Napoca, 382 p.
- Roşu, E., Pécskay, Z., Ştefan, A., Popescu, G., Panaiotu, C., Panaiotu, C.E. (1997) The evolution of the Neogene volcanism in the Apuseni Mountains (Romania): constraints from new K-Ar data. Geologica Carpatica, 48, 6, p. 353-359, Bratislava.
- Roşu, E., Udubaşa, G., Pécskay, Z., Panaiotu, C., Panaiotu, C.E. (2004) Timing of Miocene – Quaternary magmatism and metallogeny in the South Apuseni Mountains, Romania. Rom. Journal Mineral Deposit: “Fourth National Symposium on Economic Geology – Gold in Metaliferi Mountains”, 3-5 Sept. 2004, Alba Iulia, Romania; p. 33-38.
- Udubaşa, G., Roşu, E., Seghedi, I., Ivăşcanu, P.M. (2001) The “Golden Quadrangle” in the Metaliferi Mts., Romania: what does this really mean? Rom. Journ. Mineral Deposits, v. 79, Suppl. 2, Geodynamics and ore deposit evolution of the Alpine-Balkan-Carpathian-Dinaride Province. ABCD – GEODE 2001, Workshop Vaţa Băi, Romania, 8-12 June, 2001, Abstract Volume, IGR, p. 3-23, Bucureşti.

## THE Fe CONTENT IN THE SPHALERITES FROM THE BREINER-BĂIUȚ DEPOSIT

Daniel BÎRGĂOANU<sup>1,2,\*</sup>, Gheorghe DAMIAN<sup>1,3</sup>, Andrei BUZATU<sup>1</sup>

<sup>1</sup> “Alexandru Ioan Cuza” University of Iași, 20A, Carol I Blv., 700505 Iași, Romania; \*birgaoanu.daniel@yahoo.com;

<sup>2</sup> Geological Institute of Romania, 1, Caransebes Str., 012271 Bucharest, Romania;

<sup>3</sup> Technical University Cluj-Napoca, North University Center Baia Mare, 62, Victor Babes Str., 433003 Baia Mare, Romania.

**Abstract:** The study of the iron content of natural sphalerites collected from the Breiner-Băiuț epithermal deposit was performed by combining analytical methods SEM-EDS and micro-Raman spectroscopy. For this study, sphalerites containing chalcopyrite “disease” and homogeneous sphalerites were used. Following SEM-EDS analyzes, iron contents ranging from 1.68 wt.% to 6.41 wt.% were obtained. For micro-Raman spectroscopy determinations, were used the specific iron peaks  $299\text{ cm}^{-1}$  and  $330\text{ cm}^{-1}$  and the specific zinc peak  $350\text{ cm}^{-1}$  identified in the obtained spectra. Based on these, the  $h_1/h_3$ ,  $h_2/h_3$  and  $(h_1+h_2)/h_3$  ( $h_1$ ,  $h_2$ ,  $h_3$  - intensities of the three peaks) ratios were used in the equations for the determination of FeS molar fractions. The results obtained are in agreement with the results obtained on the SEM-EDS method.

**Keywords:** sphalerite, iron, SEM-EDS, micro-Raman spectroscopy, chalcopyrite disease, epithermal, Breiner-Băiuț deposit.

### 1. Introduction

Sphalerite, one of the commonly sulphides found in the base metal deposits, has been studied in numerous papers for physico-chemical deposition conditions. This mineral is known for that it can often have important iron contents, which substitutes zinc from the crystalline chain. Compositional analyses have shown that besides iron, zinc can be substituted by cadmium and manganese, and rarely cobalt, nickel, copper, germanium and indium have been identified (McClung and Viljoen, 2011). Based on these aspects, some researchers have assumed that measuring the concentration of iron in the sphalerite can determine the conditions (temperature and pressure) of the mineral crystallization (Barton and Toulmin, 1966; Borman, 1967), but this still creates controversy because, comparing the obtained results with those of fluid inclusions studies, inconsistencies were observed (Borcoș and Iosof, 1966; McClung and Viljoen, 2011). According to Scott and Barnes (1971) in hydrothermal mineralizations, the FeS content from sphalerite can only be discussed in the relationship between sulphur fugacity and temperature.

Starting from these features of the sphalerite, researchers (Osadchii and Gorbaty, 2011; Buzatu et al., 2013) developed an efficient and rapid method for determining the iron content, based on the application of Raman spectroscopy. Numerous studies using this method on natural and synthetic sphalerites have highlighted a series of fundamental vibrations, represented by the longitudinal optical vibrational modes (LO) associated with the high intensity peak  $348\text{ cm}^{-1}$  and the low intensity peak  $668\text{ cm}^{-1}$ , and the transverse optical modes (TO) attributed to the high intensity  $272\text{ cm}^{-1}$  peak and the low intensity  $613\text{ cm}^{-1}$  peak (Hope et al., 2001; Buzatu et al., 2013). In addition to optical vibrational modes, acoustic vibrations were identified for  $216\text{ cm}^{-1}$  peak (longitudinal acoustic mode - LA) and  $177\text{ cm}^{-1}$  peak (transverse acoustic mode - TA) (Hope et al., 2001). The two vibration modes appear in some cases combined, with the following peaks:  $396\text{ cm}^{-1}$  (TO + TA),  $419\text{ cm}^{-1}$  (TO + LA),  $449\text{ cm}^{-1}$  (LO + LA) and  $637\text{ cm}^{-1}$  (LO + TO) (Hope et al., 2001; Buzatu et al., 2013). The specific peaks to the presence of iron in the sphalerite were identified at  $\sim 296\text{ cm}^{-1}$  and  $\sim 331\text{ cm}^{-1}$  (Hope et al., 2001). For the determination of iron from sphalerite using only the Raman spectra, Osadchii and Gorbaty (2010) took into account the  $\sim 295\text{ cm}^{-1}$  and  $345\text{ cm}^{-1}$  peaks and developed a method by which their relative intensity ratios were projected into a correlation diagram with the molar fraction of the iron, following a calibration curve. To simplify the method, Buzatu et al. (2013), used the mathematical apparatus and presented a series of equations to determine the Fe content, in which:  $y$  - the molar fraction of iron in the sphalerite structure, and  $x$  - the three ratios determined by the intensity of all three peaks ( $h_1$ - $300\text{ cm}^{-1}$ ,  $h_2$ - $331\text{ cm}^{-1}$  and  $h_3$ - $350\text{ cm}^{-1}$ ) specific for iron and zinc:

$$\begin{aligned}h_1/h_3: & \quad y = 0.038x + 0.0033; \\h_2/h_3: & \quad y = 0.0762x - 0.001; \\(h_1+h_2)/h_3: & \quad y = 0.02551x + 7.96 \cdot 10^{-4}.\end{aligned}$$

## 2. Geology and metallogeny of the area

The Breiner-Băiut vein system is located in the Băiut-Văratec-Poiana Botizei metallogenetic field and is a base metal hydrothermal deposit accumulated in the form of three parallel branches hosted by sedimentary formations, associated with porphyritic microdioritic subvolcanic intrusions, accompanied by hornfels and cataclastic rocks (Costin, 2000). As the case of the entire Baia Mare metallogenetic district, the formation of this hydrothermal deposit was attributed to neogene magmatic events, in the context of an island-arc area in the Eastern Carpathians (Vlad and Borcoş, 1998; Borcoş et al., 1998). Sedimentological and structural studies have highlighted the presence of sedimentary rocks of Jurassic, Cretaceous, Neogene age, but the most widespread are the Paleogene sedimentary rocks represented by mudshale interposed with sandstones called Tocila-Secu flysch. In the geological context of this metallogenetic field, a series of studies on local geology of petrology and present mineralizations, relevant to this study, were made by Dimitrescu and Bleahu (1955), Dragu and Edelstein (1968), Edelstein et al. (1971); Bombiță (1972); Manilici and Kalmar (1992); Gabor et al. (1999), Plotinskaya et al. (2012); Plotinskaya et al. (2014). Regarding the metallogenetic context of the Băiut and Robu veins from the Breiner-Băiut deposit, Borcoş et al. (1977), presented extensive mineralogical and geochemical studies, Damian and Costin (1999) published compositional data of present sulfosalts and Costin (2000) highlighted the presence of some major elements.

This deposit has two major veins (the Băiut vein and the Robu vein) and a smaller vein (the Petru and Pavel vein) arranged parallel to the ENE-VSV direction. The Băiut vein has 2 km length and thicknesses between 0.5 and 2 m, but it can reach up to 10 m, being placed in the Eocene flysch. From the texture point of view, this vein has breccia zones, massive and impregnated areas. The Robu vein is about 1.5 km long and is located in the Eastern part of the Băiut vein, which is about 450 m away. From a textural point of view, this vein is comparable to the Băiut vein, but there quartz geodes quite often appear with barite and stibnite (Borcoş et al, 1977). The two veins have numerous branches, of which Kelemen I and II and Ramura 90 belong to Băiut vein, and Ramura Robu, Ramura Robu Culcuş, Ramura IV Culcuş and Realgar are ramifications of the Robu vein. Because of the small size and lack of mineralogical diversity, the Petru and Pavel vein has been described less in literature.

From the mineralogical point of view, quartz, carbonates, adularia, clay minerals and barite were identified in this deposit, these being the group of the gangue minerals. From the group of metallic minerals, pyrite, chalcopyrite, sphalerite and galena have been identified and described, and arsenopyrite, marcasite, tetrahedrite, stibnite, bournonite, semseyite, jamesonite and iron oxides are also present in smaller quantities. Quite rarely, gold and electrum as very small sized grains have been described (Costin, 2000). The identified paragenetic relations, specific to the epithermal deposits, are pyrite-chalcopyrite-sphalerite-galena-quartz-calcite and pyrite-sphalerite-galena-quartz-calcite-barite (Borcoş et al., 1998). A special interest in this study is the sphalerite. It appears to be associated in particular with chalcopyrite, pyrite and galena, but it has also been identified as sphalerites bounded in carbonate. An important feature of this mineral is the content of the chalcopyrite “disease”, and rarely identifying homogeneous sphalerite. On this criterion, Plotinskaya et al. (2012), divided the sphalerites identified in the Cisma deposit into two generations: i) sphalerite-1, without “disease”, associated with the pyrite; and ii) sphalerite-2, with abundant chalcopyrite “disease”.

## 3. Methods

To perform this study, the polished sections of the sphalerite samples collected from the Băiut and Robu veins of the Breiner-Băiut deposit were analyzed by optical microscopy in reflected light. The optical microscope used was the Zeiss Axio Imager A2m model with EC Plan-Neofluar objectives, with 10X and 20X objectives required for study. To determine the chemical composition of the sphalerites chosen for the study in the previous step, the analyzes were performed using the scanning electron microscope (SEM) Zeiss Merlin, with Gemini II column and electronic source type Schottky, from the Geological Institute of Romania. These analyzes were performed at an acceleration voltage of 15 kV with an electron beam intensity of 0.7-1.5 nA, using the Oxford Instruments X-MAX 50 EDS detector with a Si-detector with a -60° cooling, attached to the microscope. The micro-Raman spectroscopy was applied to determine the Fe content of the sphalerite and correlate with the results obtained by SEM-EDS analysis. For this, the Renishaw InVia Raman Microscope was used, equipped with two laser sources with wavelengths of 532 nm and 785 nm and full power of 500 mW, with a CCD detector, from the Geological Institute of Romania. The analyzes were performed with a 532 nm wavelength laser with 1800



1 / mm holographic grid, at a power of 10% with an exposure time of 3-5 s, to 20-30 acquisition using the zoom objective 50X from the Leica microscope attached to the spectroscope. For the determination of iron using Raman spectra, it was necessary to use the LabSpec software, which provided the necessary conditions for accurately measuring the intensity of iron and zinc peaks.

#### 4. Results and discussions

From a series of analyzed sphalerite samples, six samples, three samples from Băiut vein (BB5B, BBXB, BB9B) and three samples from Robu vein (BBXR, BB806R, BB877R) were selected for this study. Microscopic analyzes showed the presence of chalcopyrite “disease” in most of the observed sphalerites without respecting a distribution trend, therefore, for the SEM-EDS and micro-Raman analyzes, it was intended to identify areas that did not include them. Also, the primary analysis of the selected polished sections showed that the observed sphalerites occur with chalcopyrite, pyrite, galena, tetrahedrite, iron oxides, quartz and carbonates.

##### 4.1. SEM-EDS

The analyzes using the SEM-EDS method aimed to emphasize mainly Zn, Fe and S, but in addition, elements such as Mn, Cd, Cu, Ga, As, Sb, Te, Pb and Bi were measured and the results of the analyzes performed (Table 1) being normalized to 100%.

**Table 1.** Chemical composition of sphalerite samples, based on SEM-EDS measurements.

Sample	Wt. %											
	S	Zn	Fe	Cd	Mn	Cu	Ga	As	Sb	Te	Pb	Bi
BB5B	32.59	63.14	1.68	0.46	0.11	0.04	nd	0.11	0.09	0.05	1.1	0.62
BBXR	30.43	62.78	2.73	0.55	0.44	1.02	0.24	0.08	0.27	0.19	0.72	0.54
BBXB	29.82	62.69	3.30	0.72	0.11	0.90	0.23	0.13	nd	0.01	1.69	0.40
BB9B	30.17	61.28	4.54	0.40	0.39	1.74	0.01	0.02	nd	nd	0.97	0.49
BB806R	35.14	56.68	5.10	0.59	0.09	nd	nd	0.44	0.08	0.09	0.86	0.94
BB877R	29.77	59.80	6.41	0.35	0.20	1.98	nd	0.04	nd	nd	0.96	0.50

\* nd – Not determined

The presence of iron in the studied sphalerite samples shows a minimum of 1.68 wt.%, with a molar fraction equivalent of  $\text{Fe}_{0.029}$  (BB5B) and can reach up to 6.41 wt.% with a  $\text{Fe}_{0.115}$  equivalent (BB877R). Since the content of iron in the sphalerite may result from a solid solution of chalcopyrite and sphalerite (Borcoş and Iosof, 1966), the presence of chalcopyrite “disease” leads to the idea of comparing the obtained results for the iron to the copper, which shows that they are not correlated, therefore, not in all cases, high concentrations of iron can be attributed to them. Cadmium, a chemical element which may easily enter the sphalerite structure substituting zinc, is maintained at low concentrations, about 0.5 wt.% to 0.35 wt.%, minimum in the sample BB877R and a maximum of 0.72 wt.% in the sample BBXB. Manganese is poorly represented, reaching a maximum of 0.44 wt.% in the BBXR sample. Concentrations determined for gallium, antimony, arsenic and tellurium were insignificant, sometimes missing. Lead and bismuth appear in quite high concentrations, accounting for up to 1 wt.% for Pb and 0.5 wt.% for Bi. By separating the two veins, it was found that in the Băiut vein, sphalerites may present concentrations of iron of 1.68 wt.% (BB5B) up to 4.54 wt.% (BB9B) and in the Robu vein, the concentrations are between 2.73 wt.% (BBXR) and 6.41 wt.% (BB877R).

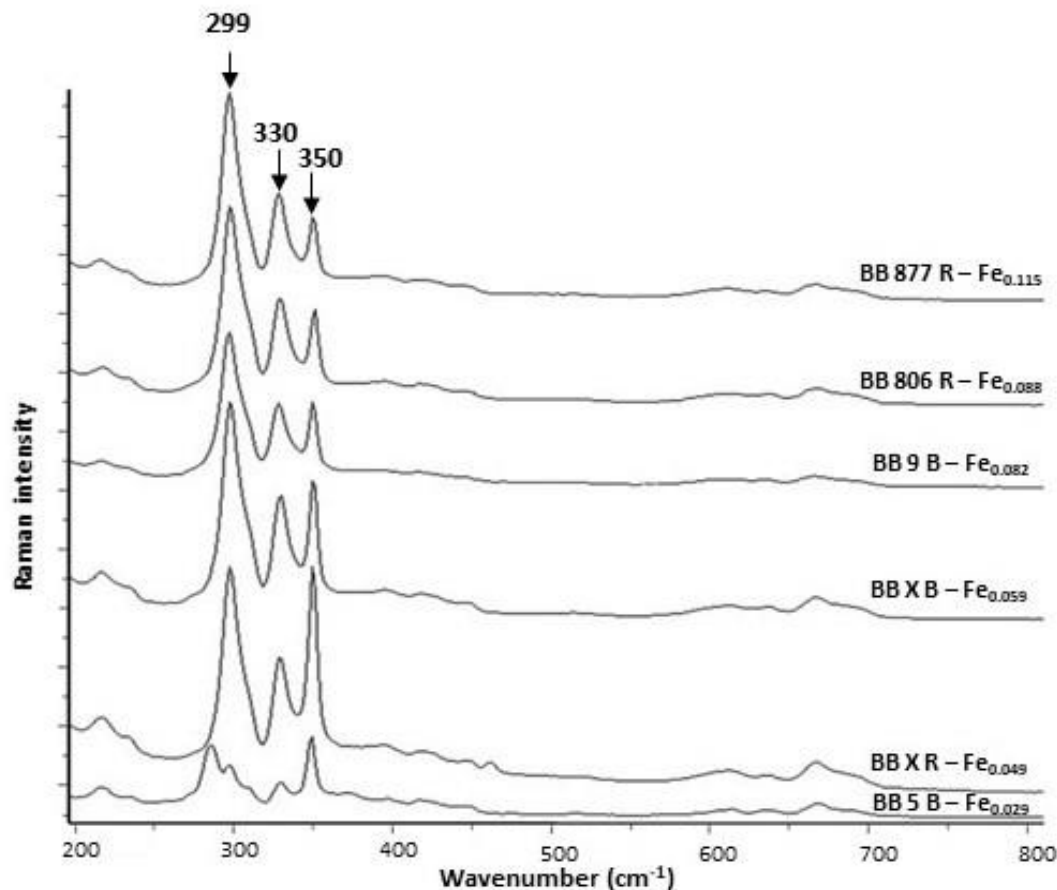
##### 4.2. Micro-Raman spectroscopy

Following the micro-Raman results obtained from the selected sphalerites, the spectra shown in Figure 1 have been arranged in order of increasing the Fe content.

According to the literature (Hope et al., 2001; Kharbish, 2007; Osadchii and Gorbaty, 2010; Buzatu et al., 2013), the spectra obtained show numerous peaks. From these, Zn-S bond LO vibrations are attributed to the  $350\text{ cm}^{-1}$  peak, and Fe-S bond vibrations are identified by the  $299\text{ cm}^{-1}$  and  $330\text{ cm}^{-1}$  peaks and Kharbish (2007) associated them with the resonance mode. The other peaks identified were associated with different types of vibrations.

The  $612\text{ cm}^{-1}$  and  $668\text{ cm}^{-1}$  peaks are associated with optical vibrations of the TO or LO type. The acoustic vibration mode is present through the  $217\text{ cm}^{-1}$  (LA) peak. The other low intensity bands present are associated with the combination of optical and acoustic vibration modes ( $\sim 396\text{ cm}^{-1}$  - TO + TA,  $\sim 419\text{ cm}^{-1}$  - TO + LA,  $447\text{ cm}^{-1}$  - LO + LA,  $\sim 638\text{ cm}^{-1}$  - LO + TO). In the case of the iron-poor sphalerite

sample (BB5B), resonance peaks of  $287\text{ cm}^{-1}$  and  $310\text{ cm}^{-1}$  were found. If the  $310\text{ cm}^{-1}$  peak was attributed to the presence of iron (Kharbish, 2007), which can be admitted because the SEM-EDS analysis showed an iron presence of 1.68 wt.%, the same author attributes the peak  $287\text{ cm}^{-1}$  to the presence of cadmium, which in the present case is unlikely, since EDS analyzes did not show any increase concentration, which were constant in all sphalerite samples and display values around 0.50 wt.%. Most likely, the  $287\text{ cm}^{-1}$  peak is due to the presence of chalcopryrite blebs in BB5B sphalerite sample, since it was observed that this peak is an intense characteristic band of chalcopryrite (Lafuente et al., 2015).



**Fig. 1.** Raman spectra of sphalerite (Fe,Zn)S samples.

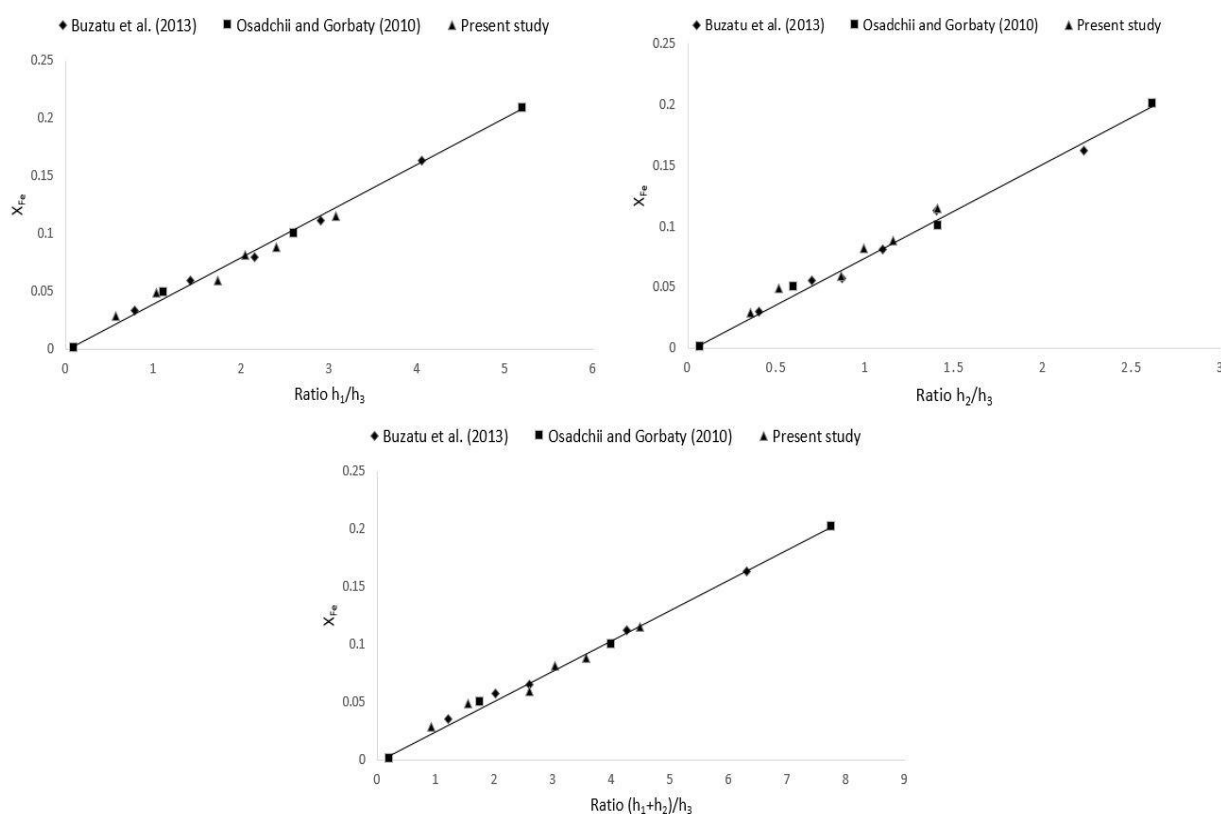
For the determination of iron by the micro-Raman spectroscopy method, the group of  $299\text{ cm}^{-1}$ ,  $330\text{ cm}^{-1}$ ,  $350\text{ cm}^{-1}$  peaks identified in the obtained spectra were taken into account and the Osadchii and Gorbaty (2010) proposed method was improved by Buzatu et al. (2013). These determinations required a series of rigorous spectral processing, which included a peak correction of the three peaks, a peak fitting procedure using the Gaussian-Lorentz function and the peaks intensities measurement, according to which we calculated  $h_1/h_3$ ,  $h_2/h_3$  and  $(h_1+h_2)/h_3$  ratios to correlate them with the SEM-EDS method (Figure 1).

Table 2 shows FeS molar fractions calculated depending of data obtained from EDS analyzes of sphalerites, in contrast to data obtained from Raman spectra. After measuring the peak intensity,  $h_1/h_3$ ,  $h_2/h_3$  and  $(h_1+h_2)/h_3$  ratios were calculated and their results were introduced into the equations of the lines indicated by Buzatu et al. (2013) to determine the molar fraction of FeS. Finally, the average of the three results obtained for each spectrum was calculated.

**Table 2.** Comparison between the results obtained by SEM-EDS and micro-Raman analyzes for Fe content from the sphalerites.

	BB5B	BBXR	BBXB	BB9B	BB806R	BB877R
<b>X<sub>Fe</sub> – EDS</b>	0.029	0.049	0.059	0.082	0.088	0.115
<b>X<sub>Fe</sub> - Raman</b>	0.025	0.040	0.066	0.078	0.091	0.113

As can be seen, the results obtained by the two methods are quite close, which demonstrates the efficiency of calculating iron contents using Raman spectroscopy.



**Fig. 2.** Correlation between the iron content in sphalerite samples and the  $h_1/h_3$ ,  $h_2/h_3$  and  $(h_1+h_2)/h_3$  ratios.

## 5. Conclusions

Microscopic observations have highlighted the presence of two types of sphalerite: i) sphalerite with chalcopyrite “disease”; and ii) homogeneous sphalerite. Contrary to expectations, the presence of iron in these sphalerites cannot be exclusively attributed to the presence of chalcopyrite “disease”, as evidenced by EDS analysis. EDS results revealed iron concentrations of 1.68 wt.% with an equivalent molar fraction  $Fe_{0.029}$  (BB5B) and 6.41 wt.% with an equivalent molar fraction  $Fe_{0.115}$  (BB877R). Iron determinations using Raman spectra were performed by measuring the intensity of the  $350\text{ cm}^{-1}$  peaks of the Zn-S bond vibrations,  $299\text{ cm}^{-1}$  and  $330\text{ cm}^{-1}$  specific for Fe-S bond vibrations. Based on these, the  $h_1/h_3$ ,  $h_2/h_3$  and  $(h_1+h_2)/h_3$  ratios were calculated, whose results were introduced into the equations of the lines suggested by Buzatu et al. (2013) to obtain the molar fractions of iron. The comparison of the results obtained by the two methods showed a good correlation, which demonstrates the effectiveness of the Raman method that has advantages in terms of sample preparation, working conditions and time for analyzes.

## References

- Barton P.B.jr., Toulmin P. (1966) Phase relation involving sphalerite in the Fe-Zn-S system. *Economic Geology* 61 (5), p. 815-849.
- Bombiță G. (1972) Studii geologice în Munții Lăpușului. *Anuarul Institutului Geologic*, vol. XXXIX, București, p. 7-110.
- Borcoș M., Iosof V. (1966) Semnificația blendei ca termometru geologic în geochimia procesului hidrotermal. *Dări de Seamă ale Ședințelor*, LII/2, p. 301-342.
- Borcoș M., Gheorghică I., Mândroiu V., Volanschi E. (1977) Considerații privind procesele metalogenetice desfășurate în extremitatea estică a Munților Gutâi (Zăcămintul Băiuț-Văratec). *Studii tehnice și economice - Studii geologice și metalogenetice în munții Oaș-Gutâi*, *Geologie economică*, seria A, nr. 11, p. 53-96.

- Borcoş M., Vlad S., Udubaşa G., Găbudeanu B. (1998) Qualitative and quantitative metallogenetic analysis of the ore genetic units in Romania. *Romanian Journal of mineral deposits*, vol. 78, vol. 2, p. 158.
- Borman R.S. (1967) Subsolidus studies in the ZnS-FeS- FeS<sub>2</sub> system. *Economic Geology* 62, p. 614-621.
- Buzatu A., Buzgar N., Damian Gh., Vasilache V., Apopei A.I. (2013) The determination of the Fe content in natural sphalerites by means of Raman spectroscopy. *Vibrational Spectroscopy*, 68, p. 220-224.
- Costin D. (2000) Major elements geochemistry of the Breiner Băiuţ ore deposit (Gutâi Mts., Eastern Carpathians). *Studia Universitatis Babeş-Bolyai, Geologia*, XLV, 1, p. 55-66.
- Damian, G., Costin D. (1999) Tetrahedrite – bournonite in Breiner – Băiuţ mineralization (Gutâi Mts., Eastern Carpathians). *Studia Universitatis Babeş – Bolyai, Geologia*, XLIV, vol. 1, p. 137-149.
- Dimitrescu R., Bleahu M. (1955) Cercetări geologice în regiunea Băiuţ (Baia Mare). Dări de seamă ale şedinţelor, *Comitetul Geologic*, vol. XXXIX, p. 48-54.
- Dragu V., Edelstein O. (1968) Asupra prezenţei panonianului la nord şi vest de Băiuţ (Baia Mare). Dări de Seamă ale Şedinţelor, vol. LIV, nr.1, Bucureşti, p. 243-248.
- Edelstein O., Dragu V., Docsănescu F., Stoicescu F., Stoicescu G. (1971) Miocenul din versantul sudic al Vârfului Văratec (Munţii Gutâi). Dări de Seamă ale Şedinţelor, vol. LVII, nr. 4, Bucureşti, p. 43-53.
- Gabor M., Kovacs M., Edelstein O., Istvan D., Bernard A. (1999) Harta geologică a munţilor Oaş-Gutâi-Țibleş, scara 1:25000, foaia Băiuţ. S.C. Cuart S.A., Baia Mare.
- Hope G.A., Woods R., Munce C.G. (2001) Raman microprobe mineral identification. *Minerals Engineering*, vol. 14-12, p. 1565-1577.
- Kharbish S. (2007) A Raman spectroscopic investigation of Fe-rich sphalerite: effect of Fe-substitution. *Physics Chemistry Minerals*, 34, p. 551-558.
- Lafuente B., Downs R.T., Yang H., Stone N. (2015) The power of databases: the RRUFF project. In: Armbruster T., Danisi R.M. (Eds.), *Highlights in Mineralogical Crystallography*. De Gruyter, Berlin, Germany, p. 1-30.
- Manilici V., Kalmar I. (1992) Asupra compoziţiei mineralogice şi a temperaturilor de cristalizare a mineralelor din zăcămintele Băiuţ, Văratec şi Cizma – Coasta Ursului. *Studii şi cercetări de geologie*, Tom 37, p. 17-28.
- McClung, C.R., Viljoen F (2011) A detailed mineralogical assessment of sphalerites from the Gamsberg zinc deposit, South Africa: The manganese conundrum. *Minerals Engineering* 24, p. 930-938.
- Osadchii E.G., Gorbaty Y.E. (2010) Raman spectra and unit cell parameters of sphalerite solid solutions (Fe<sub>x</sub>Zn<sub>1-x</sub>S). *Geochimica et Cosmochimica Acta*, 74, p. 568-563.
- Plotinskaya O.Yu., Prokofiev V.Yu., Damian Gh., Damian F., Lehmann B (2012) The Cisma deposit, Băiuţ district, Eastern Carpathians, Romania: sphalerite composition and formation conditions. *Carpathian Journal of Earth and Environmental Sciences*, 7-2, p. 265-273.
- Plotinskaya O.Yu., Damian Gh., Damian F. (2014) Sphalerite assemblages and composition in the Baia Mare region, Eastern Carpathians, Romania (preliminary data). *Romanian Journal of Mineral Deposits*, 87-1, p. 87-90.
- Scott C.D., Barnes H.L. (1971) Sphalerite geothermometry and geobarometry. *Economic Geology*, 66, p. 653-669.
- Vlad Ş., Borcoş M. (1998) Alpine Metallogenesis of the Romanian Carpathians. *Romanian Journal of Mineral Deposits*, vol. 78, Bucureşti, p. 5-20.

## NEW GEOCHEMICAL DATA AND MINERALOGICAL INTERPRETATION FOR CISMA ORE DEPOSIT, GUTÂI MOUNTAINS

Réka KOVÁCS<sup>1,2\*</sup>, Călin G. TĂMAȘ<sup>1\*\*</sup>

<sup>1</sup>Babeș-Bolyai University, Department of Geology, 1, Kogălniceanu str., 400084, Cluj Napoca, Romania;

<sup>2</sup>Victor Gordan County Mineralogical Museum of Baia Mare, 8, Traian bld., 430212, Baia Mare, Romania.

\* kovacsreka056@gmail.com; \*\*calin.tamas@ubbcluj.ro.

**Abstract:** Geochemical analyses carried out for Cisma ore deposit allow to propose several correlations between the chemical composition and the mineralogy of the ore. The presence of precious metals was also confirmed, as well as the As dominant vs. Sb subordinate character of the Cu-rich ore. Additional studies are required for a complete clarification of the mineralogical composition of the ore from Cisma as suggested by the quantitative chemical data *i.e.* significant presence of Ag, Se, and Te.

**Keywords:** geochemistry, mineralogy, tetrahedrite-tennantite, enargite, Cisma ore deposit, Băiut, Baia Mare metallogenetic district, Gutâi Mountains

### Geological setting

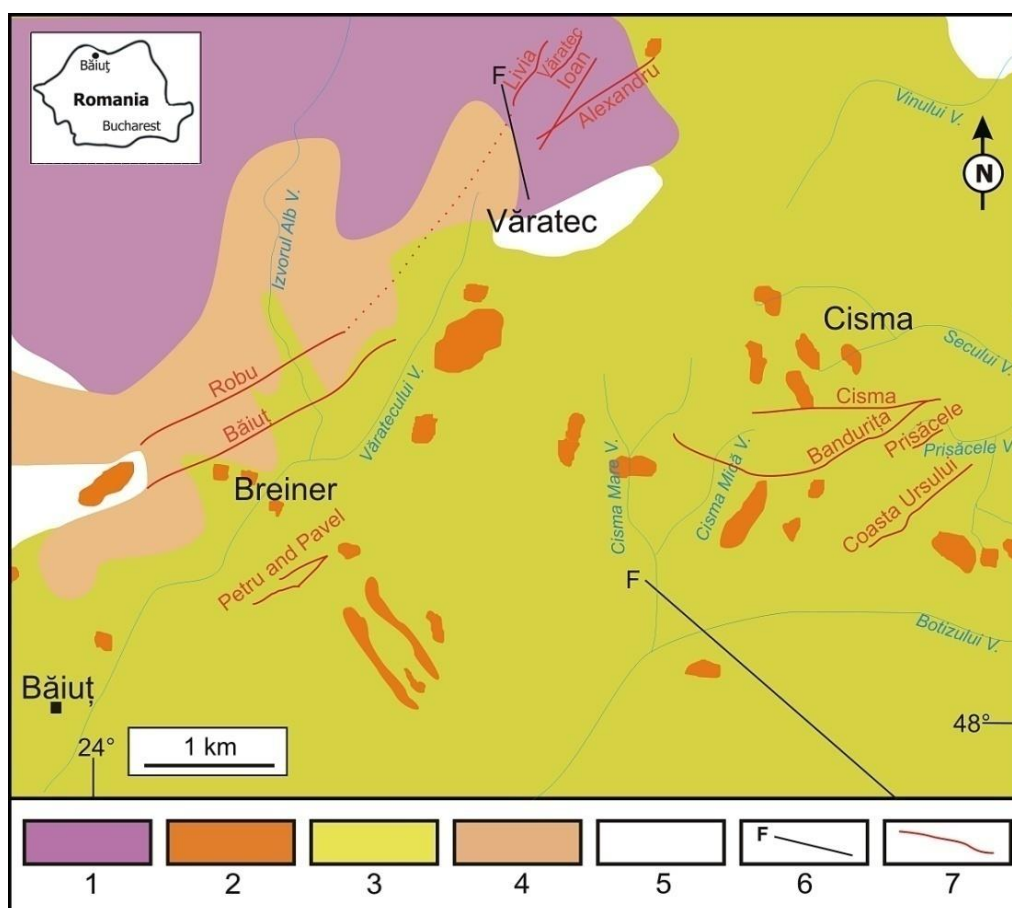
The Baia Mare Neogene metallogenetic district is situated along the southern edge of the Gutâi Mountains, from the north-western section of the Eastern Carpathian volcanic chain and hosts tens of Pb-Zn-Cu±Au-Ag and Au-Ag±Pb-Zn-Cu epithermal deposits. At the district scale Săndulescu (1984) pointed out the presence of three major structural units, *i.e.*, *i*) the pre-Neogene basement (Paleogene sedimentary rocks/flysch-like deposits); *ii*) the Neogene sedimentary rocks cover; and *iii*) the Neogene volcanic rocks. The ore deposits from Baia Mare Neogene metallogenetic district are related to the intermediate calc-alkaline arc-type magmatism that started in Sarmatian (13.4 Ma; Edelstein et al., 1992). The age of the hydrothermal activity, which was genetically linked to the volcanic activity is Pannonian (11.5-7.9 Ma; Lang et al., 1994; Kovacs et al., 1997). From geographic and from the commodities points of view, the Baia Mare metallogenetic district was divided in three metallogenetic fields (from west to east), as follows: *i*) Ilba – Nistru (Pb-Zn-Cu ±Au, Ag); *ii*) Săsar – Dealul Crucii (Au, Ag); and *iii*) Herja – Băiut (Pb-Zn-Cu and Au-Ag) (Kovacs and Fülöp, 2010).

The ore deposits from the Baia Mare metallogenetic district are controlled by the Bogdan Vodă-Drăgoș Vodă fault system with an overall west-east strike (Neubauer et al., 2005), situated on the southern slope of the Gutâi Mountains. This main metallogenetic structural control was interpreted by many authors (*e.g.* Csontos and Nagymarossy, 1998, Tischler et al., 2007) as the eastern prolongation of the so-called Mid-Hungarian Line that separates Alcapa and Tisia-Getia (Seghedi et al., 1998)/Tisza-Dacia (Csontos et al., 1992) microplates.

Representing the eastern extremity of Baia Mare Neogene metallogenetic district, the Băiut metallogenetic field is at its turn composed of the following three main ore deposits (Borcoș and Gheorghită, 1976), which from west to east are: *i*) Breiner – Băiut, *ii*) Văratec, and *iii*) Cisma-Poiana Botizei. The radiometric age of the ore deposits from the Herja-Băiut metallogenetic field (Lang et al., 1994; Kovacs et al., 1997) is 9.4-7.9 Ma and corresponds to Upper Pannonian.

The Cisma – Poiana Botizei (Cisma) ore deposit (Fig. 1) represents the easternmost ore occurrence within the Băiut metallogenetic field and the Baia Mare district as well. The ore deposit consists of several vein structures hosted in Paleogene flysch sequences that are pierced by Neogene quartz microdiorite and microgranodiorite subvolcanic bodies (Plotinskaya et al., 2012). The most important vein structures from Cisma ore deposits are Bandurița, Cisma, Coasta Ursului, Olimpiu, and Prisăcele (Borcoș and Gheorghită, 1976; Istvan et al., 1995; Mariaș, 2005; Damian et al., 2016).





**Fig. 1.** Simplified geological map (modified after Borcoş and Gheorghită, 1976; András, 2017) of the Băiut metallogenetic field, showing the location of the main veins from the Breiner (W), Văratec (N) and Cisma (E) fields. 1-Pontian pyroxene andesites; 2-Pontian pyroxene andesites±biotite; 3-Paleogene sedimentary rocks; 4-Neogene volcanic rocks; 5-Quaternary sedimentary rocks; 6-Faults; 7-Veins.

## Materials and methods

The studied sample represents an ore fragment of the former ore stock pile from Cisma ore deposit, in the neighborhood of the Băiut processing plant. According to a previous mineralogical study (András, 2017, unpubl.) the following minerals were identified by optical microscopy from similar samples: galena, chalcopyrite, tetrahedrite, sphalerite, hematite, covellite and enargite; the X-ray diffraction data by the same author confirmed the presence of kaolinite, as main alteration mineral.

Multi-elemental geochemical analyses have been carried out on the sample BT5089 from Cisma ore deposit, by ALS Romania, Roşia Montană. Macroscopically, the sample is dominated by the presence of pyrite and chalcopyrite (Fig. 2). The geochemical analyses included the grade measurement for 49 elements, including Ag, As, Au, Bi, Cd, Cu, Mn, Pb, Sb, Se, Te, Zn. The Au was measured by fire assay, with the detection limit ranging between 0.001 and 10 ppm. The Ag grade was measured by acid digestion (HF-HNO<sub>3</sub>-HClO<sub>4</sub> with HCl leach) and ICP-AES finish, with the detection limit ranging from 1 to 1500 ppm. The remaining chemical elements were measured by four acid digestion and ICP-AES finish. The detection intervals for the chemical elements presented in Table 1 is (in ppm), As 0.2-10000; Bi 0.01-10000; Cd 0.02-1000; Cu 0.2-10000; Mn 5-100000; Pb 0.5-10,000; Sb 0.05-10,000; Se 1-1000; Te 0.05-500; and Zn 2-10000 ppm. Due to the over-limit Cu grade by the above-mentioned method, Cu was additionally measured by aqua regia digestion with ICP-AES finish with the detection interval 10 ppm – 40 %.



**Fig.2.** The studied ore sample BT5089 from Cisma, used for geochemical analyses, dominated by pyrite and chalcopyrite.

## Results and Discussions

The geochemical analyses obtained on the BT5089 sample from Cisma ore deposit are presented in Table 1. These results highlight the Cu-extremely rich character of the ore (8.67 %) and the presence of precious metals (Au and Ag at 1.74 and 105 ppm respectively).

**Table 1.** The geochemistry results (selection) for the sample BT5089, Cisma ore deposit, Băiuț metallogenetic district.

Element	Ag ppm	As ppm	Au ppm	Bi ppm	Cd ppm	Cu %	Mn ppm	Pb ppm	Sb ppm	Se ppm	Te ppm	Zn ppm
Grade	105	1280	1.74	1.41	14.45	8.67	263	1470	100.5	16	1.73	1980

According to Damian and Damian (2004) and Damian et al. (2016) the ore from Cisma consists mainly of common sulfides (pyrite, chalcopyrite, galena, sphalerite) and Cu-sulfosalts (tetrahedrite and tennantite), associated to Pb-sulfosalts (semseyite, boulangerite, and jamesonite), Fe-sulfides (pyrrhotite, marcasite) and hematite, Sb- and As-sulfides (stibnite, realgar, and orpiment), Bi-minerals (lillianite-gustavite, and native Bi), wolframite and native gold.

Recent reflected light ore microscopy study and semi-quantitative SEM-EDS investigations carried out on Cisma ore samples (Kovács and Tămaș, 2017), confirmed the presence of hematite, galena, chalcopyrite, sphalerite, pyrite, tetrahedrite-tennantite, and enargite.

The high Cu content of the analyzed ore sample from Cisma is related to the abundance of chalcopyrite and the presence of Cu-sulfosalts (tetrahedrite-tennantite mineral compositions). Significant Au grade is certainly given by the presence of native gold, as this mineral was previously mentioned from Cisma by Damian and Damian (2004). With the exception of Ag-bearing tetrahedrite-tennantite mineral compositions pointed out by SEM-EDS semi-quantitative measurements by Kovács and Tămaș (2017) no other Ag-bearing minerals were mentioned previously from Cisma. Taking into account the relative low Au grade as compared to Ag grade (1.74 vs. 105 ppm respectively) it seems unlikely that the native gold could be considered as a major Ag-bearing mineral within the ore. It is more likely that some other Ag-bearing minerals apart tetrahedrite-tennantite could be also present in the ore, but these minerals are not yet identified.

The As to Sb ratio (Table 1) 1280/100.5 (in ppm) reflects accurately the predominance of tennantite versus tetrahedrite within the ore. Moreover, it also reflects the input of enargite in the bulk As-content of the analyzed ore sample.

The Zn and Pb grades mirror the presence of sphalerite and galena respectively. Taking into account the capacity of sphalerite to accommodate over 15 wt % impurities (Udubaşa et al., 1974; Cook et al., 2009), it seems that Cd, Mn and probably at least part of Se represent impurities hosted by sphalerite.

The presence of Bi-minerals (Damian and Damian, 2004) correlates well to the Bi grade within the analyzed ore sample, while for Te and Se it is possible to infer traces of Te- and Se-bearing minerals or minerals that may accommodate these chemical elements as impurities (*e.g.* sphalerite?).

## Conclusion

The geochemical analyses carried out correlate well to the overall known mineralogical composition of the ore from Cisma ore deposit. However, the new geochemical results suggest the precious metals character of the ore and the possible occurrence of Te-Se bearing mineral(s) or the presence of these elements as impurities hosted most likely by sphalerite.

## References

- András K. (2017) Mineralogical study of the ore deposits from the Băiuţ district (Maramureş county), focusing on the Văratec, Cisma, Coasta Ursului, Johan Hell, Breiner and Poiana Botizei deposits (in Romanian). Unpublished MSc Thesis, Babeş-Bolyai University Cluj Napoca, Romania.
- Borcoş M., Gheorghită I. (1976) Neogene hydrothermal ore deposits in the volcanic Gutâi Mountains. IV. Băiuţ-Văratec-Botiza metallogenetic field. *Revue Roumaine de Géologie, Géophysique et Géographie, Série de Géologie*, 20, 2, p. 197-209.
- Cook N.J., Ciobanu C.L., Pring A., Skinner W., Shimizu M., Danyushevsky L., Saini-Eidukat B., Melchner F. (2009) Trace and minor elements in sphalerite: LA-ICPMS study. *Geochimica and Cosmochimica Acta*, 73, p. 4761-4791.
- Csontos L., Nagymarosy A., Horváth F., Kovacs M. (1992) Tertiary evolution of the Intra-Carpathian area: a model. *Tectonophysics*, 208/1-3, p. 221-241.
- Csontos L., Nagymarosy A. (1998) The Mid-Hungarian Line: a zone of repeated tectonic inversions. *Tectonophysics*, 297/1-4, p. 51-71.
- Damian F., Damian Gh. (2004) Mineral parageneses of the hydrothermal ore deposits from Baia Mare area, Romania. Mining explorations, preparation of non-ferrous metallurgy, geology and environmental engineering, Series D, vol. XVIII, p. 155-172.
- Damian G., Damian F., Konecny P., Kollárová V. (2016) A new occurrence of wolframite-ferberite in Romania. *Romanian Journal of Mineral Deposits*, 89/1-2, p. 49-54.
- Edelstein O., Işţvan D., Kovacs M., Bernad A., Stan D., Işţvan E., Gabor M., Bálint B., Haranth G., Vârşescu I. (1992) Preliminary data regarding the K-Ar of some eruptive rocks from Baia Mare Neogene volcanic zone. *Revue Roumaine de Géologie*, 36, 45-60.
- Işţvan D., Vârşescu I., Halga S., Grancea L. (1995) Gold-silver epithermal levels and association of the eastern area of the Gutâi Mts. and in the Văratec Mts. (Firiza-Botiza area), East Carpathians, Romania. *Studia Universitatis Babeş-Bolyai Cluj Napoca, Geology*, XL, 1, p. 195-210.
- Kovacs M., Edelstein O., Gabor M., Bonhomme M., Pécskay Z. (1997) Neogene magmatism and metallogeny in Oaş-Gutâi-Ţibleş Mts.; a new approach based on radiometric datings. *Romanian Journal of Mineral Deposits*, 78, p. 38-45.
- Kovacs M., Fülöp A. (2010) Baia Mare metallogenetic district. In: Iancu G., Kovacs M. (2010) Ore deposits and other classic localities in the Eastern Carpathians: From metamorphics to volcanics. *Acta Mineralogica-Petrographica, Field Guide Series*, 19, p. 5-13.
- Kovács R., Tămaş C. (2017) Cu-sulfosalts in Băiuţ metallogenetic field, Baia Mare district, Gutâi Mountains – Preliminary Scanning Electron Microscopy Data. “Ion Popescu Voiteşti” Yearly Scientific Session, Babeş-Bolyai University Cluj Napoca, Geology Department, 15<sup>th</sup> December 2017, p. 24-30.
- Lang B., Edelstein O., Steinitz G., Kovacs M., Halga S. (1994) Ar-Ar dating of adularia – A tool in understanding genetic relation between volcanism and mineralization: Baia Mare area (Gutâi Mountains), Northwestern Romania. *Economic Geology*, 89, p. 174-180.
- Mariaş Z.F. (2005) Metallogeny of the Baia Mare mining district. An approach based on the Cavnic hydrothermal system, comparison with other epithermal systems in the world (in Romanian). Cornelius Publishing House, 450 pp., Cluj Napoca,

- Neubauer F., Lips A., Kouzmanov K., Lexa J., Ivășcanu P. (2005) Subduction, slab detachment and mineralization: The Neogene in the Apuseni Mountains and Carpathians. *Ore Geology Reviews*, 27, p. 13-44.
- Plotinskaya O.Y., Prokofiev V.Y., Damian Gh., Damian F., Lehmann B. (2012) The Cisma deposit, Băiut district, Eastern Carpathians, Romania: sphalerite composition and formation conditions. *Carpathian Journal of Earth and Environmental Sciences*, 7/2, p. 265-273.
- Săndulescu M. (1984) *Geotectonics of Romania* (in Romanian). Tehnică Publishing House, 336 pp., București.
- Seghedi I., Balintoni I., Szakács A. (1998) Interplay of tectonics and Neogene post-collisional magmatism in the Intracarpadian area. *Lithos*, 465, p. 483-499.
- Tischler M., Gröger H.R., Fügenschuh B., Schmid S.M. (2007) Miocene tectonics of the Maramureș area (Northern Romania): implications for the Mid-Hungarian fault zone. *International Journal of Earth Sciences, Geologische Rundschau*, 96, p. 473-496.
- Udubașă G., Medesan A., Ottemann J. (1974) On geochemistry and influence of Fe, Mn, Cd and Cu of lattice constant of natural sphalerite (in German). *Neues Jahrbuch für Mineralogie Abhandlungen*, 121, p. 229-251.





## ORE MINERALOGY AND GEOCHEMISTRY RELATIONSHIPS IN BĂIȚA BIHOR ORE DEPOSIT, APUSENI MOUNTAINS, ROMANIA - BLIDAR CONTACT CASE STUDY

Mădălina Paula ANDRII\*, Călin Gabriel TĂMAȘ\*\*

Department of Geology, Faculty of Biology and Geology, Babeș-Bolyai University, 1, M. Kogălniceanu Str., 400084 Cluj-Napoca, Romania; e-mail: \*andrii.madalina@hotmail.com, \*\*calin.tamas@ubbcluj.ro

**Abstract:** With a complex ore mineralogy, Băița Bihor ore deposit, North Apuseni Mountains, Romania represents a classic example of distal skarn related ore deposit from the northern extremity of the Banatitic Magmatic and Metallogenetic Belt. An important control factor for the ore genesis is a tectonic structure (thrust-fault) known as Blidar Contact. The geochemical analysis of the ore from Blidar Contact pointed out among others high Cu grade (22.8 wt %), and significant precious metals grades (0.91 ppm Au and > 500 ppm Ag). The W and Sn grades (530 and 110 ppm respectively) suggest the presence of scheelite and of a Sn-bearing mineral within the analyzed ore.

**Key words:** geochemistry, skarn, Băița Bihor, Apuseni Mountains.

### Introduction

Located in the north-western part of the Apuseni Mountains, Băița Bihor represents the most significant ore deposit from the northern extremity of the Banatitic Magmatic and Metallogenetic Belt - BMMB (Berza et al., 1998). This ore deposit is known for its high-grade ores and its complex mineralogy, with over 120 minerals described so far (Udubașa, 2003). Among these minerals, several have been identified for the first time from Băița Bihor ore deposit, *e.g.* cupronyite (Ilinca et al, 2010), grațianite (Ciobanu et al., 2014), makovickyite (Žák et al., 1994), and paděraite (Mumme and Žák, 1985).

The Băița Bihor is a Cu-dominated polymetallic ore deposit and represents a classic example of distal skarn related ores (Vlad, 1993). It also illustrates the outstanding metallogenetic role of the regional and local structural control (Stoici, 1974).

Despite the scientific and the economic potential of Băița Bihor ore deposit only few geochemical studies have been carried out in the last decades, and thus the reference work still remains Stoici (1983). The present contribution offers additional data for Băița Bihor ore deposit from geochemical and mineralogical perspectives regarding the so-called Blidar Contact, an important tectonic structure that favored the ore deposition (Cioflica et al., 1977; Stoici, 1974).

The access to the underground mining works and to the ore body related to Blidar contact is presently limited; therefore, the sampling was not possible. However, for the present study, we used old ore collection samples and this fact highlights the importance of ore/mineral collections for the today's science.

### Geological Setting

Băița-Bihor ore deposit is part of the Banatitic Magmatic and Metallogenetic Belt (BMMB), and its genesis is closely related to the overall geologic evolution of the belt. Over the time, the genesis of the BMMB was extremely disputed and several models have been proposed (*e.g.*, Gallhofer et al., 2015; Zimmerman et al., 2008, etc.). The most recent model stated by Gallhofer et al. (2015) suggests that the magmatic activity within the belt started during Austrian tectogenesis and was triggered by the north-dipping subduction of Neotethys (a Vardar ocean branch) with a magmatic ascension controlled by the steepening (roll-back) of the subducting slab.

The BMMB was divided based on major tectonic structures in five distinct sections (Gallhofer et al., 2015): Apuseni, Banat, Timok, Panagyurishte and Eastern Srednogorie (Fig. 1a). The onset and the end of the Banatitic magmatism within the Apuseni section of the BMMB that includes the Băița Bihor ore deposit, was determined by Cioflica et al. (1995), who suggested the time interval  $91 \pm 4$  to  $43 \pm 2$  Ma. More recently, Zimmerman et al. (2008) places the onset of the Banatitic magmatism for Apuseni Mountains (Băița Bihor skarns) at 80.6 Ma and the end at 78.7 Ma. The time span of the magmatic activity was more recently constrained by Gallhofer et al. (2015) at ~80.8-75.5 Ma.

The magmatic products hosted within the belt are known as "banatites" (according to von Cotta's term), and are generally calc-alkaline with a wide range of petrographic varieties *i.e.* diorite, andesite, granite, dacite, rhyolite, granodiorite (Berza et al., 1988; Heinrich and Neubauer, 2002; Vlad and Berza,

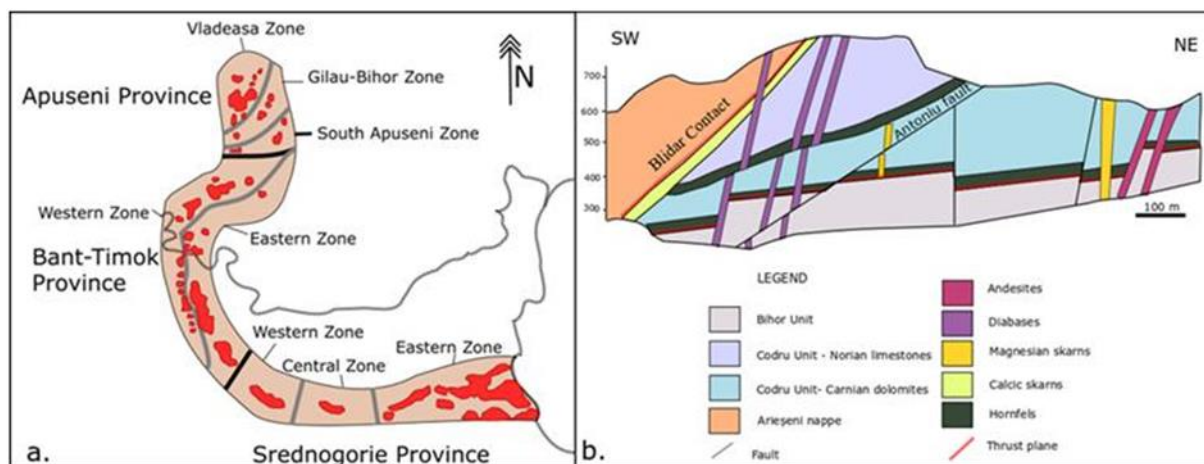
2003; Gallhofer et al., 2015; etc). However, Gallhofer et al. (2015) highlights the presence within the Apuseni section of the Banatitic belt, of high-K calc-alkaline rocks, with a dominant dacite-rhyolite petrographical range. Berza et al. (1998) mentioned for the North Apuseni, the presence of acid volcanism accompanied by granodiorite-granite pluton.

Beside the productive high-K calc-alkaline magmatism materialized through a deep-seated granite to granodiorite-diorite batholith accompanied by several dykes with a composition ranging from basic to intermediate (Stoicovici and Selegan, 1970), the structural control was the main factor that contributed to the genesis of the ores from Băița Bihor. The regional and local structural setting with thrust planes (*i.e.* Blidar Contact), fractures and faults intersections controlled the upwelling of the mineralizing fluids within the Băița Bihor perimeter. The dominant carbonatic rocks of the nappe system represented another control (lithological) that allowed the distal skarn and related polymetallic ore bodies formation.

### Local Geology

The geological structure of the Băița-Bihor area is composed of a nappe system formed mainly during pre-Gossau tectogenesis (Fig. 1b). In lower position are located Jurassic-Lower Cretaceous detritic and calcareous formations that belong to the Bihor Unit, which is thrust along the Blidar Contact by Triassic sedimentary rocks (limestones, dolomites and sandstones) of the Codru Unit (Stoici, 1983). These sedimentary units are covered by the Arieșeni nappe, which is composed of Permian (early Carboniferous?)-Lower Triassic detritic series (Stoici, 1983).

The Laramian (Upper Cretaceous) magmatism from Băița-Bihor area triggered thermal and metasomatic changes within the sedimentary rock pile and led to the development around the magmatic body of an aureole of contact metamorphism developed up to 1.5 km distance away of the batholith (Cioflica et al., 1974). Hornfels, calcic marbles and several types of skarns (*i.e.* calcic, magnesium, and calco-magnesium) and associated ore bodies were formed closely dependent on the structural peculiarities of the perimeter. One of the most important tectonic structure that facilitated the ore deposition is represented by the so-called Blidar Contact (thrust-fault) that follows a NW-SE direction and has a dip of 45-50° SW (Cioflica et al., 1971). The ore body along Blidar Contact has a tabular morphology measuring over 600 m in length and 5-15 m in width (Cioflica et al., 1971). Furthermore, the ore deposited on Blidar contact has a west to east lateral zonation, *i.e.* i) Mo (-Bi, Cu, W) deep-proximal zone; ii) Cu (-Bi, W) median zone, and iii) Pb-Zn distal zone (Stoici, 1974).



**Fig. 1.** Regional and local geological setting: a) simplified delineation of the Banatitic Magmatic and Metallogenetic Belt (BMMB) sections (Vlad, 2011; adapted after Vlad and Berza, 2003); b) simplified geological cross-section through Băița Bihor ore deposit (Stoici, 1974).

### Materials and methods

Due to the unsafe passage through the underground mining works that give access to the Blidar Contact ore body, the studied material consists of several ore samples collected by Professor Ioan Mârza in 1971 and presently preserved in "Valeriu Lucca" Ore Deposit Collection, Department of Geology, Babeș-Bolyai University, Cluj-Napoca.

The macroscopic observations allowed to select a representative sample for the bulk composition of the ore. The sample dimensions are 23x16 cm and it is bornite rich. A slice from this sample (Fig. 2) was selected for multi-elemental geochemical analyses.



**Fig. 2.** Slice of the ore sample from Blidar Contact ore body used for geochemical analyses. Bornite (dark purple) is the main ore mineral and is associated to wollastonite (white).

The multi-elemental geochemical characterization of the ore was carried out within ALS Romania, Roşia Montana Geochemistry facility. The concentrations of 49 chemical elements in the ore were measured including Ag, Au, Bi, Cd, Cu, Fe, Mn, Pb, S, Se, Sn, Te, W, and Zn.

The gold grade was measured by fire assay and ICP-AES and the detection limit has a range between 0.005 and 10 ppm. Ag was analyzed by HF-HNO<sub>3</sub>-HClO<sub>4</sub> digestion with HCl leach, ICP-AES finish and the concentrations interval ranging between 1-1500 ppm. The Cu assay was carried out with four acid digestion and ICP finish, the detection limits ranging from 0.001 to 40 %. These analyses were combined with a four acid and ICP-AES method, and Bi, Cd, Fe, Mn, S, Sn, Zn, Pb, Te, Se, W, etc. were tracked. The detection range for each element mentioned is, *i.e.* Bi, 0.01-10,000 ppm; Cd, 0.02-1,000 ppm; Fe, 0.01-50 %; Mn, 5-100,000 ppm; S, 0.01-10 %; Sn, 0.2-500 ppm; Zn, 2-10,000 ppm; Pb, 0.5-10,000 ppm; Te, 0.05-500 ppm; Se, 1-1,000 ppm; and W, 0.1-10,000 ppm.

## Results and Discussions

The geochemical analyses aimed to point out the presence of certain metallic elements and their grade. Significant results were obtained for several metallic elements presented in Table 1 by combining the analytical methods mentioned above. The concentration of two metals presented in Table 1, *i.e.* Bi and Sn, exceeds the upper detection limit of the analytical methods. However, the abundance of Bi (> 1 wt %), and the high grade Sn was certified for the analyzed ore sample.

**Table 1.** The main chemical components in the ore deposit from Blidar Contact, Băița Bihor ore deposit.

Element	Ag ppm	Au ppm	Bi wt%	Cd ppm	Cu wt%	Fe wt%	Mn wt%	Pb wt%	S wt%	Se ppm	Sn ppm	Te ppm	W ppm	Zn wt%
Content	530	0.91	>1	115	22.8	13.5	0.16	0.29	7.85	110	>500	120.5	530	0.69

The geochemistry results (Table 1) indicate the polymetallic character of the ore. Copper grade is extremely elevated (over 22 wt %) and it is accompanied by less economically attractive Pb and Zn grades. The precious metals are well represented with significant Au and Ag grades, *i.e.* about 1 ppm and 530 ppm respectively. The couple W-Sn has also high grades with over 500 ppm for each element. Te, Se and Cd also show high concentrations that precisely reflect the mineralogy of the ore.

Recent mineralogical results on similar ore samples from Blidar Contact (Andrii and Tămaş, 2015 and 2017) obtained by optical microscopy, SEM-EDS semi-quantitative chemical data and back-scattered electrons images presently allow to correlate at least in part the geochemical results to the mineralogy of the ore. The above-mentioned authors confirmed the copper-rich character of the Blidar Contact ore body with bornite as main Cu-bearing mineral, which shows partial replacement by several

secondary Cu-sulfides, *i.e.* digenite, chalcocite and covellite, and is accompanied by chalcopyrite, sphalerite, hessite, electrum, wittichenite, and kesterite.

According to the above mentioned results, the abundance of Cu bearing sulfides, *e.g.* digenite, chalcopyrite, and especially bornite is responsible for high Cu grade and in part (*i.e.* bornite and chalcopyrite) for Fe grade. Wittichenite was identified for the first time in Băița Bihor ore deposit by Giușcă (1941) from the Blidar Contact area, and was confirmed by SEM-EDS data by Andrii and Tămaș (2017). The presence of wittichenite and other related Bi-bearing minerals could explain the high-bismuth grade (over 1 wt %; Table 1).

According to the available mineralogical data, *e.g.* Andrii and Tămaș (2015 and 2017), the main source of silver seems to be hessite. The presence of native gold in the ore from Blidar Contact, reported recently by Andrii and Tămaș (2015) is also confirmed by the Au bulk grade (0.91 ppm, Table 1). Hessite seems to be the most important source of Te as well. However, one cannot exclude the possible occurrence of other Te-bearing minerals, which were previously described from Băița Bihor, *e.g.* cervelleite (Cook and Ciobanu, 2003), tetradymite (Cook et al., 2002), joseite-A (Cioflica and Lupulescu, 1995), and for this reason Băița Bihor is an ore deposit with a dominant Bi(-Te) trace signature (Harris et al., 2013).

The high Se grade could be related to Se-bearing minerals or to minerals that host Se impurities. It is worth to be mentioned that naumannite ( $\text{Ag}_2\text{Se}$ ) and clausthalite ( $\text{PbSe}$ ) have been mentioned by Cook et al. (2002) from Băița Bihor ore deposit. Pekoite ( $\text{PbCuBi}_{11}(\text{S},\text{Se})_{18}$ ) and friedrichite ( $\text{Pb}_5\text{Cu}_5\text{Bi}_7(\text{S},\text{Se})_{18}$ ) that can incorporate small amounts of Se have been also described from Blidar Contact by Shimizu et al. (1998).

The Zn grade in the analyzed ore (Table 1) is certainly related to sphalerite that was described from similar samples by Andrii and Tămaș (2015 and 2017). Sphalerite can accommodate significant quantities of impurities, *e.g.* Fe, Mn, Cd, etc (Cook et al., 2009). It seems that Mn and Cd from the analyzed ore (Table 1) are related to sphalerite. Another Mn-bearing mineral was recently described from Băița Bihor, *i.e.* grațianite (Ciobanu et al., 2014), but this mineral was not identified so far in the studied samples. The Pb grade (Table 1) is likely linked to the presence of galena within the ore.

The geochemical data (Table 1) indicate high W and Sn grades. The occurrence of kesterite (Andrii and Tămaș, 2017) correlates with the high Sn grade, while W should correlate with a W-bearing mineral. It is worth to mention that scheelite ( $\text{CaWO}_4$ ) has been described from Blidar Contact by Superceanu (1956) and seems to be the likely candidate for the significant W grade in the analyzed sample.

## Conclusions

The present work brings new geochemical data regarding the so-called Blidar Contact ore body from Băița Bihor. These new data validate the polymetallic character of the ore (Cu, Au, Ag, Bi, Sn, W) and allow to propose some possible correlations among these data and the already published mineralogical data. While for most of the analyzed chemical elements it was possible to tight up a connection mineralogy-geochemistry based on recent mineralogical investigation on similar samples, *i.e.* Cu, Bi, Ag, Te, Sn, etc., for W and Se the connection is inferred based on broader mineralogical data reported earlier (*e.g.* Superceanu, 1956; Shimizu et al., 1998; Cook et al., 2002).

## References

- Andrii M.P., Tămaș C.G. (2015) Mineralizații cuprifere în zăcămintul Băița Bihor, Munții Apuseni - studii mineralogice comparative. In: Bucur I.I. et al. (eds.) - Sesiunea științifică anuală „Ion Popescu Voitești”, Cluj-Napoca, 4 decembrie 2015, p. 1-4
- Andrii M.P., Tămaș C.G. (2017) Preliminary Mineralogical Data on Bi- and Sn-minerals from Băița Bihor Ore Deposit, North Apuseni Mountains, Romania. Sesiunea Științifică “I.P. Voitești” 2017, 15 decembrie, 2017, Departamentul de Geologie, Universitatea Babeș-Bolyai, p. 1-8
- Berza T., Constantinescu E., Vlad Ș.N. (1998) Upper Cretaceous Magmatic Series and Associated Mineralisation in the Carpathian - Balkan Orogen. Resource geology, vol. 48, no. 4, p. 291–306.
- Ciobanu C.L., Brugger J., Cook N.J., Mills S.J., Elliot P., Damian G., Damian F. (2014) Grațianite,  $\text{MnBi}_2\text{S}_4$ , a new mineral from the Băița Bihor skarn, Romania. American Mineralogist, 99(5-6), p. 1163-1170.

- Cioflica G., Vlad Ș., Stoici S. (1971) Repartition de la mineralization dans le skarn de Băița Bihorului. *Revue Romaine de Geol., Geoph., Geogr., Seie Geologie*, 15, p. 43-58.
- Cioflica G., Vlad Ș., Iosif V., Panican A. (1974) Metamorfismul termic și metasomatic al formațiunilor paleozoice din unitatea de Arieșeni de la Băița Bihorului. *St. cerc. geol., geofiz., geogr., Seria geologie*, 19, p. 43-68.
- Cioflica G., Vlad Ș., Volanschi E., Stoici S. (1977) Skarnele magneziene cu mineralizațiile asociate de la Băița Bihorului. *St. cerc. geol., geofiz., geogr., Geologie*, 22, p. 39-57.
- Cioflica G., Jude R., Lupulescu M. (1995) Petrometalogenetic models in the areas with the end Maastrichtian-Paleocene granitoid intrusions of Romania. *Studia Univ. Babeș-Bolyai, Geologia (Petrometalogeny)* 40/1, Cluj-Napoca, p. 41-54.
- Cioflica G., Lupulescu M. (1995) New data on joseite-A from Baita Bihor Mine (Bihor Mountains, Romania). *Romanian Journal of Mineralogy* 77, Suppl. 1, p. 12-13.
- Cook N.J., Ciobanu C.L., Bogdanov K. (2002) Trace mineralogy of the Upper Cretaceous Banatitic Magmatic and Metallogenetic Belt, SE Europe. 11th IAGOD Symp. Geocongress. CD vol. of ext. Abstr, *Geol. Surv. Namibia*.
- Cook N., Ciobanu C. (2003) Cervelleite,  $\text{Ag}_4\text{TeS}$ , from three localities in Romania, substitution of Cu, and the occurrence of the associated phase,  $\text{Ag}_2\text{Cu}_2\text{TeS}$ . *Neues Jahrbuch für Mineralogie - Monatshefte*, 7, p. 321-326.
- Cook N.J., Ciobanu C.L., Pring A., Skinner W., Shimizu M., Danyushevsky L., Saini-Eidukat B., Melcher F. (2009) Trace and minor elements in sphalerite: a LA-ICPMS study. *Geoch. Cosmoch. Acta*, 73, p. 4761-4791.
- Gallhofer D., Quadt A., Peytcheva I., Schmid, S., Heinrich C. (2015) Tectonic, magmatic and metallogenic evolution of the Late Cretaceous Arc in the Carpathian - Balkan orogen. *Tectonics*, 34, 1813–1836.
- Giușcă., D. (1941) Note préliminaire sur la minéralisation des gisements de contact de Băița Bihorului. *Mem. Sect. Științ. Acad. Roum. ser. II, XVI/6*, p. 681-693.
- Harris C., Pettke T., Heinrich C.A., Rosu E., Woodland S., Fry B. (2013) Tethyan mantle metasomatism creates subduction geochemical signatures in non-arc Cu–Au–Te mineralizing magmas, Apuseni Mountains (Romania). *Earth and Planetary Science Letters*, 366, p. 122-136.
- Heinrich A., Neubauer F. (2002) Cu – Au – Pb – Zn – Ag metallogeny of the Alpine – Balkan – Carpathian – Dinaride geodynamic province. *Mineralium Deposita*, 37, p. 6-7.
- Ilinca G., Makovicky E., Topa D., Zagler G. (2010) Cuproneite,  $\text{Cu}_7\text{Pb}_{27}\text{Bi}_{25}\text{S}_{68}$ , a new mineral from Băița Bihor, Romania. *Canadian Mineralogist*, 50, p. 353-370.
- Mumme W.G., Žák L. (1985) Paderaitite,  $\text{Cu}_{5.9}\text{Ag}_{1.3}\text{Pb}_{1.6}\text{Bi}_{11.2}\text{S}_{22}$ , a new mineral of the cuprobismutite-hodrushite group. *Neues Jahrb. Mineral. Monatsh'*, p. 557 -567.
- Shimizu M., Kato A., Cioflica G., Lupulescu M., Shimizu M. (1998) Friedrichite from Băița Bihor, Romania. *Canadian Mineralogist* 36, p. 861-868.
- Stoici D.S. (1974) Studiul geologic și petrografic al bazinului superior al Crișului Negru - Băița Bihor cu privire specială asupra mineralizației de bor și a skarnelor magneziene. *Inst. Geol. Geofiz., Stud. tehn. econ., Ser. I, Min.-Petr.*, 7, 198 p.
- Stoici D.S. (1983) Districtul metalogenetic Băița Bihorului: cercetări geologice și miniere. Editura Academiei Republicii Socialiste România, București, 189 p.
- Stoicovici E., Selegean I. (1970) Considerațiuni la cunoașterea magmatismului banatitic din Munții Bihorului. *Studia Universitatis Babe-Bolyai, Seria Geologia*, vol. 15/2, p. 3-15.
- Superceanu C. (1956) Noi apariții de scheelit în zăcămintele de conact din provincia geochimică a banatitelor. *Rev. min.*, p. 4-5.
- Udubașa G. (2003) Outstanding mineral occurrences in Romania: what's new? *Acta Mineralogica-Petrographica, Abstract Series* 1, 106 p.
- Vlad Ș.N. (1993) *Geologia resurselor minerale. Curs universitar. Partea I: Zăcămintele metalifere și nemetalifere*. Universitatea Ecologică, București, 90 p.
- Vlad Ș.N. (2011) Perspective targeting CuAuMo porphyries of Romanian Carpathians: blind porphyry mineralization and its variable distal expression as vein and skarns. *Cent. Eur. J. Geosci*, 3(3), p. 318-335.
- Vlad Ș.N., Berza T. (2003) Banatitic magmatic and metallogenetic belt: metallogeny of the Romanian Carpathians segment. *Studia Universitatis Babes-Bolyai, Geologia*, XLVIII, 1, p. 113-122.



- Žák L., Fryda J., Mumme W.G., Paar W.H. (1994) Makovickyite,  $\text{Ag}_{1.5}\text{Bi}_{5.5}\text{S}_9$  from Băița Bihorului, Romania. The 4P natural member of the pavonite series. *Neues Jahrb. Mineral., Abh.* 168, p. 147-169.
- Zimmerman A., Stein H.J., Hanah J.L., Koželj D., Bogdanov K., Berza T. (2008) Tectonic configuration of the Apuseni-Banat-Timok-Srednogorie belt, Balkans-South Carpathians, constrained by high precision RE-OS molybdenite ages. *Miner. Deposita*, 43, p 1-21.

## DEPOSITIONAL SYSTEMS FOR THE SEDIMENTARY DEPOSITS FROM THE LIGHIDIA PERIMETER, BOZOVICI, CARAŞ-SEVERIN COUNTY

Ioan E. BARBU<sup>1,2\*</sup>, Gheorghe BRĂNOIU<sup>2</sup>

<sup>1</sup> Petroleum-Gas University of Ploiesti, 39 Bucureşti Street, 100680 Ploieşti, Romania;

<sup>2</sup> Geological Institute of Romania, 1 Caransebes Street, 012271 Bucureşti, Romania;

\*johann.geology@gmail.com; Tel.: 0741365134.

**Abstract:** In this paper it's about the mineralogical composition of the sedimentary rocks in the Miocene of the Bozovici basin. The perimeter studied is between the Lighidia valley and Agriş valley. The Bozovici basin formed during the lifting and subsidence movements of the Neozoic basement in the Southern Carpathians. The studied deposits are represented by different types of claystones, sandstones, conglomerates, carbonate nodules and coal (lignite). Data on the mineralogical and petrographic composition of the rocks in the perimeter studied were determined by facies analysis, optical microscopy and X-rays diffraction. The identified minerals and lithoclasts are represented by quartz, feldspar, micas, carbonates, metamorphic and sedimentary lithoclast in sandstones and conglomerates, and clay minerals from the smectite group (montmorillonite) and kaolinite group in claystones. The highest concentration in montmorillonite was identified in tonstein (bentonite). The mineralogical data of tonstein suggests a felsic composition of initial volcanic material that has been transformed in conditions of a negative redox potential and an acidic pH of the swamps during Badenian. The X-rays diffraction was done in the laboratory of Oil-Gas University of Ploiesti. This method was used to characterize minerals from 8 samples collected from the Lighidia quarry. The results of the facies analysis, optical microscopy and X-rays diffraction provide us the evidence of the continental environments that correspond to an alluvial fan and overbank environments that evolves in a warm and humid climate.

**Keywords:** Bozovici basin, lignite, facies analysis, montmorillonite, tonstein, X-rays diffraction, delta plain

### 1. Introduction

Bozovici basin is an intramontane post-tectonic depression from the south of the Southern Carpathian. The objective of this study it represents Badenian deposits from Lighidia perimeter, represented by clay, marl, sandstone, conglomerate, carbonate nodules and coal. The purpose of the study is to show the evidence of the seasonal lake, swamp and alluvial fan depositional environments based on the mineralogical composition resulted from sedimentary facies analysis, optical microscopy and x-ray diffraction.

This paper aims to bring a better understanding of the relationship between alluvial fan and associated overbank sedimentation, which may be important for coal seam and sedimentary deposits with big amount of montmorillonite extent and their exploitation.

### 2. Regional setting

The basin is located in the Caraş-Severin county along the higher course of the Nera River (Fig.1. A). It is delimited in north of Semenice and Anina Mountains, in south and south-east of Almăj Mountains and in south-west of Locva Mountains. The perimeter studied is located in the northern part of the basin, at the exit from the Bozovici (Fig.1.B).

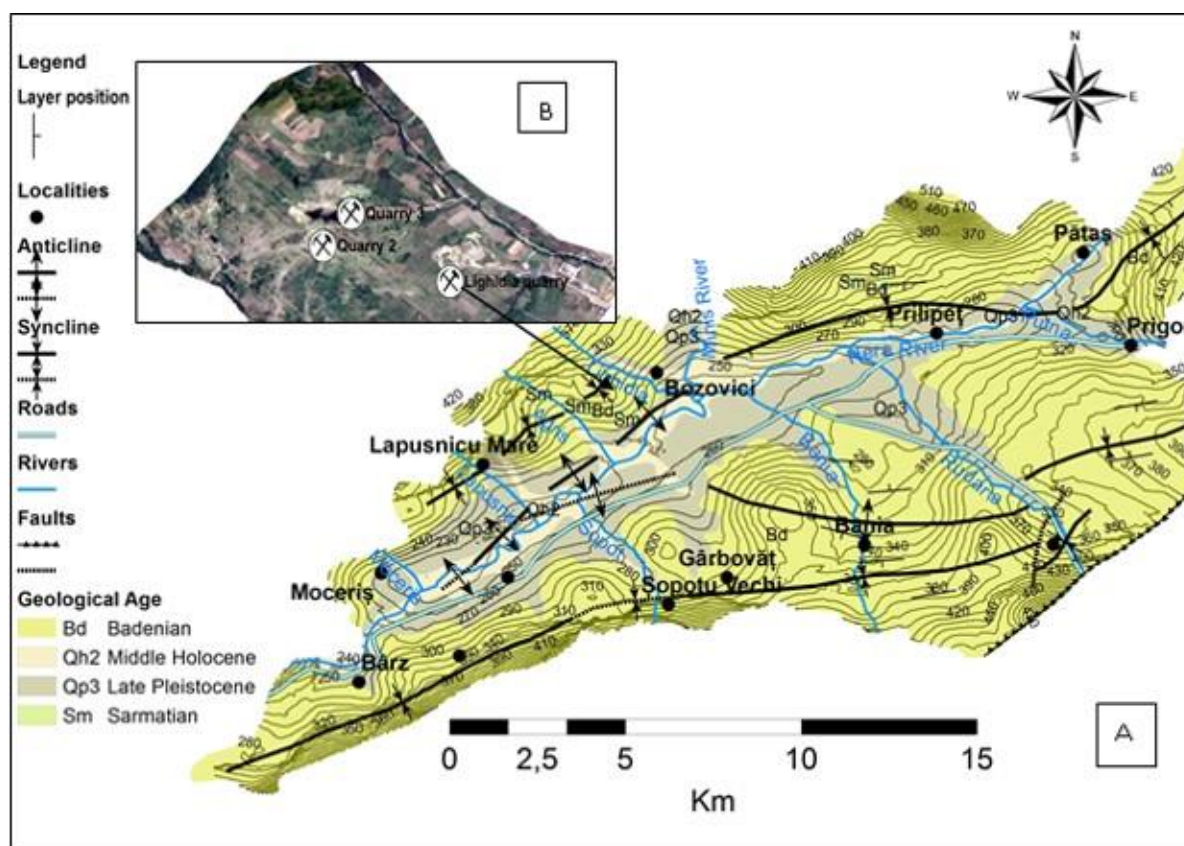
The length of the basin is 40 km and the maximum width is almost 15 km. The thickness of sedimentary deposits is up to 600 m.

The sedimentary deposits of the basin are transgressively and discordantly arranged over the Getic basement and their sedimentary cover. The Getic basement are represented by Sebeş-Lotru, Miniş and Buceava series and the sedimentary cover are represented by upper Jurassic and lower Cretaceous limestones and of upper Cretaceous conglomerates (Balintoni, 1997).

Sedimentary deposits of the basin are composed from Miocene deposits (Badenian) with a similar geological composition to that of Neogene deposits in the Caransebeş-Mehadia basin, of which it was bound by a narrow strip of Miocene deposits in the east part of basin. According to Iliescu et.al (1967), the Badenian deposits in the Bozovici basin are composed from three levels: 1) the lower level that are formed from two small levels: claystone level with marl and coal, and sandstone level with sandstone and claystone; 2) The Dalboset Strata that are formed from conglomerate level with sandstone; and 3) The Sopot Strata with claystone and marl with tuff strata. Petrescu et al. (1986) add a new level represented by sandstones and gravels which they attribute to the Sarmatian. The Quaternary is represented by claystones, sandstones and gravels.

#### 2.1 Tectonic setting

The Bozovici basin formed during the lifting and subsidence movements of the basement in the Neozoic period that led to rise of some crystalline areas along to the sedimentary cover and shedding of some narrow areas that have led to the appearance of the intramontane depression, in which accumulated molasses deposits and it formed coal (Mutihac and Ionesi, 1974).



**Fig. 1.** A. Geological map of Bozovici basin (modified after geological maps Reșița and Baia de Arama – scale 1:200.000); B. Satellite map of Lighidia perimeter.

The most important fault is situated in the east part of basin, which represents an overthrust fault, which delimit Getic unit from the Danubian unit (Preda et al., 1994). The overthrust of Getic unit over Danubian unit occurred during Laramic tectogenesis. Structurally the basin is represented by anticline and syncline folds that are affected of numerous fractures, which appear during Stric tectogenesis.

### 3. Materials and methods

**Facies analysis.** In the field were determined features of the rocks related of their color, thickness, grain size, sedimentary structures, overall lithofacies characteristics and stratum of boundary, were collected samples from which were made 18 thin sections. Based on characteristics of sedimentary rocks were determined the processes and depositional environments.

**Optical microscopy.** In the laboratory were analyzed, with optical microscope, 18 thin sections which were made from samples that derive from facies F14, F10, F8, F3, F2, F1, P1. The study of the 18 thin sections allowed determination of mineralogical composition from sandstones and, in some wise, from carbonate nodules.

**X-ray diffraction.** The bulk samples were grinded in an agate mortar to a fine powder ( $< 2 \mu$ ). X-ray powder diffraction data were measured at 24°C using an automated Bruker D8 Advance  $\theta$ - $\theta$  diffractometer with  $\text{CuK}\alpha$  radiation ( $\lambda = 1,54\text{\AA}$ ; 40kV; 40mA), LynxEye detector and Bragg-Brentano geometry.  $\text{K}\beta$  radiation was eliminated by a Ni filter. Primary and secondary Soller slits were 2.5°. In the measurements were used a 0.6mm divergence slit, a 0.6mm antivergence slit and 0.1mm width detector slit. Data were obtained using 0.1° 2 $\theta$  steps from 1° to 60° 2 $\theta$  counting for 2 seconds per step. The device and emission source profile were modeled using NIST SRM 660a and SRM 676 profile standards.

Qualitative analyses were carried out using Diffracplus EVA software and database PDF-ICDD 2-2008. The Rietveld refinements (quantitative analysis) were carried out using the TOPAS 4.1 software. Pseudo-Voigt (pV) profile function was used for the fit of the peaks. Rietveld refinement quality was expressed by R-values indices represented by Rwp (R-weighted pattern), GOF (goodness-of-fit), DW (the weighted form of Durbin-Watson). (Young, 1996; Pecharsky and Zavalij, 2009).

### 4. Results and discussion

Based on grain size, sedimentary structures, overall lithofacies characteristics and stratum boundary were separated 13 sedimentary facies and a pedofacies represented by carbonate nodules, and then compared with those defined by Miall (2006) (Fig. 2). At facies analysis have been added data determined from X-ray diffraction (Table 1) and optical microscopy analysis.

*Facies A.* The lithofacies consists of sand with gravel sized material (2-10 mm). Grain size is generally very coarse sand to silt, with an admixture of gravels, which consists of sub-angular to sub-rounded grains. The gravels are dispersed in sand. The lithofacies are represented by quartzite, greenschist and carbonate rock fragments. The fossils of microfauna, bivalve, freshwater gastropods remains, and tree stumps are present in this lithofacies. The thickness is between 0.8 to 100 cm and the base boundary is irregular, with non-erosional character. This deposit mould to the bed form. The massive structure and weak normal grading are interpreted as structures produced by high-viscosity mass flows. Matrix-supported massive gravel deposits are formed by mass flow under the condition of balanced viscosity and shear strength (Miall, 2006; Hatano and Yoshida, 2017). This facies is defining for alluvial fans environments, or/ and for proximal sections of the braided rivers (Anastasiu et al., 2007). This lithofacies corresponds to Gmm facies in Miall (2006).

*Facies B.* Dark grey claystones, massive occur in beds 5 to 100 cm thick and the base boundary is sharp. In this lithofacies occur tree stumps. The mineralogical composition determined based on X-ray diffraction of the sample of the *facies B* consists of montmorillonite, kaolinite, chlorite, quartz, albite and muscovite (Table 1). The existence of montmorillonite and kaolinite in claystone suggest a poorly drained, tropical to subtropical areas of low relief marked by flooding during humid season and substantial pore water in the soil during dry season (Hong et al., 2012). The amount chlorite is probably derived from greenschist lithoclasts and is a characteristic mineral of cold regions and dry marked by very low rates of weathering (Hallam et al., 1991). The presence of chlorite together with montmorillonite and kaolinite indicate a particularly cold and arid episode. This lithofacies represent soil development and is common in vegetated floodplains and is equivalent to Fr facies in Miall (2006).

*Facies C.* The coal appears seamed between claystones and have a tend to break up in flags. On the surface of coal appear dispersed sulphur. Allochthonous plant fossils are very abundant. This facies formed by quick accumulation of plants fragments in a warm and humid climate, under lower energy conditions. Coal is typically associated with fluvial floodplains environments and indicates deposition in swamps with stagnant water (Hatano and Yoshida, 2017). This facies is equivalent to C facies in Miall (2006).

*Facies D.* This lithofacies is represented by calcareous claystone without sandy fraction. Leaves fossils and freshwater gastropods remains are abundant. The mineralogical composition identified by X-ray diffraction consists of montmorillonite, calcite, kaolinite, quartz, albite, chlorite and muscovite (Table 1). This lithofacies formed in a specific swamp, created during the floods that had part to sorting of sandy fraction from the clay and silty fraction. The mineralogical composition suggests a warm and humid climate and the apparition of calcite suggest an unusually warm and seasonal arid climate (Hong et al., 2012) consistent with the expansion of C4 biomass (Saylor et al., 2009). This lithofacies represents a floodplain deposit somewhat more distal relative to clastic sources and is equivalent to Fsm facies in Miall (2006).

*Facies E.* This lithofacies consists of alternating beds of reddish-yellowish marl with micro-ripples and horizontal lamination with silt and sandy lenticular lamination. Lucchi (1992) offers us two explains of form of this facies: 1) the fine material deposited slow and continuous from suspension deposits, when the flow begins calm, and the sandy and silty fraction deposited when appear a strong current; 2) every marl level represents a decrease of the current speed, and the sedimentation beginning with sand followed by silt and mud, which suggest that the flooding of overbank area occurred progressive. This two explains indicate deposition from suspension and from weak traction currents. This lithofacies is common in overbank areas and is equivalent to Fl facies in Miall (2006).

*Facies F.* This lithofacies consists of interlamination of horizontally bedded sand and ripple cross-laminated sand with reddish yellowish marl. The structures that compound this facies are represented by horizontal lamination, micro-ripples, cross lamination and coal laminae. Horizontal lamination shows deposits from an upper flow regime of a grain flow, parallel with the bed of flow. Sandy ripples indicate the transition from an upper flow regime to a lower flow regime as a result of change velocity of flow current. The mineralogical composition identified in thin section is show off by quartz, feldspar (orthoclase, microcline and plagioclase), opaque minerals (probably pyrite) and lithic fragments caught in a carbonate cement that show an erosional process due to abundant flooding. These lithofacies are defining for laminated sand architecture and are equivalent with Sh and Sr facieses in Miall (2006).

*Facies G.* This lithofacies consists of pebble to cobble grained conglomerates, that consists of sub-rounded grains. The lithoclasts are represented by quartzite, micaschist, greenschist, sandstone and limestone rock fragments of centimetric to decimetric size. The thickness of this lithofacies is about 250 cm, and the base boundary is non-erosional, irregular and mould to the bed form. The massive structures are interpreted as structures produced by low-strength, pseudoplastic debris flow, deposited from viscous, laminar or turbulent flows (Miall, 2006). This clast matrix supported is defining for alluvial fan environment, and/or for the proximal sections of the braided rivers and is equivalent to Gcm facies in Miall (2006).

*Facies H.* This lithofacies consists of grey fine to medium grained sandstone, massive. Bed thickness range from 30 to 40 cm. In the thin section were identified quartz, feldspar (plagioclase and microcline), calcite and lithic fragments caught in carbonate cement. The fossils content is represented by plant remains in bottom and gastropods in top. The lithofacies can be attributed to rapid dumping of sediment directly from turbulent suspension (Lowe, 1988; Widera, 2016). Its massive nature is considerate indicative of hyper-concentrated flows (Widera, 2016). Such beds are the deposits of gravity flows. A characteristic occurrence of this lithofacies is in small channels resulting from bank collapse (Miall, 2006). This lithofacies is equivalent to Sm facies in Miall (2006).

*Facies I.* Red brown and dark grey marls, massive, occur in beds between 10 to 200 cm (the mostly over 100

cm) thick. The mineralogical composition determined based on X-ray diffraction of the sample of the gray marls consists of calcite, quartz, albite, chlorite, kaolinite and muscovite (Table 1), and indicate a warm and humid climate for this lithofacies. This lithofacies is interpreted to result from deposition of suspended material in deep (over 2 m), relatively long-lived lakes covering the overbank area (backswamp). The massive structure is the evidence of the low variability in settling rate and grain sized of these fines (Widera, 2016). The grey color of this lithofacies is indicative of subaqueous accumulation in anoxic conditions caused partially by decomposition of organic matter (Widera, 2016). This lithofacies is defining for the most distal floodplains facies, including deposition in floodplain ponds, and is equivalent to Fm facies in Rust (1978) and Miall (2006).

*Facies J.* The black shale lithofacies consists of thinly laminated black claystones, very rich in gastropods. The mineralogical composition identified by X-ray diffraction consists of calcite (62.29 % - due to fossils), quartz, chlorite, montmorillonite, kaolinite, muscovite and pyrite (Table 1), and suggest a humid and cold climate. The interpretation of this facies is that mud and gastropods settling in a deep subaqueous domain under anoxic condition (Tavares, 2015). This lithofacies is defining for sediments from lake and is characterized by sediment carried in suspension deposited below the storm wave level. This lithofacies corresponds to Fp in Teixeira (2012).

*Facies K.* This lithofacies consists of interlamination of claystones, siltstones and very fine grained sandstone, including same sparse plant fossils and freshwater bivalve and gastropods remains. Very small scale ripples are present in the sandstone and siltstone beds. Individual layers are between a few millimeters to a few centimeters. The mineralogical composition identified by X-ray diffraction consists of Calcite, Quartz, Muscovite, Kaolinite, Montmorillonite (Table 1), and indicate a warm and humid climate. The concretions (of the smectic claystone), fine lamination and micro-ripples suggest the transition from a cold and humid climate to a warm and humid climate with incipient processes of form soil. Alternation of sandstone layers with claystone layers suggest the repetition of transportation of sediments by traction processes followed by weakening of flows and deposition by suspension currents. Sharp layer boundaries between sandstone and fine grained layers suggest rapid changes of depositional processes due to flooding in overbank area (Hatano and Yoshida, 2017). This lithofacies is common in overbank areas, including deposition from suspension and from weak traction currents, and is equivalent to Fl facies in Miall (2006).

*Facies L.* This lithofacies consists of tonstein. The mineralogical composition identified by X-ray diffraction show that montmorillonite is the dominant mineral, with only small amounts of cristobalite and quartz (Table 1). Cristobalite is usually widely spread in sedimentary deposits, due to the transformation of volcanic ash under alkaline or weakly alkaline conditions (Yudovich and Ketris, 2010; Abruzov et al., 2015). The tonstein result from the weathering of volcanic ash falls in a freshwater swamp.

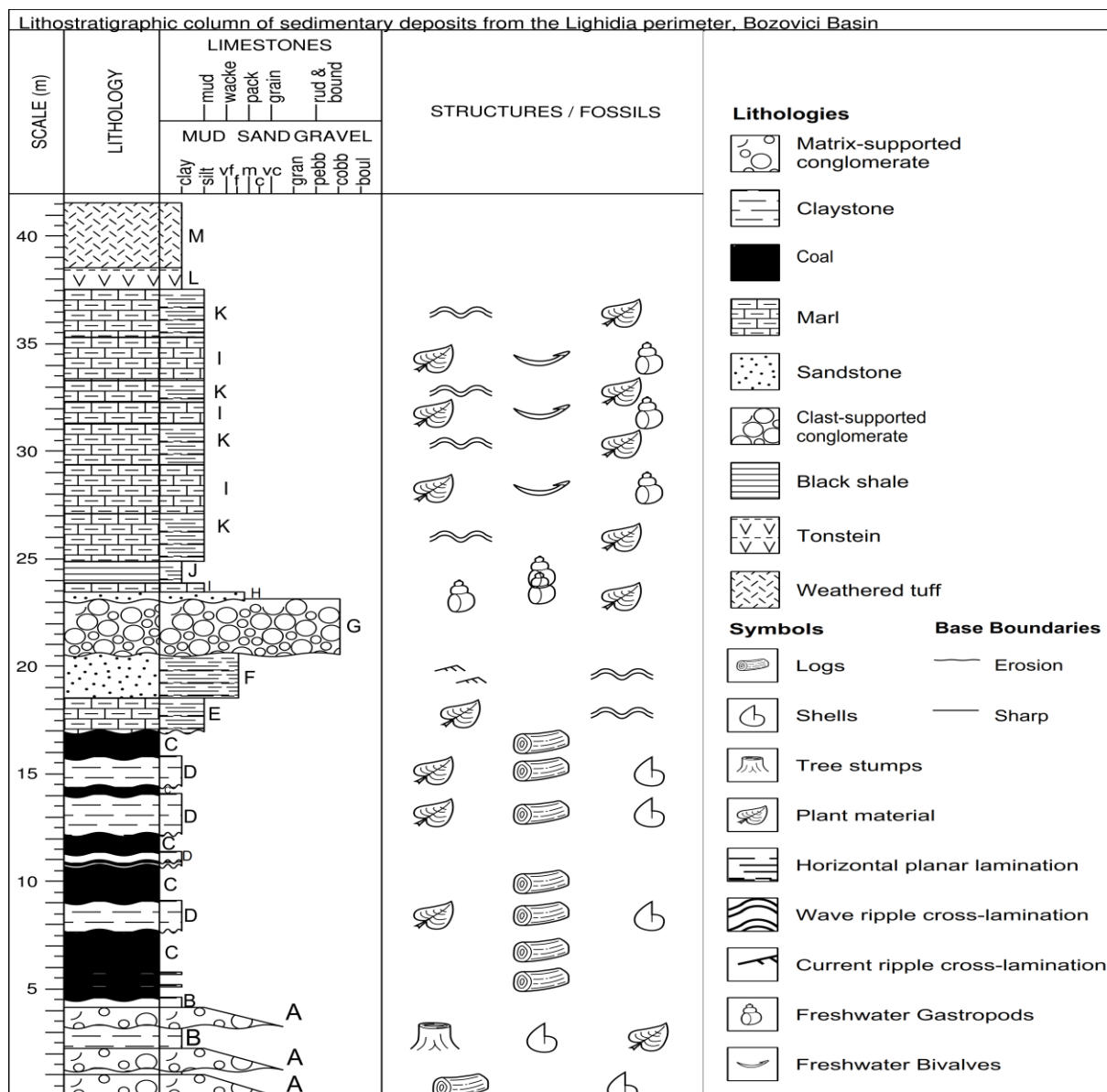
*Facies M.* This facies consists of weathering tuff. The mineralogical composition identified by X-ray diffraction highlighted calcite, cristobalite, quartz, muscovite and tridymite (Table 1). The mineralogical data for tuff show an alkaline composition by presence of calcite. The association of quartz-cristobalite-trydimite were probably inherited from primary volcanic ash (Mitoza et al., 1987, Arbuzov et al., 2015). According to Addison et al. (1983) the high amount of montmorillonite from tonstein and tuff is due of the depositional environment (salinity, pH of water and early diagenesis) and probably suggests that the environment conditions changed.

*The pedofacies (P)* is represented by carbonate nodules in the form of lens which are main formed from calcite and siderite and small amounts of quartz, kaolinite, chlorite, albite and muscovite (Table 1). The increasing of pedogenic carbonates under the form of nodules suggest a particularly arid episode and the large amounts of detrital quartz, albite, muscovite and chlorite suggest a seasonally high water influx and a strong physical erosion under dry climate conditions (Hong et al. 2012).

**Table 1.** X-ray diffraction analyses (%) of the sedimentary deposits in the Lighidia perimeter.

Samples/ Minerals	Tonstein (L) %	Altered tuff (L) %	Black shale (J) %	Smectic claystone (K) %	Marl (I) %	Carbonate nodule (P) %	Clay (B) %	Calcareous clay (D) %
Montmorillonite	92,30	76,10	4,48	70,45	-	-	45,42	35,71
Kaolinite	-	0,73	1,46	1,13	5,34	12,11	21,72	17,60
Clinocllore	-	-	24,77	-	25,43	8,30	18,81	7,50
Cristobalite	6,91	1,49	-	-	-	-	-	-
Quartz	0,79	3,91	5,08	5,21	27,53	18,29	12,30	14,13
Trydimite	-	0,03	-	-	-	-	-	-
Albite	-	-	-	0,56	1,57	2,25	1,10	2,87
Calcite	-	17,39	62,29	22,27	39,11	52,94	-	21,87
Siderite	-	-	-	-	-	5,18	-	-
Muscovite	-	0,36	0,63	0,38	1,02	0,92	0,65	0,31
Pyrite	-	-	1,30	-	-	-	-	-





**Fig. 2.** Lithostratigraphic column of sedimentary deposits from Lighidia quarry, Bozovici basin with original data.

## 5. Conclusions

The warm and humid climate led to apparition of coal-forming swamps with stagnant water. The presence of calcite is due to the biggest amount of fossils. The black shale lithofacies was deposited in the lake center, where anoxic conditions were fitted up. The big amount of chlorite suggest a cold climate. The alluvial fan sediments in association with nearby lithofacies provide evidence of the braided-alluvial fan processes. Claystone and marl were deposited in depression located on the overbank surface.

In conclusion the rock units were deposited in the alluvial fans and subenvironments of the braided-river system. The coal seams occurred in well-drained swamps and the coal distribution was controlled by braided channels. At the end of sedimentation stage, the basin was occupied by shallow lakes and these were filled rapidly by volcanoclastic products and flood sediments.

The Lighidia perimeter consists from tonsteins and smectitised tuffs with minor kaolinite. The mineralogical composition of these is a function of depositional environment and the volcanic source was probably of intermediate or acidic composition. The economic importance of deposits from studied perimeter is due on the one hand to the existence of large amount of montmorillonite mineral form the tonstein, altered tuff and smectic clay (> 50 %), and on the other hand to the existence of lignite that are wide-spread in the wholly basin.

**Acknowledgements.** The authors are grateful to I. Mariş for her assistance in samples collection and making of lithological column, and to T. Creţ for his permission to collect samples from the Lighidia quarry.

## 6. References

- Addison R., Harrison R.K., Land D.H., Young B.R. (1983) Volcanogenic tonsteins from Tertiary coal measures, East Kalimantan, Indonesia. In: *International Journal of Coal Geology Series*, 3, p. 1 – 30.
- Anastasiu N., Popa M., Roban R.D. (2007) *Sisteme depoziționale. Analize secvențiale în Carpați și Dobrogea*. Editura Academiei Române, 614 pp., București.
- Arbuzov S.I., Mezhibor A.M., Spears D.A., Ilenok S.S., Shaldybin M.V., Belaya E.V. (2015) Nature of tensteins in the Azeisk deposits of the Irkutsk Coal Basin (Siberia, Rusia). In: *International Journal of Coal Geology Series*, 153, p. 99 – 111.
- Balintoni I. (1997) *Geotectonica terenurilor metamorfice din România*. Editura Carpatica, 227 pp., Cluj-Napoca.
- Codardea A., Răileanu Gr. (1968) Republica Socialistă România. Harta geologică, L-34-XXIX, scara 1:200.000, foaia Baia de Aramă. Institutul geologic cartografii, București.
- Codardea A., Răileanu Gr. (1968) Republica Socialistă România. Harta geologică, L-34-XXVIII, scara 1:200.000, foaia Reșița. Institutul geologic cartografii, București.
- Hallam A., Grose J.A., Ruffell A.H. (1991) Paleoclimatic significance of changes in clay mineralogy across the Jurassic-Cretaceous boundary in England and France. In: *Palaeogeography, Palaeoclimatology and Palaeoecology Series*, 81, p. 173 – 187.
- Hatano N., Yoshida K. (2017) Sedimentary environment and paleosols of middle Miocene fluvial and lacustrine sediments in central Japan: Implications for paleoclimate interpretations. In: *Sedimentary Geology Series*, 347, p. 117 – 129.
- Hong H., Wang C., Zeng K., Zhang K., Yin K., Li Z. (2012) Clay mineralogy of The Zhada sediments: Evidence for climatic and tectonic evolution since 9 Ma in Zhada, Southwestern Tibet. In: *Clay and Clay Mineral*. Vol. 60. No 3., p. 240 – 253.
- Iliescu O., Radu A., Lica M. (1967) Geologia bazinului Bozovici. D.S. Inst. Geol., LIII 1.
- Lowe D. R. (1988) Suspended-load fallout rate as an independent variable in the analysis of current structures. In: *Sedimentology Series*, 35, p. 765-776.
- Lucchi F.R. (1992) *Sedimentographica. A petrographic atlas of sedimentary structures*. Second edition., Columbia University Press, 282 pp., New York.
- Petrescu I., Bițoiianu C., Nicorici M., Ionescu E., Mărgărit Gh, Nicorici E., Pătruțoiu I., Todroș C., Popescu D. (1986) *Geologia zăcămintelor de cărbuni*. Vol. 1. Editura Tehnică, 314 pp., București.
- Miall A. (2006) *The geology of fluvial deposits. Sedimentary facies, basin analysis, and petroleum geology*. Springer, 582 pp., Toronto, Canada.
- Mizota C., Toh N., Matsuhisa Y. (1987) Origin of cristobalite in soils derived from volcanic ash in temperate and tropical regions. In: *Geoderma Series*, 39, p. 323 – 330.
- Mutihac V., Ionesi L. (1974) *Geologia României*. Editura Tehnică, 646 pp., București.
- Pecharsky V.K., Zavalij P.Y. (2009) *Fundamentals of Powder Diffraction and Structural Characterization of Materials*. Second Edition. Springer – Verlag US, 744 pp.
- Preda I., Turculeț I., Androhovici A., Barus T. (1994) *Geologia Zăcămintelor de cărbuni*. Partea a II-a. Răspândirea zăcămintelor de cărbuni. Editura Universității București, București.
- Saylor J.E., Quade J., Dellman D.L., DeCelles P.G., Kapp P.A., Ding L. (2009) The late Miocene through present paleoelevation history of southwestern Tibet. In: *American Journal of Science Series*, 309, p. 1 – 42.
- Tavares A.C., Borghi L., Corbett P., Nobre-Leopes J., Câmara R. (2015) Facies and depositional environments for the coquinas of the Morro do Chaves Formation, Sergipe-Alagoas Basin, defined by taphonomic and compositional criteria. In: *Brazilian Journal of Geology Serie*, 45, p. 415-429.
- Teixeira B.F.L. (2012) *Coquinas de Formacao Morro do Chaves (Cretaceo Inferior), secao Rifte da Bacia Sergipe-Alagoas*. Trabalho de conclusao de curso, Graduacao em Geologia, Departamento de Geologia, Universidade Federal do Rio de Janeiro, 107 pp.
- Widera M. (2016) Depositional environments of overbank sedimentation in the lignite-bearing Grey Clays Member: New evidence from Middle Miocene deposits of central Poland. In: *Sedimentary Geology Sedries*, 335, p. 150-165.
- Young R.A. (1996) *The Rietveld Method (IUCr Monographs on Crystallography)*. Oxford University Press, 308 pp.
- Yudovich Y.A.E., Ketris M.P. (2010) *Geochemical and Mineralogical Indicators of Volcanic Products in Sedimentary Rocks*. UB RAS Ekaterinburg, 412 pp.

## DECONTAMINATION OF MIDDLE TO LOW-GRADE CONTAMINATED AREAS, USING A LOWCOST METHOD

Heloiza M. HORN<sup>1\*</sup>, Adolf H. HORN<sup>2</sup>, Regynaldo A. SAMPAIO<sup>1</sup>, Essaid BILAL<sup>3</sup>

<sup>1</sup> Universidade Federal de Minas Gerais, Montes Claros, MG, Brazil;

<sup>2</sup> Universidade Federal de Minas Gerais, Belo Horizonte, MG, Brazil;

<sup>3</sup> École des Mines de St. Etienne, St. Etienne, France;

\* hmfhorn@uol.com.br; Tel.: 0055 31 34417505 21;

**Abstract:** Protected areas and wetlands often suffer contamination due to outcrops or by passage of contaminated fluids as rain, subsurface water or river infiltration. Due to legislation, in these areas activities which alter the natural environment are not permitted. Here we suggest and describe a methodology that can be used in all low to middle-grade contaminated areas without the necessity of structure changes, intense human interference and/or supervision.

**Keywords:** contaminated regions; plants; Si-Phytoliths; heavy metals; soils; native plants.

### 1. Introduction

With the increase of industrial and mining activities, larger areas are affected by contamination, often passing the limits established by local authorities or causing hazardous effects for living-, especially human beings.

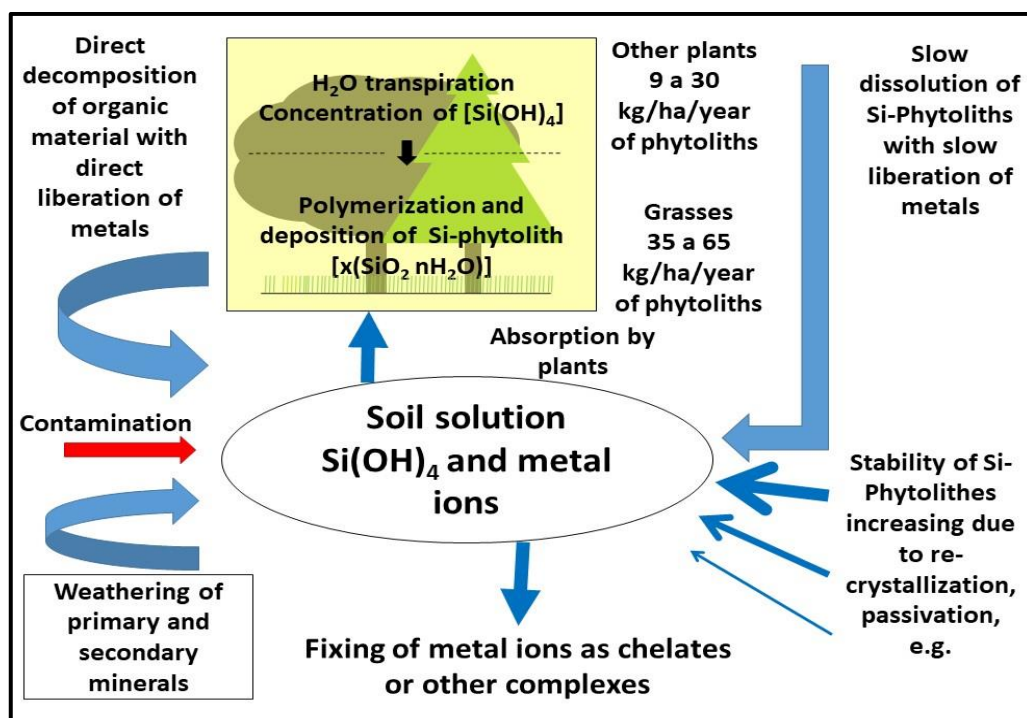
Many different decontamination techniques, like mechanical, chemical or biological/biochemical intervention were developed and suggested (e.g.: Cunningham et al., 1996; Accioly and Siqueira, 2000; Meurer, 2004; Melo et al., 2006), but nearly all are based on a strong interaction with the contaminated soil, destroying natural structures and biotopes, or need a permanent supervision during their execution.

The method here suggested is simple to apply, cheap, very adaptable and does not imply great monitoring efforts during its execution and is qualified to be applied under a wide spectrum of climate situations and different types of contaminations. Here in this text an example from the Savanna system in Brazil is shown (Fernandes-Horn, 2016).

The methodology is based on two concepts:

**a.** Plants absorb metals in their parts and trap them especially in Si-Phytoliths (Figure 1).

**b.** Organic opal is nearly insoluble and has a long resistance to attack under normal soil conditions (Fig. 2; Table 1).



**Fig. 1:** Schematic diagram of heavy metal behavior in the soil-plant system. Other important factors are temperature, water flux quantity and velocity. Metal trapping per ha is estimated.

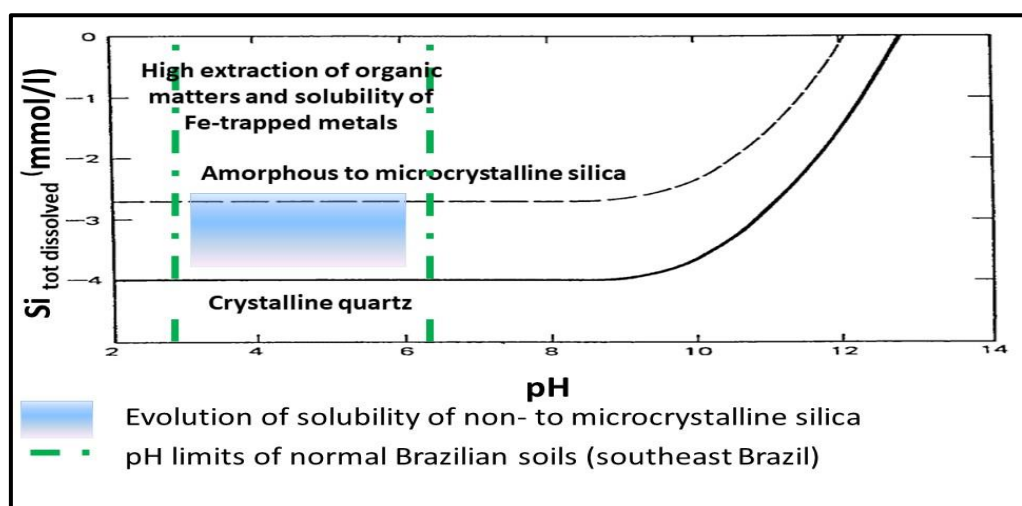


Fig. 2: Opal conditions in the natural environment (Sources: Ondo and Sase, 1986; Iller, 1979).

Table 1: Opal properties and element trapping compared to other SiO<sub>2</sub>- compounds.

Mineral	Density	Hardness	Impurities g kg <sup>-1</sup>	H <sub>2</sub> O g kg <sup>-1</sup>
Quartz	2,65	7,0	traces	0
Plant opal	1,5 –	5,5 – 6,5	50-150*	40-90
Geol. opal	2,3 1,2 -2,9	5,5 – 6,5	up to 200**	2 - 10

\*Al<sub>2</sub>O<sub>3</sub>, C, Fe, K, Na, Cu, Ti and others;

\*\*not only in the structure.

## 2. Regional setting

The target area of about 500 m<sup>2</sup> is localized at the northern border of the Minas Gerais State (UTM 702600E – 702300E and 8230750N – 8230350N), near the town of Riacho dos Machados in the transition zone between semiarid to arid conditions (Fig. 3). It belongs to a region where the mineralized rocks were explored by the Carpathian Gold Inc. crop out and caused anomalies of Zn, Pb and Cu.

Typical plant associations (Campos and Labouriau, 1969; Buján, 2013) form the vegetation in these hot and dry conditions.

## 3. Geology of the study area

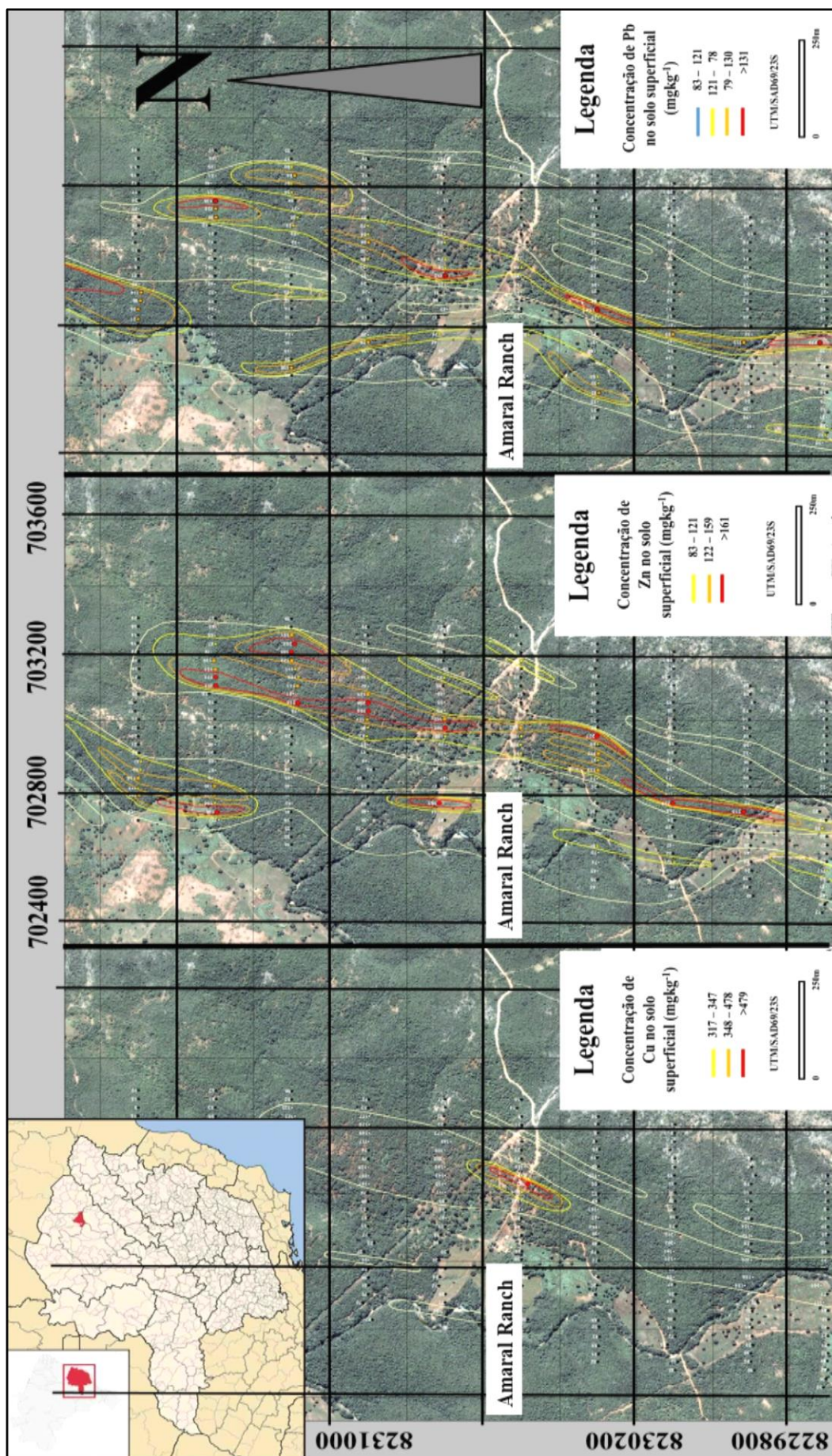
The study area consists mainly of Precambrian rocks, migmatites and schists with intrusive granites, which suffered tectonism and hydrothermalism during the Brasiliano Event, causing impregnation with metals, especially Zn, Pb, Cu and Au by ascending liquids. Heavy metal concentration is limited on fractures and surrounding contacts. All is covered by soils, predominantly quartzitic sand, not well developed (~10–40cm) Ultisols and Inceptisols, disposed over an undulated landscape.

## 4. Materials and methods

The existent natural species, occurring in the working areas, were sampled. Three species of them adequate to the conditions and with favorable biological properties, were selected (Table 1). In this case *Rollinia leptoptella*, *Piptadenia gonoacantha* and *Sida sp.*

To compare metal concentration from plants with that from soil-Phytoliths, soil samples were collected over the investigated area.





**Fig. 3:** Location and element-distribution at the experimental area (Source: Crocco et. al., 2006).



The separation of the Si-Phytoliths was executed using the extraction methodologies of Coe (2009) for soil samples and of Parr et al. (2001) for plants.

The separated Si-Phytoliths were dissolved using hot HF/HNO<sub>3</sub> mixtures to separate metal concentrations. The soil samples were treated with different solutions (H<sub>2</sub>O; HNO<sub>3</sub> 10%; HNO<sub>3</sub> conc.) to obtain information about total and available concentration of metals.

The analyses for total metal concentrations in soil were performed using a Shimatzu X-ray fluorescence (XRF) equipment at the multiuse laboratory at UFVJM, Diamantina. The Si-Phytolith extracts were analyzed by ICP-OES, model M 4165, Spectroflame-Spectro, at the laboratory of NGqA of the UFMG in Belo Horizonte. All applied methods were according to international and national standards.

## 5. Results

### 5.1. Element behavior in the plants

All three plants formed nearly the same totalized Si-Phytolith quantities. The highest concentration was found in the leaves, which also showed the highest dry mass, followed by roots and stems.

The element showed a peculiar distribution in plants and their organs. It seems that there are groups with homogeneous correlated behavior while other ones have no correlated behavior. In addition, variations in the deposited elements concentrations can be observed in the leaves, stems and roots of the investigated plants (Table 2). This may be a result of element inherent chemical properties or related to the accessible soil concentrations (Fig. 3).

**Table 2:** Phytolith mass of the selected plants, metal content per plant and the calculation per kg dry mass. ps = wet mass (100g); pc = dry mass; pf = Mass of Si-Phytoliths.

Species		Pc (g)	Pf(g)	ps/pc (%)	ps/pf (%)
<b>Rollinia leptopetala</b>	<b>Leaves</b>	109,76	15,18	11	1,5
	<b>Stems</b>	88,86	13,12	8,9	1,3
	<b>Roots</b>	76,84	15,48	7,7	1,6
<b>Piptadenia gonoacantha</b>	<b>Leaves</b>	70,38	13,67	7	1,4
	<b>Stems</b>	74,98	8,62	7,5	0,9
	<b>Roots</b>	35,98	8,20	3,6	0,8
<b>Sida sp</b>	<b>Leaves</b>	90,97	22,71	9,1	2,2
	<b>Stems</b>	98,86	16,39	9,9	1,7
	<b>Roots</b>	85,75	7,71	8,6	0,8

Each one of the three investigated plant species enriches metals differently in leaves, roots and stems. For *Rollinia leptopetala* and *Piptadenia gonoacantha* the leaves, followed by roots and stems concentrate more metals. *Sida sp.* shows a different behavior with a sequence from root and stems to leaves.

The highest metal concentrations are that of Mn, Ba, Zn, Pb, Ni, Cu, Co, Cd and Cr. This order correlates with the element's concentration in the substrate.

Table 3 shows the trapped element concentrations in the selected plants, which are similar to those observed in other plants and biotopes (Campos and Labouriau, 1969).

**Table 3:** Metal trapping per selected plants and parts of the plants.

Species		Ba	Cr	Co	Cu	Cd	Ni	Pb	Ti	Mn	Zn
<b>Rollinia leptopetala</b>	<b>Leaves</b>	61021	49	293	6329	216	5434	1603	21886	112016	17171
	<b>Stems</b>	27375	73	270	7550	200	1505	1627	16969	31358	34821
	<b>Roots</b>	57943	2689	824	20911	357	9643	11244	312192	80589	16172
<b>Piptadenia gonoacantha</b>	<b>Leaves</b>	37252	3291	726	8862	210	4044	2971	60569	148271	32811
	<b>Stems</b>	90686	717	461	8785	182	2892	2061	26316	75980	32314
	<b>Roots</b>	8526	3352	580	3489	642	2563	3580	74659	37813	32670
<b>Sida sp</b>	<b>Leaves</b>	19788	193	157	5290	127	874	1825	8068	92732	22714
	<b>Stems</b>	25721	116	618	8121	572	7499	3503	6040	118652	32214
	<b>Roots</b>	32369	749	303	4192	108	1328	30546	53467	31172	14562

## 5.2. Soil (substrate) evolution

The observations made over a period of four years (2015-2018) permit to suggest that there is a real reduction in available metals in the treated soils.

In Table 2 it can be seen the respective concentration of Phytoliths in the selected plants related with dry mass. Combined with the data from Table 3 it is possible to evaluate the transfer factor from available metal ions to fixed metal compounds in soil after plant activity.

Table 2 shows the relation between plant mass, dry plant mass and Phytolith content. We may calculate 10 to 80 kg/ha/year of Si-Phytolith production (Fig. 1) with a trapping between 150 to 150000 ppm of Metal-ions/kg of Phytoliths (Table 3) to the total element immobilization of about 100-300 g/ha/year.

In Fig. 4 a schematic element balance is shown.

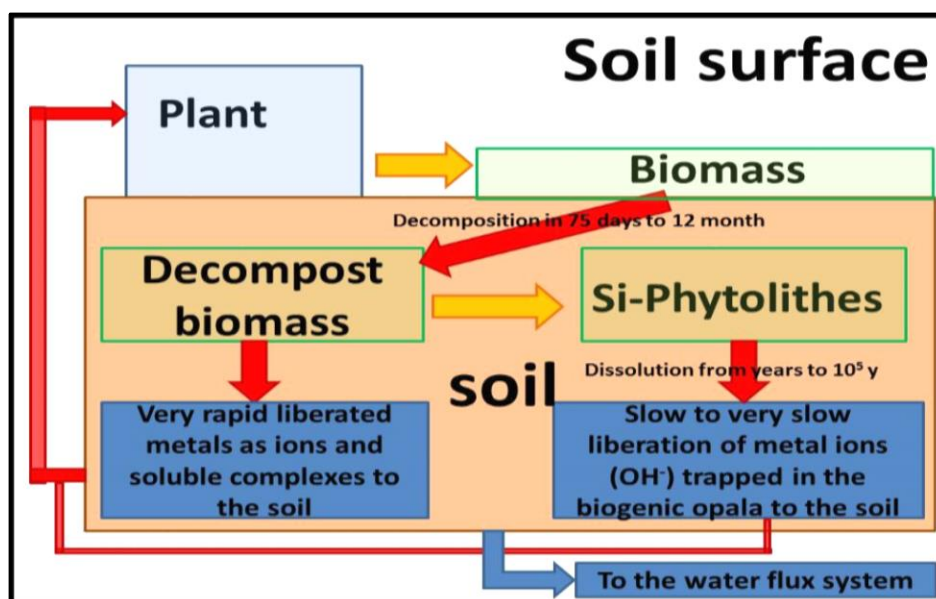


Fig. 4: Schematic decontamination process, using plants with Si-Phytoliths.

## 6. Conclusions

This paper presents a methodology to reduce metal concentrations in soils affected by natural enrichment or by industrial and mining site contributions, if the concentrations are not too high. The overall reduction of available metal is higher than the annual production by natural processes like weathering (Fig. 4).

The results show that it is possible to use invaders, or better, natural species to transform available element concentration from a contaminated soil or substrate in compounds of low solubility, and to reduce in this way the contamination of the soil making the area available for agricultural activities like cattle breeding or plantations after a certain period.

Before the use of this method, it is necessary to select adequate plant species and to obtain information about the soil properties to estimate the time between fixing and slow liberation to the aquatic system.

## 7. Acknowledgements

We thank CNPq, FAPEMIG and CAPES for financial and local Farmers and the Carpathian Gold Ltda. for logistic support.

## 8. References

- Accioly A.M.A., Siqueira J.O. (2000) Contaminação química e biorremediação do solo. In: Novais, R. F.; Alvarez V.; V. H.; Schaefer, C. E. G. R. Tópicos em ciência do solo. Viçosa: Sociedade Brasileira de Ciência do Solo, v. 1, p. 299-352.
- Buján E. (2013) Elemental composition of phytoliths in modern plants (ERICACEAE). Quaternary International, n. 287, p. 114-120.
- Campos A.C., Labouriau L.G. (1969) Corpos silicosos de gramíneas dos cerrados. II. Pesquisa Agropecuária Brasileira. 4, p. 146-151.

- Coe H. (2009) Estudo de Fitólitos: Protocolo de Extração de Fitólitos e Extração de Sedimentos de Solos. Departamento de Geografia. UERJ/FFP.
- Crocco F.A., Abreu F.R. de, Teixeira N., Cançado F.L.L., Maciael J.D., Sena F., Ramos M.M. (2006) Mineralizações de Zinco e chumbo do depósito salobro, Porteirinha, MG. p. 359-377.
- Cunningham S.D., Anderson T.A., Schwab A.P. (1996) Phytoremediation of soils contaminated with organic pollutants. *Adv. Agron.*, v. 56, p. 55-114.
- Fernandes-Horn H.M.F., Sampaio R.A., Horn A.H., Oliveira E.S.A. de, Lepsch I., Bilal E. (2016) Use of Si-Phytoliths in depollution of mining areas in the Cerrado-Caatinga region, MG, Brazil. *Int. J. of GEOMATE*, p. 2186-2990.
- Iler R.K. (1997) The chemistry of silica: solubility, polymerization, colloid and surface properties, and biochemistry. New York: John Wiley and sons Interscience, 896 p.
- Jones L.H.P., Handreck K.A. (1967) Silica in soils, plants and animals. *Adv. Agron.* 19, p. 107-149.
- Kondo R., Sase T. (2006) Opal phytoliths, their nature and application. *Quarter. Res.*, 25, p. 31-63.
- Melo E.E.C., Nascimento C.W.A., Santos A.C.Q. (2006) Solubilidade, fracionamento e fitoextração de metais pesados após aplicação de agentes quelantes. *R. Bras. Ci. Solo*, 30, p. 1051-1060.
- Meurer E.J. (2004) Fundamentos de Química de Solo. Ed. Gênese, Porto Alegre, 2<sup>nd</sup> ed., 290 p.
- Parr J.F., Lentfer C.J., Boyd W.E. (2001) A comparative analysis of wet and dry ashing techniques for extraction of phytoliths from plant material. *J. of Arch. Sci.*, 28, p. 875-886.

## CHARACTERIZATION OF CLAY MINERALS FROM THE REJECT OF THE SAND EXTRACTION IN CAPELA DE SANTANA-RS, BRAZIL

João P. S. KESSLER<sup>1</sup>, Thiago P. ARAUJO<sup>1\*</sup>, Fernando M. MELLO<sup>2</sup>, Essaid BILAL<sup>3</sup>

<sup>1</sup> Universidade do Vale do Rio dos Sinos (UNISINOS), São Leopoldo-RS, Brazil;

<sup>2</sup> Universidade Federal Rural do Rio de Janeiro (UFRRJ), Seropédica-RJ, Brazil;

<sup>3</sup> Ecole des Mines de Saint Etienne (EMSE), GSE, CNRS UMR 5600, F42023 Saint-Etienne France.

\* [tpeixotoa@unisin.br](mailto:tpeixotoa@unisin.br)

**Abstract:** Clay minerals are largely used in various industries and engineering works, as an essential raw material. In the municipality of Capela de Santana/RS, Brazil, several sand deposits are explored, and in a specific manner the beneficiation process of this material generates large amounts of sediment of very fine grain size in its tailing basin. The characterization of this material can add economic value to the slag mineral, previously discarded, and supply market demands. This study aims to characterize that sand mining reject, by classing its granulometry, mineralogical composition and physico-chemical behavior, with the purpose of evaluating their future application in geotechnical works.

**Keywords:** clay minerals, raw material, environment, Brazil, natural resources, valuation, geotechnical works.

### 1. INTRODUCTION

Clay minerals are in general, secondary minerals and are mainly composed of the kaolinite groups ( $\text{Al}_4(\text{OH})_8\text{Si}_4\text{O}_{10}$ ), illites (complex hydrated silicates of Al, Mg, Fe and Na), montmorillonites (complexes hydrated silicates of Al, Mg and Na), among others.

Due to their specific physical and chemical properties these mineral groups are used in a wide range of industrial and engineering works. Its applications are related to its structure, composition, physical and chemical behavior. Thus, knowledge of these characteristics can define their use, improve their utilization or even open new areas of application (Savicet et al., 2014).

With interest in the possibilities of application of clay minerals in geotechnics, such as the construction of dams, use as a waterproofing layer in engineering works, road paving, liners in sanitary landfills, constituents of geomembranes, or stabilization of soils and slopes, this work will seek to characterize its mineralogy and define the physical-chemical parameters of clays to define their applicability.

Clay minerals can be widely used in engineering works, from the geological drilling process where clays are used as drilling fluid to slope stabilization works, foundations for structures, chemical or water containment barriers, etc.

Due to this, the current market demands a large range of clays with specific characteristics; with the study being developed it will be possible to define the applicability of an existing clay deposit, adding value to the sand mining activity and possibly supply a niche market.

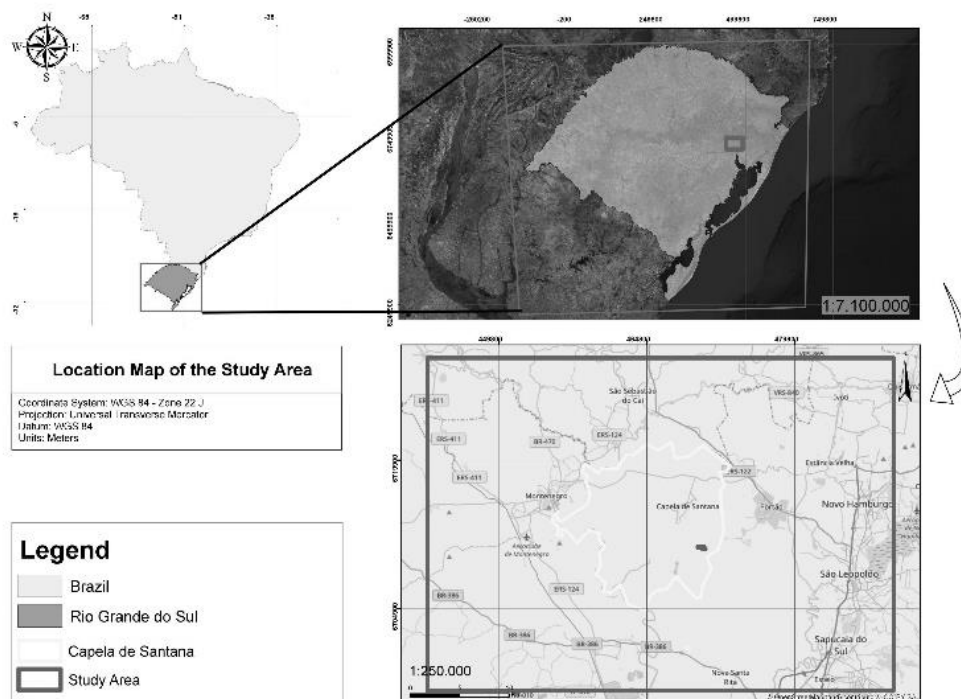
The main objective of this work is to characterize the waste material from a sand deposit in the municipality of Capela de Santana/RS, in Brazil, and to evaluate its applicability as a sealing layer in sanitary landfills (mineral liner).

### 2. LOCATION AND GEOLOGY OF THE STUDIED AREA

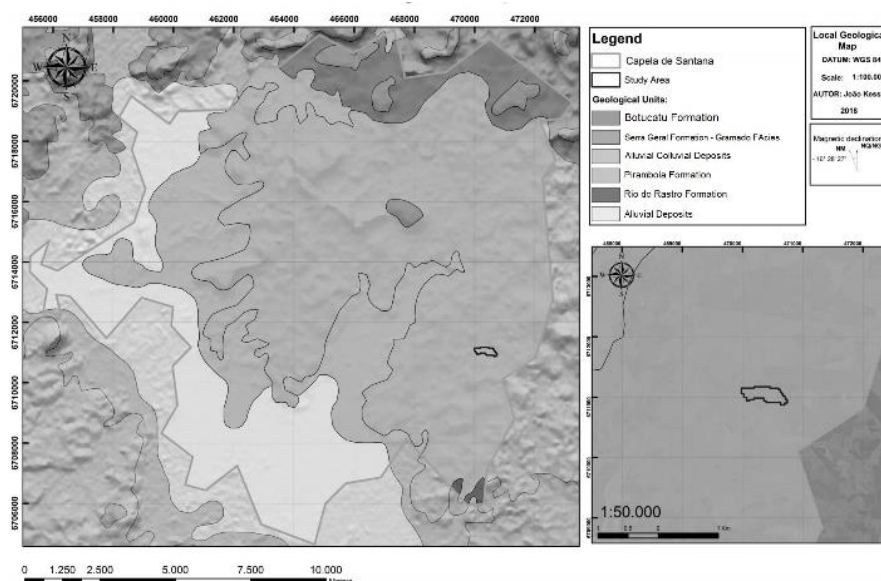
This work was carried out at Sanga Funda, in the Capela do Santana county (Fig. 1), in the state of Rio Grande do Sul, Brazil, located on the southern flank of the huge Paraná Sedimentary Basin comprising near shore environments stratigraphic units of Neopaleozoic to Mesozoic ages. The Mesozoic units are represented by the Sanga do Cabral Formation (Rosário do Sul Group) and Pirambóia, Botucatu and Serra Geral Formations (São Bento Group) (Milani et al, 2007). The Pirambóia Formation is one of the units with the largest outcrops areas in Capela de Santana (Fig. 2) and encompasses a large portion of the municipality, from its center-west to the east, and covers the region of the area under study (Zalán et al., 1990; Montardo, 1982; Lavina et al., 1993; Grehs, 1976; Bilal et al., 1998; Bilal et al., 2000).

### 3. MATERIALS AND METHODS

The object of this study is a geotechnical characterization of the existing material in the reject pond from the mineral extraction of sand. Sand mining at the site is accomplished by the hydraulic removal of soil horizons and saprolitic material from the alteration of the sedimentary rocks of the Piramboia Formation.



**Fig. 1.** Location map of the study area in relation to the state of Rio Grande do Sul, Brazil.



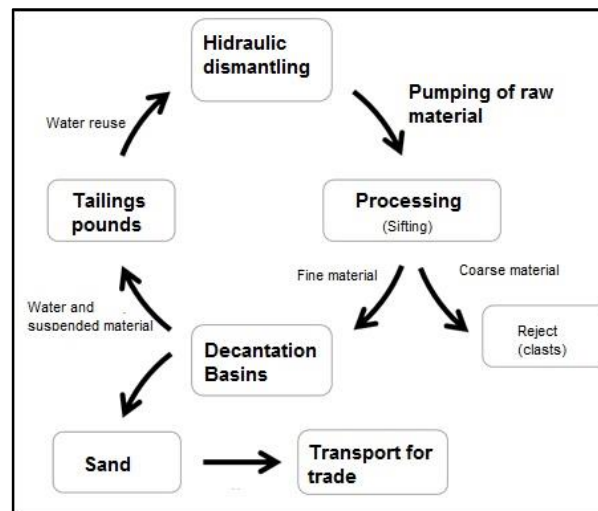
**Fig. 2.** Geological map of the study area.

The plowed material is selected by density in decantation basins and the sands are currently commercialized from fine-grained to medium-grained, the remaining material is sent to reject basins. With the plowing process used, as shown in Fig. 3, the discarded material is composed of fine granulometry sediments, and it may become viable the economic exploitation of this mineral good, now discarded as waste from the process.

In order to carry out the characterization of the reject, samples were collected from two reject ponds that were already in their maximum capacity in the period in which the samples were collected. Material from each sampled basin has clearly compositional variations, highlighted by the etching of the material.

As a preliminary analysis, sedimentation, liquid limit (LL) and plasticity limit tests were performed according to Brazilian standards NBR 6457/86, 6508/84, 7181/16, 7180/84 and 6459/84, in order to obtain a prior knowledge of the grain size distribution and some behavior of the samples. These characteristics are essential for the application of materials such as sealing layer in landfills. In addition, the determining factor for the use of this material as mineral liner is percolation velocity and water through the material.





**Fig. 3.** Flowchart of the extraction method of the material.

It is very important to define the mineral specimens in the reject, because different clay minerals will present different behaviors. For this, X-Ray Diffraction and X-Ray Fluorescence analyzes were performed on samples from the two reject basins, since these methods are well suited for the identification of different types of clays, as they have very characteristic diffraction profiles and easy distinction (Albers et al., 2002; Arab et al., 2015; Benson et al., 1994).

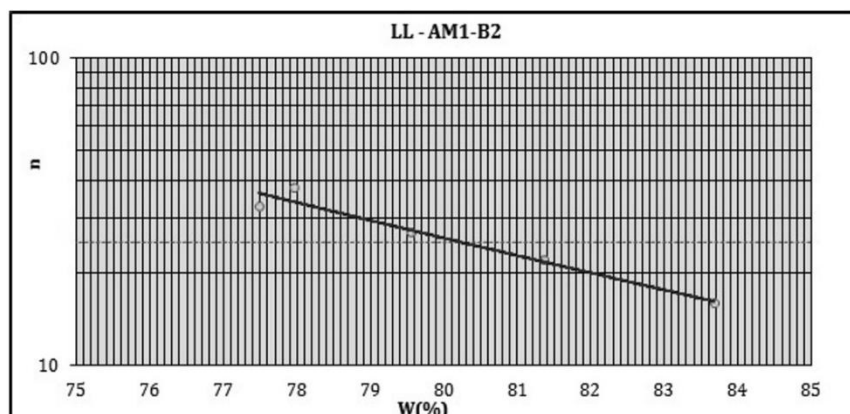
From the data obtained so far it is possible to say that the material has potential to be used in the purpose proposed by the study. Still remaining to assess the permeability coefficient to ensure that all the requirements implied by the standards for the construction of landfills are met.

The sedimentation tests and the Attenberg Limits performed initially were redone. After the sedimentation test was carried out pH was measured from the deflocculant solution ( $(\text{NaPO}_3)_6$ ) and it was found to be pH below the ideal provided by the standard, which may lead to a reduction in the efficiency of particle disintegration, resulting in a larger particle size than the real sample. Therefore, it was necessary to retake the deflocculant solution, with greater control in the preparation.

In addition, sedimentation tests were performed with two sample preparation methods. In the first one the material was disaggregated using a ball mill and then subjected to the action of the deflocculant and the second, the material was only subjected to manual disaggregation and then applied the deflocculant solution for the sedimentation test. These two preparation methodologies were applied due to the behavior resulting from the granulometry of very fine nature of the material since both the methods are questionable. Due to the disintegration in the mill, grain breakage and granulometry reduction can occur, and disintegration can only be achieved by the action of the deflocculant solution, the possibility that grains remain aggregated and decant more rapidly, resulting in an increase in granulometry.

#### 4. RESULTS AND DISCUSSION

So far, the tests for two samples, one of each reject basin, denominated AM1-B1 and AM1-B2 (Reject basin 1 and 2, respectively), have been carried out. The sample AM1-B2 has a LL of 81% (Fig. 4) and a plasticity limit of 29.94%. The sample has a high plasticity, having a plasticity index of 51,06.



**Fig. 4.** Graph of sample liquidity limits AM1-B2

The sample AM1-B2 presents high clay contents, as shown in the grain size distribution curves presented in Fig. 5.

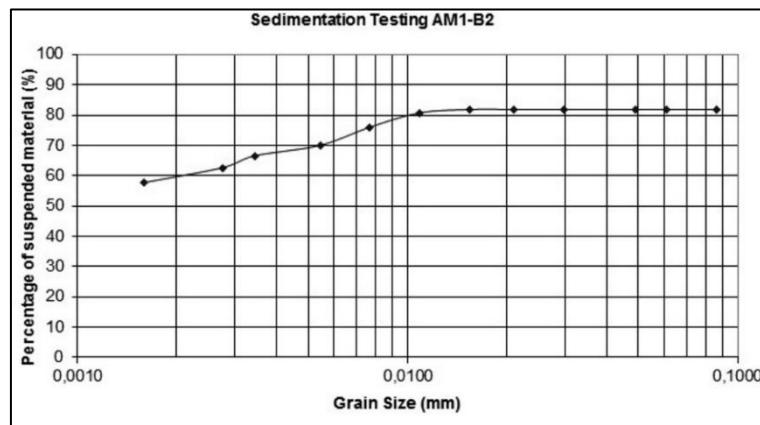


Fig. 5. Sample size curve AM1-B2.

The sample AM1-B1 has a liquidity limit of 71.9% (Fig. 6) and a plasticity limit of 31.7%. The sample has a high plasticity, with a plasticity index of 40.2.

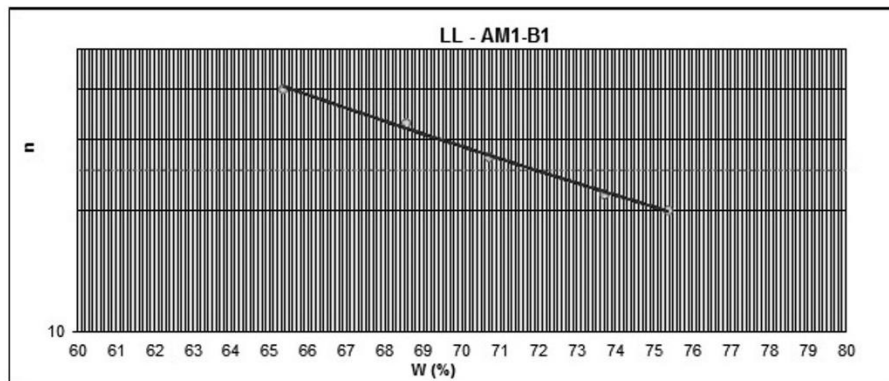


Fig. 6. Graph of sample liquidity limits AM1-B1.

The AM1-B1 sample also appears to have a high clay content, since after the time of 24 hours of sedimentation 69.5% of the particles remained in suspension, however due to the low specific weight of the particles, it was not possible to reach the expected particle size, only the silt fraction (0.002 mm), as shown in the grain size curve shown in Fig. 7.

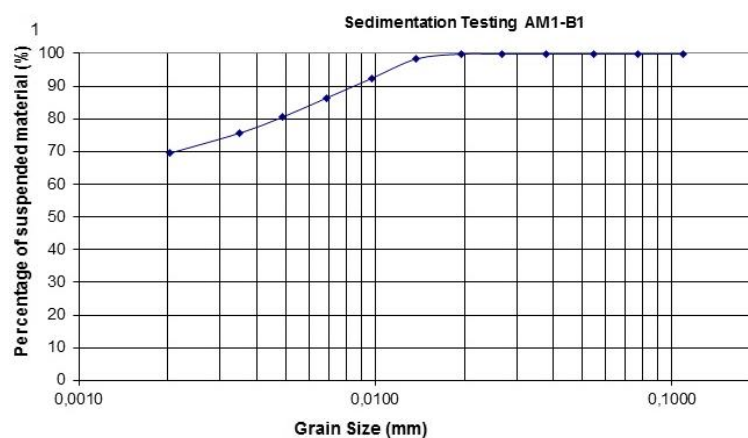


Fig. 7. Grain size distribution curves of sample AM1-B1.

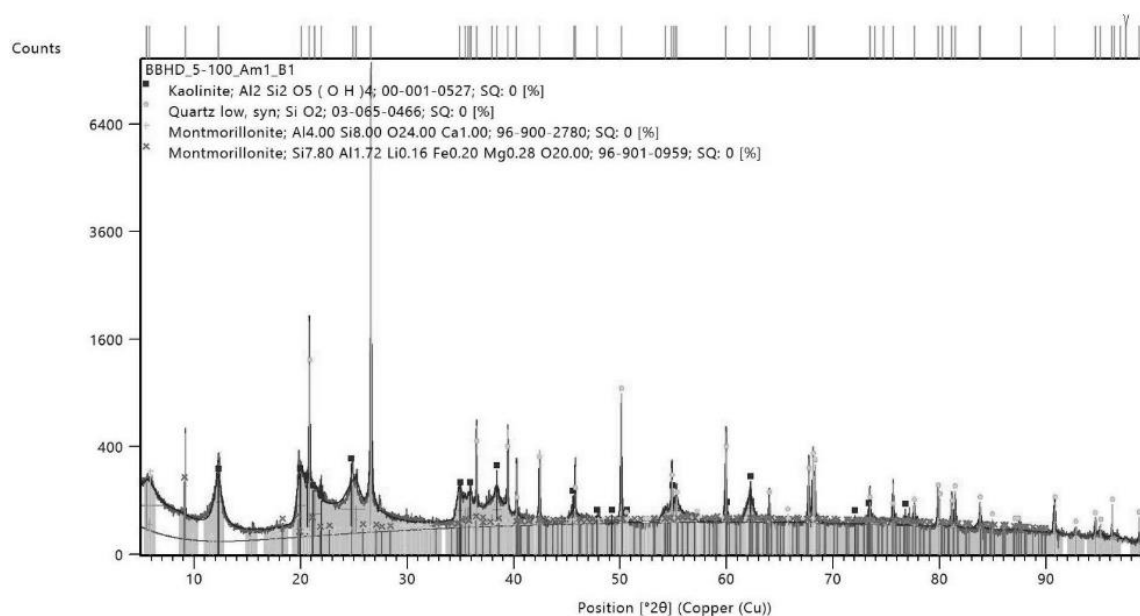
X-ray (XRF) analyzes were performed on the samples from the two reject basins, through which quantitative data were obtained of the chemical composition of the samples, mainly composed of  $\text{SiO}_2$ ,  $\text{Al}_2\text{O}_3$ , organic matter and  $\text{Fe}_2\text{O}_3$ , which corresponds to the basic composition of most of the clay mineral

groups (Gomes, 1988), as shown the Fig. 8. The main mineral phases in the samples were identified by X-Ray diffraction, being montmorillonite, kaolinite, quartz, muscovite and microcline (Figs. 9 and 10).

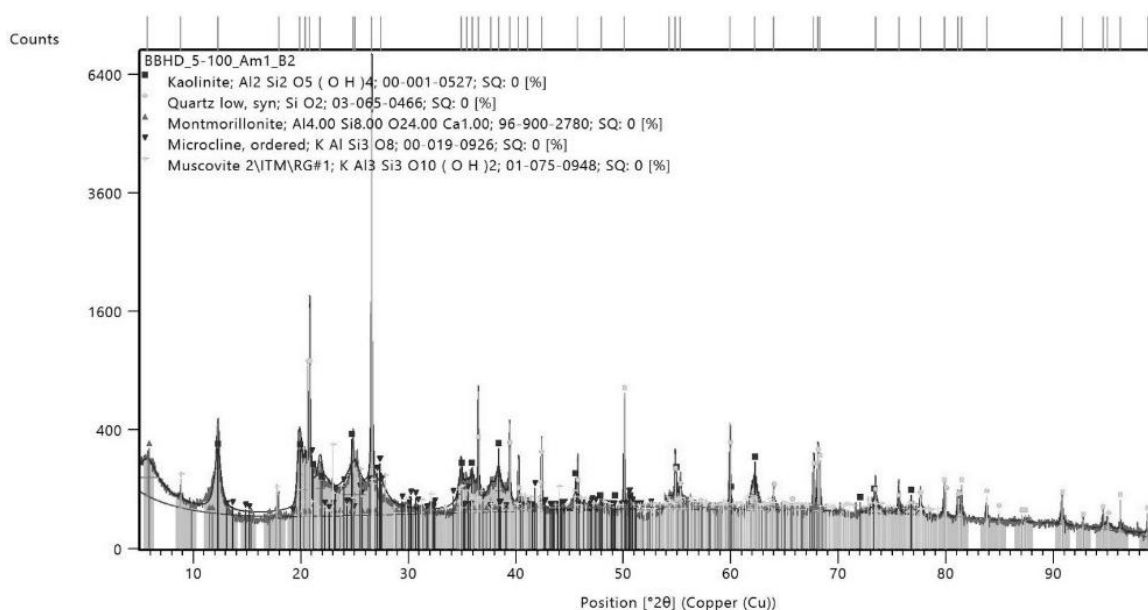
Quantitative Result	
Analyte	Result
====[No. 1 Layer]====< Layer1	
Layer1	6.000 um
C3H6	100.000 %
====[Base]=====< Base	
Na2O	0.522 %
MgO	0.408 %
Al2O3	17.269 %
SiO2	51.002 %
P2O5	0.191 %
SO3	0.034 %
K2O	0.610 %
CaO	0.032 %
TiO2	0.987 %
MnO	0.019 %
Fe2O3	3.513 %
L.O.I	10.605 %

Quantitative Result	
Analyte	Result
====[No. 1 Layer]====< Layer1	
Layer1	6.000 um
C3H6	100.000 %
====[Base]=====< Base	
Na2O	0.455 %
MgO	0.611 %
Al2O3	20.715 %
SiO2	48.139 %
P2O5	0.035 %
K2O	0.600 %
CaO	ND %
TiO2	1.582 %
MnO	0.010 %
Fe2O3	3.218 %
L.O.I	12.097 %

**Fig. 8.** Results of XRF sample from the reject basin 1 (AM-01/B1) in left, and basin 2 (AM-01/B2) at right.



**Fig. 9.** XRD result of reject sample 2 (AM-01/B1).



**Fig. 10.** XRD result of reject sample 2 (AM-01/B2).

## 5. CONCLUSIONS

Through the analyses carried out so far, it was possible to assess some behavior of the studied material and to verify by the grain size distribution, that showed its very fine nature, with a high percentage of clays. The possible application of the material is, in a first approach, as a waterproofing layer. Another necessary aspect to be investigated will be the causes of the compositional variation in the different reject basins.

In order to do this, future research is pointing to carry out other field visits and sampling at the study area to evaluate the method of beneficiation of the deposit and possible variables in the process. Moreover, an analysis of possible lithological variations of the prospected rock. If the possibility of changes in the beneficiation method is eliminated and compositional variations in the lithology are identified, the aim is to collect samples from the lithology and perform petrographic analyzes in order to understand the origin of the clay material.

## REFERENCES

- Arab P.B, Araujo T.P, Pejon O.J. (2015) Identification of clay mineral in mixtures subjected to differential thermal and thermogravimetry analyses and methylene blue adsorption tests. In: *Applied Clay Science* 114, p. 133–140.
- Albers A.P.F., Melchades F.G., Machado R., Baldo J.B., Boschi A.O. (2002) A simple method for the characterization of clay minerals by X-ray diffraction. In: *Cerâmica* vol.48 no.305 São Paulo Jan./Feb./Mar.
- Benson C., Zhai H., Wang. X. (1994) Estimating the hydraulic conductivity of compacted clay liners. *Journal of Geotechnical Engineering, ASCE* 120, p. 366-387.
- Bilal E., Nalini Jr., Horn H.A., Correia-Neves J., Giret A., Fuzikawa K., Fernandes, Mello F.M., Moutte J. (1998) Neoproterozoic granitoid suites of Rio Doce Region, Brazil. In: *Proceedings of "Precambrian and Craton"* - the 14th International conference on basement tectonics, Ouro Preto, Brazil, p. 41-43.
- Bilal E., Horn H.A., Nalini jr. H., Mello de F.M., Correia-Neves J.M., Giret A., Moutte J., Fuzikawa K., Fernandes M.L. (2000) The Neoproterozoic granitoid suites in Southeastern Brazil. *Revista Brasileira de Geociência*, 30 (1), p. 51-54.
- CPRM (2006) Mapa Geológico Integrado. Scale 1:250.000. Porto Alegre, Brazil.
- Faccini U.F. (1989) O Permo-Triássico do Rio Grande do Sul. Uma análise sob o ponto de vista das sequências deposicionais. Curso de Pós-Graduação em Geociências, 121p. MSc. Dissertation - Instituto de Geociências, Universidade Federal do Rio Grande do Sul.
- Gomes C.F. (1988) Argilas: o que são e para que servem. Fundação Calouste Gulbenkian.
- Grehs S.A. (1976) Mapeamento geológico preliminar de Santa Cruz do Sul visando obter informação básica ao planejamento integrado. *Acta Geológica Leopoldensia* 1, p. 121-152
- Lavina E.L.C., Faccini U.F., Ribeiro H.J.S. (1993) A Formação Pirambóia (Permo-Triássico) no Estado do Rio Grande do Sul. *Acta Geológica Leopoldensia*, 38 (1), p. 179- 197.
- Milani E.J., Melo J.H.G., Souza P.A., Fernandes L.A., França A.B. (2007) Bacia do Paraná. In: *Cartas Estratigráficas. Boletim de Geociências da Petrobras*, Rio de Janeiro, v. 15, n. 2, p. 265-287,
- Montardo D.K. (1982) Estudo geológico dos sedimentos do Gondwana Superior na região de Candelária a Santa Cruz do Sul, RS. Porto Alegre. Unpublished MSc. Dissertation UFRGS, 111p.
- Savic I., Stojiljkovic S., Savic I., Gajic D. (2014) Industrial Application of Clays and Clay Minerals. In: *Clays and Clay Minerals*, Nova Science Publishers, Inc., ISBN: 978-1-63117-779-8
- Zalán P.V., Wolff S., Astolfi M.A.M., Vieira I.S., Conceição J.C.J., Appi V.T., Santos Neto E.V., Cerqueira J.R., Marques A. (1990) The Paraná Basin, Brazil. *American Association of Petroleum Geologists*, (AAPG. Memoir, 51), p. 681-708.
- Wenzel J.A. (1996) Mapeamento geológico estrutural geotécnico da Zona Urbana de Santa Cruz do Sul visando obter informação básica ao planejamento integrado. Technical report. PMSCS.

## PRELIMINARY ASSESSMENT OF ANTHROPOGENIC CONTRIBUTION AND INFLUENCING FACTORS ON MAJOR ELEMENTS AND TOTAL ORGANIC CARBON IN TAZLĂU RIVER SEDIMENTS, ROMANIA

Andreea-Elena MAFTEI<sup>1\*</sup>, Andrei BUZATU<sup>2</sup>, Nicolae BUZGAR<sup>2</sup>, Andrei-Ionut APOPEI<sup>2</sup>

<sup>1</sup>“Alexandru Ioan Cuza” University of Iasi, Department of Research, Faculty of Geography and Geology, 20A Carol I Blv., 700505 Iasi, Romania;

<sup>2</sup>“Alexandru Ioan Cuza” University of Iasi, Department of Geology, 20A Carol I Blv., 700505 Iasi, Romania.

\* andreea.maftei@uaic.ro

**Abstract:** The concentration of major elements (Si, Al, Ca, Mg, Na, K, Ti, Fe, Mn and P), as well as the total organic carbon (TOC) were studied in surface sediments from 29 sampling points in Tazlău River catchment.

The river sediments are characterized by lower concentrations of the studied major elements in almost all sampling points, with the exception of s3 sample, where the concentrations slightly exceed the geochemical threshold. The mean values of major elements in Tazlău river sediments are in decreasing order of Si (75.74 wt%) > Al (4.44 wt%) > Ca (3.39 wt%) > Fe (2.47 wt%) > K (1.56 wt%) > Mg (0.65 wt%) > Ti (0.34 wt%) > Na (0.30 wt%) > P (0.09 wt%) > Mn (0.04 wt%). The pollution load index (PLI) values for Fe and Mn elements in Tazlău River sediment were found to be from 0.50 to 2.42 and are confirming that s3 sampling point is moderately contaminated (PLI > 1).

**Keywords:** Major elements; sediments; Tazlău River; TOC, background; PLI

### 1. Introduction

Investigation of the chemical composition of river sediments is an important approach because the human activity can strongly influence the environmental quality of the fluvial systems (Dinelli et al., 2005). Strong urbanization and industrialization in recent years has resulted in increases heavy metals concentration discharged into the rivers.

Tazlău basin, with a total area of 1117 km<sup>2</sup> located in the central-eastern part of the Eastern Carpathians and Subcarpathians overlaps three distinct geological units: Tarcău nappe, Vrancea nappe (external flysch) and molasse sediments (pericarpathian nappe). Geological surface in the Eastern Carpathian region is primary composed by bituminous rocks (menilites, bituminous shale and brown marl) which have a high content of organic matter (Țabără et al., 2015). Total organic carbon (TOC) has a major influence on chemical and biological process that take place in sediments (Agah et al., 2013).

The main objectives of this study are as follows: (1) to determine the major elements and total organic carbon in sediment samples collected from Tazlău River and, (2) to evaluate how different sampling locations are polluted with Mn and Fe.

### 2. Material and methods

#### 2.1. Samples preparation

Twenty-nine stream sediment samples were collected from Tazlău River and some of its main tributaries at an equidistance of 3-4 kilometers (Fig. 1). Each sample was sieved and the fraction less than 0.63 mm diameter was used for analysis by X-ray fluorescence spectrometry (XRF).

The major elements measurements were carried out with an EDXRF Epsilon 5 Spectrometer at Geology department from “Alexandru Ioan Cuza” University, Iași.

To measure the total organic carbon (TOC%) the sediment samples were treated for 24 hours with 4N HCl, washed with distilled water, dried at 60° C and analyzed on Elementar EURO EA 3000 equipment.

#### 2.2. Metal pollution assessment in Tazlău River sediments

Interpolation maps were made only for Fe and Mn elements by using the kriging method. The assessment of anthropogenic contribution of Fe and Mn in Tazlău River sediments was possible by determining the geochemical background and pollution load index (PLI). Geochemical background was calculated as Reimann et al. (2005) suggested:

$$\text{Geochemical background} = \text{Median} \pm 2\text{MAD}$$

In order to evaluate the degree of contamination with Fe and Mn, the pollution load index (PLI) was calculated in this study according to the formula used by Ali et al. (2016), Islam et al. (2015) and Maftei et al. (2014):

$$PLI = (CF_1 \times CF_2 \times CF_3 \times \dots CF_n)^{1/n}$$



where CF is the ratio obtained by dividing concentration of the studied metal in sediment to the background value:  $CF_{metals} = C_{metal}/C_{background}$ . Therefore, the values greater than 1 indicate pollution and the values smaller than 1 indicate that the sediments are unpolluted.

### 3. Results and discussion

#### 3.1. Geochemical distribution of major elements and TOC in surface sediments

The major elements composition and total organic carbon values are listed in Table 1. The Pearson's correlation coefficients between major elements and TOC of 29 sediment samples were calculated and presented in Table 2.

**Table 1.** Major elements concentrations in Tazlău River sediments and geochemical background calculated for Fe and Mn.

	Na	Mg	Al	Si	P	K	Ca	Ti	Mn	Fe	TOC
	wt%										
s1	0.60	0.57	7.75	75.22	0.05	1.88	1.78	0.43	0.06	3.57	0.66
s2	0.38	0.63	6.70	75.47	0.06	1.72	1.79	0.36	0.06	3.31	0.59
s3	1.64	2.69	7.91	66.04	0.09	2.25	5.91	0.54	0.10	5.14	1.32
s4	0.46	0.96	6.10	75.65	0.09	1.86	2.84	0.43	0.05	3.36	0.68
s5	0.19	0.47	5.70	75.63	0.06	1.60	2.05	0.33	0.05	2.82	0.51
s6	0.18	0.65	4.67	74.96	0.09	1.56	2.20	0.38	0.04	2.45	0.49
s7	1.41	0.84	2.50	74.87	0.11	1.40	7.32	0.27	0.07	2.59	0.53
s8	0.03	0.65	5.04	74.36	0.08	1.72	2.96	0.38	0.05	2.98	0.57
s9	0.19	0.61	4.85	74.51	0.10	1.66	3.06	0.39	0.05	2.88	1.25
s11a	0.80	0.99	6.63	69.81	0.10	1.97	4.09	0.53	0.06	3.29	0.80
s11b	0.11	0.43	3.86	78.79	0.11	1.51	2.07	0.26	0.03	2.19	0.44
s12	0.13	0.64	4.91	76.51	0.11	1.68	3.02	0.39	0.04	2.61	1.04
s13	0.02	0.23	3.63	79.18	0.07	1.42	2.59	0.25	0.02	1.90	0.40
s14a	0.03	1.34	7.14	69.34	0.07	2.04	5.03	0.59	0.06	3.40	0.61
s14b	0.03	0.23	2.85	81.20	0.09	1.29	2.23	0.25	0.02	1.71	0.35
s15a	0.02	0.37	3.01	78.07	0.07	1.34	2.26	0.23	0.02	1.62	0.48
s15b	0.02	0.42	4.68	74.13	0.10	1.61	3.43	0.36	0.05	2.38	0.67
s16a	0.04	0.44	3.61	74.17	0.08	1.45	3.19	0.34	0.03	1.92	0.55
s16b	0.02	0.33	2.89	80.14	0.11	1.28	2.73	0.19	0.02	1.62	0.76
s18	0.04	0.66	2.82	81.42	0.08	1.31	2.56	0.27	0.02	1.54	0.41
s19	1.35	0.79	3.32	73.77	0.08	1.40	3.56	0.30	0.02	1.78	0.47
s21a	0.35	0.69	4.05	79.32	0.06	1.56	3.13	0.30	0.03	1.97	0.57
s21b	0.09	0.19	2.76	77.30	0.09	1.32	3.47	0.21	0.03	1.61	0.34
s22	0.03	1.02	4.61	74.89	0.05	1.60	4.11	0.29	0.04	2.24	0.73
s23	0.06	0.39	2.27	81.07	0.08	1.13	2.58	0.18	0.02	1.26	0.38
s24	0.05	0.42	3.46	75.05	0.14	1.45	4.84	0.38	0.04	2.14	0.36
s25	0.06	0.48	4.03	73.97	0.10	1.52	5.09	0.34	0.05	2.36	0.60
s26	0.04	0.45	4.22	71.86	0.10	1.54	5.18	0.36	0.05	2.85	0.42
s28	0.29	0.23	2.93	79.76	0.08	1.26	3.35	0.23	0.03	2.16	0.79
Geochemical background			Geochemical threshold				Mean content				
Fe	1.34 – 3.39				3.39				0.04		
Mn	0.02 – 0.07				0.07				2.29		

The major elements abundance is described by Si dominance, values ranging from 66.04 wt% to 81.42 wt% (Table 1). Silica does not show any specific relationships with phosphor and the negative correlation with all elements suggest a dilution effect due the higher quartz content in sediments (Maharana et al., 2018). The mean values of major elements in Tazlău river sediments are in decreasing order of Si (75.74 wt%) > Al (4.44 wt%) > Ca (3.39 wt%) > Fe (2.47 wt%) > K (1.56 wt%) > Mg (0.65 wt%) > Ti (0.34 wt%) > Na (0.30 wt%) > P (0.09 wt%) > Mn (0.04 wt%). The variable contents of Al, Fe, Ca and K may suggest the feldspars control in sediments. The distribution of Fe, Ti, K and Mn is similar with Al concentrations, showing a strong positive correlation with Pearson coefficients between 0.76 and 0.95 at  $p < 0.05$  and  $n = 29$  (Table 2).

TOC content in Tazlău River surface sediments ranges between 0.34 wt% and 1.32 wt% with a mean of 0.61 wt%. The maximum value of TOC was recorded in s3 sample point located near of natural gases exploitation area. Biological input characterized by nutrient availability can significantly contribute in carbon absorption and water chemistry. The highest concentration of TOC recorded in s3 sampling site

could be due to the organic matter decomposition through the biological process that occurs in sediments (Kamaruzzam et al., 2009).

According to Environmental Protection Agency of United State (Agah et al., 2013, USEPA, 2002), TOC in sediments river is evaluated based to the following categories:  $\leq 1\%$  - low impact, between 1% to 3% - intermediate impact and  $> 3\%$  high impact. Therefore, in Tazlău River sediments, the carbon level was found to be in the range of low to medium impact. The geochemical correlation between the total organic carbon and Fe and Mn (pairs TOC-Fe and TOC-Mn), can suggest the same local source for the higher concentrations, especially in *s3* sampling point.

A highest relationship described by *r* can being significant at  $p < 0.05$  and has been obtained between the pairs  $K_2O - TiO_2$ ,  $Fe_2O_3 - Al_2O_3$ ,  $K_2O - Al_2O_3$ ,  $MnO - Fe_2O_3$  and  $K_2O - Fe_2O_3$  (Table 2).

**Table 2.** Pearson correlation matrix between major elements and TOC in Tazlău river sediments ( $n = 29$ ).

	Si	Ti	Al	Fe	Mg	Mn	Ca	Na	K	P	TOC
Si	1										
Ti	<b>-0.84</b>	1									
Al	<b>-0.70</b>	<b>0.86</b>	1								
Fe	<b>-0.79</b>	<b>0.83</b>	<b>0.90</b>	1							
Mg	<b>-0.72</b>	<b>0.68</b>	<b>0.63</b>	<b>0.77</b>	1						
Mn	<b>-0.80</b>	<b>0.77</b>	<b>0.76</b>	<b>0.93</b>	<b>0.74</b>	1					
Ca	<b>-0.59</b>	0.32	0.02	0.32	<b>0.49</b>	<b>0.55</b>	1				
Na	<b>-0.48</b>	0.31	0.30	<b>0.51</b>	<b>0.65</b>	<b>0.56</b>	<b>0.47</b>	1			
K	<b>-0.81</b>	<b>0.93</b>	<b>0.95</b>	<b>0.93</b>	<b>0.77</b>	<b>0.83</b>	0.24	0.39	1		
P	-0.12	0.03	-0.30	-0.07	-0.07	0.10	<b>0.44</b>	0.04	-0.12	1	
TOC	<b>-0.47</b>	<b>0.49</b>	<b>0.52</b>	<b>0.63</b>	<b>0.60</b>	<b>0.60</b>	0.21	0.36	<b>0.59</b>	0.07	1

Values in bold are different from 0 with a significance level  $\alpha < 0.05$

### 3.2. Estimating the level of pollution of Fe and Mn in Tazlău River sediments

Fe and Mn are considered the most important environmental contaminants due to their toxicity and risk that they pose. In this study Fe is one of the most abundant elements and its concentration ranges between 1.26 wt% and 5.14 wt% with the highest contents recorded in *s3* sampling point (Fig. 2). The concentration of Mn in Tazlău River sediments is characterized by a uniformity of data with a low dispersion degree. The Mn concentration is slightly exceeding the geochemical threshold in *s3* sampling point and the chemical composition ranges between 0.02 wt% and 0.10 wt% (Fig. 2).

The *s3* sampling point is located near natural gas drillings and the studies describe the association between oil and natural gases extraction processing with environmental pollution by heavy metals (Adesodun and Mbagwu, 2008, Essiet et al., 2010, Muniz, 2004, Yang et al., 2015).

The calculated pollution load index (PLI) values of Fe and Mn elements in sediments are summarized in Fig. 3. The values range from 0.50 to 2.42 and are confirming that *s3* sampling point was moderately contaminated ( $PLI > 1$ ).

The higher PLI values recorded in *s3* sampling point indicate that Mn is the major contributor to the sediment pollution (percentage contributions for each element: 53.87 % - Mn and 46.13% - Fe). Therefore, the higher PLI observed in *s3* sample might be due to the anthropogenic effects already explained.

For the other sampling points that exceed the value of 1, the PLI indicates a certain uniformity based on the following percentages: *s3* (11.07%)  $>$  *s1* (7.22%)  $>$  *s11a* (7.00%)  $>$  *s14a* (6.80%)  $>$  *s2* (6.62%)  $>$  *s7* (6.51%)  $>$  *s4* (6.46%)  $>$  *s9* (6.01%)  $>$  *s8* (5.99%)  $>$  *s26* (5.76%)  $>$  *s5* (5.60%)  $>$  *s25* (5.47%)  $>$  *s12* (5.14%)  $>$  *s15b* (5.05%)  $>$  *s24* (4.71%)  $>$  *s6* (4.60%).

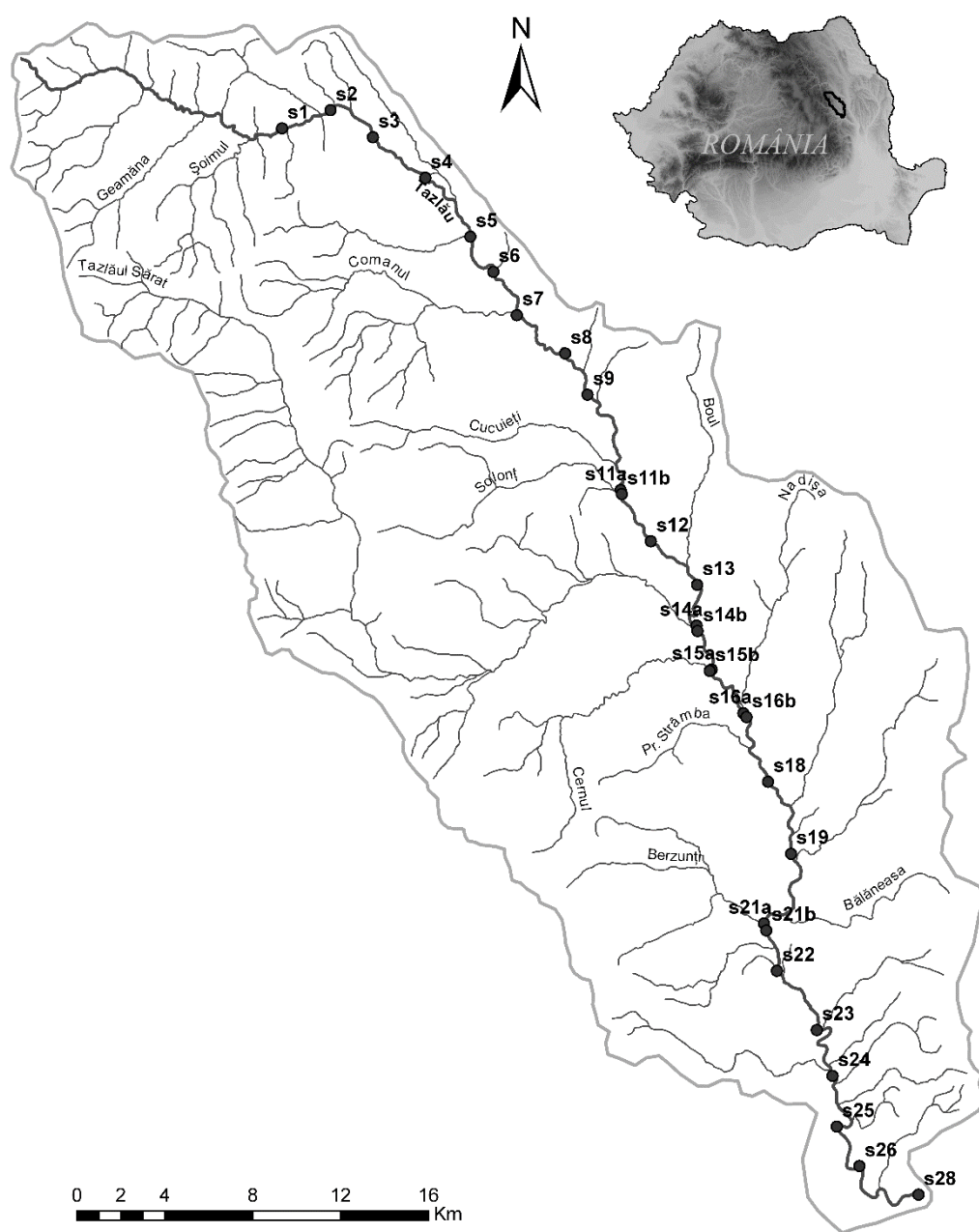
As a general overview the sources could be controlled by human as well as environmental factors such as geogenic input, oil and gas drilling, pesticides and fertilizers used in agricultural soils, or natural disasters. For example, the *s1* and *s2* sampling points are located in a natural background area without any anthropogenic source. Nevertheless, the high values identified in this region might be of natural source, controlled by the lithogenic substrate of the sediments (external flysch). For the rest of sampling points the PLI values that slightly exceeded the threshold could accumulate from a variety of sources such as industrial and

agricultural activities, traffic, atmospheric deposition or rainfalls, since the downstream area of the basin is a very populated one and several local agricultural activities are present.

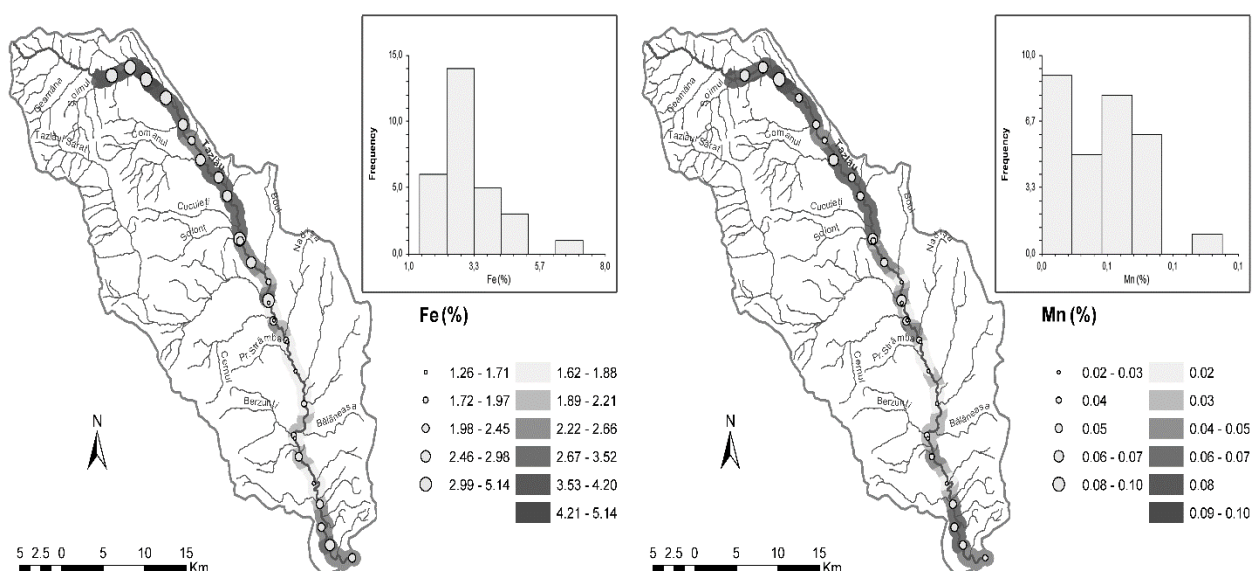
However, because the PLI values are slightly exceeding the value of 1 the human impact seems under control and safe. Of course, further investigations are required in order to control the health of the ecosystem and the contaminants caused by anthropogenic activities.

#### 4. Conclusions

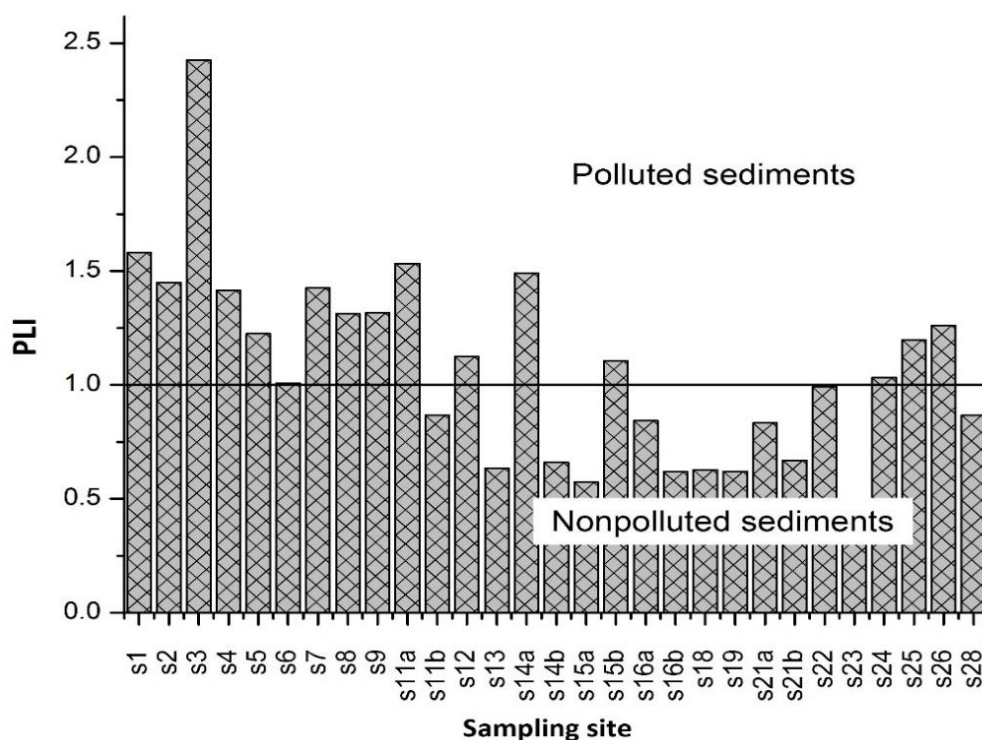
The chemical analysis of sediments in Tazlău River and its catchment indicate a high content of  $\text{SiO}_2$  and anthropogenic pollution in  $s_3$  sampling point with some heavy metals (Fe and Mn) and organic carbon. The TOC content in Tazlău River surface sediments range between 0.34 wt% and 1.32 wt% with a mean of 0.61 wt% and the maximum value was recorded in  $s_3$  sample point located near natural gases exploitation area. The calculated pollution load index (PLI) values for Fe and Mn elements in sediments were found to be in the interval of 0.50 - 2.42 and are confirming that  $s_3$  sampling point is moderately contaminated ( $\text{PLI} > 1$ ).



**Fig. 1.** Map of the study area with sampling sites.



**Fig. 2.** Distribution map of Fe and Mn (%) in Tazlău River sediments.



**Fig. 3.** Pollution load index value of Fe and Mn (%) metals in Tazlău River sediments.

## References

- Adesodun J. K., Mbagwu J. S. (2008) Distribution of heavy metals and hydrocarbon contents in an alfisol contaminated with waste-lubricating oil amended with organic wastes. *Bioresource Technology*, 99, p. 3195-3204.
- Agah H., Rahmanpour S., Sheijooni Fumani N. (2013) Organic Carbon and Organic Matter Levels in Sediments of the Strait of Hormoz, the Persian Gulf. *Journal of the Persian Gulf*, 4, p. 31-37.
- Ali M. M., Ali M. L., Islam M. S., Rahman M. Z. (2016) Preliminary assessment of heavy metals in water and sediment of Karnaphuli River, Bangladesh. *Environmental Nanotechnology, Monitoring & Management*, 5, p. 27-35.

- Dinelli E., Cortecchi G., Lucchini F., Zantedeschi E. (2005) Sources of major and trace elements in the stream sediments of the Arno river catchment (northern Tuscany, Italy). *Geochemical Journal*, 39, p. 531-545.
- Essiett U. A., Effiong G. S., Ogbemudia F. O., Bruno E. J. (2010) Heavy metal concentrations in plants growing in crude oil contaminated soil in Akwa Ibom State, South-Eastern Nigeria. *African Journal of Pharmacy and Pharmacology*, 4(7), p. 465-470.
- Islam M. S., Ahmed M. K., Raknuzzaman M., Habibullah -Al- Mamun M., Islam M. K. (2015) Heavy metal pollution in surface water and sediment: A preliminary assessment of an urban river in a developing country. *Ecological Indicators*, 48, p. 282-291.
- Kamaruzzam B. Y., Siti Wazna A., Ong M. C., Shahbudin S., Jalal K. C. A. (2009) Variability of Organic Carbon Content in Bottom Sediment of Pahang River Estuary, Pahang, Malaysia. *Journal of Applied Sciences*, 9, p. 4253-4257.
- Maftei A. E., Iancu O. G., Buzgar N. (2014) Assessment of minor elements contamination in Bistrița River sediments (upstream of Izvorul Muntelui Lake, Romania) with the implication of mining activity. *Journal of Geochemical Exploration*, 145, p. 25-34.
- Maharana C., Srivastava D., Tripathi J. K. (2018) Geochemistry of sediments of the Peninsular rivers of the Ganga basin and its implication to weathering, sedimentary processes and provenance. *Chemical Geology*, 483, p. 1-20.
- Muniz P. (2004) Assessment of contamination by heavy metals and petroleum hydrocarbons in sediments of Montevideo Harbour (Uruguay). *Environment International*, 29, p. 1019-1028.
- Reimann C., Filzmoser P., Garrett R. G. (2005) Background and threshold: critical comparison of methods of determination. *Science of the Total Environment*, 346, p. 1-16.
- Țabără D., Pacton M., Makou M., Chirilă G. (2015) Palynofacies and geochemical analysis of Oligo-Miocene bituminous rocks from the Moldavidian Domain (Eastern Carpathians, Romania): Implications for petroleum exploration. *Review of Palaeobotany and Palynology*, 216, p. 101-122.
- USEPA. (2002) Mid-Atlantic Integrated Assessment (MAIA) Estuaries 1997-98: Summary Report, EPA/620/R-02/003. US Environmental Protection Agency, Washington, DC, p. 115.
- Yang X., Yuan X., Zhang A., Mao Y., Li Q., Zong H., Wang L., Li X. (2015) Spatial distribution and sources of heavy metals and petroleum hydrocarbon in the sand flats of Shuangtaizi Estuary, Bohai Sea of China. *Marine Pollution Bulletin*, 95, p. 503-512.



## PRELIMINARY STUDY ON THE GEOCHEMISTRY OF STREAM SEDIMENTS FROM GRINTIESUL MARE BROOK, EASTERN CARPATHIANS, ROMANIA

Marius C. SANDU<sup>1\*</sup>, Gabriel O. IANCU<sup>1</sup>, Ciprian CHELARIU<sup>1</sup> Mihai NICULITA<sup>2</sup>

<sup>1</sup> Al. I. Cuza" University of Iași, Department of Geology, 20A Carol I Av., 700505 Iași, Romania;

\**cristi2sandu@yahoo.com*;

<sup>2</sup> Al. I. Cuza" University of Iași, Department of Geography, 20A Carol I Av., 700505 Iași, Romania.

**Abstract:** The Grintiesul Mare Brook located in the East Carpathian Mountains in the vicinity of closed Uranium mine exploration is the subject of this study. There are plans to open a new uranium mining facility in the Tulgheș-Grintieș area, where geological surveys have proven that the area holds the largest uranium deposit in the country. Geochemical analysis of the stream sediments samples collected from Grintiesul Mare Brook, and the water quality analysis (physical parameters) were made to establish the pollution level and the potential pollution sources. The elemental analysis shows normal values for U and Th, with values under the pollution limit. For the rest of the elements, V, Cr, Cu, Zn, As, Sr, Mo, Rb, Pb, Co, Nb, Zr, except Ni, higher values have been detected comparing to those published for the Upper Continental Crust. The water quality parameters analyzed by using a multiparameter probe have an increasing trend from upstream to downstream for Salinity, Conductivity and TDS, probably due to the influence of the human factor. The XRD analysis of the stream sediments identified the following minerals: quartz as a predominant mineral, followed by illite-muscovite, albite and clinocllore. The XRF and XRD analyses were carried out at Geolog International, Geochemistry Department, Milan, Italy.

**Key words:** Grinties Brook, major elements, trace elements, stream sediments, XRF, XRD, water quality parameters

### 1. INTRODUCTION

Romania is one of the few European states (alongside the Czech Republic, France, Germany, Ukraine) and one of the few in the world with uranium deposits, mainly used in the energy sector. The geological survey of the area started in 1963, when the first gamma anomalies and ore deposits were found. After a short prospecting period, the perimeter began to be excavated. During 1994-1997, the mining activity involved an experimental face cut, later followed by proper mining procedures, single geological block only, and single gallery (between the second semester of 1997 and the first semester of 2001). Later, in 2005, the National Uranium Company proposed a project aiming to reopen the mining operations for the existing uranium deposits found in Tulgheș and Grintieș area. The area currently holds several mining galleries, in different conservation stages (Tofan et al, 2016). The main objective of this study is to determine the geochemistry of stream sediments from Grintiesul Mare Brook.

### 2. GEOLOGICAL FRAMEWORK

The perimeter of the study area lies in the Central Group of the Eastern Carpathians (Fig. 1), in Bistricioara Mountains (Bistriței Mts.), Preluca Ursului-Pietrele Roșii subunit, between Harghita and Neamț counties. Hovering at approximately equal distance (20 km) from Durău and Borsec mountain spas, the perimeter is crossed by the Prisecani, Bradu, Primatar and Grintieș streams, left side tributaries of Bistricioara river.

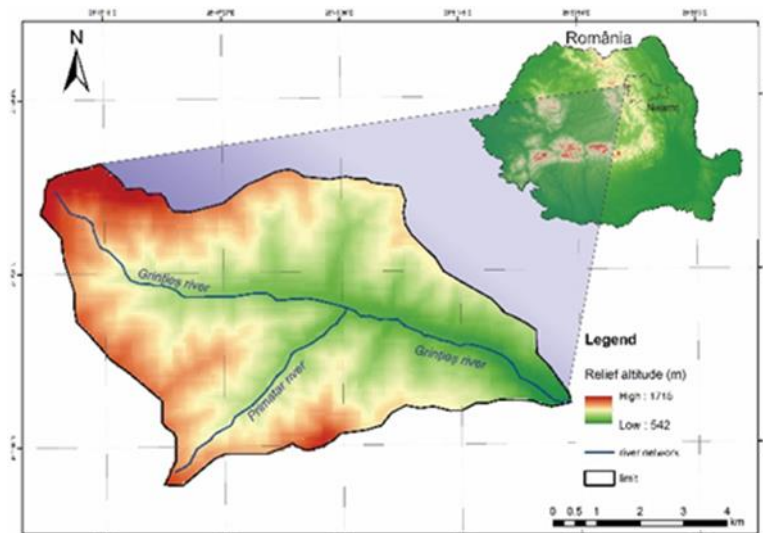
The studied area is located in the Crystalline-Mesozoic Zone of the Eastern Carpathians, in the Tulgheș terrane (Fig. 2). The geological formations from this area were formed during Precambrian to Upper Cretaceous. Most of the geological formations are composed of metamorphic rocks. The Tulgheș metamorphic unit is a low-grade sequence lithostratigraphically subdivided into 5 formations (from bottom to top): a blastodetrital, quartzitic formation; a mainly graphitic with metalydites and associated manganese carbonate ore bodies formation; a rhyolitic meta-sedimentary formation with associated base metal ore bodies; a blastodetrital formation with phyllites; a mainly graphitic formation with greenschists and limestones (Balintoni and Balica, 2013).

The flysch area is represented by the marly limestone series known in the literature as the "Layers of Sinaia" (Fig. 2).

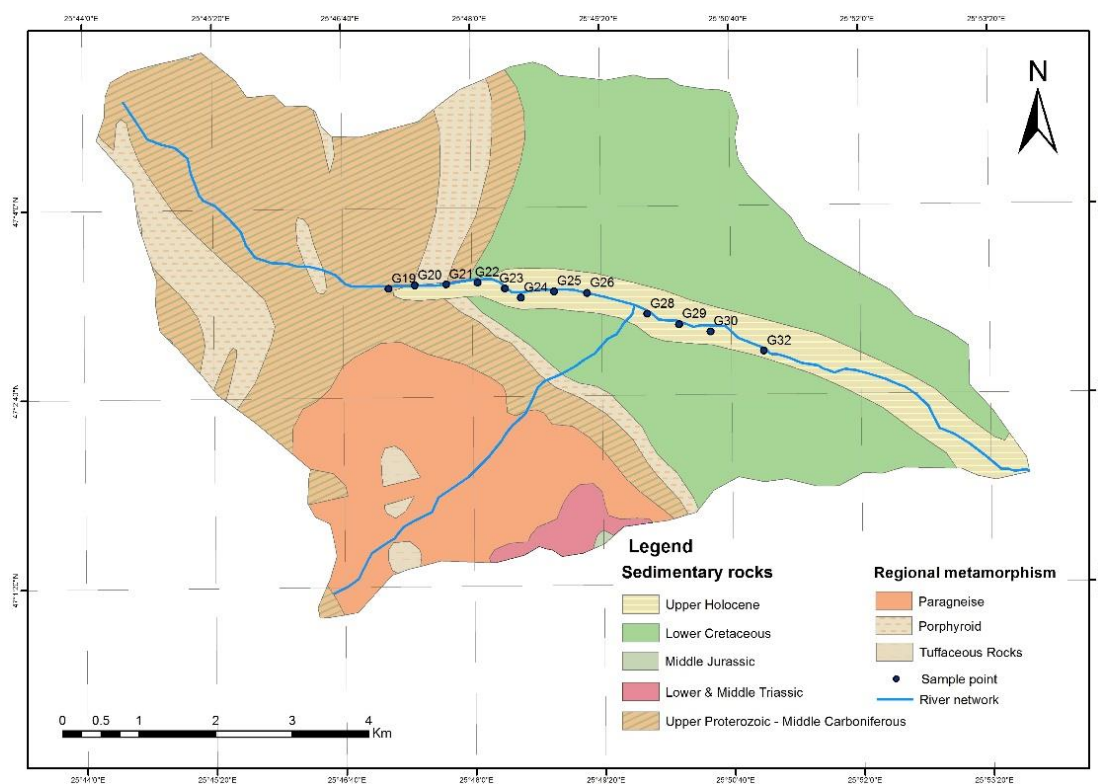
### 3. MATERIAL AND METHODS

Twelve alluvial sediment samples were collected during November 2017 from the bed of the Grintiesul Mare brook located in the North East part of Romania. About 2 kg of sediments were collected manually

from the main stream using a metal bucket. The samples were dried in the electrical oven at 50° C and



**Fig. 1.** Localization of Grintiesul Mare Brook.



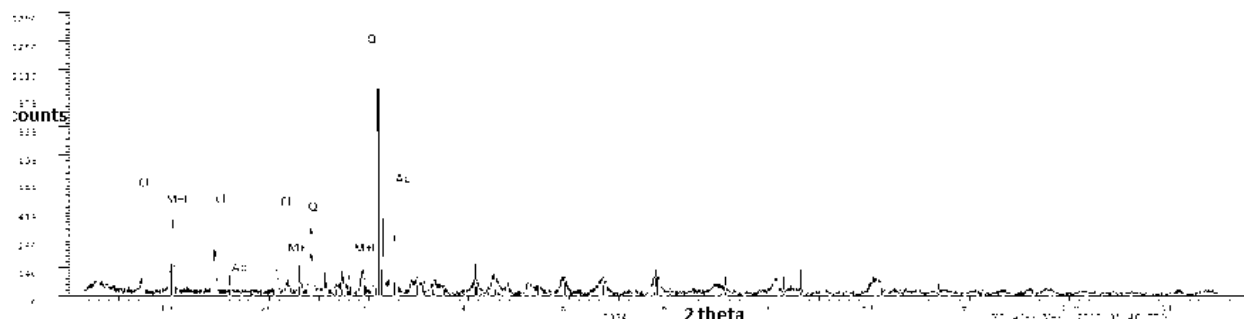
**Fig. 2.** Geological map of the study area (after Geological Map of Romania, scale 1:200000, Toplita sheet, modified from Alexandrescu et al., 1968).

sieved at 0.063 mm. The XRD analyses were carried out at Geolog International, Geochemistry Department, Milan, Italy. The elemental composition was determined by using Energy dispersive X-ray fluorescence spectrometer (XRF) Benchtop, and the calibration method is based on more than 20 certified standards from USGS, NIST and NGS to provide the most accurate results. XRD measurements were performed by X-Ray Diffraction benchtop instrument - Equinox 100, equipped with a Cobalt tube (Co K $\alpha$  radiation  $\lambda = 1.78896 \text{ \AA}$ ), and a Curved Position Sensitive X-ray Detector scanning simultaneously from 5 to 120° 2 $\theta$ . Water quality parameters were measured for each sampling point using the multiparameter probe SmarTROLL in order to determine the following parameters: conductivity, pH, oxydation reduction potential (ORP), dissolved oxygen (DO), water level/pressure, salinity, total dissolved solids (TDS), resistivity, density, air and water temperature, and barometric pressure.

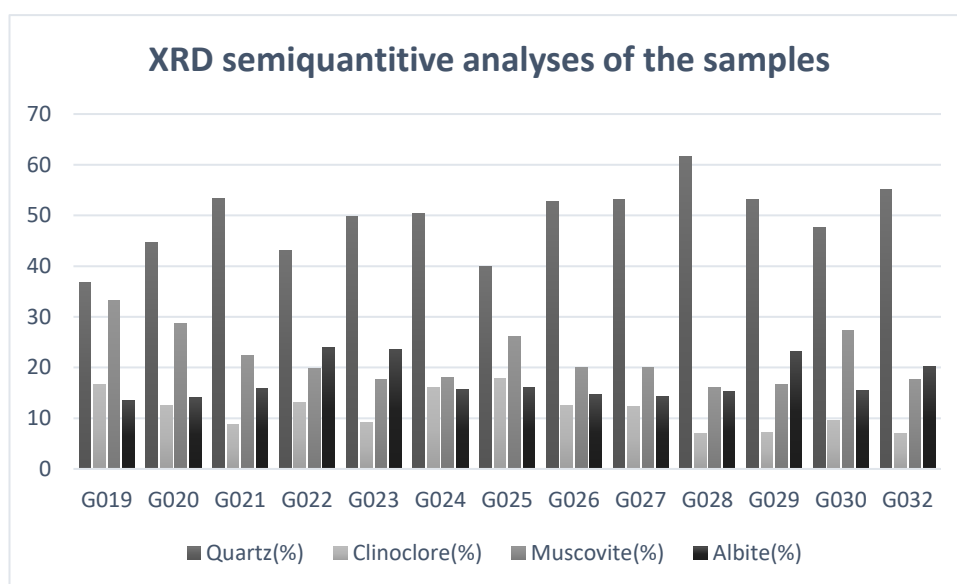
## 4. RESULTS

### 4.1 Mineralogy

The X-ray diffractograms (XRD) for the sediment samples collected from Grintiesul Mare brook revealed the presence of quartz, illite-muscovite, albite, clinochlore, as shown in Fig. 3. These minerals were determined semi-quantitatively as well (Fig. 4).



**Fig. 3.** The diffractogram of the G024 sample: Q=Quartz, M+I=Muscovite + Illite, Cl=Clinochlore, Ab=Albite



**Fig. 4.** XRD semiquantitative analyses of stream sediments from Grințieșu Mare Brook

### 4.2 Major oxides:

The bulk geochemistry of the major elements of twelve samples of the Grintiesul Mare alluvial sediment is presented in Table 1. The stream sediments have a content of SiO<sub>2</sub> with an average concentration of 56.14%. They have relative low contents of CaO (average 1.21 %), MgO (average 1.73%), K<sub>2</sub>O (average 3.45 %), MnO (average 0.10%), TiO<sub>2</sub> (average 1.21%) and P<sub>2</sub>O<sub>5</sub> (average 0.23%). MgO follows the trend of Al<sub>2</sub>O<sub>3</sub> indicating that MgO and Al<sub>2</sub>O<sub>3</sub> are associated with micaceous clay minerals (Akarish and El-Gohary, 2011). This is further confirmed by their correlation with Al<sub>2</sub>O<sub>3</sub> (i.e. Al<sub>2</sub>O<sub>3</sub> has positive strong correlation with MgO,  $r=0.67$  and TiO<sub>2</sub>,  $r=0.17$ , Fig. 5), showing that Al<sub>2</sub>O<sub>3</sub> and MgO are associated and most likely from the same source. Furthermore, Al<sub>2</sub>O<sub>3</sub> has positive correlation with Fe<sub>2</sub>O<sub>3</sub> ( $r=0.41$ ), CaO ( $r=0.56$ ) and P<sub>2</sub>O<sub>5</sub> ( $r=0.77$ ). However, Al<sub>2</sub>O<sub>3</sub> has a very good correlation with K<sub>2</sub>O ( $r=0.85$ ) which depicts the same origin, (Fig. 5). This suggests that most of the oxides result from aluminosilicate minerals like the plagioclase feldspars and mica group minerals (Jin et al., 2006).

### 4.3 Trace elements

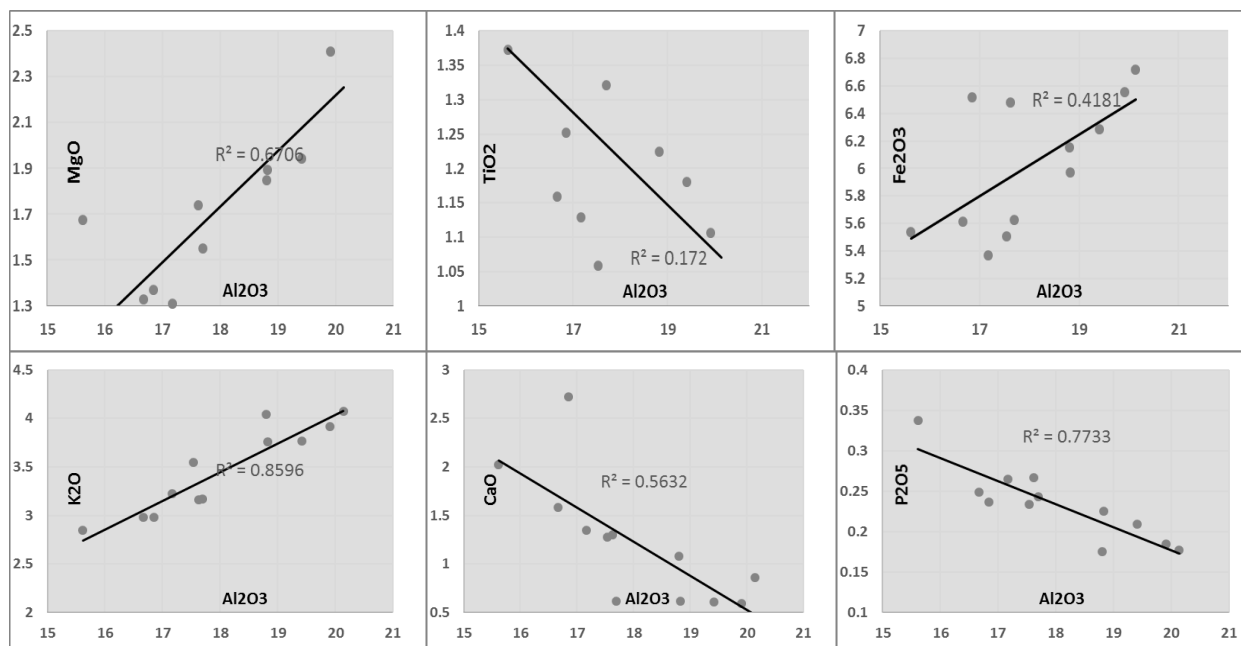
The trace elements analyzed from the alluvial sediments are presented in Table 1. Their descriptive statistical summary is presented in Table 2 in comparison to published Upper Crust Concentrations (Rudnick and Gao, 2003) and Crucea river sediment analysis (Petrescu et al., 2010).

**Table 1.** XRF analyses of major and trace elements

Major oxides in %												
	G19	G20	G21	G22	G23	G24	G25	G26	G28	G29	G30	G32
SiO <sub>2</sub>	53.06	57.71	54.95	56.72	55.59	58.27	55.98	58.27	57.09	56.08	59.55	57.48
Al <sub>2</sub> O <sub>3</sub>	18.82	17.69	20.13	19.91	19.41	16.84	17.62	16.66	18.80	17.53	17.17	15.61
Fe <sub>2</sub> O <sub>3</sub>	5.97	5.62	6.72	6.55	6.28	6.51	6.48	5.61	6.15	5.50	5.36	5.53
CaO	0.61	0.61	0.86	0.59	0.60	2.72	1.30	1.58	1.08	1.27	1.34	2.02
MgO	1.89	1.55	2.53	2.41	1.94	1.37	1.73	1.33	1.84	1.27	1.31	1.67
K <sub>2</sub> O	3.76	3.17	4.07	3.91	3.76	2.98	3.16	2.98	4.04	3.54	3.22	2.84
MnO	0.11	0.10	0.11	0.11	0.10	0.10	0.11	0.10	0.08	0.08	0.08	0.09
TiO <sub>2</sub>	1.22	1.32	0.96	1.10	1.18	1.25	1.81	1.15	0.97	1.05	1.12	1.37
P <sub>2</sub> O <sub>5</sub>	0.22	0.24	0.17	0.18	0.20	0.23	0.26	0.24	0.17	0.23	0.26	0.33
Trace elements in ppm												
S	410	300	510	435	430	280	450	290	500	850	123	125
Cl	NQ	NQ	34.4	NQ	NQ	20.5	NQ	NQ	NQ	NQ	27	10.6
As	15.2	13.4	13.9	13.4	13.7	14.5	15.9	13.4	13.4	11.2	12.8	12.9
Ba	728.8	611	877.1	805	762.3	586.5	677.7	600.3	749.5	807.4	672.2	861.6
Co	34.6	36.1	36.9	36.6	38.1	40.6	37.7	36.3	38.6	36.9	36	35.1
Cr	123.4	127.7	123.5	121.7	112.9	124.1	120.9	126.1	125	121.8	121.6	122.7
Cs	29.4	37.3	11.5	33.9	31.8	36.7	61.6	27.4	18.2	21.2	25.4	47.6
Cu	38.8	34.3	31.4	36.8	34.9	36.7	39.1	35	38.5	39.2	35.3	43.9
Ga	25.6	21.4	25.7	26.2	25.4	19.2	23.1	20.2	25.2	21.2	19.5	18.7
Gd	5.7	5.4	6	6.2	5.8	5.7	5.9	5.4	5.7	5	4.9	5.1
Mo	1.6	2.1	2.1	2.6	2.1	4.6	3.2	2	2.8	0.5	1.5	1.3
Nb	20.4	22.1	18.5	20.7	19.7	22.4	27.6	16.2	19.4	15.5	18.9	24.7
Nd	22.6	16	23.5	26.6	15.6	31.2	22	25.2	37.6	24.1	33.2	25.3
Ni	40.2	38.7	36.6	40.3	38.4	47.5	43.8	41.5	40.2	41.9	38.9	43.1
Pb	24.6	25.2	24.6	25.4	25.8	23.4	24.5	21.7	28.3	21.1	23.8	22.1
Rb	144.3	119.4	159.2	151.3	144.1	120.5	119.9	107.4	153.3	104.8	113.2	98.8
Sr	125.8	120.8	112	113.4	117.7	148.6	129.8	119.5	137.5	107.9	124.6	132.4
Th	18	17.4	17	17.7	18.3	16.4	18.7	14.9	14	11.7	13.5	12.4
U	4.7	4.7	3.9	5.2	5.1	3.4	4.4	3.5	4.7	3.8	4.6	5.3
V	117.5	108	112.7	116.8	122.5	112.8	120.2	106.8	115.7	114.5	98	94.8
Zn	114.8	110.4	125.5	121.5	114.2	120.8	113.7	105	130.8	113.8	106.4	108.7
Zr	463.5	356.4	289.2	326.9	350.2	336	726.5	294.2	262.5	218.7	290.9	564.4

**Table 2.** Statistical Summary of Trace Elements concentrations in comparison to published Upper Crust Concentrations - UCC (Rudnick and Gao, 2003) and Crucea river sediments analyses (Petrescu et al., 2010).

This study						Crucea region					UCC
Element (ppm)	Min	Max	Median value	Mean value	Std Dev.	Min	Max	Median value	Mean value	Std Dev.	
V	94.8	122.5	112.8	110.65	8.91	105.23	123.29	117.39	115.29	5.70	97.00
Cr	109.2	127.7	122.7	121.58	5.10	81.82	110.68	88.88	90.74	6.34	92.00
Ni	36.6	47.5	40.2	40.84	2.79	35.78	125.09	46.03	50.41	19.92	47.00
Cu	31.4	43.9	36.7	36.82	3.12	39.83	70.86	54.64	55.12	9.29	28.00
Zn	96.6	130.8	113.8	114.01	9.13	124.63	161.68	142.00	141.18	10.48	67.00
Sr	100.0	148.6	120.8	122.30	12.97	100.26	120.17	106.57	108.96	7.36	320.00
U	3.4	5.3	4.6	4.36	0.68	17.20	5023.96	63.46	236.81	291.09	2.70
Th	11.7	18.7	16.4	15.55	2.53	18.70	6643.92	47.78	309.89	391.16	10.55
Pb	18.0	28.3	24.5	23.73	2.56	37.16	371.57	183.54	192.16	97.16	17.00
Co	30.9	40.6	36.6	36.49	2.29	15.03	21.54	18.34	18.41	1.87	17.30



**Fig. 5.** Relationships among major oxides (%) from Grintiesul Mare stream sediments samples.

V/Cr ratio has been used as a paleo – oxygenation indicator (Dill et al., 1988, Garver et al., 1996 and Ghandour et al., 2003), so that the V/Cr > 2 is thought to represent anoxic depositional condition, and the V/Cr < 2 represents deposition under relatively oxidizing conditions. In this study, the V/Cr ratio ranges from 0.7 to 1.08 with an average of 0.91, suggesting a deposition under relatively oxidizing conditions.

The Mn belt is situated at the bottom of Tulghes Group and the sulphide belt at the top of it. The Ba mineralization is present in the whole Tulghes Group together with both Mn and sulphide belts. The Mn belt also contains other Ba minerals, including celsian, hyalophane, barite and cymrite as accessory minerals (Hirtopanu et al, 2012). This indicates a genetic link between the Ba and Mn mineralizations, suggesting to have formed by the same submarine hydrothermal processes on the Cambrian sea floor. In the analyzed samples, Ba follows the same trend as MnO, this may suggest they have the same provenance.

Vanadium concentrations (94–122 ppm) are relatively higher than the levels commonly recorded in sediments (about 20 ppm) and given that V is concentrated in mafic rocks, they suggest some mafic input into the depositional system (McCann, 1991).

#### 4.4 Water quality parameters

For each sampling point the main quality parameters have been measured using a multiparameter probe. The results are presented in Table 3. The investigations have been made during the first part of November 2017. The Conductivity increases from upstream to downstream, from 95 to 234  $\mu$ S/cm and follows the same trend (increase from upstream to downstream) as Salinity and TDS. The pH is between 7.85 and 8.3 (average 8.11) with no significant variations in the sampling points. Dissolved oxygen is almost constant with values between 9 and 10 mg/l.

### 5. CONCLUSIONS

The XRF analyses conclude that for the radioactive elements such as U and Th, the values are in normal limits. For the rest of the elements, V, Cr, Cu, Zn, As, Sr, Mo, Rb, Pb, Co, Nb, Zr, except Ni, higher values have been measured comparing to published UCC but may be comparable with the elemental concentration reported in Crucea Brook sediments (except U and Th with high values in Crucea river sediments). Using XRD the following minerals have been identified: quartz as a predominant mineral, illite-muscovite, albite and clinocllore. The XRF elemental analysis (major elements) confirms as well the presence of the above mentioned minerals in the analyzed samples from the stream sediments. Some ratios such as V/Cr may be used as a paleo – oxygenation indicator. In this study this ratio has an average value of 0.91, suggesting deposition under relatively oxidizing conditions. High values of V may suggest some mafic input into the depositional system. The water quality parameters such as



Conductivity, Salinity and TDS increase from upstream to downstream. This behavior is due to natural processes in the upstream sector, while in downstream it is enhanced by anthropogenic activities.

**Table 3.** Water quality parameters measured in the sampling points.

Sample ID	Temperature °C	Conductivity ( $\mu$ S/cm)	Salinity (PSU)	TDS (ppt)	pH	ORP (mV)	DO (mg/l)
G019	8.09	95.29	0.065	0.091	8.06	75.33	10.02
G020	8.56	99.09	0.067	0.093	8.02	65.8	9.91
G021	8.73	102.8	0.069	0.096	8.05	63.53	9.93
G022	8.8	104.02	0.07	0.09	8.13	66.88	9.98
G023	9.51	111.24	0.074	0.102	8.07	65.92	9.94
G024	9.71	111.53	0.073	0.102	8.17	64.86	9.74
G025	10.11	148.17	0.097	0.134	7.85	68.11	8.99
G026	10.01	154.31	0.102	0.14	8.12	64.85	9.67
G028	10.17	187.35	0.124	0.169	8.3	63.57	9.66
G029	10.23	203.56	0.134	0.184	8.2	66.15	9.49
G030	10.22	220.53	0.146	0.199	8.11	65.74	9.27
G032	10.25	234.18	0.155	0.211	8.27	63.00	9.59

## REFERENCES

- Akarish A.I.M., El-Gohary A.M. (2011) Provenance and Source Area Weathering Derived from the Geochemistry of Pre-Cenomanian Sandstones, East Sinai, Egypt. *Journal of Applied Sciences*, 11, p. 3070-3088.
- Alexandrescu Gr., Muresan G., Peltz S., Sandulescu M. (1968) Harta Geologica a Romaniei, Scara 1:200000, L-35-VIII, 12. Toplita. Nota explicativa.
- Balintoni I., Balica C. (2013) Peri-Gondwanan terranes in the Romanian Carpathians: A review of their spatial distribution, origin, provenance, and evolution. *Gondwana Research* 23, p. 1053-107.
- Dill H., Teschner M., Wehner, H. (1988) Petrology, inorganic and organic geochemistry of Lower Permian Carbonaceous fan sequences "Brandschiefer Series". Federal Republic of Germany. Constraints to their paleogeography and assessment of their source rock potential. *Chem. Geol.* 67, p. 307-325.
- Garver J. I., Royce P.R., Smick T.A. (1996) Chromium and nickel in shale of Taconic Foreland: A case study for the provenance of fine – grained sediments with ultramafic source. *J. Sedim. Res.*, 66, p. 100-106.
- Ghandour I.M., Masuda H., Maejima W. (2003) Mineralogical and chemical characteristics of Bajocian –Bathonian shales, G. Al-Maghara, North Sinai, Egypt: Climatic and environmental significance. *Geochemical Journal*, 37, p. 87-108.
- Hirtopanu P., Scott P.W., Andersen J.C., Fairhurst R.J. Chukanov N.V., Jakab Gy., Petrescu L. (2012) Barium mineralization within the Tulghes group, East Carpathians, Romania. Joint 5th Mineral Sciences in the Carpathians Conference and 3rd Central-European Mineralogical Conference, 20–21 April, University of Miskolc, Miskolc, Hungary, *Acta Mineralogica-Petrographica*, Abstract Series 7, p. 55.
- Jin Z., Li F., Cao J., Wang S., Yu J. (2006) Geochemistry of Daihai Lake sediments, Inner Mongolia, north China: Implications for provenance, sedimentary sorting and catchment weathering. *Geomorphol.*, 80, p. 147-163.
- McCann T. (1991) Petrological and geochemical determination of provenance in the southern Welsh Basin. In: Morton A.C., Todd S.P., Haughton P.D.W. (eds.) *Developments in Sedimentary Provenance*. *Geol. Soc. Spec. Publi.* 57, p. 215–230.
- Petrescu L., Bilal E., Iatan L.E. (2010) The impact of a uranium mining site on the stream sediments (Crucea mine, Romania). *Scientific Annals of the School of Geology, Aristotle University of Thessaloniki, Greece*, Special vol. 100, *Proceedings of the XIX CBGA Congress 2010*, p. 121-126.
- Rudnick R.L., Gao S. (2003) Composition of the continental crust. *Treatise of Geochemistry*, 3. Elsevier, Amsterdam, p. 1-64.
- Tofan G. B., Nita A., Nimara C., Pacurar B. N. (2016) The exploitation of the Tulghes-Grinties uranium deposit between benefits and controversy. *Studia UBB Geographia*, LXI, 1, p. 105-114.

# THE DYNAMICS, GEOMORPHOLOGY AND THE RELATIONSHIP OF THE MASS MOVEMENT WITH THE GEOLOGY IN THE SUBCARPATHIAN AREA, BETWEEN THE BUZĂU AND THE CÂLNĂU RIVERS

Lucica NICULAE\*

Institute of Geodynamics, 19-21 Jean-Louis Calderon St., Bucharest–37, 020032, Bucharest, Romania

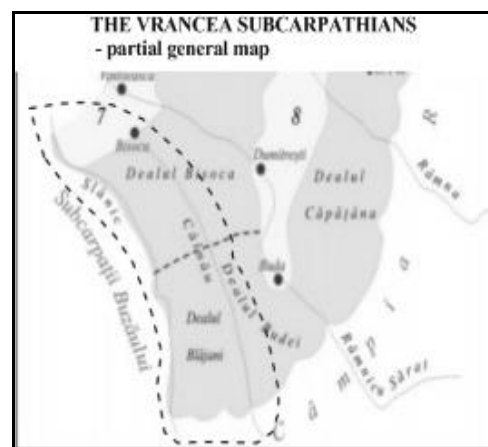
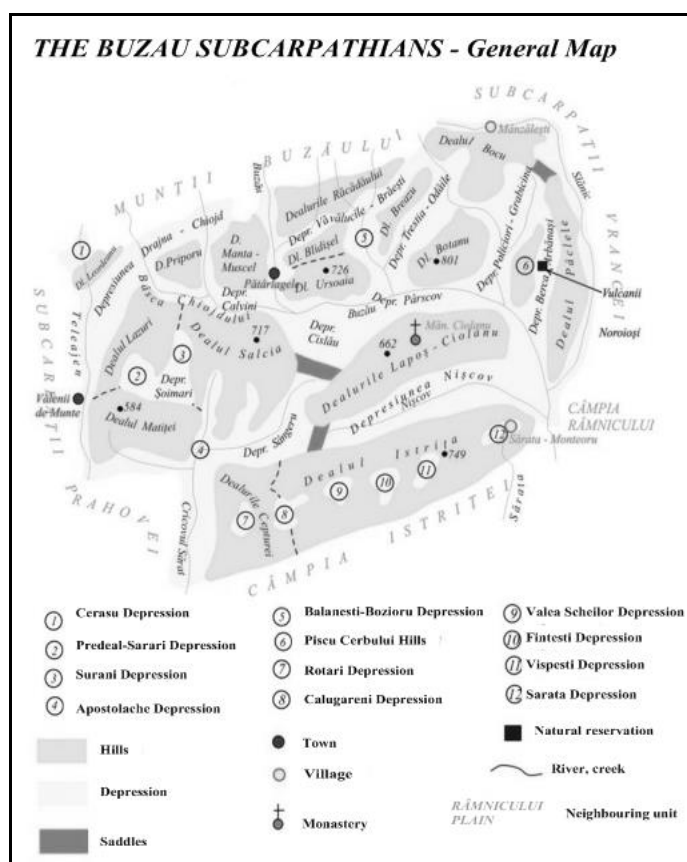
\*niculaelucica@yahoo.com, lniculae55@gmail.com; Tel.: 0726.733.751

**Abstract:** The the Subcarpathian Area, between the Buzău and the Călnău Rivers, belongs to the young Subcarpathian areal, and it is defined by an extraordinary dynamic of the geomorphological processes, evolved on the background of a severe neotectonic activity. This is reflected by the fragmentation and display of the geological formations, together with the shape of the relief. The processes are fueled by an intense neotectonic activity and earthquakes. As a consequence, the landslides are extremely diverse, classified according to a wide range of criteria, which eventually leads to affecting the agricultural soil and human habitat, even to their complete destruction.

**Keywords:** dynamics, geomorphology, tectonics, landslides, human habitat

**Introduction:** The landslides became part of the research sphere at the beginning of the 20th century, precisely because of the special effects on relief and human habitat. Their complexity is due to the diversity of relief forms, geological composition, tectonic activity and land use.

**1. Regional settings and geology features:** Of the entire eastern Subcarpathian area, the one formed by the Subcarpathians of the Buzău and the Prahova, displays a complex geomorphology defined by the structure of relief (Fig. 1 – a, b), by the interference of the paleogene sandstone flysch with the miocene and pliocene formations (clay-sandy), the presence of NE-SV, but also EV-shaped structures and different tilting.



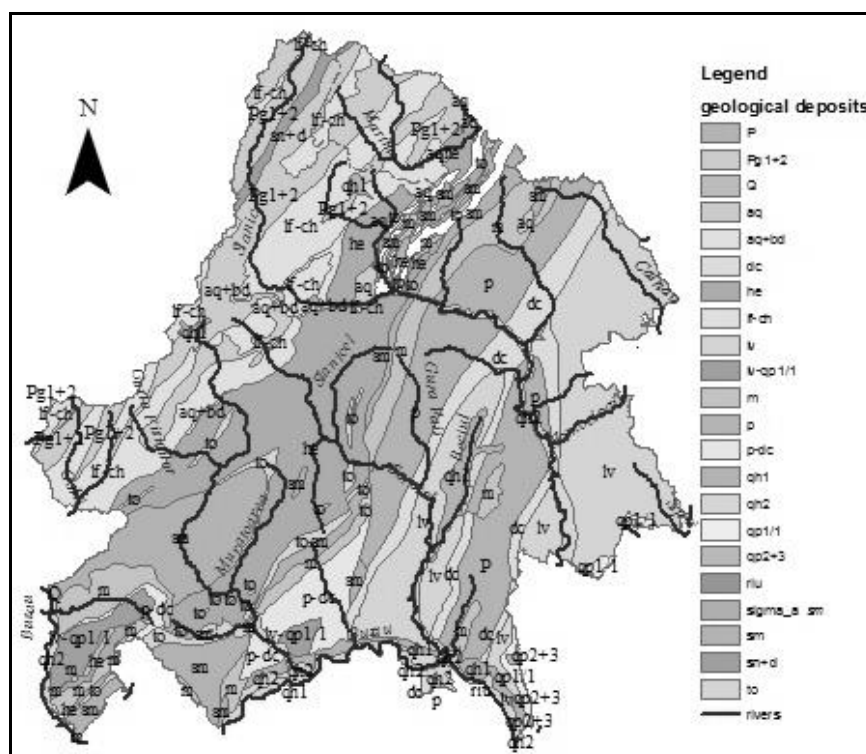
**Fig. 1.** The main units of the study area (a and b) – Subcarpathian area between the Buzău and Călnău Rivers

The tectonic activity occurs in the west-east direction, following the plans of the initial faults, and the direction of the fall of the strata, as well as in the north-south direction, following the plans of the

secondary faults, perpendicularly or obliquely oriented on the original ones. The Buzău Valley is outlined on the newest system of faults reflected by the particularly sinuous aspect of the main bed. The relief within the sub-Carpathian area, between the Călnău and the Buzău Rivers, is characterized by a great variety of relief the outcome of the tectonic processes that have affected the regional and local geological formations.

As a result, the hydrographic network created depressions on syncline and narrowings on the anticline, causing high values of relief energy. Also, there is a varied dynamic in both the slopes, the creation of a terraced relief, and in the low rivers, through the creation of large meadows and accelerated bed processes.

The relief developed on the marlstone and clays is perhaps the largest spread, the weight of these litofacies being important in the petrographic mosaic existing in the Subcarpathians. The clays are plastic rocks with a very high porosity and absorption degree, impermeable due to the material made up of fine granules, called pellets, with a diameter of less than 0.039 mm, which causes their cementation or consolidation (Ene, 2005). Depending on the dominant material, we can encounter sandy clays, clay and charcoal. Marlstones are characterized by increased hardness compared to clays, being rocks of transition between clays and limestones; may be marl itself, marl-lime, sandy marl (Fig. 2).



**Fig. 2** Lithological map of the study area – Subcarpathian area between the Buzău and Călnău Rivers (data processing in ArcGis software)

Ages: *Quaternary* (qp1, qp2+3, qh1, qh2), *Pliocene* (m, p, p-dc, dc, lv), *Miocene* (to), *Upper and Lower Paleogene* (Oligocene – lf-ch, aq, bd, he), *Cretaceous* (sn+d, sm)

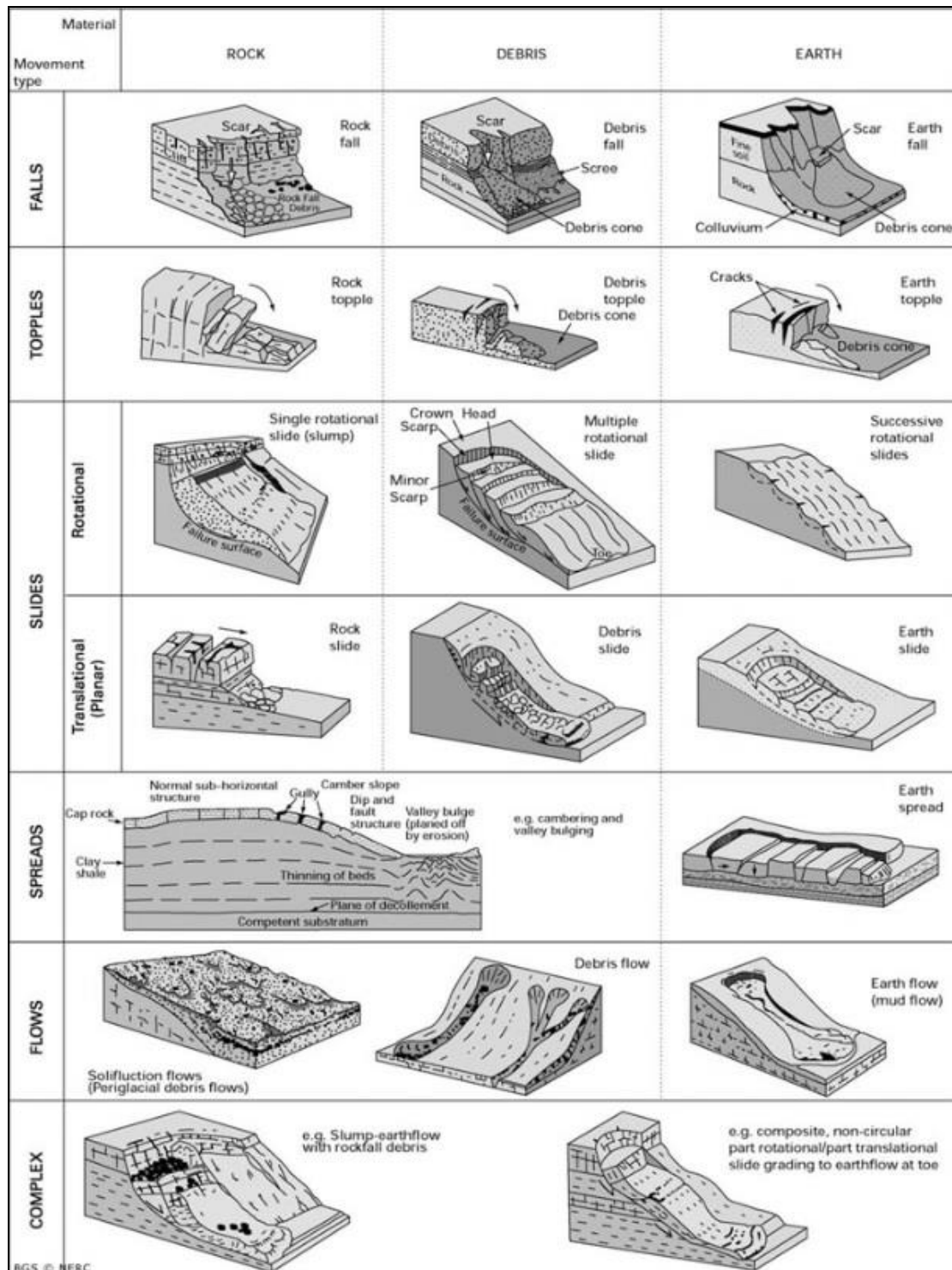
**2. Materials:** The analysis of the land movements in the Buzău Subcarpathians area, between the Buzău and the Călnău Rivers, was based on two types of activities:

- in the office, including the extraction of information from topographic maps at 1: 25,000 scale, topographic blueprints, aerial images or from certain software like Google Earth, and
- in the field, including the observation, recording and monitoring (limited by the financial and material support).

Subsequently, the information was centralized in the form of thematic maps designed by the ArcGis software package.

**3. Methods and results:** The methods of study were varied, conditioned by the physico-geographic features of the analyzed space, and by the logistic support available. For example, the Varnes classification system (Fig. 3) has been used, which divides the movements into 6 categories: falls,

topples, slides, spreads, flows and complexes, and which, depending on the mass of the collapsed or slid, is the displacement developed in rock (hard rock), debris (rock fragments) and earth (earthen type). The current paper approaches a brief classification, considering that the field displacements occur under the impulse of gravity, at different speeds. Depending on the speed of travel, we encounter sudden gravitational processes in the Buzău Subcarpathians: collapses, landslides, slope flows and slow gravitational processes (dry drift, freeze-thaw).



BGS © NERC

**Fig. 3** The classification of landslides (scheme based on Varnes – 1978, source [http://www.bgs.ac.uk/landslides/how\\_does\\_bgs\\_classify\\_landslides.html](http://www.bgs.ac.uk/landslides/how_does_bgs_classify_landslides.html)).

The physical and chemical characteristics of rocks, modeling agents and new-tectonic influence are just some of the determining factors in the development of geo-morphological processes and the formation of relief units. This paper deals with some forms of movement, but with a wide spread in the analyzed space, and they are as follows:

**3.1 Bad-lands** are generated by the processes of drainage and sedimentation affecting the clay and marl-stone, with sandy and sandstone interlaces. They accompany the slopes of the tributaries on the left side of the Buzău, but also appear at the base of the internal hills, such as Bisoca Hill, whose slopes are scattered with ravens, drainage ditches to give the specific ruinous appearance, and the landslides further accentuate the dramatic character. The main factors contributing to forming these reliefs are: the tilting of the slopes, the deforestation of the slopes, the torrential precipitations in summer and late spring.

A particular aspect is also determined by the occurrence of salt pits requiring a pseudocarst specific to bad-land areas: horizontal and vertical ballasts, drainage ditches, dissolution alveoli. All these forms are the outcome of the advanced degradation of the land without the protection of the vegetal carpet. Falls occur where the marl strata stand almost upright and are in succession with other harder strata (sandstones, conglomerates), and underlying erosion of the strata occur, or, as the case may be, mechanical disintegration. As a result, in the absence of a support, the layers above collapse under the impulse of gravity (Ielenicz et al., 2013).

Slow movements of land are differentiated according to speed of displacement, so we meet:

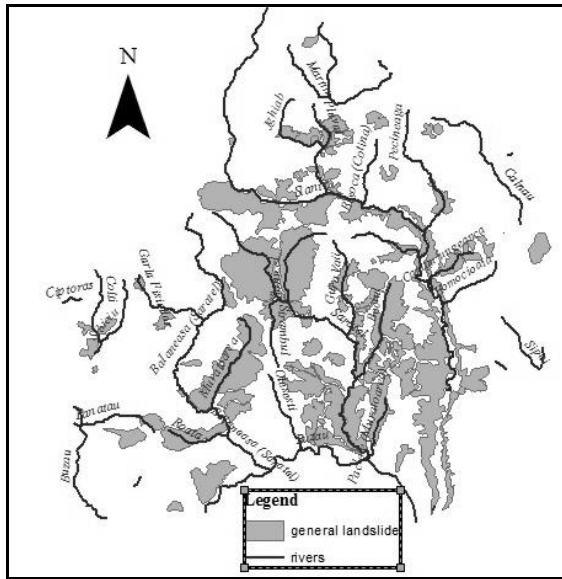
**3.2. Solifluctions** occur on most of the slopes of average tilting, used for grazing. These processes are conditioned by the daily freeze-thaw cycle and affect the soil cover. These gravitational movements are invisible to the human eye but affect the field farmland and change the physiognomy of the slopes with a wavy appearance (Grecu, 2018, Florea, 2003). Solifluction terraces represent a more advanced form of land degradation by solifluction and are spread over slopes with tilts larger than 10-12 degrees, with lengths of several tens of meters and widths of 1-2 m.

**3.3. Landslides** are the most widespread Geo-morphological processes in the sub-Carpathian area due to the large expansion of marls and clays. Their complexity gives them the quality of relief forms (Ene, 2005). For example, in the monocline area, genuine landslide valleys are formed, consisting of a spring (the feeding area), the sliding mass (the main course) with variable dimensions and shapes similar to those formed in the mountain glacier space, the sliding cone, formed in the lower part of the slope, and, depending on the consistency and speed of the material, it can take various forms, from the funnel, to the cloths of landslide diluvium.

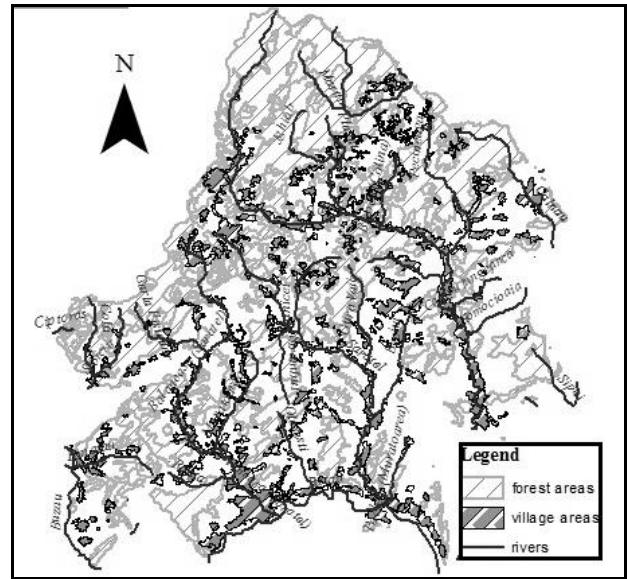
**3.4. The mud flow (muddy torrent)** show a high degree of spreading and affect important areas of agricultural land. These are a consequence of the water overflow of marls or clays, which exceeds the upper limit of plasticity. The flow rate of the torrents varies depending on the viscosity of the moving material from a few meters per week to a few meters per day. The spreading cone flows to the downstream side and has a sharp 1-2 m. The most representative forms of flow are formed in the external part of the Subcarpathians of the Buzău, in the monocline area. For example, in the Călnău Basin, in the Valea Largă-Sărulești Valley - Salcie Valley, on the right slope to the valley of the Călnău; the flows were formed on the gentle slope of a cuesta, parallel layout, over a distance of about 2 km (The mud flow in Valea Largă-Sărulești-Valea Salciei area). Most of the times, they cross the access roads, temporarily damming the Călnău river bed; upstream lakes are formed. On the left slope, represented by the forehead of a cuesta, there are deep, topless and rotational slides (Complex landslide with mud flow in Valea Largă-Sărulești-Valea Salciei area).

**4. Discussion:** A rather controversial topic of discussion is given by the age of landslides. For example, the oldest landslides appear to be contemporary to the main relief units, but due to the fact that they no longer function, being basically incorporated into the current relief forms, it is questionable whether they can still be classified as landslides (Fig. 4). One thing is certain, namely, the current slides are grafted on the older landslides, now monitoring their reactivation, amid extreme triggering conditions: intense precipitation, earthquakes, the formation of accentuated slopes, excessive grazing, extreme deforestation (Fig. 5).





**Fig. 4.** General landslide map of the study - Subcarpathian area between the Buzău and Călnău Rivers (data processing between 2014-2016).

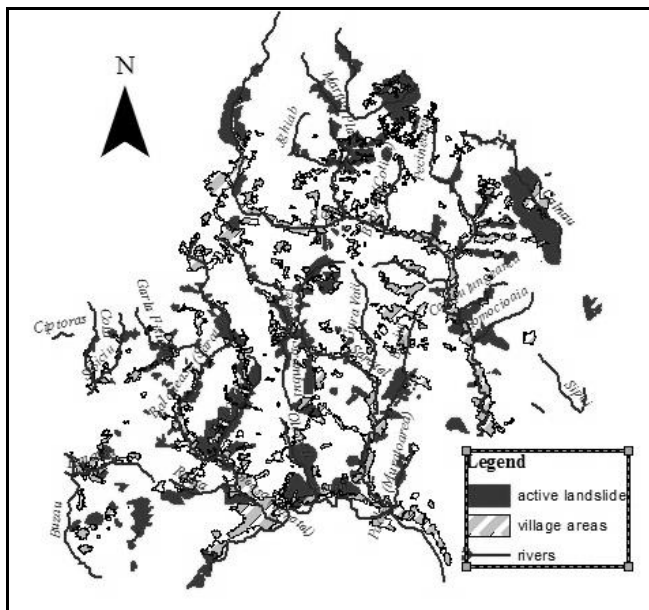


**Fig. 5.** The forest map of the study area - Subcarpathian area between the Buzău and Călnău Rivers (Land Cover -2007).

Another subject of discussion refers to the zonal tectonic activity. It plays an important role in the development and orientation of landslides, an example of such being the landsliding in the area of Rătești Monastery (October 2014, Fig. 6). It developed in the area of a tectonic-erosive depression, located between the Soimului Coast to the west and north, the Coast of Rătești, to the east and the Buzău Valley, to the south. The depression developed on an inverted fault system, to the north-south and the fall to the west; later, to the south, a series of normal secondary faults appeared, perpendicular to the main fault system, which are set up in steps towards the Buzău Valley. Anyway, the Buzău Valley, especially on the left side, is affected by sliding systems developed on the background of particularly active tectonic activities (Fig. 7).



**Fig. 6.** Landslide in Rătești – October 2014.



**Fig. 7.** Active landslide map of the study – Subcarpathian area between the Buzău and Călnău Rivers (data processing between 2014-2016).

**5. Conclusions:** The study of the dynamics of land movements is of great importance because these processes and forms of relief affect both human habitats and agricultural land, often having an irreversible character. At present, the lithological factor plays an important role in differentiating the land movements and slope withdrawal mechanisms, but the regionalization of these phenomena is a complex process conditioned by a series of physical and climatic factors. Their monitoring is therefore seasonal in nature, with the aim of monitoring the reactivating movements, especially if they affect the human habitat, including its support (infrastructure and agricultural land).

From a geomorphological point of view, the general evolution of the slopes shows their parallel withdrawal, together with the gradual decrease of the slope. The slopes affected by mud, ravenous and torrential floods are classified as severely degraded and therefore require afforestation and other measures to prevent materials from moving on the slopes.

**6. Acknowledgements:** This work was partially supported both project, by EEA Financial Mecanism 2009-2014, project number 22 SEE/2014 and the 29 PCCDI/2018 “GEORES” project financed by UEFISCDI, ROMANIA.

## References:

- Ene M. (2005) The Ramnicu Sarat River Basin. Dynamics relief in Carpathian and Subcarpathian area (Bazinul hidrografic Râmnicu Sărat. Dinamica reliefului în sectoarele montan și subcarpatic). Editura Universitară, București.
- Grecu F. (2018) Dynamic rainfall and fluvial geomorphology. Theory and Practice (Geomorfologie dinamică pluvio-fluvială. Teorie și aplicații). Editura Universitară, București.
- Florea N. (2003) Soil and Land Degradation, Protection and Improvement (Degradarea, protecția și ameliorarea solurilor și terenurilor). Editura Universitară, București.
- Ielenicz M., Nedelea A., Comănescu L. (2013) Geomorphology Thesaurus (Lexicon de Geomorfologie). Editura Universitară, București.
- Varnes D.J. (1978) Slope movement types and processes. In: Schuster R.L. and Krizek R.J. (eds.) Landslides - Analysis and control: National Research Council, Washington, D.C., Transportation Research Board, Special Report 176, p. 11–33.

## BACKGROUND AND REFERENCE VALUES FOR THE CADMIUM CONTENTS OF BRAZILIAN SOILS COMPARED

Fernando M. MELLO<sup>1</sup>, Essaid BILAL<sup>2</sup>, Gustavo N. C. MESQUITA<sup>1\*</sup>, Maria Eduarda L. R. TEODORO<sup>1\*\*</sup>, Thiago P. ARAUJO<sup>3</sup>, Frédéric GALLICE<sup>2</sup>

<sup>1</sup> Universidade Federal Rural do Rio de Janeiro (UFRRJ). Seropédica-RJ, Brazil; *fermamll@ufrrj.br*;

<sup>2</sup> Ecole des Mines de Saint Etienne-EMSE, CNRS UMR 5600, F42023 St.-Etienne, France; *bilalessaid@gmail.com*;

<sup>3</sup> Universidade do Vale do Rio dos Sinos (UNISINOS). São Leopoldo-RS, Brazil; *thiagopeixotoaraujo@gmail.com*;

\* *gustavonevescm@gmail.com*; \*\* *me.loureiro@yahoo.com.br*

**Abstract:** The difficulty on quality assessment of soils arises is in part due to distinguish pollutant sources, natural or anthropogenic. Compare this different sources backgrounds and guiding values is very important to instruction on regulations and legislation in general, for heavy metals contents, among other chemical components, and are pointing to more restrictive use of cadmium-rich phosphate fertilisers in many countries. Recognize and characterize contaminated soils is a serious concern with issues that whole society have to deal with today and one of the largest and most neglected problems in Brazil. This work intends to obtain an insight in the natural sources and loads of heavy metals, especially cadmium to soils in Brazil, mainly with the application of huge volume of mineral fertilisers, directly linked with their dangerous concentrations. This is a threat to public health in many regions, and it is one of the priorities to protect it from all sources of anomalous concentration in the ground. Decreasing soil quality by means of contamination and pollution by heavy metals is now recognized also as a serious risk for environmental quality and to the health of people.

**Keywords:** soil, Brazil, heavy metals, cadmium, contamination, legislation, reference values, fertilisers

### 1. INTRODUCTION

Soil contamination by Heavy Metal Elements (HME) is largely due to agricultural practices, mining and metallurgy. The current paper has the purpose to analyze and compare how this major issue is receiving attention in Brazil and in some developed countries, their guiding values and behavior of some heavy metals in the soil, with emphasis in cadmium from fertilisers and mining industry; to compare protocols of sampling, methods of detection and regulations around the world and also compare the minimum concentrations to establish levels of intervention and assess the risk. The distribution of most elements in soil shows a pattern related to geology and/or mineralization. Past climates and the prevailing particular tropical conditions in Brazil caused strong argillic and ferrallitic weathering of some rocks, with a change in mineralogy, and a modification of vertical and lateral distribution patterns of most major elements, but the main source of the anomalous enrichment remains the HME generated through time by agricultural activities on the environment, particularly in Latosols over volcano-sedimentary basins. In the actual brazilian norm, the CONAMA Resolution N° 420/2009, each state (federation) must determine the guiding values of prevention. Quality control and risk assessment associated to the soil contamination requires the knowledge of the total content in those elements and the influence of source rock contents in HME in the various constituent compartments of the ground. In the present work, HME are considered as the sense of Alloway (1995), the metals/metalloids which behaves geochemically as Siderophiles (Co, Ni, Au, Mo, Pb, As), Calchophiles (Cu, Ag, Au, Zn, Cd, Hg, Pb, As, Sb, Se, Tl, Mo) and the Lithophiles (V, Cr, Mn, U, Ti).

Soil contamination by HME became a problem in large agricultural areas, especially in extensive plantations, with the continuous use of phosphate based fertilisers, rich in HME, especially cadmium. The option to protect this natural resource is by using the legislation to establish, in a clear manner the rules, regulations and norms. This is the base to support and increase the controls and monitoring of those elements. In the last years, biomedical research has shown a strong correlation caused by cadmium in diseases of humans.

### 2. CADMIUM CONTENTS IN ROCKS, SOILS, FERTILISERS AND SEWAGE SLUDGE

The phosphate rocks which are mined in Brazil, Finland, Russia, and South Africa are mainly igneous rocks and have very low cadmium contents (sometimes below 10 mg•kg<sup>-1</sup>). In the other hand, those found in North and West Africa and in the Middle East are sedimentary rocks formed in environments rich in organic matter, and generally have much higher cadmium levels. In Tunisia, Togo, Senegal, they are reaching frequently values of 60 mg•kg<sup>-1</sup> while in Morocco deposits, the most important supplier of Brazil and European Union (EU), the cadmium contents in fertilisers are above 60 mg•kg<sup>-1</sup>. Most natural soils contain less than 1 mg•kg<sup>-1</sup> of cadmium resulted from the weathering of parent materials (Alloway, 1995). Generally lower levels are found in acid igneous rocks (granite average 0.09 mg•kg<sup>-1</sup>) than basic (basalt

average 0.13 mg•kg<sup>-1</sup>). In seds, sandstone and limestone show lower levels, higher contents are found in black shales (0.3 to 219 mg•kg<sup>-1</sup>), organic-rich seds or marine manganese nodules and phosphorite (Fergusson, 1990).

The average Cd content in soil surface is estimated to be 0.53 mg•kg<sup>-1</sup>, with all higher values reflecting anthropogenic influences (Kabata Pendias and Pendias, 2001). Although uneven distributed by different regions of Brazil, the dominant soil type is the Latosol, with 56,30% in total area of the country, followed by the Argisol (20,68%) and Neosol (9,38%) (Coelho et al. 2002). That distribution is mostly due to the geologic ground and by extreme climatic differences in the country. Proposed HME baseline values of natural concentrations in brazilian soils by Amaral Sobrinho (1993) suggests that different values of HME could be found in the same class and level of soil or between different classes as a function of the variation of soil characteristics.

Studies assessing natural contents of HME in some soil types of Brazil by Fadigas (2006), divides the soils in seven groups (see Table 1), the first one (1) distinguished by high contents in Mn, Fe and clay is composed by Red Distrophic Latosol, Brun Latosol and Red Argisol mainly formed in terrains of basaltic compositions, some of them over the huge Paraná Sedimentary Basin. This is the group that naturally concentrates the highest values of HME. The second group (2) includes those with high levels of silt, Mn and high CEC (Cation Exchange Capacity), including Chernosols, Luvisols, Eutrophic soils, and some samples of Yellow Latosol, Red-Yellow Latosol and Red Argisol. The sixth and seventh groups (6 and 7) shows the lowest levels in HME and share the same composition but are differentiated by clay and Fe contents, includes Yellow Dystrorphic Latosols and Argisols, and in minor quantity by soils derived by Tertiary and Quaternary sediments. Third, fourth and fifth (3, 4 e 5) groups share intermediate characteristics of those cited above and are mainly constituted by a great variety of Latosols and Argisols, and, with minor importance by Plinthosol, Cambisol, Nitosol with dystrophic character. Average values showed in Table 1 are near the quality reference values (Casarini, 2000) for the State of São Paulo-Brazil, in which the concentrations, in mg•kg<sup>-1</sup> are: Cd (0.5), Co (12.5), Cu (35.1), Cr (40.2), Ni (13.2), Pb (17), Zn (59.9). The adsorption/desorption of Cd and Zn presents a great sensibility to pH, compared with Cu and Pb. This chemical behaviour could contribute to explain the accumulation Zn and Cd in soil surficial layers in locals with higher pH (Alloway, 1990), *i.e.* in topsoils, the upper, outermost layer of soil, usually the top 5 cm to 20 cm depth. It has the highest concentration of SOM (Soil Organic Matter) and microorganisms and is where most of the biological soil activity occurs. Plants generally concentrate their roots there to obtain nutrients.

**Table 1.** Normal considered values of Cd, Co, Cr, Cu, Ni, Pb and Zn in natural soils, proposed as a Reference Value (RV)<sup>1</sup>. Modified from Fadigas et al. (2006).

GROUP (G)	ELEMENT						
	Cr	Co	Ni	Cu	Zn	Cd	Pb
	Soil Concentration (mg kg <sup>-1</sup> )						
1	55	20	35	119	79	<b>1.0</b>	19
2	48	10	18	19	44	<b>0.8</b>	28
3	65	4	25	16	23	<b>1.6</b>	16
4	35	10	17	12	35	<b>0.9</b>	18
5	23	4	7	6	12	<b>0.4</b>	22
6	43	2	12	2	12	<b>0.4</b>	3
7	19	2	5	3	6	<b>0.3</b>	40
QSm <sup>2</sup>	41	8	17	25	30	<b>0.8</b>	20

<sup>1</sup> Concentration considered normal for the soils belonging to each group and corresponding to the value of the upper quartile (75%) of the frequency distribution of the sample data in each group.

<sup>2</sup> Mean upper quartile between groups

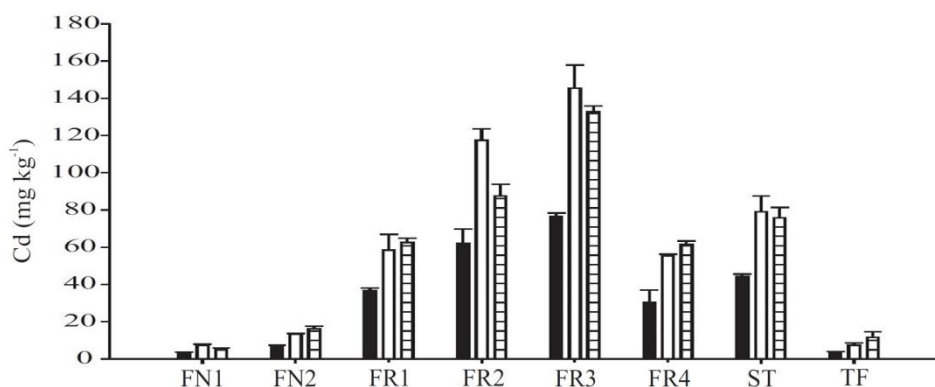
Phosphate fertilisers contain between 5 and 100 mg•kg<sup>-1</sup> Cd and up to 300 mg•kg<sup>-1</sup> Cd may be present in sewage sludge. Cadmium is a trace element in fertilisers, which have been applied extensively to arable and pasture land around the world. In United Kingdom (UK) the European Risk Assessment Report (ECB, 2007) related that current fertilisers contain around 79 mg•kg<sup>-1</sup> Cd of P. Based on the use of fertilisers in the 1980s and early 1990s, Alloway (1995) estimated that around 4.3 g of cadmium per hectare per year has been added to agricultural soils in the UK. Across the European Union, 231 tonnes of cadmium are added to agricultural soils each year from fertiliser use European Union Regulation (EC, 2007). It was concluded that this average cadmium content of european fertilisers, 138 mg•kg<sup>-1</sup>, would lead to a radical increase in the concentrations of cadmium in soil and crops, therefore in cadmium leaching.

Only 10% of the applied P as a fertiliser is taken by the plants, differing in this aspect by the higher taken of N and K. This difference is due to the higher P fixation in tropical soils, with high Fe-Al oxides (Raij, 2003). The Brazilian consumption of  $P_2O_5$  was in 2002 about 2,777,000 t (Lopes, 2003), 43% of monoammonium phosphate (MAP), 30% in the form of simple superphosphate (SSP), 15% triple superphosphate (TSP) and 12% of other sources of the market.

Langenbach and Sarpa (1985) compared the Cd concentration in eleven brazilian phosphates and observed that their Cd contents are lesser than  $2.0 \text{ mg}\cdot\text{kg}^{-1}$  Cd. The brazilian phosphate rock from Catalão-GO contains  $4 \text{ mg}\cdot\text{kg}^{-1}$  of Cd,  $19 \text{ mg}\cdot\text{kg}^{-1}$  Cr and  $58 \text{ mg}\cdot\text{kg}^{-1}$  Pb, and the fine apatitic concentrate from Araxá-MG shows contents of  $7 \text{ mg}\cdot\text{kg}^{-1}$  Cd,  $44 \text{ mg}\cdot\text{kg}^{-1}$  Cr and  $127 \text{ mg}\cdot\text{kg}^{-1}$  Pb (Gabe and Rodella, 1999). Amaral Sobrinho et al. (1992) presented typical ranges of HME in phosphate fertilisers as  $0.1\text{--}170 \text{ mg}\cdot\text{kg}^{-1}$  Cd,  $7\text{--}225 \text{ mg}\cdot\text{kg}^{-1}$  Pb,  $7\text{--}38 \text{ mg}\cdot\text{kg}^{-1}$  Ni,  $1\text{--}300 \text{ mg}\cdot\text{kg}^{-1}$  Cu and  $50\text{--}1450 \text{ mg}\cdot\text{kg}^{-1}$  Zn.

### 3. HEAVY METALS EXTRACTION ANALYTICAL METHODS COMPARED

Comparison of three extraction procedures was carried out by Campos et al. (2005) to assess HME in mineral fertilizers (Embrapa, 1999; USEPA 3051A and USEPA 3050B) for Cd, Cr, Cu, Ni, Pb, and Zn from the market in Brazil. The methods described do not fully solubilize the solid fraction of phosphates and are more indicated than total extractions for soil pollution studies, due to representation of maximum potentially bioavailable of a certain pollutant (Fig. 1).



**Fig. 1.** Average contents of Cd in brazilian natural phosphates FN1 and FN2, brazilian triple superphosphate and reactive non-brazilian phosphates FR1, FR2, FR3 and FR4, determined by different methods: USEPA 3051A (in black bars), USEPA 3050B (white bars) and EMBRAPA (dashed bars). Higher traces are the standard deviation of average values. Modified from Campos et al. (2005).

The USEPA 3050B method, from the Environmental Protection Agency, EPA (USEPA, 1998a), takes 1 g of the material, while USEPA 3051A (USEPA, 1998b) less material, 0.5 g to 1.0 g. The Brazilian method (EMBRAPA, 1999) uses approximately 0.5 g of the material added to 20 ml of  $HCl$   $2 \text{ mol}\cdot\text{l}^{-1}$ . The quantification of trace elements content was performed by air acetylene flame atomic absorption spectroscopy. Among the studied phosphates, the thermophosphate presented significantly greater concentrations of Cd, Cr, Cu, Ni, and Zn whereas Cu, Ni, Pb, and Zn were found in greater contents in the natural phosphate FN2. The reactive phosphate FR3 presented the greatest quantity of Cd ( $145\pm13 \text{ mg}\cdot\text{kg}^{-1}$ ) and the natural phosphate FN2, the highest quantity of Pb ( $234\pm9 \text{ mg}\cdot\text{kg}^{-1}$ ).

The tested methods can be applied in studies concerning heavy metals in samples of brazilian natural phosphate fertilisers phosphates (FN1 and FN2) which showed an average of  $8.7 \text{ mg}\cdot\text{kg}^{-1}$  of Cd content, while non-brazilian ones presented higher values, in average,  $77 \text{ mg}\cdot\text{kg}^{-1}$  Cd (Campos et al., 2005). Phosphate rocks presented contents between  $5\pm0.6$  and  $145\pm13 \text{ mg}\cdot\text{kg}^{-1}$  (Figure 1). Those values are in the range cited by Kabata Pendias and Pendias (2001) for phosphate fertilisers, namely  $0.1\text{--}170 \text{ mg}\cdot\text{kg}^{-1}$  of Cd. Amaral Sobrinho et al. (1992) encountered lower contents for apatite rocks ( $2\text{--}7 \text{ mg}\cdot\text{kg}^{-1}$  Cd).

For Cu content, there was no difference between the extraction methods. For Ni and Zn contents, there was no statistical difference between USEPA 3051A and USEPA 3050B, but they were superior than the Embrapa method (1999). The USEPA 3050B extracted more Cd than other methods, while for Cr contents, Embrapa method extracted the most.



#### 4. GUIDING VALUES IN BRAZIL AND EUROPE

The Brazilian Environmental Council (CONAMA, 2009), through the Resolution n.420/2009, established that each state in the country must determine its own guiding values for heavy metal concentrations based on a set of soil samples that represent the local geomorphology, pedology and lithology. This was decided because the international values, or those from other regions, might result in erroneous interpretation regarding areas suspected of being contaminated. The Brazilian resolution establishes three types of guiding values: quality reference values (QRVs), which should be determined by each state, prevention values (PVs) and investigation values (IVs), which are established and are valid for the whole country. In São Paulo state the risk limits were recently determined by CETESB (2016) mainly in topsoil and are, in  $\text{mg}\cdot\text{kg}^{-1}$ , as follows: (As -15), (Cd -1.3), (total Cr - 75), (Cu - 60), (Hg - 0.5), (Ni - 30), (Pb - 72) and (Zn - 1,900).

Cadmium in fertilizer phosphate rock, animal manures and land applied municipal sewage sludge is increasingly regulated in different parts of the world. Initially, cadmium was regulated primarily because of concerns about the metal leaching from fertilized soil into ground and surface waters. However, as knowledge increased about cadmium as a major human toxicant in our food, the emphasis on allowable cadmium in fertilizer has shifted to the amount of uptake seen in agricultural commodities grown on soils that include added cadmium in fertilizer. In the Netherlands the Soil Quality Regulation (2006) and the Soil Remediation Circular (2009) focuses on the elaboration of the remediation criterion used to determine whether urgent remediation is necessary. To be compared worldwide, all values presented in Table 2 are taken only from soils with 10% of organic matter and 25% of clay minerals. This restriction is due to strong correlation between HME, clay minerals and SOM contents. Higher the SOM content, higher levels of HME. Sandy soils are poor in HME than argillic ones and the SOM. The highest allowed levels in EU community are  $3 \text{ mg}\cdot\text{kg}^{-1}$  Cd,  $150 \text{ mg}\cdot\text{kg}^{-1}$  Zn;  $140 \text{ mg}\cdot\text{kg}^{-1}$  Cu and  $50 \text{ mg}\cdot\text{kg}^{-1}$  Pb (Chaudri et al., 1993). In Poland, those limits are, for arable soil  $3 \text{ mg Cd kg}^{-1}$ ,  $300 \text{ mg}\cdot\text{kg}^{-1}$  Zn and  $200 \text{ mg}\cdot\text{kg}^{-1}$  Pb (Chlopecka et al., 1996).

According to the EU recommendations, soil fertilised with sewage sludge should not contain more than  $3 \text{ mg}\cdot\text{kg}^{-1}$  Cd (86/278/EC/12-6-1986). Soil Guideline Values (SGVs) for cadmium in the Netherlands are presented according to land use in Table 2.

**Table 2.** Background values, Intervention Values and Maximum Values in soil in function of its destination: Soil Quality Regulation 2006 (a), Soil Remediation Circular 2009 (b). Modified from Ribeiro (2013, unpubl.).

Elements	Background values) <sup>a</sup> ( $\text{mg kg}^{-1}$ )	Sediment <sup>a</sup> ( $\text{mg kg}^{-1}$ )	Max Values $\text{mg kg}^{-1}$		Intervention Value) <sup>a</sup> ( $\text{mg kg}^{-1}$ )	Intervention Value) <sup>b</sup> ( $\text{mg kg}^{-1}$ )
			Residential <sup>a</sup>	Industrial <sup>a</sup>		
As	20	29	27	76	76	76
<b>Cd</b>	<b>0.6</b>	<b>0.8</b>	<b>1.2</b>	<b>4.3</b>	<b>13</b>	<b>13</b>
Cr total	55	100	62	180	180	-
Cu	40	36	54	190	190	190
Hg Total	0.15	0.6	0.83	4.8	36	-
Pb	-	-	-	-	-	4
Ni	50	85	210	530	530	530
Zn	140	140	200	720	720	720

The SGVs apply only to cadmium and its inorganic compounds. For residential ( $10 \text{ mg Cd kg}^{-1}$ ) allotment ( $1.8 \text{ mg}\cdot\text{kg}^{-1}$  Cd) and commercial ( $230 \text{ mg}\cdot\text{kg}^{-1}$  Cd) land uses, SGVs are based on estimates representative of lifetime exposure. Although young children are generally more likely to have higher exposures to soil contaminants, the renal toxicity of cadmium are based on considerations of the kidney burden accumulated over 50 years or so (Environment Agency, 2009). It is therefore reasonable to consider exposure not only in childhood but averaged over a longer time period.

#### 5. PROPOSED REDUCTION OF CADMIUM CONTENTS OF PHOSPHATE FERTILISERS IN EUROPEAN UNION

European Commission recently proposed a regulation (European Union Regulation - EC 2016) envisaging stringent limits of cadmium in phosphate fertilisers. Besides the proposals of no action and general actions for market incentives, the limits are synthetically: (i) an initial limit of  $60 \text{ mg}\cdot\text{kg}^{-1}$  Cd will apply as soon as the regulation comes into force; (ii) more stringent limit of  $40 \text{ mg}\cdot\text{kg}^{-1}$  Cd will phase in three years later; (iii) the lowest limit of  $20 \text{ mg}\cdot\text{kg}^{-1}$  Cd will come into force nine years after the regulation initiation and (iv) a new regulation setting a Community limit value for cadmium content in phosphate

fertilisers at  $60 \text{ mg}\cdot\text{kg}^{-1}$  Cd decreasing over time to 40 and eventually  $20 \text{ mg}\cdot\text{kg}^{-1}$  Cd if decontamination becomes available on industrial scale.

A new Regulation converges to a common proposal: establish an EU limit value of  $60 \text{ mg}\cdot\text{kg}^{-1}$  Cd as a starting point. This limit would take effect after an appropriate transition period of *e.g.* 2 to 3 years. Flexibility should be given to allow Member States to set limit values at either 40 or  $20 \text{ mg}\cdot\text{kg}^{-1}$  in the light of specific conditions in their territories. Fertilisers would be labelled to provide an indication which limit value for cadmium they comply with.

## 6. DISCUSSION AND CONCLUSIONS

The metallic elements tracks (Cd, Cr, Cu, Hg, Ni, Pb, Zn) are rapidly increasing in soils with the indiscriminate use of fertilizers, manures and urban sewage sludge. As some of them are potentially toxic and present no agronomic interest, their presences generate a major concern. The agricultural use of the residual mud allows the recycling of precious components such as the organic matter and many nourishing elements of the plant (Logan and Harrison, 1995). Residual muds can replace or reduce the use of these imported and expensive fertilisers. Economic and environmental issues are in the center of this debate, and this paper intends to expose the main advances in the knowledge.

The estimated Cd increase with the application of  $200 \text{ kg ha}^{-1}$  of the FR3 incorporated in 0.1 m depth of soil would reach  $0.094 \text{ mg}\cdot\text{kg}^{-1}$ , and in that way needs 111 applications to attain the intervention level of  $10 \text{ mg}\cdot\text{kg}^{-1}$  Cd (CETESB 2016). In the other hand, they noticed that in five years, Cd contents could double, from one average soil of  $0.5 \text{ mg}\cdot\text{kg}^{-1}$  Cd (Campos et al., 2005).

The possibility to attain the maximum permissible concentration, not only for Cd, but also for other evaluated elements, increases with larger quantities of phosphates fertilizers associated with sewage sludge and other fertilizers containing trace elements. Ramalho et al. (1999) availed the use of polluted water and phosphate fertilisers combined and observed that soils that received 25 years of phosphate fertilisers, showed a noticeable increase of Cd ( $0.66 \text{ mg}\cdot\text{kg}^{-1}$ ) when compared with the control area ( $0.5 \text{ mg}\cdot\text{kg}^{-1}$ ), without however elevate it to critical levels. The conditions that determine the adsorption capacity, such as pH, organic matter content, content of clay and oxides of Fe and Al, affect the availability and mobility of heavy metals present in phosphates (Abdel-Haleem et al., 2001). It is also important to consider local conditions that could lead to losses by erosion of soil particles enriched with heavy metals, transported to other areas or water bodies.

The ground contamination by heavy metals elements is a major environmental problem for two main reasons. Beside the risk in food, this contamination can have very long-term effects because its continuous concentration and strong chemical and physical affinity for the solid matrix of distinct geologic grounds and a long residence time in soils (Echevarria and Morel, 2006).

Current limits of cadmium on fertilisers in Brazil are insufficient to meet health and environmental protection goals. The states that have previously established base levels need to review recent research on the health effects of cadmium, the increment of cadmium in soils, and the contribution of fertiliser to cadmium loading in surface waters.

## REFERENCES

- Abdel-Haleem A.S., Scroon A., El-Bahi S.M., Zohny E. (2001) Heavy metals and rare earth elements in phosphate fertilizer components using instrumental neutron activation analysis. *Applied Radiation and Isotopes*, v. 55, p. 569-573.
- Alloway B.J. (1995) Cadmium. In: Alloway B.J (ed.) *Heavy Metals in Soils* (2nd ed.). London: Blackie Academic & Professional. 368 p.
- Amaral Sobrinho N.M.B., Costa L.M., Oliveira C., Velloso A.C.X. (1992) Metais pesados em alguns fertilizantes e corretivos. *Revista Brasileira de Ciência do Solo*, v. 16, p. 271- 276 .
- Amaral Sobrinho N.M.B. (1993) Interação dos metais pesados de resíduos siderúrgicos com um podzólico Vermelho Amarelo [Interaction of Heavy Metals from siderurgy waste with Red-Yellow Podzolic sol]. Viçosa UFV. Dsc.Thesis, 163 p.
- Campos M.L., Pierangeli M.A.P., Guilherme L.R.G., Marques J.j., Curi N. (2003) Baseline concentration of heavy metals in Brazilian Latosols. *Communications in Soil Science and Plant Analysis*, v. 34, p. 547-558.
- Casarini D. C. P. (2000) Proposta de valores de referência de qualidade e intervenção para solos e águas subterrâneas no estado de São Paulo. In: *Sem. Internacional sobre Qualidade de Solos e Águas Subterrâneas*, 2., SP. An. CETESB, 165p.

- CETESB (Companhia de Tecnologia de Saneamento Ambiental) (2016) Relatório de estabelecimento de valores orientadores para solos e águas subterrâneas no Estado de São Paulo [Report of the establishment of guiding values for soils and underground water]. São Paulo: Secretaria de Estado do Meio Ambiente, 230p.
- Chaudri A.M., McGrath S.P., Giller K.E., Rietz E., Sauerbeck D.R. (1993) Enumeration of indigenous *Rhizobium leguminosarum* biovar *trifolii* in soil previously treated with metal-contaminated sewage sludge. *Soil Biol. Biochem.*, 25, p. 301-309.
- Chlopecka A., Bacon J.R., Wilson M.J., Kay J. (1996) Forms of Cadmium, Lead, and Zinc in contaminated Soils from Southwest Poland. *J. Environ. Qual.*, 25, p. 69-79.
- Coelho M.R., Santos H.G., Silva E.F., Aglio M.L.D.O. (2002) Recurso natural solo [Natural resource soil]. *Uso agrícola dos solos brasileiros*. Rio de Janeiro, Embrapa Solos, p. 1-11.
- CONAMA- Conselho Nacional de Meio Ambiente (2009) Resolução CONAMA n 420, de 28 de janeiro de 2009. Brasília, 16 p.
- Echevarria G., Morel J.-L. (2006) Caractérisation de la biodisponibilité des éléments en traces dans les sols et validation de mesures fiables. *Sols et environnement*. Vandœuvre-lès-Nancy, 57 p.
- ECB (2007) European Union Risk Assessment Report. Volume 72, Cadmium oxide and cadmium metal, Part 1 - Environment (EUR 22919 ENV). Luxembourg: Office for Official Publications of the European Communities, 2007.
- Environment Agency (2009). Contaminants in soil: updated collation of toxicological data and intake values for humans. Cd Science Report SC050021/SR TOX7. Bristol: Environment Agency. 11p
- EMBRAPA (1997) Manual de métodos de análise de solo. 2nd ed., Rio de Janeiro, 212 p.
- Environment Agency (2009) Soil Guideline Values for cadmium in soil. Science Report SC050021 / Cadmium SGV. Bristol, UK: Environment Agency, 11 p.
- European Union Regulation EC (2016) Limits for cadmium in phosphate fertilisers. Proposal for a Regulation of the European Parliament and of the Council amending Regulations (EC) No 1069/2009 and (EC) No 1107/2009. 91 p.
- Fadigas F. S., Amaral Sobrinho N.M.B., Mazur N., Anjos L.H.C., Freixo A.A. (2006) Proposição de valores de referência para a concentração natural de metais pesados em solos brasileiros [Proposition of Reference Values to natural brazilian soils]. *Revista Bras. de Eng. Agrícola e Ambiental* v.10, n.3. p. 699-705.
- Fergusson J.E. (1990) *The Heavy Elements: Chemistry, Environmental Impact and Health Effects*. Oxford: Pergamon Press. p. 382–399.
- Gabe U., Rodella A.A. (1999) Trace Elements in Brazilian Agricultural Limestones and Mineral Fertilizers. *Communication Soil Science Plant Anal.* 30(5/6), p. 605-620.
- Greenwood N.N., Earnshaw A. (1997) Zinc, cadmium and mercury. *Chemistry of the Elements*, 29, p. 1201–1226.
- Kabata-Pendias A., Pendias H. (2001) *Trace Elements in Soils and Plants*, Third Edition. Boca Raton: CRC Press LLC.
- Langenbach T., Sarpa M. (1985) Teor de cádmio nos fertilizantes fosfatados brasileiros. *Revista Brasileira de Ciência do Solo*, v.9, p.179-181,
- Logan T.J., Harrison B.J. (1995) Physical characteristics of alkaline stabilized sewage sludge (Nvitro soil) and their effects on soil properties. *J. Environ. Quality*, 24, p. 153-164.
- Lope A.S. (2003) Reservas de fosfatados e produção de fertilizantes fosfatados no Brasil e no mundo [Phosphate reserves and phosphate fertiliser production in Brazil and the world]. In: *Simpósio sobre fósforo na agricultura brasileira, 2003*, Piracicaba. Anais. Piracicaba: Potafos/Anda., 1 CD-ROM.
- Raij B. van (2003) Fósforo no solo e interação com outros elementos. In: *Simpósio sobre fósforo na agricultura brasileira*. Piracicaba. Anais. Piracicaba: Potafos/Anda. 1 CD-ROM.
- Ramalho J.F.G.P., Amaral Sobrinho N.M.B., Velloso A.C.X. (1999) Acúmulo de metais pesados em solos cultivados com cana-de-açúcar pelo uso contínuo de adubação fosfatada e água de irrigação. *Revista Brasileira de Ciência do Solo*, v.23, p. 971-979 .
- Ribeiro M.A.C. (2013) Contaminação do solo por metais pesados [Soil contamination by heavy metals]. Lisbon. Universidade Lusófona de Humanidades e Tecnologias. Unpublished M.Sc Dissertation. 249 p.
- Usepa (1998a) Method 3050B Available at: [http:// www.epa.gov/SW-846/pdfs/3050b.pdf](http://www.epa.gov/SW-846/pdfs/3050b.pdf). Accessed in Feb. 2004.
- Usepa (1998b) Method 3051A. Available at: <http://www.epa.gov/SW-846/3051a.pdf>. Accessed in March 2004.

## EVALUATION OF THE PRESENT DEMAND AND SUPPLY OF GEMS, MINERALS AND ROCKS OF AESTHETIC VALUE IN THE EXHIBITIONS ORGANIZED BY THE GEOLOGICAL INSTITUTE OF ROMANIA - NATIONAL MUSEUM OF GEOLOGY

Adrian Theodor TONCO<sup>1\*</sup>, Antonela NEACȘU<sup>1\*\*</sup>, Delia Georgeta DUMITRAȘ<sup>2\*\*\*</sup>

<sup>1</sup> University of Bucharest, Faculty of Geology and Geophysics, 1, N. Bălcescu Ave., 010041 Bucharest, Romania

<sup>2</sup> Geological Institute of Romania, 1, Caransebeș Str., Bucharest, Romania, RO-012271

\**adrian-tonco@gmail.com*; \*\**antonela.neacsu@gmail.com*; \*\*\**d\_deliaro@yahoo.com*.

**Abstract:** Exhibitions of gems, jewelry, decorative rocks and fossils are taking place at the National Museum of Geology in Bucharest since 2006. In an attempt to evaluate the supply and demand, as well as the cultural and social impact of these events, a protocol was concluded between the Department of Mineralogy of the Faculty of Geology and Geophysics, and the Geological Institute of Romania. An inventory of the exhibits was carried out during November 2017 and June 2018, and details about their origin countries, gemological treatments, processing methods and authenticity were found. The risk of acquiring imitations and synthetic materials becomes more and more higher. Without a good experience to allow a rapid and accurate macroscopic assessment, they can be difficult to distinguish from genuine gemstones. Where possible, gems were verified by X-ray diffractometry.

**Key words:** gems exhibition, gemological treatments, gems' sources, gemological varieties, quiz.

### I. INTRODUCTION

In our country, the Geological Institute of Romania through the National Museum of Geology (NMG) is the traditional host of the sales exhibitions of gems, jewelry, minerals and rocks of gemological quality. Interesting is that the events are connected to important religious holidays and/or traditional festivals, providing the opportunity to make good business. Thus, the most modern trends in the processing of minerals and rock gems can be admired, getting information about treatments applied to them, and obtaining certifications and advice from experts. There is a wide range of minerals and rocks that came from Romania, as well as around the world. The gems are either rough, rolled or faceted, either in advanced processing stages, including heat or chemical treatments to improve their quality. The most modern trends in the processing of minerals and rock gems can be admired, getting information about treatments applied to them and obtaining certifications and advice from experts.

For visitors, quiz about color preferences was elaborated, as well as about processing and intervention through various procedures on raw material, also about the degree of product information. Another question was about the purpose for which the gems are purchased, knowing the tendency to be used increasingly more in alternative medical therapies. For exhibitors, questionnaires were focused on origin countries of crystals and rocks, how to purchase (personally or through intermediaries, participation in international fairs), and also on the possibility to check the quality and authenticity of gems and decorative rocks. In order to confirm the authenticity of the gems, some of the dealers allowed extracting fragments of mineral and rock exhibits for RX diffraction, using the equipment of the Geological Institute of Romania. X-ray powder diffraction analyses were performed on a Bruker D8 Advance automated diffractometer equipped with a graphite-diffracted beam monochromator (Cu  $K\alpha$  radiation,  $\lambda = 1.54056$  Å), at an operating voltage of 40 kV and a beam current of 40 mA, ICDD PDF Release 2013 data base, software including Diffrac Basic (Eva V3.1) and Topaz 4-2 programs.

### II. RESULTS AND DISCUSSION

Questionnaires designed for 15 dealers and retailers focused on the origin countries of the gem-quality stones which they sell: Brazil, India, China, South Africa, Peru, Afghanistan, Russia and Madagascar. Other countries, such as Argentina, Mexico, the USA, Canada, Namibia, Congo, Ethiopia, Morocco, Myanmar, Dominican Republic, Australia, Turkey, as well as European countries like Germany, Spain, Norway, the Czech Republic and France, contribute to a lesser extent to the shaping of the Romanian gem market. Some specimens come from the former famous mining areas of Romania (Baia Mare, Apuseni Mountains, Banat). The exhibits are purchased personally or through intermediaries, usually from international gems exhibitions and trade fairs in Germany, France, USA, rarely directly from the origin countries. Many of the gems found at these international events (Tab. 1) are originally transported to India, where they are often processed and then sold to collectors and dealers. The exhibitors who participate to the NMG events sometimes ask the expertise of GIR specialists for gems certification. Some of them are geologists, or have specialized gemological training.

70 questionnaires designed for visitors were distributed and received answers are illustrated in Fig. 1.

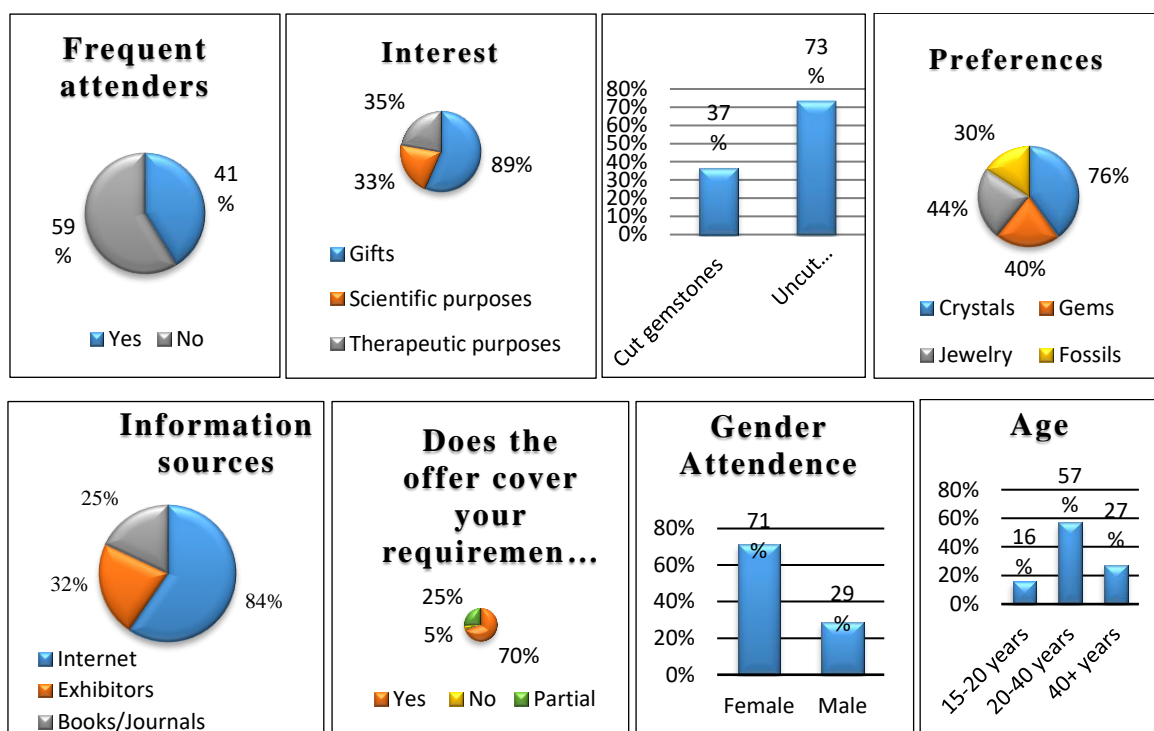














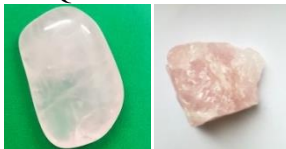






Fig. 1. Received answers from the visitors to the questionnaires.


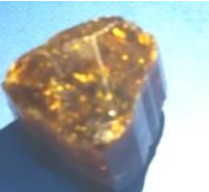




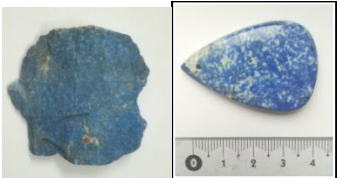

Table 1. The most spectacular minerals and rocks with gemological properties marketed in the NMG exhibitions (November 2017-June 2018).





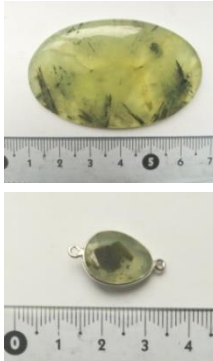
MINERAL / ORIGIN COUNTRIES	CHEMICAL COMPOSITION The New IMA List of Minerals – A Work in Progress – Updated: March 2018	GEMOLOGICAL VARIETIES	MACROSCOPIC DESCRIPTION
Beryl  Madagascar Brazil Russia	$\text{Be}_3\text{Al}_2\text{Si}_6\text{O}_{18}$	Morganite (Rose Beryl) 	Rare variety of beryl. Rose color with an intense lilac shade. Fine brown inclusions into internal cracks. Dichroic. Non-heat-treated for the rose color improvement. The crystals with a strong rose color are the most valuable (Andrei, 2013).
		Aquamarine (Blue Beryl)  	A distinct greenish blue to blue color, due to the low content of iron oxide ( $\text{Fe}^{2+}$ ). Few inclusions and fractures. Dichroic. Pale greenish cloudy and almost opaque in beads for necklaces, earrings and bracelets. Some of them present the <i>chatoyant</i> effect. There are raw, greenish-blue stones, and it is assumed that they were not heat-treated for color intensification (Crowe, 2007). Others have probably been heat-treated to get the pale blue or the dark blue of the so-called <i>Brazilian aquamarine</i> , the most popular (Andrei, 2013).
		Heliodore (Gold Beryl) 	Less intense yellow, meaning a low Fe content. But the color can often be changed by heating and irradiation, so treatments cannot be excluded. Internal fine cracks and a relatively good transparency. Because it can be mistaken for peridot, chrysoberyl and some tourmaline varieties (Andrei, 2013), it was subjected to the RX investigation. Rarely used in jewelry, because of the absence of brightness.



		Goshenite (White Beryl) 	Incolore specimen of beryl. Free of inclusions. Rarely used in jewelry, excepting just this pure appearance named <i>the mother of gemstones</i> .
Corundum  <i>India</i>	Al <sub>2</sub> O <sub>3</sub>	Sapphire 	<i>Geuda</i> type (Andrei, 2013). Inferior gemological varieties, green to yellow-green color, because of the less Fe content in comparison with the most valuable and expensive blue to violet sapphires. Fine inclusions and a relatively low transparency. RX tested.
		Ruby  	Dark red color and lack of transparency show that rubies are of inferior quality. Thermally untreated (heating can remove inclusions and improve the clarity). Ruby cabochons in zoisite, zoisite ruby and dark red ruby in necklaces, earrings and bracelets. RX tested.
Chrysoberyl  <i>Russia</i> <i>South Africa</i>	BeAl <sub>2</sub> O <sub>4</sub>	Alexandrite 	Genuine alexandrite displays a color change ( <i>alexandrite effect</i> ) depending upon the nature of ambient lighting ( <i>metamerism</i> ). Never observed in the case of alexandrite marketed in the NMG. Russian pendants of red-raspberry alexandrite. Raw bicolored green to dark green stones, with a relatively low transparency (South Africa). It can be mistaken for topaz, beryl, peridot and tourmaline. RX tested.
Quartz  <i>India</i> <i>Uruguay</i> <i>Brazil</i> <i>Madagascar</i> <i>Bolivia</i>	SiO <sub>2</sub>	Amethyst 	A purple variety of quartz. Sometimes bicolored crystals. The color is due to the presence in the crystalline structure of Fe <sub>2</sub> O <sub>3</sub> and Al <sub>2</sub> O <sub>3</sub> . The most popular gem in NMG: raw and faceted crystals, cabochons and beads in silver for earrings, rings, trinkets or pendants. It can be mistaken for fluorite, kunzite, spinel, tourmaline, topaz and tanzanite (Andrei, 2013). RX tested.
		Citrine 	Yellow to brownish-colors, by the presence of iron and aluminum traces in the crystalline structure. It is the most popular quartz variety in NMG after amethyst: beads, pendants raw and faceted crystals. As gemologists mention, about 10 to 30 % of the total citrine found on the market is synthetic, being almost impossible to distinguish from the natural one. It can be mistaken for beryl, topaz, sapphire, tourmaline and zircon (Andrei, 2013). RX tested.
		Aventurine 	A variety of translucent quartz with abundant small plate- or flake-shaped of fuchsite mica inclusions. Aventurine is usually green, but also brown, gray and blue. Beautiful beads and cabochons.

		<p>Rose Quartz</p> 	Color ranges from a very light to a rich translucent pink. The pink color is attributed to microscopic inclusions of minerals containing Ti, Mn, Fe, Al, Li (Andrei, 2013). Sold as raw and faceted crystals, jewelry made of spheres or cabochons presenting the phenomenon of <i>asterism</i> , necklaces, ashtrays, cassettes.
		<p>Ametrine</p> 	Is a variety of rare bicolored quartz presenting amethyst and citrine in contact with one another in a single crystal. Almost all of the world's commercial ametrine comes from Anahi Mine in Bolivia (Andrei, 2013).
		<p>Smoky quartz. <i>Cairngorn quartz</i>. <i>Morion</i> (black)</p> 	A grey, translucent variety of quartz that ranges in clarity from almost complete transparency to an almost-opaque brownish-gray (smoky quartz) ( <i>Cairngorn quartz</i> ) or black crystal ( <i>morion</i> ). The color is due to the presence in the crystal lattice of aluminum and/or lithium (Andrei, 2013). Some samples show rutile needle inclusions. Faceted crystals in white metal mount.
<p>Jadeite</p>     <p><i>Nephrite</i></p> <p><i>China</i> <i>Canada</i> <i>Africa</i></p>	<p><math>\text{Na(Al,Fe)Si}_2\text{O}_6</math></p>    <p><math>\text{Ca}_2(\text{Mg,Fe})_5\text{Si}_8\text{O}_{22}(\text{OH})_2</math></p> <p><i>Gem Reference Guide</i>. Gemological Institute of America 1988.</p>	<p><i>Jade</i></p> 	As a result of iron content, green jadeite has a typical marble appearance and a resinous luster. RX tested. Nephrite is exposed as various shades of cream-colored (rich in magnesium), and also as white and dark green (due to the presence of iron oxide) (Crowe, 2007), sometimes gray. Both are durable, colorful materials that are admired and sold in the NMG exhibitions as jewelry (bangles), art and decorative objects (carvings). Jadeite jade is rarer and generally more valuable than nephrite.
<p>Malachite</p>   <p><i>Russia</i> <i>Congo</i></p>	<p><math>\text{Cu}_2(\text{CO}_3)(\text{OH})_2</math></p>	<p>Malachite</p> 	All specimens are green and range from a pastel green to an extremely dark green. Made in silver for earrings, bracelets and pendants. Also decorative and luxury objects (carvings, ashtrays, cassettes). RX tested.
<p>Spinel</p>   <p><i>India</i> <i>Myanmar</i> <i>Madagascar</i></p>	<p><math>\text{MgAl}_2\text{O}_4</math></p>	<p>Gahnit. Gahnospinel <i>Burma Spinel</i></p> 	Greenish-purple blue stones cheaper and less sought than other color spinel (Crowe, 2007). It is one of the few gemstones that can be purchased with the certainty of being natural, as it is rarely treated thermally or irradiated to intensify or change the color. Made in silver for earrings, bracelets and pendants. It can be mistaken for corundum, zircon, tourmaline, amethyst and garnet. RX tested.
<p>Fluorite</p>  <p><i>China</i></p>	<p><math>\text{CaF}_2</math></p>	<p>Fluorite</p> 	Typically purple, green, and yellow. Also colorless, blue, red, and black. Specimens with exceptional diaphaneity and color are found as unpolished crystals or beaded stone, and as beautiful cabochons. Also art and ornamental objects (ashtrays, vases, clock dials). RX tested.

<p><b>Turquoise</b></p> <p><i>USA</i> <i>Tibet</i> <i>Iran</i></p>	$\text{CuAl}_6(\text{PO}_4)_4(\text{OH})_8 \cdot 4\text{H}_2\text{O}$	<p><b>Turquoise</b></p> 	<p>Shades of blue, bluish green, green and yellowish green. Made in silver in beads for necklaces, earrings, rings, trinkets or pendants. Treatments that even traders do not know about (reconstitution, pressing, stabilization, and painting) are not excluded (Crowe, 2007). Because of the frequent use of howlite and magnesite imitations (Andrei, 2013), it was RX tested.</p>
<p><b>Tourmaline</b></p> <p><i>Madagascar</i> <i>India</i></p>	$\text{NaMg}_3\text{Al}_6(\text{BO}_3)_3[\text{Si}_6\text{O}_{18}](\text{OH})_4$	<p><b>Dravite</b></p> 	<p>Brown-yellow color due to the presence of magnesium in the mineral network (Crowe, 2007). Dichroic, with two different colors when viewed from different angles.</p>
	$\text{CaMg}_3\text{Al}_6(\text{BO}_3)_3[\text{Si}_6\text{O}_{18}][(\text{OH})_3\text{O}]$	<p><b>Uvite</b></p> 	<p>The official IMA name for this mineral species is <i>uvite</i>, redefined as part of a nomenclature revision of the Tourmaline group (Henry <i>et al.</i>, 2011). Beautiful green crystals occasionally striated. RX tested.</p>
	$\text{Na}(\text{Al}_{1.5}\text{Li}_{1.5})\text{Al}_6(\text{BO}_3)_3[\text{Si}_6\text{O}_{18}](\text{OH})_4$	<p><b>Bicolored Elbaite</b> <i>Watermelon</i>      <i>Pink elbaite</i></p>  	<p>It is most used in jewelry. The green color of the <i>watermelon</i> variety is due to ferric ions, chrome or vanadium. Manganese in the crystal network usually gives the pink color (Andrei, 2013). Raw bicolored pink elbaite crystals, watermelon elbaite in copper mounts. The higher the colors contrast and the more transparent elbaite is, the more expensive it is.</p>
	$\text{NaFe}_3\text{Al}_6(\text{BO}_3)_3[\text{Si}_6\text{O}_{18}](\text{OH})_4$	<p><b>Schorl</b></p> 	<p>Ferric black tourmaline. It can be mistaken for onyx, with which it is sometimes substituted. Used like mourning stone (Andrei, 2013), in silver mounts.</p>
<p><b>Lazurite</b></p> <p><i>Afghanistan</i> <i>Iran</i></p>	$(\text{Na,Ca})_8\text{Si}_6\text{Al}_6\text{O}_{24}[(\text{SO}_4),\text{S},\text{Cl},(\text{OH})]_2$	<p><b>Lapislazuli</b></p>  	<p>Lazurite is the blue component of the gemstone or, more usually, ornamental rock <i>lapislazuli</i>. It is an ultramarine to midnight-blue, opaque mineral, often containing calcite inclusions. Sold as jewelry (cabochon, boards, drops, spheres), art and decorative objects (cassettes, ashtrays, statuettes). Treatments are not excluded in order to obtain a uniform color by masking calcite diaclasses. Substituted by synthetic spinel or blue glass paste (Andrei, 2013). It can be often mistaken for azurite. RX tested.</p>

<p>Topaz</p> <p><i>Brazil</i> <i>Ukraine</i></p>	$\text{Al}_2\text{SiO}_4(\text{F},\text{OH})_2$	<p><i>Imperial topaz.</i> Rare and precious bicolored topaz</p>  <p>Light yellow topaz.</p>	<p>The color ranges from colorless to yellow-orange (<i>imperial topaz</i>), brown and pink yellow, as well as rare bicolored topaz crystals. Light yellow topaz has a lower gemological value. Thermal treatments are not excluded, by which the defects in the crystalline network are repaired, with the transformation of light yellow to pink or pink-orange color, belonging to the most sought-after topaz varieties (Andrei, 2013). It can be mistaken for citrine or smoky quartz.</p>
<p>Pectolite</p> <p><i>Dominican Republic</i></p>	$\text{NaCa}_2\text{Si}_3\text{O}_8(\text{OH})$	<p><i>Larimar. Lorimar</i></p> 	<p>Calcium substitution by copper produces the blue color. Also called <i>Stefilia's Stone</i>, is a rare blue variety of pectolite found only in the Dominican Republic. An intense silky chatoyance can be observed (<a href="http://www.jmarcano.com/mipais/recursos/larimar2.html">http://www.jmarcano.com/mipais/recursos/larimar2.html</a>).</p>
<p>Spodumene</p> <p><i>Afghanistan</i> <i>USA</i> <i>Pakistan</i></p>	$\text{LiAlSi}_2\text{O}_6$	<p>Kunzite</p>  <p>Hiddenite</p> 	<p>Pink to lilac specimens of gem-quality spodumene. The color is attributed to the presence of manganese as a chromophore. Greasy luster. Kunzite is the most commonly encountered gem spodumene. Very hard to cut and polished (Crowe, 2007).</p> <p>Rare green variety of the gem spodumene. The color is attributed to the presence of chromium as a chromophore. Only light green hiddenite. The dark green stones are even rare and very expensive (Crowe, 2007), and they are not marketed yet in the NMG exhibitions.</p>
<p>Prehnite</p> <p><i>India</i></p>	$\text{Ca}_2\text{Al}_2(\text{Si}_3\text{O}_{10})(\text{OH})_2$	<p>Prehnite</p> 	<p>Typically silky semi-transparent to translucent. Usually yellow-green to apple-green or mint green. Faceted shiny beads sometimes with black tourmaline inclusions. It can be mistaken for nephrite, jadeite, chrysoprase and peridot (Crowe, 2007).</p>

## References

- Andrei M.-D. (2013) Practical gemology. The gems identification (in Romanian). Punct Edit., Bucharest, 444 p.
- Crowe J. (2007) The jeweler's dictionary of gemstones: a complete guide to appraising and using precious stones from cut and color to shape and settings (in Romanian). Rao Edit., 176 p.
- Henry D.J., Novák M., Hawthorne F.C., Ertl A., Dutrow B.I., Uher P., Pezzotta F. (2011) Nomenclature of the tourmaline-supergrout minerals. American Mineralogist, volume 96, p. 895–913
- The New IMA List of Minerals - A Work in Progress. Updated: March 2018.  
[http://nrmima.nrm.se/IMA\\_Master\\_List\\_%282018-03%29.pdf](http://nrmima.nrm.se/IMA_Master_List_%282018-03%29.pdf)  
<http://www.jmarcano.com/mipais/recursos/larimar2.html>





## CONTENT

– continued from the front cover –

page

<b>Daniel BÎRGĂOANU, Gheorghe DAMIAN, Andrei BUZATU</b> The Fe content in the sphalerites from the Breiner-Băiuț deposit .....	37
<b>Réka KOVÁCS, Călin G. TĂMAȘ</b> New geochemical data and mineralogical interpretation for Cisma ore deposit, Gutâi Mountains .....	43
<b>Mădălina Paula ANDRII, Călin Gabriel TĂMAȘ</b> Ore mineralogy and geochemistry relationships in Băița Bihor ore deposit, Apuseni Mountains, Romania - Blidar Contact case study .....	49
<b>Ioan E. BARBU, Gheorghe BRĂNOIU</b> Depositional systems for the sedimentary deposits from the Lighidia perimeter, Bozovici, Caraș-Severin county .....	55
<b>Heloiza M. HORN, Adolf H. HORN, Reginaldo A. SAMPAIO, Essaid BILAL</b> Decontamination of middle to low-grade contaminated areas, using a lowcost method .....	61
<b>João P. S. KESSLER, Thiago P. ARAUJO, Fernando M. MELLO, Essaid BILAL</b> Characterization of clay minerals from the reject of the sand extraction in Capela de Santana-RS, Brazil .....	67
<b>Andreea-Elena MAFTEI, Andrei BUZATU, Nicolae BUZGAR, Andrei-Ionut APOPEI</b> Preliminary assessment of anthropogenic contribution and influencing factors on major elements and total organic carbon in Tazlău River sediments, Romania .....	73
<b>Marius C. SANDU, Gabriel O. IANCU, Ciprian CHELARIU Mihai NICULITA</b> Preliminary study on the geochemistry of stream sediments from Grintiesul Mare brook, Eastern Carpathians, Romania .....	79
<b>Lucica NICULAE</b> The dynamics, geomorphology and the relationship of the mass movement with the geology in the Subcarpathian Area, between the Buzău and the Călnău Rivers .....	85
<b>Fernando M. MELLO, Essaid BILAL, Gustavo N. C. MESQUITA, Maria Eduarda L. R. TEODORO, Thiago P. ARAUJO, Frédéric GALLICE</b> Background and reference values for the cadmium contents of brazilian soils compared .....	91
<b>Adrian Theodor TONCO, Antonela NEACȘU, Delia Georgeta DUMITRAȘ</b> Evaluation of the present demand and supply of gems, minerals and rocks of aesthetic value in the exhibitions organized by the Geological Institute of Romania - National Museum of Geology .....	97